Investigating the Effects of Variant Calmodulin on RyR2 in Generating Arrhythmogenic Ca^{2+} Release

Aisha Abdullah Faraj Gendra

A thesis submitted for the degree of Doctor of Philosophy

Cardiff University

December 2025

Summary

The human cardiac ryanodine receptor (hRyR2) is a Ca^{2+} channel located on the sarcoplasmic reticulum of cardiomyocytes. In regulating Ca^{2+} release, it maintains both electrical and contractile function, and in these tasks its normal function is modulated by the Ca^{2+}-binding accessory protein calmodulin (CaM). Several CaM mutations have been linked to cardiac arrhythmias, such as Catecholaminergic Polymorphic Ventricular Tachycardia (CPVT), but their arrhythmogenic mechanisms are not fully resolved. This research aimed to investigate the effects of two arrhythmia-linked CaM mutations (D132E and Q136P) on RyR2 function (either directly, or by virtue of CaM's regulation of its associated kinase: CaMKII) and how this might lead to aberrant Ca^{2+} signalling.

RyR2 and CaM were recombinantly co-expressed in HEK293 cells and live-cell confocal Ca^{2+} imaging was used to assess recursive Ca^{2+} release dynamics. The effect of wild type (WT) CaM co-expression on RyR2 is inhibitory - decreasing the duration of Ca^{2+} release events. Co-expression of D132E and Q136P CaM was shown to diminish this inhibitory effect by increasing the duration of Ca^{2+} release transients. Additionally, D132E CaM significantly reduced the endoplasmic reticulum Ca^{2+} store load in non-oscillating HEK293 cells compared to WT CaM. It is, therefore, likely that D132E variant CaM is causing diastolic Ca^{2+} leakage from the channel which results in smaller Ca^{2+} stores. A reduction in Ca^{2+} sparks frequency was also observed in permeabilised mouse ventricular myocytes with both D132E and Q136P CaM variants compared to WT CaM. Additionally, Q136P CaM was found to impair CaMKII signalling, showing reduced CaMKII autophosphorylation and consequent decreased phosphorylation of RyR2 at the S2814 CaMKII phosphorylation site.

Despite D132E and Q136P CaM variants showing similar RyR2-mediated Ca^{2+} release profiles at the cellular and spark level, these findings suggest that D132E and Q136P CaM exert their dysfunction in different ways. D132E seems to exert a greater Ca^{2+} leak under diastolic conditions, while Q136P CaM disrupts CaMKII-dependent RyR2 regulation, suggesting that calmodulinopathy in CPVT is likely mechanistically complex.

Acknowledgments

My first and foremost thanks go to my supervisor, Dr Lowri Thomas. Not many people have the privilege of working under someone as caring, understanding, and supportive as you. Thank you for your unwavering belief in me, for your patience during moments of doubt, and for your insightful guidance that always steered me in the right direction. I could not have asked for a more caring or supportive supervisor.

I would like to thank Dr Ewan Fowler for his assistance with the sparks experiments and for his invaluable and constructive feedback. I would also like to thank Dr Nordine Helassa for his input and support and valuable discussions throughout my PhD.

A special thank you to Tessa, my wonderful lab partner. Your positivity, teamwork, and shared commitment made the lab a place of both productivity and friendship.

My deepest appreciation is for my family and friends, whose love forms the foundation of everything I do.

To my parents, Abdullah and Samira, despite the vast distance between us, you were always present. Your constant support, wise counsel, and those precious video calls bridged the continents between us.

To all my wonderful sisters and brothers, thank you for your unconditional support and encouragement and for always being there when I needed you.

To my son, Ismail, your smiles and laughter were the fuel for this journey. I'm even grateful for the random strings of letters you typed on my unattended laptop.

Finally, to my husband, Mohamed, thank you for being my rock, so supportive and encouraging, cheering for my ups and holding me steady through my downs. This achievement is as much yours as it is mine.

Publications

Published abstracts arising from this thesis

Gendra, A., Fowler, ED., Helassa, N., Thomas, NL. 2024. Mechanistically Complex Effects on Variant Calmodulin on Ryanodine Receptor in CPVT. Physiology in Focus 2024. Northumbria University, Newcastle. PCA009.

Contents

List of Figures

List of Tables

List of abbreviations

ACMG	American College of Medical Genetics and Genomics
ADP	Adenosine diphosphate
AM	Acetoxymethyl
AMP	Adenosine monophosphate
AP	Action potential
Apo-CaM	Ca^{2+} -free calmodulin
ATP	Adenosine triphosphate
BCA	Bicinchoninic acid
Bp	Base pair
Ca^{2+}	Calcium ion
CaCaM	Ca^{2+}-bound calmodulin
$CaCl_2$	Calcium chloride
CaM	Calmodulin
CaMBD	CaM binding domain
CAMKII	Ca^{2+} /calmodulin-dependent protein kinase II
cAMP	Cyclic adenosine monophosphate
$CaPO_4$	Calcium phosphate
cDMEM	Complete DMEM
CHAPS	3-[(3-cholamidopropyl) dimethylammonio]-1-propanesulfonate
CICR	Calcium-induced calcium release
CPVT	Catecholaminergic polymorphic ventricular tachycardia
CPVT1	CPVT caused by mutations in RyR2
CRU	Ca^{2+} release unit
Cryo-EM	Cryogenic electron microscopy
CSQ2	calsequestrin isoform 2, cardiac
DAD	Delayed after depolarisation
dH_2O	Deionised water
DMD	Duchenne muscular dystrophy

DMEM	Dulbecco's Modified Eagle Medium
DMSO	Dimethyl sulphoxide
DTT	Dithiothreitol
EAD	Early after depolarisation
ECACC	European Collection of Authenticated Cell Cultures
ECC	Excitation-contraction coupling
ECG	Electrocardiogram
E-coli	Escherichia coli
EDTA	Ethylenediaminetetraacetic acid
Epac	The exchange protein activated by cAMP
ER	Endoplasmic reticulum
FBS	Fetal Bovine Serum
F-CaM	Fluorescently labelled CaM
FKBP	FK506-binding protein
FoV	Field of view
FRET	Fluorescence-resonance-energy-transfer
GSH-CaM	Gly-Ser-His-CaM
HA-CaM	High Affinity-CaM
HBS	HEPES Buffered Saline
HeNe	helium-neon
HF	Heart failure
hRyR2	Human RyR2
ICalmR	International Calmodulinopathy Registry
ICD	Implantable cardioverter defibrillator
IF	Immunofluorescence
iPSC-CMs	Induced pluripotent stem cell-derived cardiomyocytes
IRES	Internal ribosome entry site
K^+	Potassium ion
KRH	Krebs-Ringer-HEPES
LB	Luria Bertani

LCSD	Left cardiac sympathetic denervation
LQTS	Long QT syndrome
LTCCs	L-type Ca^{2+} channels
MDCK	Madin-Darby canine kidney
mDMEM	Minimal DMEM
Mg^{2+}	Magnesium ion
Na^{+}	Sodium ion
NaB	Sodium butyrate
NCBI	National Centre for Biotechnology Information
NCX	Na^{+}-Ca^{2+} exchanger
NO	Nitric oxide
NTA	Nitrilotriacetic acid
PBS	Phosphate buffered saline
PC	L-α-Phosphatidylcholine
PE	Phosphatidylethanolamine phospholipid
PKA	Protein kinase A
PKC	Protein kinase C
PKG	Protein kinase G
PLB	Phospholamban
PLM	Phospholemman
PMCA	Plasmalemmal Ca^{2+} ATPase
P_o	Open probability
PP	Protein Phosphatase
PP1	Protein Phosphatase 1
PP2A	Protein Phosphatase 2A
PP2B	Protein Phosphatase 2B
PSG	Penicillin-Streptomycin-Glutamine
PVDF	polyvinylidene difluoride
ROIs	Regions of interest
RT	Room temperature

RyR	Ryanodine receptor
RyR2	Ryanodine receptor isoform 2, cardiac
RyR2-DKI	Ryanodine receptor type 2 double knock-in mouse
SAN	Sinoatrial node
SDS	Sodium dodecyl sulphate
SDS-PAGE	Sodium Dodecyl Sulfate-Polyacrylamide Gel Electrophoresis
SERCA	Sarcoplasmic/endoplasmic reticulum Ca^{2+} ATPases
SERCA2a	The cardiac isoform of SERCA
SHEW	Safety, Health, Environment and Welfare
SK channels	Small-conductance Ca^{2+}-activated K^{+} channels
SM2	Spark Master 2
SOC	Super optimal medium with catabolic repressor
SOICR	Store overload-induced Ca^{2+} release
SPEG	Striated muscle preferentially expressed protein kinase
SR	Sarcoplasmic reticulum
TAE	Tris Acetate-EDTA
TBS-T	Tris-buffered saline-tween
T_c	Median closed time
TCaM	therapeutic CaM
T_d	Dead time
T_m	Melting temperature
T_o	Median open time
T-tubules	Transverse tubules
UV	Ultraviolet
WT	Wildtype

Chapter 1: General introduction

1.1 Calcium signalling

1.1.1 Versatility of calcium signalling

The calcium ion (Ca^{2+}) is one of the most ubiquitous signalling molecules that controls many biological functions including cellular proliferation and differentiation, neuronal signalling and muscle contraction (Berridge et al. 2000; Lytton 2013; Landstrom et al. 2017). A simple rise in Ca^{2+} concentration from 100nM to around 500-1000nM in cells can control such a versatile variety of processes by varying signal speed, frequency, magnitude, and spatial patterns (Berridge et al. 2000). The intracellular availability of Ca^{2+} is controlled through several signalling proteins which increase or decrease the level of cytoplasmic Ca^{2+}, a balance which establishes the resting cellular Ca^{2+} levels (Bootman et al. 2001).

The release of sequestered Ca^{2+} from intracellular stores or the influx of Ca^{2+} ions through integral plasma membrane Ca^{2+} channels both raise the intracellular Ca^{2+} concentration, which in turn triggers numerous Ca^{2+}-sensitive processes. In order to return cytosolic Ca^{2+} concentrations to resting levels and enable termination of the Ca^{2+}-initiated cellular event, the elevated intracellular free Ca^{2+} concentration must drop. Ca^{2+} is extruded from the cell by plasma membrane Ca^{2+} ATPases or exchangers, sequestered into intracellular stores by sarcoplasmic/endoplasmic reticulum Ca^{2+} ATPases (SERCA), or taken up into the mitochondria by the mitochondrial uniporter (Berridge et al. 2000).

1.1.2 Compartmentalisation of calcium signalling

Ca^{2+} governs a wide range of complex cellular functions by varying the localisation, amplitude and duration of a signal. The free diffusion of Ca^{2+} throughout the cell is controlled by cytoplasmic buffering, Ca^{2+} extrusion and store uptake by proteins and organelles within the cell. Therefore, Ca^{2+} signals must enter the cell close to its target protein or travel across the cell via the process of signal propagation. Ca^{2+} is stored within the endoplasmic reticulum (ER) of cells, or equivalent organelle in myocytes, the sarcoplasmic reticulum (SR). The release of Ca^{2+} from the SR stores in myocytes occurs

predominantly through ryanodine receptors (RyRs) on the junctional SR membranes and is an example of signal compartmentalisation (Berridge et al. 2000; Bootman et al. 2001).

Activation of a single RyR channel results in a localised, nanoscopic Ca^{2+} release event (~30 nM), that spreads to a distance of approximately 2 μm and is termed a Ca^{2+} "quark" (Lipp and Niggli 1996; Niggli and Shirokova 2007). The activation of several neighbouring RyR channels in a cluster produces a Ca^{2+} spark (Cheng et al. 1993). Historically, estimates of the number of RyR2 channels involved in the generation of a calcium spark varied widely, from a single channel to over 100 channels (Cheng et al. 1993; Franzini-Armstrong et al. 1999). Current estimates indicate that a typical calcium spark is generated by the concurrent opening of one to five RyR2 channels in a cluster (Hou et al. 2023a) and result in greater increase in localised Ca^{2+} levels (~100-300 nM) and spreads for no more than 6 μm and typically lasts ~10-100 ms (Song et al. 2016). If several Ca^{2+} sparks occur in close proximity simultaneously, this could result in the propagation of a Ca^{2+} wave that spreads rapidly throughout the cell (Cheng et al. 1993) (see **Figure 1.1**). Waves can move between cells to create an intercellular wave when gap junctions are present (Berridge et al. 2000). The propagation and degeneration of these elementary Ca^{2+} release events are dependent on the buffering ability of the proteins and organelles met by the Ca^{2+} signal (Bootman et al. 2001).

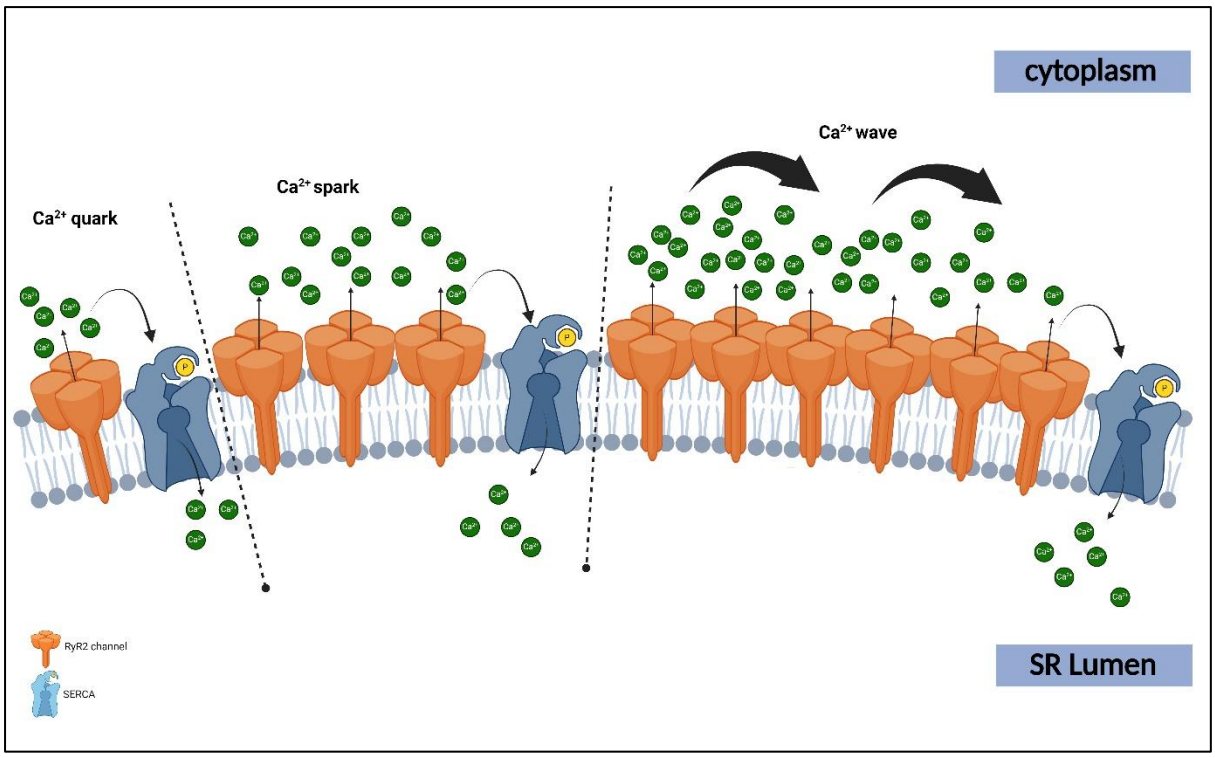

Figure 1.1. Elementary Ca^{2+} release events from the SR store. Ca^{2+} is released from the SR through RyR2 channels, and is sequestered back into the SR lumen through SERCA pumps. Activation of a single RyR2 channel results in nanoscopic, localized Ca^{2+} release event termed "quark". Activation of a cluster of neighbouring RyR2 channels produces a Ca^{2+} spark. Sequential activation of neighbouring RyR2 channels leads to the formation of a Ca^{2+} wave that can spread rapidly throughout the cell, and from one cell to the other through gap junctions. Created with BioRender.com.

1.2 Calcium signalling in the heart

1.2.1 Cardiac muscle structure and mechanism of contraction

The myocardium is predominantly composed of cardiac myocytes whose highly specialised structure enables their contraction, making them fundamental to heart function. A ventricular myocyte is normally cylindrical in shape, measuring 50-100 µm in length and 10-20 µm in diameter. These cells are bound together longitudinally, *i.e.*, end-to-end, by intercalated discs, allowing for electrical and mechanical communication between cells (Shimada et al. 2004; Cerrone et al. 2017b).

The sarcolemma, which is a lipid bilayer that forms the outer layer of the cardiac myocyte, houses numerous channels and receptors that allow selective ion transport in and out of the myocyte. Invaginations of the sarcolemma form transverse tubule

structures (t-tubules) that penetrate into the intracellular space of myocytes and form tight connections with the SR. This means that the L-type Ca^{2+} channels (LTCC), located on the sarcolemma, and the cardiac ryanodine receptors (RyR2), present on the SR membrane, are in close proximity. T-tubules are approximately 100-300 nm in diameter and occur every 1.8 μm along the axis of every myocyte (Walker and Spinale 1999; Song et al. 2005).

The sarcomere, the myocyte contractile apparatus, is made up of titin and repeating units of "thin" actin and "thick" myosin filaments, and each individual myocyte is filled with these highly ordered arrays of myofilament proteins. The Z-line marks the boundary of the sarcomere, giving it mechanical stability, and connects neighbouring sarcomeres together, allowing for force transmission (Frank & Frey, 2011). Thin filaments primarily consist of actin, tropomyosin and troponin complex (troponin T, I and C), while thick filaments are composed of myosin and accessory proteins (Gautel and Djinović-Carugo 2016). The interaction between these filaments and proteins is the driver of myocyte contraction (see **Figure 1.2**).

When the cardiac myocyte is relaxed during diastole (at intracellular Ca^{2+} concentration <100 nM), tropomyosin is wrapped around the actin filament, blocking the myosin binding site and preventing the interaction between thin and thick filaments. During systole, an action potential (AP) triggers a rapid increase in intracellular Ca^{2+} concentration (~1 μM), which binds to and causes a conformational change in troponin C, exposing the myosin binding site on the actin filaments. Cross-bridge formation between myosin heads and actin active sites is induced by the hydrolysis of adenosine triphosphate (ATP) by ATPase on myosin, which is no longer blocked by troponin I. The release of adenosine diphosphate (ADP) from the myosin heads causes a change in the angle of the cross-bridge, and causes myosin filaments to slide past the actin filaments, shortening the sarcomere and resulting in muscle contraction. Subsequent extrusion of Ca^{2+} from the myocytes dissociate Ca^{2+} from troponin C, which allows myofilaments to return to their resting positions and myocyte relaxation occurs (Gautel and Djinović-Carugo 2016). The process by which an AP triggers cyclical release and re-sequestration of Ca^{2+} in the SR and results in the contraction and relaxation of myocytes is termed

excitation-contraction coupling (ECC) (see **Section 1.2.3**) (Bers 2002).

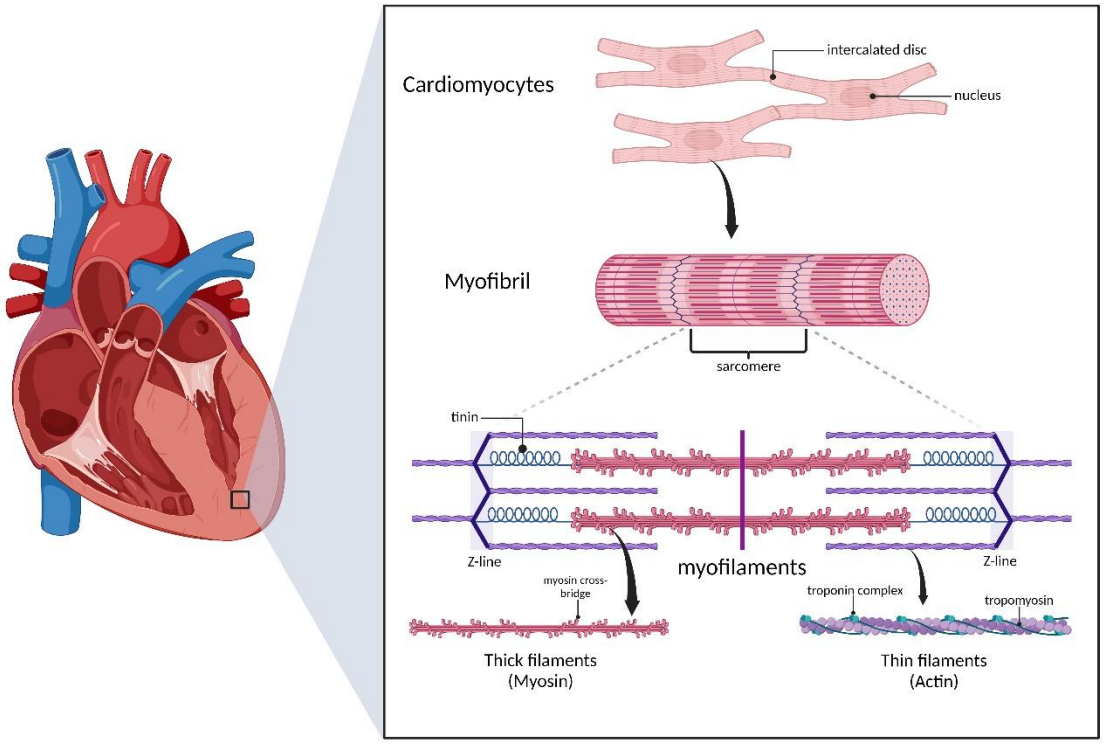

Figure 1.2. Cardiac muscle structure. Cardiac myocytes form muscle fibres, connected by intercalated discs. Each myocyte consists of sarcomeres, the contractile apparatus of the cell, which is made up of titin and repeating units of actin and myosin filaments. The interaction between these filaments is the driver of myocyte contraction. Created with BioRender.com.

1.2.2 The cardiac action potential

An electrical impulse known as the cardiac AP is the origin of ECC. Channels and transporter proteins, which allow positively or negatively charged ions to enter or exit cells, mediate the delicate balance of polarising and depolarising ionic currents that create cardiac excitability. The primary initiator of AP in the heart are the sinoatrial node (SAN) cells located in the right atrium. The AP transmission from cell to cell is mediated by current flow through gap junction channels located in the intercalated discs (Van Veen et al. 2001). The AP in cardiac cells can be divided into five distinct phases, each marked by different ion movements (see **Figure 1.3**):

- Phase 4 - resting potential

This phase represents a cardiac myocyte under diastolic conditions, exhibiting a resting membrane potential (E_m) of -85 mV. This is produced by the selective permeability of the membrane to potassium ions (K^+) and the K^+ concentration gradient across the cell membrane.

- Phase 0 – depolarisation

  A voltage-dependent activation of fast inward sodium ion (Na^+) currents, coupled with decreased membrane permeability to K^+, resulting in a rapid depolarisation to approximately +40 mV, and is presented by the sharp upstroke in AP.

- Phase 1 – initial repolarisation

  A decrease in Na^+ permeability and the Efflux of K^+ and Cl^- ions from the cell causes partial repolarisation and the membrane potential slightly decreases.

- Phase 2 – plateau

  Membrane permeability to Ca^{2+} through LTCCs increases during this phase, balancing the outward K^+ current, thus maintaining depolarisation and extending the AP. Toward the end of phase 2, membrane permeability to Ca^{2+} somewhat reduces, and an inward Na^+ current partially maintains the plateau.

- Phase 3 – repolarisation

  RyR2-mediated Ca^{2+} release stops the inward Ca^{2+} current, SERCA2a (the cardiac isoform of SERCA) replenishes the SR Ca^{2+} store, and the outward K^+ channels remain open, allowing K^+ ions, and therefore positive charge, to be extruded from the cell until a resting potential of -85 mV is reached again.

The duration of the cardiac AP is roughly 300 ms. The cell is completely refractory to further stimulation during this period, *i.e.*, until repolarisation is almost finished, no more APs will be produced. This refractory period is vital in protecting against arrhythmia occurring (Bers 2002; Pinnell et al. 2007).

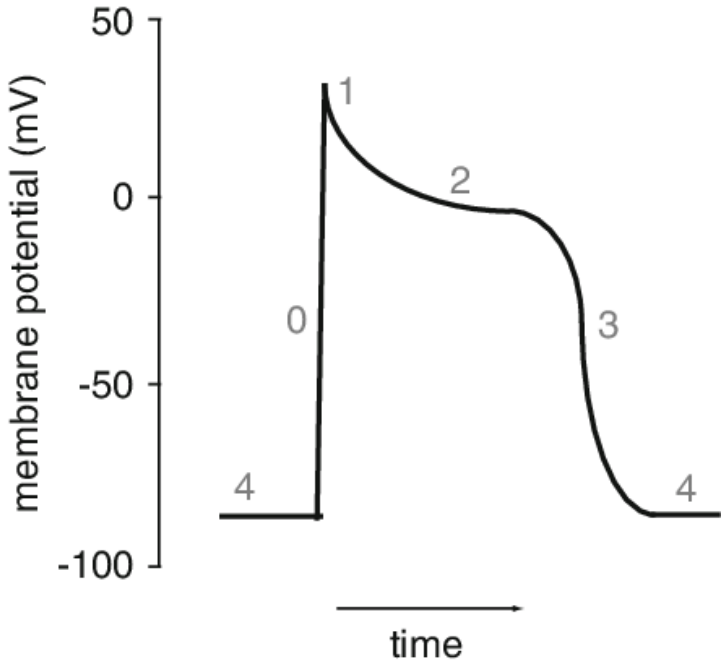

Figure 1.3. The cardiac action potential. Phase 0: depolarisation, phase 1: initial repolarisation, phase 2: plateau due to delay in repolarisation, phase 3: repolarisation, phase 4: resting potential. Figure adapted from Kaestner et al. (2012).

1.2.3 Excitation- contraction coupling

ECC is the process whereby an AP (electrical stimulation) is converted into a contractile force (Fearnley et al. 2011; Landstrom et al. 2017). As previously described in **Section 1.2.2**, the AP induces Ca^{2+} influx through LTCCs situated in the sarcolemma and in the t-tubules. The entry of Ca^{2+} through LTCCs increases Ca^{2+} concentration in the dyadic space; the space between the t-tubules and the SR. This small increase in Ca^{2+} concentration (200-400 μM) is sufficient to stimulate the opening of the RyR2 Ca^{2+} release channels, situated in the SR membrane, allowing even more Ca^{2+} to be released from the SR into the cytosol. This process is termed calcium-induced calcium release (CICR). The increased availability of intracellular Ca^{2+} causes activation of the contractile machinery in the myocytes and results in myocyte contraction (as outlined in **Section 1.2.1**). For myocytes to relax following a contraction, Ca^{2+} must be removed from the cytosol. This is achieved by pumping Ca^{2+} from the cytosol into the lumen of the SR through SERCA2a transporter, and by moving Ca^{2+} out of the cell via Na^{+}-Ca^{2+} exchanger (NCX) and plasmalemmal Ca^{2+} ATPase (PMCA). Additionally, Ca^{2+} is returned to the

mitochondria via the mitochondrial Ca^{2+} uniporter (see **Figure 1.4**) (Bers 2002; Eisner et al. 2017; Landstrom et al. 2017).

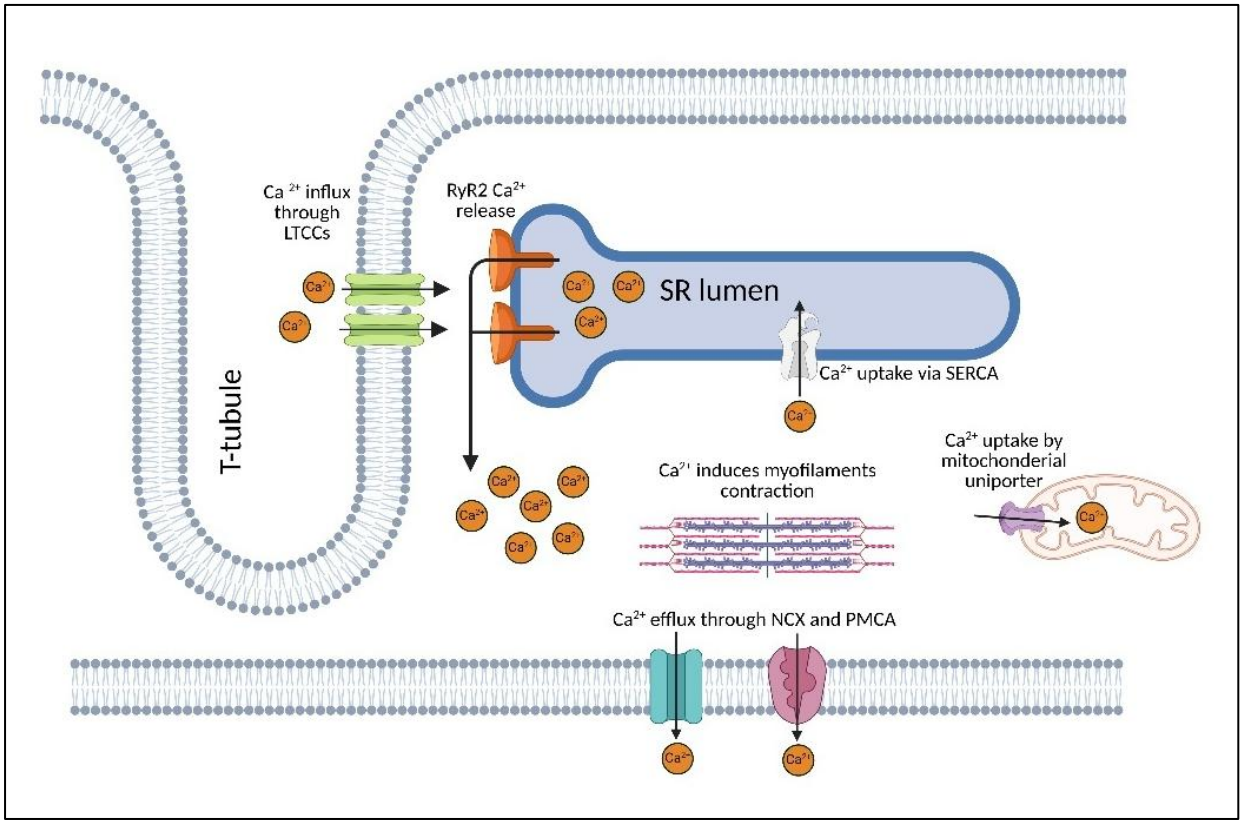

Figure 1.4. Excitation-contraction coupling within a ventricular myocyte. Upon membrane depolarisation, Ca^{2+} influx through LTCCs induces RyR2 channels to release Ca^{2+} from the SR store. High cytosolic Ca^{2+} initiates myofilaments contraction. During relaxation, Ca^{2+} is sequestered in the SR via SERCA2a, pumped out of the cell through NCX and PMCA and taken up by the mitochondria via the uniporter. Created with BioRender.com.

1.2.4 β-adrenergic stimulation of the cardiac myocyte

During periods of high metabolic demand, *i.e.*, physical or emotional stress, sympathetic stimulation of the heart through the β-adrenergic pathway is critical in order to increase cardiac output. When β-adrenergic receptors are stimulated by catecholamines such as adrenaline, this leads to increased production of cyclic adenosine monophosphate (cAMP), which in turn triggers SAN cells to depolarise faster. This accelerates heart rate (chronotropy). cAMP also activates protein kinase A (PKA) and increases PKA-mediated phosphorylation of several proteins involved in ECC. Phosphorylation of LTCCs by PKA increases Ca^{2+} influx into the cell. Additionally, PKA-mediated phosphorylation of RyR2 increases Ca^{2+} release from the SR. Ca^{2+} /calmodulin-dependent protein kinase II

(CaMKII) is also activated by β-adrenergic pathway which in turn phosphorylates RyR2, increasing the channel's open probability (P_o) and thus increasing cytosolic Ca^{2+} (Wehrens 2011; Uchinoumi et al. 2016) (see **Section 1.4.2.2**). A positive inotropic effect is produced by this elevated cytosolic Ca^{2+} concentration, meaning that more Ca^{2+} ions are accessible to bind to the contractile machinery in myocytes, accelerating the formation of actin-myosin cross bridges and, consequently, increasing contractile force.

During β-adrenergic activation of the heart, PKA phosphorylation also accelerates myocyte relaxation (lusitropy) through phosphorylation of phospholamban (PLB), an inhibitor of SERCA2a, whose phosphorylation relieves its inhibitory effect on SERCA2a, increasing SR Ca^{2+} uptake and enhancing myocyte relaxation. PKA phosphorylation of troponin I also decreases myofilaments Ca^{2+} sensitivity and increases the rate of Ca^{2+} dissociation from troponin C which leads to faster relaxation (Kentish et al. 2001). PKA also mediates phosphorylation of phospholemman (PLM), a protein that associates with and inhibits Na^+/K^+-ATPase, reducing its affinity for internal Na^+. Once phosphorylated, PLM's inhibition is relieved, increasing Na^+ extrusion and K^+ influx, which contributes to faster cardiac relaxation (Despa et al. 2005; Han et al. 2010).

PKA has been shown to phosphorylate NCX, but the functional regulation of PKA on NCX is still debatable, with some reports of no alteration (Fan et al. 1996; Ginsburg and Bers 2005; Lin et al. 2006), and others showing upregulation (Han and Ferrier 1995; Linck et al. 1998; Perchenet et al. 2000; Ruknudin et al. 2000; Zhang et al. 2001).

In summary, cAMP's lusitropic effect occurs concurrently with its inotropic effect, and the interplay between them increases heart muscle contractility while allowing the ventricles to fill, which culminate to increased cardiac output to meet the demand.

1.3 RyR2 as an ion channel

RyR channels are large transmembrane Ca^{2+} release channels located on the ER/SR membrane that regulate Ca^{2+} release during Ca^{2+} signalling events, such as ECC. The channels were named after the plant alkaloid ryanodine, which was shown to have a

paralytic action on both skeletal and cardiac muscles by inhibiting Ca^{2+} release from the ER/SR by binding to high molecular weight channels located on the SR membrane (Sutko and Kenyon 1983; Fabiato 1985); later purified and named RyR channels (Inui et al. 1987). There are three identified isoforms of ryanodine receptors. RyR2 is predominantly expressed in the heart muscle, although also found in the brain, and in low levels in the stomach, kidney, adrenal glands, ovaries and lungs (Nakai et al. 1990; Otsus et al. 1990; Lanner et al. 2010), RyR1 is mainly found in skeletal muscle cells (Takeshima et al. 1989; Zorzato et al. 1990) and RyR3 is found in low levels in several other tissues including brain tissues and smooth muscle tissues (Furuichi et al. 1994; Ledbetters et al. 1994). The three RyR isoforms are encoded by three different genes, and exhibit ~70% gene homology among them (Zalk et al. 2007). Although the three isoforms are tissue-specific, they all function as high-conductance, Ca^{2+} release channels, regulated by various ligands, such as Ca^{2+}, ATP and caffeine, with different degree of sensitivity.

Experimental work by Takeshima et al. (1994) with RyR-deficient mice highlighted the developmental importance of RyR expression. RyR1-deficient mice showed aberrant skeletal and muscular development as well as respiratory failure (Takeshima et al. 1994), whereas RyR2 knockout mice died around embryonic day 10 with heart tube abnormalities (Takeshima et al. 1998). Despite having normal muscle function and development, RyR3-deficient animals showed increased locomotor activity, which may indicate altered neural function (Takeshima et al. 1996).

The work presented in this thesis was conducted solely on the cardiac RyR isoform, RyR2. The remainder of this Introduction focuses on the structure and function of RyR2.

1.3.1 RyR2 channel structure

RyR2 protein has a large homotetrameric structure (~2.2 MDa), with each subunit consisting of around 5,000 amino acids (Otsu et al. 1993; Tunwell et al. 1996; Lanner et al. 2010). The cytoplasmic view of the channel shows a distinctive square appearance. Around 80% of the total protein structure lies in the cytoplasmic region, and a smaller part of the channel occupies the transmembrane region.It has been challenging to

separate sufficient amounts of pure, structurally intact RyR2 channels from the cardiac muscle for cryogenic electron microscopy (cryo-EM) characterisation of RyR2 channels until 2016 when Peng et al. determined the structure of porcine RyR2 stabilised in 3-[(3-cholamidopropyl) dimethylammonio]-1-propanesulfonate (CHAPS) using cryo-EM at the near-atomic resolutions of 4.2 Å and 4.4 Å in the open and closed state, respectively (see **Figure 1.5**).

The overall architecture and domain structure of RyR2 was found to be identical to that of RyR1, consistent with their 70% sequence homology (Peng et al. 2016). Each RyR2 monomer consists of a N-terminal domain which protrudes into the cytosol and are recognised as "foot-like" structures at the junction between terminal cisternae and the t-tubule network. The N-terminal domain provides an area for channel modulators and ligands interaction with the channel (Franzini-Armstrong et al. 1999; Peng et al. 2016). The smaller C-terminal transmembrane domain contains 6 transmembrane helices that form the pore for ion movement in the centre of the channel. A conformational change takes place upon channel activation which shifts the pore restriction site from I4868 (I4867 in human) in the closed state to Q4864 (Q4863 in human) in the open structure. The four Q4864 residues enclose a pore with ~4 Å diameter which allows Ca^{2+} to pass in a single file (Peng et al. 2016).

The Central domain of RyR2 is a cytoplasmic domain that interacts with the transmembrane domain and is thought to be the primary transducer of conformational changes (outward rotations of the cytosolic ends of S6 helices) that regulates channel opening and closing. The N-terminal domains, the Handle and Helical domains, and a second tier of transmitters encircle the Central domain, offering a framework for communication with several peripheral domains and channel modulators (Peng et al. 2016; Gong et al. 2021).

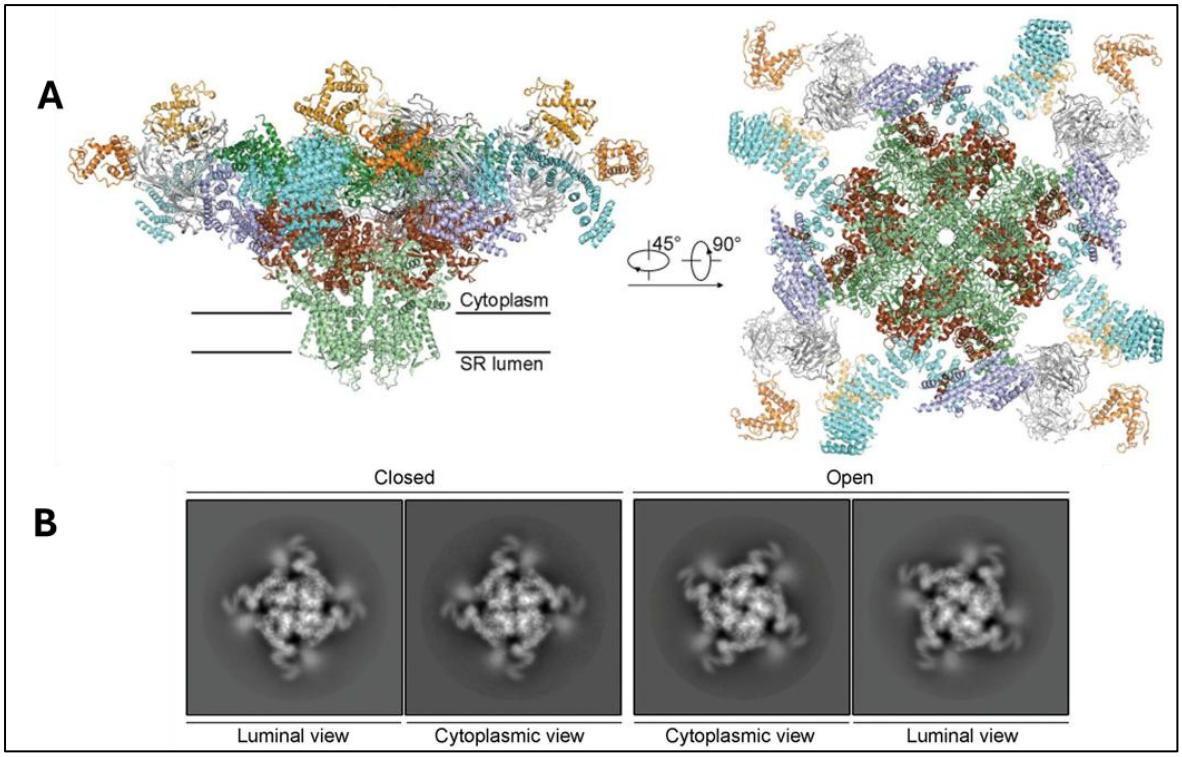

Figure 1.5. RyR2 structure (A) Shows structure of RyR2 homotetramer from porcine heart at 4.2 Å. Most of the channel structure lies in the cytoplasmic region and a smaller part occupies the transmembrane region. The cytoplasmic view of the channel shows a distinctive square appearance with the channel pore visible in the middle which allows Ca^{2+} ions to pass through. The structure is colour coded to indicate different sub-domains (the nature of which is not relevant to the context of this thesis). **(B)** Representative 2D averages of cryo-EM images of RyR2 in its open and closed state, showing the marked difference of the central pore. Figure adapted from Peng et al. (2016).

1.3.2 RyR2 channel regulation by endogenous modulators

A variety of physiological ligands regulate RyR2 channel function, including Ca^{2+} itself, magnesium (Mg^{2+}) and ATP. Some of these modulators of RyR2 are accessory proteins that associate to the channel and constitute the macromolecular complex. Other modulators regulate RyR2 function indirectly by altering the intracellular ionic environment. The functional effect of some of the relevant RyR2 channel regulators will be discussed in this section.

1.3.2.1 RyR2 regulation by cytosolic and luminal Ca^{2+}

Ca^{2+} is the most important regulator of RyR2 channel function. Nevertheless, there are many unanswered questions regarding the regulation of RyR2 by Ca^{2+}, and identifying the precise locations of Ca^{2+}-sensing/binding sites in the large RyR2 structure has been

difficult, but four Ca^{2+}-binding sites per monomer has been proposed by Laver (2007) as shown in **Figure 1.6**. Laver suggested one activating cytoplasmic-facing Ca^{2+}-binding site, termed the A-site and one luminal Ca^{2+} activating site, termed the L-site. A low-affinity inhibition site was also proposed called the I_1-site, which is also referred to as the Ca^{2+}/Mg^{2+} inhibition site because of its proposed inability to distinguish between these divalent cations. A second high-affinity inhibitory site termed the I_2-site was also predicted which causes partial channel inactivation upon binding Ca^{2+} (Laver 2007).

Single channel recording of human RyR2 (hRyR2) channels from explanted hearts of patients with end-stage heart failure (HF) revealed that when the luminal Ca^{2+} concentration was kept at 67 mM, increasing the cytosolic Ca^{2+} concentration from 1 to 100 µM dramatically increased the number of channel opening events (Holmberg and Williams 1989). Additionally, cytosolic Ca^{2+} increases the P_o of recombinant hRyR2 and RyR2 channels isolated from healthy human hearts (Mukherjee et al. 2012; Walweel et al. 2014). Mukherjee et al. (2012) showed that recombinant hRyR2 channels' P_o increased most at cytoplasmic Ca^{2+} concentrations between 100 nM-1 µM at 5 nM luminal Ca^{2+}, while channel P_o reached saturation levels when cytosolic Ca^{2+} concentration increased to over 10 µM.

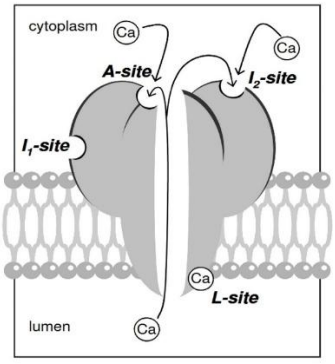

Site	Proposed effect	Ligand	Dissociation constant
A-site	Cytoplasmic activation	Ca^{2+}	1-10 µM
I_1-site	Cytoplasmic inhibition	Ca^{2+} and Mg^{2+}	10 mM
I_2-site	Cytoplasmic inactivation	Ca^{2+}	1 µM
L-site	Luminal activation	Ca^{2+}	60 µM

Figure 1.6. Schematic representation of proposed RyR2 Ca^{2+} binding sites. Figure adapted from Laver (2007). The precise positions of these binding sites are still unknown.

It was originally proposed that elevated intracellular cytosolic Ca^{2+} concentration terminates SR RyR2-mediated Ca^{2+} release via binding of Ca^{2+} to the cytosolic low-affinity inhibition site on RyR2. In the Laver model, this is termed the I_1 site. However, there is evidence that the termination of CICR is not significantly impacted by the inactivation of RyR2 by cytosolic Ca^{2+}, but rather by fall in SR luminal Ca^{2+} concentration. Multiple research groups have demonstrated that luminal Ca^{2+}-dependent deactivation caused RyR2 spark termination (Sitsapesan and Williams 1994; Györke and Györke 1998; Brochet et al. 2005; Terentyev et al. 2008; Zima et al. 2008). A number of hypotheses have been proposed to explain how luminal Ca^{2+} controls the activation and inactivation of RyR2 channels, although the exact mechanism is still debated. Some of these theories will be discussed below.

Ca^{2+} feed-through hypothesis

The hypothesis proposes that luminal Ca^{2+} can modulate the RyR2 channel by passing through the channel pore and binding to its cytoplasmic regulatory sites (A-, I_1- and I_2-sites) (Xu and Meissner 1998; Laver 2007). To support this hypothesis, Xu and Meissner (1998) reported that in the absence of cytoplasmic Ca^{2+} or other activating factors, *i.e.*, when the channel is closed, increasing luminal Ca^{2+} up to 10 mM did not cause channel activation (Xu and Meissner 1998).

Direct luminal Ca^{2+} activation

Some evidence suggests that distinct Ca^{2+}-binding sites on the luminal face of RyR2 channels act as Ca^{2+} sensors that regulate channel activity (Györke and Györke 1998; Laver 2007). In the Laver model, this site is termed the L-site. Györke and Györke (1998) showed that under conditions which prevented luminal-to-cytoplasmic Ca^{2+} flux, increasing luminal Ca^{2+} concentration increased channel P_o. Ching et al. (2000) also reported that trypsin digestion of the luminal side of RyR2 altered the channel activity in a way that an increase in luminal Ca^{2+} concentration no longer enhanced RyR2 P_o, but rather reduced the channel activity, suggesting the presence of a luminally located Ca^{2+} activation site (L-site) that was destroyed with trypsin digestion, and a luminal inactivation site (not shown on the Laver model) that remained intact following protease digestion.

Luminal-triggered Ca^{2+} feed through mechanism

This proposed mechanism incorporates both previously discussed activation mechanisms. It suggests that RyR2 is activated by Ca^{2+} binding to either cytoplasmic (A-site) or luminal (L-site) Ca^{2+} binding sites, and is inactivated by Ca^{2+} binding to inhibitory Ca^{2+} binding sites on the cytoplasmic side (I_1-and I_2-sites) (Laver 2007). According to this hypothesis, Ca^{2+} binding to the L-site results in brief channel openings that permit small amount of luminal-to-cytoplasmic Ca^{2+} flow, leading to localised increase in Ca^{2+} concentration at the A-site. Activating the A-site would increase channel P_o and increase SR Ca^{2+} release. Eventually, if Ca^{2+} release was high enough, the channel becomes inactivated by Ca^{2+} binding to I_1 - and I_2-sites (Laver 2007).

Luminal Ca^{2+} sensitised cytosolic Ca^{2+} activation

This model suggests that increasing luminal Ca^{2+} concentration renders the channel more sensitive to activation by cytoplasmic Ca^{2+} and leads to an increase in P_o (Qin et al. 2008).

Calsequestrin-dependent luminal Ca^{2+} activation

This model suggests that the RyR2 associated protein, calsequestrin (CASQ2), acts as a luminal Ca^{2+} sensor. When SR Ca^{2+} content increases, CASQ2 senses that increase and undergoes a conformational change and dissociates from RyR2, relieving its inhibitory effect. As SR luminal Ca^{2+} decreases, CASQ2 exerts an inhibitory effect on RyR2, reducing channel P_o (Györke et al. 2009).

1.3.2.2 RyR2 regulation by Mg^{2+} and ATP

Mg^{2+} has a multifaceted effect on RyR2 channels. It is primarily known for its inhibitory action on RyR2 channel activity in the millimolar concentration range (reducing channel P_o) at low cytosolic Ca^{2+} concentrations; indicating that Mg^{2+} exhibits its physiological effect during diastole (Rousseau et al. 1987; Holmberg and Williams 1989; Rousseau and Meissner 1989). It is suggested that Mg^{2+} competes with Ca^{2+} at the low-affinity Ca^{2+} inhibition I_1-site (Györke and Györke 1998; Laver 2007). Additionally, Laver proposed that Mg^{2+} may also occupy the A- and L- activation sites on RyR2 during diastole when SR Ca^{2+} content is depleted, reducing RyR2 activation. Once Ca^{2+} is sequestered back into the SR

and luminal Ca^{2+} concentration increases, Laver proposed that Ca^{2+} displaces Mg^{2+} at the L-site, reducing inhibition and allowing RyR2 channel activation at the A-site (Laver 2010). Mg^{2+} has also been shown to increase RyR2 channel activation at intermediate cytosolic Ca^{2+} concentrations of ~10-100 µM. However, this was only seen in rabbit RyR2 which does not exhibit typical biphasic Ca^{2+}-dependence of activation/inactivation (Chugun et al. 2007).

At millimolar levels, ATP binds to and activates RyR2 channels, enhancing channel P_o, but only in the presence of cytosolic Ca^{2+}. ATP activates RyR2 by stabilising the open conformational state of the channel, increasing the frequency and duration of openings. Additionally, ATP is thought to activate RyR2 by sensitising the channel to activation by Ca^{2+} rather than directly activating the channel (Witcher et al. 1991; Xu et al. 1996; Kermode et al. 1998; Laver 2007). Adenosine monophosphate (AMP) and ADP, which are by-products of ATP hydrolysis, can also increase RyR2 Ca^{2+} release, though they seem to be less efficient (Kermode et al. 1998).

1.3.2.3 RyR2 regulation by accessory and associate proteins

The cytoplasmic assembly of RyR2 channels acts as a scaffold for many regulatory proteins. While most RyR2 regulators act on the cytoplasmic region, other RyR2 regulators act as luminal accessory proteins. Accessory and associated proteins of the RyR2 macromolecule complex will be described below (see **Figure 1.7**).

<u>Regulation by CASQ2, junctin and triadin</u>

CASQ2, an RyR2 associated protein, plays a crucial role in RyR2 channel regulation. This 42 kDa protein serves as a high-capacity, low-affinity Ca^{2+} buffering protein that traps Ca^{2+} within the SR (~50 per monomer), ensuring that Ca^{2+} is readily available at the pore during CICR (Kim et al. 2007). CASQ2 has also been proposed as the SR luminal Ca^{2+} sensor in cardiac muscle cells (see **Section 1.3.2.1**). At low luminal Ca^{2+} concentration, CASQ2 exists as organised aggregates (monomers and dimers), and as long polymers at high concentrations (Beard et al. 2005; Kim et al. 2007). When SR Ca^{2+} concentration is low, CASQ2 binds to junctin and triadin (26 kDa and 32 kDa proteins bound to the luminal side of RyR2), and presumably form a quaternary complex with RyR2 that anchors CASQ2

near the channel and inhibits Ca^{2+} release, allowing efficient SR Ca^{2+} refill (Zhang et al. 1997). At high luminal Ca^{2+} concentration, CASQ2 undergoes a conformational change as its Ca^{2+}-binding sites become occupied, and subsequently dissociate from the quaternary complex, relieving the inhibitory effect on RyR2 and allowing SR Ca^{2+} release (Zhang et al. 1997; Kim et al. 2007).

Regulation by FKBP12 and FKBP12.6

FK506-binding proteins (FKBPs) are accessory proteins that directly interact with the cytoplasmic assembly of RyR2. FKBPs are also known as immunophilins due to their interactions with the immunosuppressant drugs FK506 and rapamycin (Timerman et al. 1996; Zissimopoulos and Lai 2005). There is a single FKBP binding site on each RyR2 subunit, *i.e.*, RyR2 binds FKBP in a 1:4 stoichiometry (Timerman et al. 1996; Jeyakumar et al. 2001). There are two isoforms of FKBPs detected in cardiac myocytes, FKBP12 and FKBP12.6 (also known as calstabin and calstabin2), named after their molecular weight (12 and 12.6 kDa respectively) (Timerman et al. 1996; Guo et al. 2010).

Evidence has shown that although FKBP12 is more abundant in cardiac myocytes than FKBP12.6 (Timerman et al. 1996), it may not be relevant to the function of RyR2 as it was not shown to affect RyR2 Ca^{2+} spark frequency (Guo et al. 2010) or alter recombinant RyR2 in systems of heterologous expression (George et al. 2003b; Goonasekera et al. 2005). A recent study by Galfré et al. (2012) suggested that FKBP12 activates RyR2 channels and its effect is antagonised by FKBP12.6. FKBP12.6, on the other hand, has ~600-1000 fold increased affinity for RyR2 binding compared to FKBP12 (Timerman et al. 1996; Guo et al. 2010). The effect of FKBP12.6 on RyR2 function is controversial, with some reports showing that FKBP12.6 stabilises the closed state of the channel, thus preventing diastolic Ca^{2+} leak (Brillantes et al. 1994; Marx et al. 2000; Prestle et al. 2001; George et al. 2003b; Wehrens et al. 2003). Supporting this idea, single RyR2 channels from FKBP12.6-knockout mice and wildtype (WT) channels treated with drugs that suppressed FKBP12.6:RyR2 interaction showed an increase in P_o and exhibited a number of sub-conductance states (Wehrens et al. 2003). Additionally, FKBP12.6 overexpression in mice reduced Ca^{2+} spark frequency and enhanced cardiac output (Prestle et al. 2001; Huang et al. 2006; Gellen et al. 2008). Other reports, however, suggest that FKBP12.6

does not affect RyR2 channel biophysical properties or spontaneous Ca^{2+} release events in FKBP12.6-deficient mouse models compared to WT (Xiao et al. 2007). Another study by Timerman et al. (1996) also demonstrated that FKBP12.6 does not affect RyR2 channel function and P_o. It has been hypothesised that the relationship between FKBP12.6 and RyR2 is dependent on RyR2 phosphorylation status. This will be discussed further in **Section 1.5**.

Regulation by calmodulin and EF-hand proteins

Calmodulin (CaM) is a relatively small (17 kDa) Ca^{2+}-binding protein that influences RyR2 through direct binding or indirectly by activating CaMKII, upregulating channel phosphorylation (Sorensen et al. 2013a; Walweel et al. 2017). Four CaM molecules bind to each RyR2 channel, one for each monomer. RyR2 can bind to CaM in both its Ca^{2+}-free (Apo-CaM) and Ca^{2+}-bound (CaCaM) states at overlapping sites known as the CaM binding domain (CaMBD). Binding of CaCaM to RyR2 at cytosolic Ca^{2+} concentrations above 1 μM reduces the open probability of the channel, and thus reduces Ca^{2+} release from the SR. Apo-CaM binding to RyR2 also inhibits SR release of Ca^{2+} by stabilising the closed conformation of the channel at lower cytosolic Ca^{2+} concentrations (Balshaw et al. 2001; Fruen et al. 2003; Sorensen et al. 2013a; Walweel et al. 2017). Therefore, CaM inhibition of RyR2 could be largely Ca^{2+}-independent (Badone et al. 2018). CaM regulation of RyR2 will be discussed in more detail in **Section 1.4.2**.

Sorcin, a 22 kDa EF hand-containing Ca^{2+} binding protein, directly interacts with RyR2 channels. Although its precise role is yet to be established, sorcin is thought to act in a similar way to CaM, inhibiting RyR2 channel function over a wide range of Ca^{2+} concentrations (Lokuta et al. 1997; Meyers et al. 1998; Valdivia 1998; Farrell et al. 2003). Sorcin was also shown to inhibit CaMKII activity, while CaMKII has been shown to phosphorylate sorcin, indicating a collaborative regulation of RyR2 activity (Anthony et al. 2007).

S100A1 is another EF-hand containing protein that has not been well studied. It is a 21 kDa accessory protein that has been shown to enhance RyR2 channel's P_o (Prosser et al. 2011). S100A1 binds RyR2 at the same site as CaM, so it was originally proposed that S100A1's regulation of RyR2 involves direct competition with CaM at the CaMBD (Prosser

et al. 2008; Wright et al. 2008). However, a recent study by Rebbeck et al. (2016) suggested that S100A1 and CaM can concurrently bind to RyR2 and regulate its function, but this does not involve direct competition at the CaMBD.

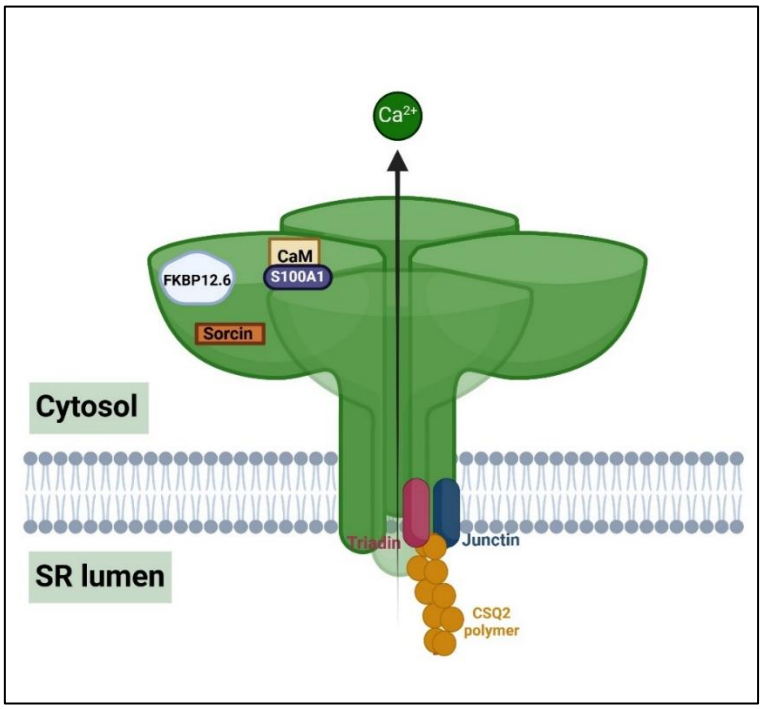

Figure 1.7. RyR2 macromolecule complex. Schematic presentation of RyR2 accessory and associate proteins. Proteins may not be constitutively bound to RyR2 as their interaction can be dependent on physiological conditions. Created with BioRender.com.

1.3.3 RyR2 channel organisation and coupled gating

RyR2 channels are assembled into clusters within the SR membrane known as Ca^{2+} release units (CRUs), and the propagation of an intracellular Ca^{2+} signal requires coordinated activation of neighbouring channels. Recent super-resolution studies reported means of 9-19 RyR2 channels per cluster in human and rat ventricular myocytes (Jayasinghe et al. 2018; Shen et al. 2019; Asghari et al. 2020).

The behaviour of RyR1 channels, which has been shown to form clusters by assembling into lattices with a regular "checkerboard" configuration, served as the basis for many of the original assumptions on RyR2 clustering properties (Yin and Lai 2000). However, it is now recognised that RyR2 channels are not uniformly organised but rather exist within

clusters with different channel density and topologies. Single and dual-tilt tomograms of human and rat cardiomyocytes have revealed that RyR2 tetramers can be seen in checkerboard, side-by-side or isolated configurations (see **Figure 1.8**). However, this arrangement is dynamic and can shift according to changes in the environment such as varying Mg^{2+} concentration and phosphorylation which could be due to interprotein allosteric interactions (Asghari et al. 2012; Asghari et al. 2014; Hiess et al. 2018; Asghari et al. 2020). The distance between RyR2 tetramers in a cluster varies between different configurations, with tetramers in a side-by-side configuration exhibiting closer spacing to one another (~31 nm) compared to checkerboard (~37 nm) and isolated configurations (~42 nm) (Asghari et al. 2014; Waddell et al. 2023).

RyR2s in a cluster are proposed to exhibit coupled gating, whereby neighbouring channels influence each other's activity and leading to synchronous opening and closing, a critical component of CICR. Coupled RyR2 channels were reported to exhibit longer open times under activating conditions in comparison to single RyR2 channels (Marx et al. 2001).

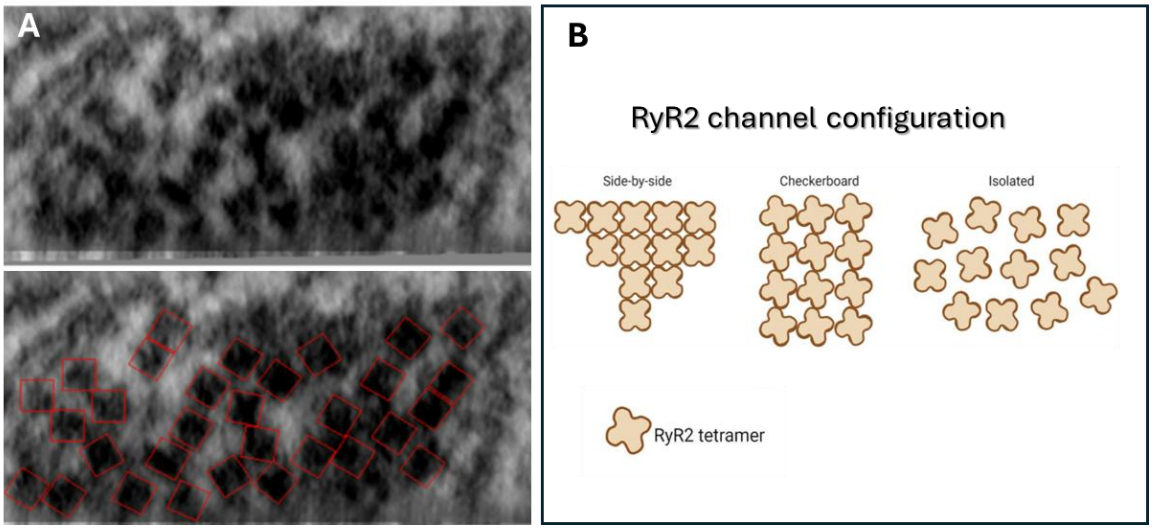

Figure 1.8. Example image of RyR2 cluster. (A) Figure show RyR2 channels distribution in rat cardiac cells fixed *in situ*. The arrangement is variable, and channels can be seen isolated, side-by-side or in checkerboard arrangement. Figure adapted from Asghari et al. (2014) **(B)** cartoon illustration of the different arrangements of RyR2 tetramers observed in clusters. Figure adapted from Waddell et al. (2023).

1.4 Calmodulin: A key regulator of calcium signalling

CaM is a highly conserved and ubiquitous Ca^{2+}-binding protein found in all eukaryotic cells (Brostrom and Wolff 1981), as well as many plants, fungi and protists species (Kuźnicki et al. 1979; Muthukumar et al. 1987; Zhu et al. 2015). This small protein consists of 148 amino acids (17 kDa) and plays a crucial role in Ca^{2+} signalling pathways, including muscle contraction, metabolism and apoptosis (Stevens 1983). CaM associates directly with RyR2 channels, as well as over 300 proteins and ion channels (Yap et al. 2000). CaM structure and regulation of RyR2 will be discussed in this section.

1.4.1 Calmodulin structure

In mammals, three paralogous, non-identical genes (*CALM1*, *CALM2* and *CALM3*) express the same CaM protein in response to various stimuli (Nojima and Sokabe 1986; Fischer et al. 1988; Pegues and Friedberg 1990; Toutenhoofd et al. 1998). In terms of structure, CaM consists of two globular domains, the N-lobe and the C-lobe, connected by a flexible central linker. Each lobe contains two EF-hand motifs capable of binding two Ca^{2+} ions with a micromolar-range binding affinity (see **Figure 1.9**). Ca^{2+}-binding domains in the C-terminal lobe have a 10-fold higher Ca^{2+} affinity (10^{-6} M) compared to those in the N-terminal lobe (10^{-5} M) (Black et al. 2000). Ca^{2+} binds to the two sites in the C-lobe first, followed by the two sites in the N-lobe, in a cooperative and sequential manner (Crouchl and Klee 1980). After binding Ca^{2+}, the EF-hand domains open, exposing the hydrophobic target-interacting pocket that can bind to different target proteins. In the absence of Ca^{2+}, the C-lobe is in a partially open conformation, providing limited access to the hydrophobic pocket, which may enable Apo-CaM binding to target proteins (Swindells and Ikura 1996).

Single-molecule fluorescence resonance energy transfer (FRET) studies have demonstrated the existence of at least three discrete conformations of CaCaM and Apo-CaM in solution. CaCaM favours a conformational change that is more compact, while Apo-CaM tends to favour a more extended conformation. This structural elasticity is thought to facilitate CaM's target recognition and interaction with numerous target proteins. Additionally, the compact state of CaCaM is thought to facilitate interdomain

communication, although the coupling mechanism is still unclear (Johnson 2006; Villarroel et al. 2014).

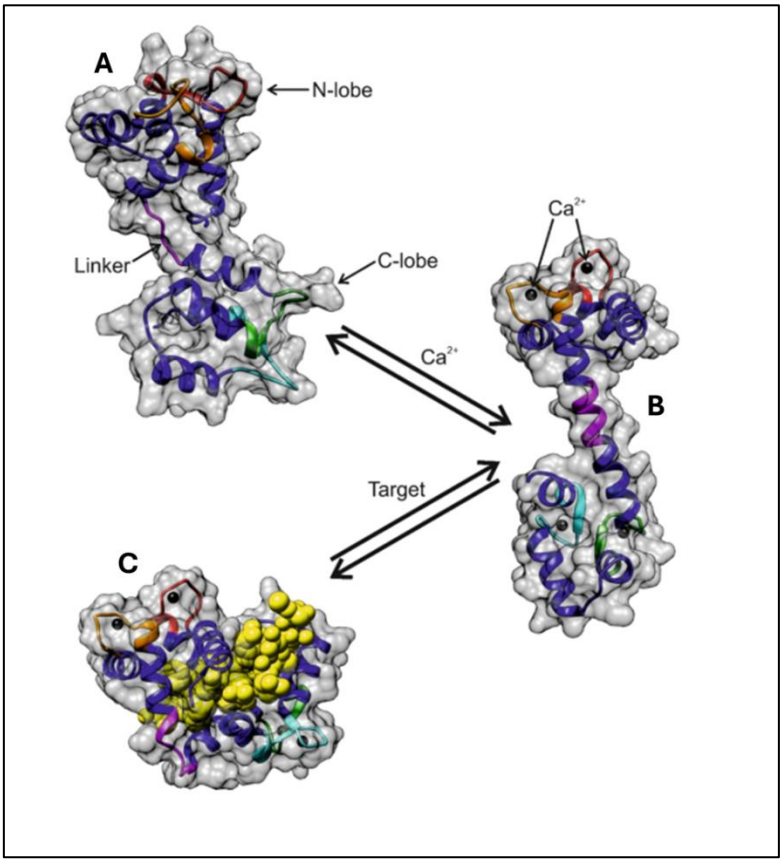

Figure 1.9. Molecular models of Apo-CaM and CaCaM structures. The figure shows Ca^{2+}-induces conformational change that enables CaM to bind to target proteins. Ca^{2+} binds to four binding sites (red, orange, green, cyan). **(A)** Figure shows the more extended conformation of Apo-CaM. **(B)** Figure demonstrates CaCaM; a more compact conformation. **(C)** Demonstrates an example of CaCaM binding and engulfing a target protein, *e.g.,* CaMKII peptide (yellow). Figure adapted from Calver (2019).

One CaM molecule binds to each RyR2 monomer, *i.e.*, four for each RyR2 channel. Both Apo-CaM and CaCaM bind to RyR2 at distinct but overlapping sites in the elongated cleft formed by the handle, helical and central domains, known as the CaMBD (Gong et al. 2019) (see **Figure 1.10**). The shift in CaMBD on RyR2 is controlled by Ca^{2+} binding to CaM, rather than to RyR2 (Gong et al. 2019).

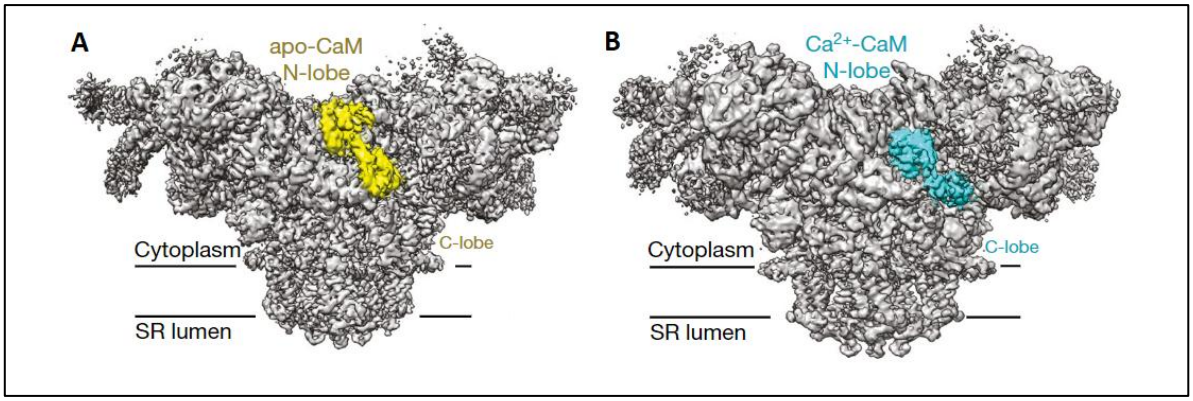

Figure 1.10. Cryo-EM structures of CaM binding to porcine RyR2. (A) shows RyR2-apoCaM complex (3.6 Å). **(B)** demonstrates RyR2- CaCaM complex (3.9 Å). Figure adapted from Gong et al. (2019).

1.4.2 Calmodulin regulation of RyR2 channels

CaM regulates RyR2 function through direct binding, or indirectly by virtue of CaM's regulation of its associated kinase: CaMKII, upregulating channel phosphorylation. Interestingly, CaM's modulation of RyR2 activity differs from that of other RyR isoforms, indicating that CaM has a distinct function in ECC regulation (Tripathy et al. 1995; Hamilton et al. 2000).

1.4.2.1 RyR2 regulation by direct CaM binding

Although CaM binding to target proteins often depends on its binding to Ca^{2+} (Zhang et al. 2012b), in the case of RyR2, CaM can bind in both its Ca^{2+}-free and Ca^{2+}-bound states (Balshaw et al. 2001). Both CaCaM and Apo-CaM inhibit RyR2 Ca^{2+} release from the SR by stabilising its closed state conformation and reducing the channel's P_o, suggesting that this inhibitory mechanism is Ca^{2+}-independent. However, CaM inhibition is more pronounced at high Ca^{2+} concentration (Balshaw et al. 2001; Fruen et al. 2003; Sorensen et al. 2013a; Walweel et al. 2017; Badone et al. 2018).

1.4.2.2 RyR2 regulation by CaMKII

CaMKII is a serine/threonine-specific protein kinase activated by CaCaM that plays a crucial role in various signalling cascades. Its regulation of RyR2 is essential for Ca^{2+} homeostasis in cardiomyocytes. CaMKII has four main isoforms expressed in humans that are derived from different genes (α, β, γ, and δ) (Tombes et al. 2003), with CaMKIIδ

being the most commonly expressed isoform in the heart (Hoch et al. 1999) and referred to here simply as CaMKII. CaMKII proteins form large oligomeric structures. The N-terminal catalytic domain is connected via an autoinhibitory or regulatory domain and a linker of various lengths to a C-terminal association domain, which arranges the kinase into ring-shaped hub that ties the subunits together (Chao et al. 2011; Myers et al. 2017). 3D single-particle EM images revealed that CaMKII assembles into a large dodecameric holoenzyme in most physiological conditions (Hoelz et al. 2003). This assembly takes the form of a pair of parallel hexameric rings (Rellos et al. 2010) (see **Figure 1.11A**).

In its inactive form, access to the catalytic domain of CaMKII is blocked by the autoinhibitory pseudo-substrate domain of the protein, *i.e.*, the tight association between the catalytic and regulatory domains results in autoinhibition of the kinase (Rosenberg et al. 2005; Chao et al. 2011; Myers et al. 2017). CaCaM binds to the regulatory segment with a K_D of 10-70 nM at elevated Ca^{2+} concentration (Gaertner et al. 2004). CaCaM binding to CaMKII induces a conformational change that removes the regulatory domain from the catalytic domain, exposing the catalytic site (Erickson et al. 2014), (see **Figure 1.11B**).

Prolonged CaCaM associated with CaMKII (when Ca^{2+} transients are long or have high frequency) triggers CaMKII autophosphorylation at T287 site (equivalent to T286 in CaMKIIα as shown in the figure), which is located in the regulatory domain (see **Figure 1.11C**) (Hanson et al. 1994; De Koninck and Schulman 1998; Erickson et al. 2014). The addition of phosphate group to the T287 site affects CaMKII function in two ways. Firstly, the negatively charged phosphate group prevents the reassociation of the catalytic and regulatory domains, preventing autoinhibition and generating kinase activity that continues even following CaCaM dissociation (Lai et al. 1987; Braun and Schulman 1995; Buard et al. 2010). Secondly, T287 phosphorylation also increases CaMKII's regulatory domain's affinity for CaCaM by between 10-1000 fold (Meyer et al. 1992; De Koninck and Schulman 1998). Conversely, under basal, non-stimulated conditions, autophosphorylation of T305 and T306 sites located in the CaCaM binding site of the regulatory segment prevents CaCaM binding and the full activation of CaMKII (Colbran and Soderling 1990; Hanson and Schulman 1992). CaMKII autophosphorylation in the

heart is particularly observed during β-adrenergic signalling (Grimm and Brown 2009; Erickson et al. 2011).

Under β-adrenergic stimulation, CaCaM-activated CaMKII phosphorylates RyR2 at the Serine 2814 (S2814) phosphorylation site (Wehrens et al. 2004), rendering the channel more sensitive to Ca2+-dependent activation and increasing channel Po and spark frequency (Guo et al. 2006a; Wehrens 2011; Respress et al. 2012). It is believed that CaMKII activation of RyR2 plays a crucial role in enhancing SR Ca^{2+} release in response to adrenergic stress, enhancing CICR and leading to stronger contractions and increased heart rate (Wu et al. 2009; Kushnir et al. 2010; Wehrens 2011) (see **Section 1.2.4**). Although adrenergic stimulation is the main mechanism of positive inotropy, under pathological conditions, it is also widely recognised to be an activator of undesired SR Ca2+ leak that contributes to heart disease, such as cardiac arrhythmia and HF (Anderson et al. 2011; Baier et al. 2021). More detailed information on RyR2 phosphorylation will be discussed in **Section 1.5**.

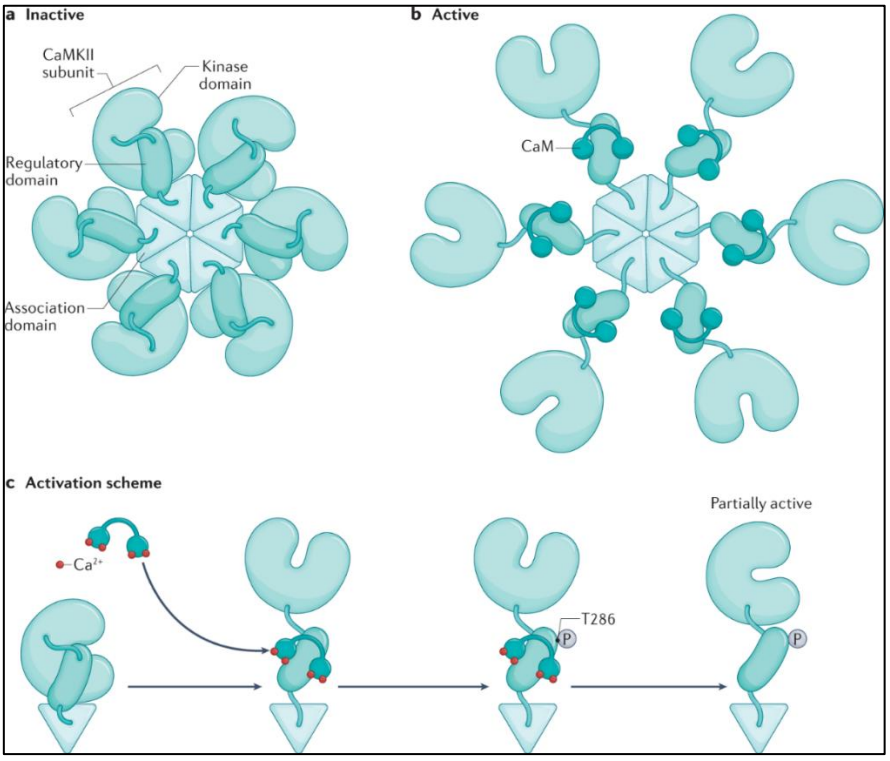

Figure 1.11. Structure of CaMKII holoenzyme. (A) Shows CaMKII structure in its inactive form, which consists of 12 subunits assembled as two hexameric rings stacked on top of each other with rotational and planar symmetry. Each subunit consists of a kinase domain, regulatory domain and am association domain. **(B)** Shows activated CaMKII upon CaCaM binding. The induced conformational change dissociates the regulatory domain from the kinase domain, exposing the catalytic site. **(C)** Shows CaMKII

autophosphorylation of T286 (equivalent to T287 in CaMKIIδ) following CaCaM binding. Figure adapted from Yasuda et al. (2022).

1.5 Phosphorylation as a post-translational modification of RyR2

Post-translational modifications refer to the chemical changes made to proteins, which play a crucial role in regulating channel function. One example of post-translational modifications to RyR2 is ubiquitination where a ubiquitin group covalently attaches to the RyR2 protein and promote its degradation (Pedrozo et al. 2010). The ubiquitin-conjugating enzyme UBE2C was found to act as the primary driver for the ubiquitination and degradation of the RYR2 protein in breast cancer cells (Zhai et al. 2022). The RyR2 protein is also very susceptible to redox, which is another important post-translational modifier of its function. Reversible oxidation of RyR2 was found to increase the P_o of the channel and enhance Ca^{2+} release, while reduction decreased channel P_o (Marengo et al. 1998; Xu et al. 1998; Sun et al. 2008). Severe oxidative stress was also linked to diastolic Ca^{2+} leak through RyR2 due to irreversible channel activation (Xu et al. 1998). The major type of post-translational modification affecting RyR2 is phosphorylation, which will be discussed in detail in this section.

As outlined in **Section 1.2.4**, β-adrenergic stimulation of the heart, as part of the fight-or-flight response, leads to phosphorylation of multiple ECC target proteins, including RyR2 channels, by kinases. This, in turn, leads to upregulation of channel activity, increasing heart rate and myocytes contraction in order to meet the metabolic demand of the body (Bers 2002; Eschenhagen 2010; Terentyev and Hamilton 2016).

1.5.1 Effects of protein kinases on RyR2

Experimental evidence has shown that RyR2 could be phosphorylated by multiple serine/threonine kinases including PKA, protein kinase C (PKC), protein kinase G (PKG) and CaMKII (Takasago et al. 1989; Takasago et al. 1991). PKA is a major kinase that consists of a regulatory subunit that traps the catalytic subunit and renders it inactive. Once activated by cAMP following β-adrenergic stimulation, the catalytic subunit of PKA dissociates, ready to phosphorylate target ECC proteins (as described in **Section 1.2.4**)

(Knighton et al. 1991b; Knighton et al. 1991a; Cheng et al. 2001; Johnson et al. 2001). The effects of PKA phosphorylation on RyR2 function in health and disease is controversial. This will be discussed further in **Section 1.5.2**. CaMKII is another kinase that phosphorylates multiple ECC proteins in cardiomyocytes in response to CaCaM activation, including LTCCs, PLB and RyR2 (the latter was discussed in **Section 1.4.2.2)**.

PKC and PKG have also been shown to phosphorylate RyR2, primarily at the Serine 2808 (S2808) site. Takasago et al. (1991) reported that PKC-treated RyR2 channels enhance [^{3}H] ryanodine binding, suggesting an increase in P_o. Additionally, The PKCα isoform phosphorylates many other proteins involved in ECC and muscle contraction, including LTCCs and troponin (Sumandea et al. 2003; Yang et al. 2005; Hidalgo et al. 2009; Kooij et al. 2013). PKG, on the other hand, is activated via parasympathetic muscarinic stimulation. PKG phosphorylates RyR2 at the S2808 site in a nitric oxide (NO)-dependent manner facilitating systolic SR Ca^{2+} release, particularly when the SR Ca^{2+} content is low. Concurrently, muscarinic stimulation of the heart was also shown to promote a reciprocal dephosphorylation of RyR2 at S2814 site, thereby inhibiting aberrant SR Ca^{2+} leak (Ho et al. 2016; Baine et al. 2020).

The exchange protein activated by cAMP (Epac) is another kinase known to influence RyR2 function. As the name suggests, Epac is directly activated by cAMP during β-adrenergic stimulation, and is thought to enhance RyR2 activity primarily via CaMKII-dependent and PKA-independent manner. Epac was found to activate CaMKII and increase RyR2 phosphorylation at the CaMKII site, without significant effect on LTCCs or NCX (Pereira et al. 2007; Pereira et al. 2013; Lezoualc'H et al. 2016). It is yet unclear whether Epac and PKA regulate cellular function independently, synergistically or in opposition to one another (Bers 2007; Ruiz-Hurtado et al. 2013).

1.5.2 Potential phosphorylation sites of RyR2

The hRyR2 sequence has 42 potential phosphorylation sites (Hamilton and Terentyev 2024). However, only three sites have been investigated widely for over 20 years; these are S2808, Serine 2030 (S2030) and S2814 and will be discussed below. Advances in

structural data on RyR2 has revealed that S2808 and S2814, by virtue of proximity, form part of a larger "phosphorylation hotspot", that also includes S2811 and potentially T2810 ([2805]RRI**S**Q**TS**QV**S**V[2815]) (Yuchi et al. 2012; Camors and Valdivia 2014; Hamilton and Terentyev 2024). This phosphorylation hotspot is situated on the cytosolic face of the channel, allowing easy access for various kinases.

1.5.2.1 S2808

The S2808 phosphorylation site was initially identified by Witcher et al. (1991) as a CaMKII phosphorylation site. However, later studies by Marx et al. (2000) and Wehrens et al. (2006) classified it as an exclusive PKA site. Since Marx *et al.*'s (2000) study which proposed that S2808 is hyperphosphorylated by four fold in HF (in dogs and humans), and that its phosphorylation significantly increases RyR2 channel activity, this phospho-site has since drawn the attention of several research groups (Jiang et al. 2002; Rodriguez et al. 2003; Stange et al. 2003; Currie et al. 2004; Xiao et al. 2004; Ai et al. 2005; Carter et al. 2006; Kohlhaas et al. 2006; Huke and Bers 2008; MacDonnell et al. 2008; Fischer et al. 2013), with most evidence suggesting that S2808 is a target for PKA, CaMKII, and possibly PKG. The Marks model proposes that the observed hyperphosphorylation by PKA at S2808 causes FKBP12.6 dissociation from RyR2, destabilising the closed state of the channel and consequently leads to SR Ca^{2+} leak, ultimately contributing to systolic dysfunction in HF (Bellinger et al. 2008). The group reported that S107, a RyR2-FKBP12.6 interaction stabiliser, inhibited diastolic Ca^{2+} leak in post-myocardial infarct hearts of mice with S2808D mutation which mimics PKA hyperphosphorylation (Shan et al. 2010). They also found that mice harbouring RyR2 channels that cannot be phosphorylated by PKA at S2808 (S2808A) exhibit limited β-adrenergic response and impaired exercise capacity (Shan et al. 2010).

Although Marks' group continuously validated and extended their scheme by additional reports, many prominent research groups were unable to replicate or confirm most of the aspects of the Marks model. Multiple studies done by other groups reported a substantially high basal phosphorylation at S2808 (~50-75%) in healthy animal species and humans. This raised doubts about whether this site could be considered a reliable

indicator of PKA phosphorylation in HF (Jiang et al. 2002; Rodriguez et al. 2003; Xiao et al. 2004; Carter et al. 2006; Huke and Bers 2008). In studies with S2808 phosphoablative RyR2 (S2808A) mouse models (although not from the same mouse line used by Marks group), the β-adrenergic response of the cardiomyocytes was not altered and their function was almost unchanged, and there was no observed protection against HF dysfunction (Benkusky et al. 2007; MacDonnell et al. 2008; Zhang et al. 2012a). However, western blot analysis using site-specific phospho antibodies showed that genetic ablation of the S2808 site induces a compensatory increase in phosphorylation at the S2814 and S2030 sites under β-adrenergic stimulation with isoproterenol; suggestive of possible functional redundancy between all three sites (Terentyev and Hamilton 2016).

The proposed role of S2808 phosphorylation in FKBP12.6 dissociation leading to RyR2 Ca^{2+} flux, especially at diastolic Ca^{2+} concentrations, was also contested. Ablating the S2808 phospho-site (S2808A) or inducing constitutive activation (S2808D) was shown to have no impact on channel activity or binding affinity for FKBP12.6 (Stange et al. 2003). Other groups also found that RyR2 phosphorylation did not cause FKBP12.6 dissociation (Xiao et al. 2004; Guo et al. 2010). Therefore, while it is agreed that S2808 is phosphorylated by PKA, CaMKII and potentially other kinases, the functional consequence of this phosphorylation remains a topic of ongoing debate.

1.5.2.2 S2030

The S2030 phospho-site was discovered by Xiao et al. (2005) using classical two-dimensional mapping of RyR2. S2030 is preferentially phosphorylated by PKA and not CaMKII, and phosphoablation of this site did not affect FKBP12.6 binding to RyR2, nor did it change Ca^{2+} dependence of [^{3}H] ryanodine binding (Xiao et al. 2005). Basal phosphorylation of this site is very low in quiescent cardiac myocytes and its phosphorylation is prompted by β-adrenergic stimulation (Xiao et al. 2005; Huke and Bers 2008). Recombinant RyR2 with S2030A mutation showed a diminished response to PKA. Additionally, the phosphomimetic mutation, S2030D, was shown to have enhanced sensitivity to SR luminal Ca^{2+}(Xiao et al. 2007). A diminished β-adrenergic response was also reported in S2030 phosphoablative mouse models (Potenza et al. 2019). Double

knock-in mice with S2808 and S2814 phosphoablation (RyR2-DKI) were recently generated to investigate the functional relevance of S2030 phosphorylation on RyR2. Increased spark frequency was reported in permeabilised cAMP-treated RyR2-DKI cardiomyocytes compared to WT (Janicek et al. 2024). This important finding suggests that S2030 phosphorylation increases RyR2 activity and that S2030 phosphorylation might be enough for a β-adrenergic-mediated response in RyR2. Recent work by Asghari et al. (2024) demonstrated that phosphoablation of S2808, S2814 and S2030 increased the abundance of RyR2 isolated tetramers. However, under β-adrenergic stress, the rearrangement of RyR2 tetramers within clusters was restored in S2808 and S2814 phosphoablative mouse cardiomyocytes, but not for S2030 ablated cells. This suggests that rearrangement of RyR2 in a cluster under β-adrenergic stimulation could be influenced primarily by S2030 phosphorylation.

1.5.2.3 S2814

The S2814 phosphorylation site of RyR2 was discovered by the Marks' group as a CaMKII-specific site (Wehrens et al. 2004). Although it is generally agreed that CaMKII is the primary kinase for this site, there is less consensus on whether it is the only CaMKII phosphorylation site on RyR2. As mentioned above, S2808 is also a target for CaMKII phosphorylation (Witcher et al. 1991). Although S2814 forms part of the same phosphorylation hotspot with S2808, there is less controversy on its role because it appears to be more likely regulated by CaMKII.

Unlike S2808, the basal level of phosphorylation of S2814 in quiescent cardiomyocytes is very low, and it increases in the presence of β-adrenergic agonists (Huke and Bers 2008). Although CaMKII inhibitors may prevent activity-dependent phosphorylation at S2814, the basal phosphorylation level at rest was found to be maintained by a Ca^{2+}-dependent kinase other than CaMKII (Huke and Bers 2008). A significant increase in S2814 basal level of phosphorylation was reported in HF in human cardiomyocytes (Fischer et al. 2014).

Mouse models with germline ablation of S2814 site (S2814A) did not show significant change in SR Ca^{2+} release in comparison to WT. However, the phosphomimetic

counterpart S2814D showed SR Ca^{2+} leak and consequently reduced SR Ca^{2+} load (Van Oort et al. 2010). S2814D mice with structurally and functionally normal hearts developed persistent ventricular tachycardia and sudden cardiac death following catecholaminergic provocation (Van Oort et al. 2010). On the other hand, the S2814A mouse models appeared to be more resilient to multiple cardiac insults, *e.g.,* S2814A and protected mice from developing catecholaminergic and pacing-induced arrhythmias following transverse aortic constriction surgery (Van Oort et al. 2010). Additionally, crossbreeding S2814A mice with the Duchenne muscular dystrophy (DMD) mouse model suppressed arrhythmogenic spontaneous Ca^{2+} sparks and waves that were prevalent in the DMD model (Ather et al. 2013).

Allthough several lab groups have demonstrated that inhibiting S2814 phosphorylation prevents functional and structural damage to the heart induced by HF and other insults, it is important to remember that it is unlikely that phosphorylation of S2814 (a common and natural reaction) was designed to harm the heart's function. Therefore, it is crucial to define the conditions under which S2814 phosphorylation becomes harmful, especially given the fact the mice with constitutive activation of S2814 (S2814D) have structurally and functionally normal hearts (Van Oort et al. 2010; Camors and Valdivia 2014).

1.5.2.4 Other investigated phosphorylation sites

Mass spectrometry of RyR2 has identified other potential phosphorylation sites such as S2811, S2367, S2797 and T2810. The S2811 site is another serine residue located in the phosphorylation hotspot that appears to be phosphorylated by both PKA and CaMKII *in vitro*, and in mice stimulated by β-adrenergic agonists *in vivo* (Huttlin et al. 2010; Yuchi et al. 2012). It remains unclear whether S2811 plays a role in CaMKII and PKA phosphorylation of RyR2, or interferes with the signal of phospho-specific antibodies for S2808 and S2814, complicating the identification of kinase specificity for these sites (Camors and Valdivia 2014).

A recent study has shown that the previously uncharacterised S2367 site is

phosphorylated by a striated muscle preferentially expressed protein kinase (SPEG), and that phosphorylation of S2367 reduces RyR2-mediated SR Ca^{2+} release; unlike PKA and CaMKII phosphorylation that are known to increase RyR2 activity. Loss of S2367 phosphorylation by reducing SPEG levels was also shown to cause diastolic Ca^{2+} leak and increase susceptibility to atrial fibrillation (Campbell et al. 2020).

Due to their location that is within or immediately preceding the phosphorylation hotspot, S2797 and T2810 are also thought to be accessible for phosphorylation by protein kinases. Yuchi et al. (2012) showed that PKA phosphorylates both T2810 and S2797, although their functional relevance to RyR2 remains unclear.

1.5.3 Effects of serine/threonine phosphatases on RyR2

Protein phosphatases (PP) dephosphorylate RyR2 channels (and other proteins involved in ECC) to counterbalance the phosphorylation induced by kinases. The extent of channel phosphorylation is therefore determined by the balance of activities of kinases and phosphatases. The RyR2 macromolecular complex includes several protein phosphatases, including protein phosphatase type 1 (PP1), protein phosphatase type 2A (PP2A) and Ca^{2+}-dependent protein phosphatase type 2B (PP2B) (MacDougall et al. 1991). The PP scaffold to RyR2 via adaptor proteins, *e.g.,* mAKAP and spinophillin (Marks et al. 2002). Studies demonstrated that PP1 can dephosphorylate S2808 and S2814, while PP2A can dephosphorylate S2814 and S2031. The specificity of PP2B has not been investigated yet (Huke and Bers 2008; Terentyev et al. 2009; Terentyev and Hamilton 2016). Whereas kinase-dependent phosphorylation of RyR2 increases RyR2 P_o and SR Ca^{2+} release, PP1 and PP2A were found to reverse this action; reducing channel activity (Carter et al. 2006; Carter et al. 2011; Little et al. 2015). Some of the inconsistent findings in studies that looked into phosphorylation of RyR2 have been attributed to the activity of PP and their inhibitors and the initial RyR2 phosphorylation levels during experimental procedures (Reiken et al. 2003; Terentyev and Hamilton 2016).

1.6 RyR2 dysfunction and disease

Given the complex regulation of myocyte Ca^{2+} signalling and the critical role of RyR2 in

this process, it is not surprising that dysfunctional RyR2-mediated SR Ca^{2+} release is a driver of cardiac pathology. Destabilised or "leaky" RyR2 channels can precipitate aberrant Ca^{2+} release, which in turn triggers early and delayed after depolarisation (EADs and DADs) that can lead to premature AP and arrhythmias (Bers 2006). Over the last two decades, evidence has accumulated suggesting a link between abnormal RyR2 function associated to mutations and disease (ryanopathies) (Sleiman et al. 2021). Additionally, CaM mutations have been linked to RyR2 dysregulation and disease (calmodulinopathy) (Badone et al. 2018). Catecholaminergic polymorphic ventricular tachycardia (CPVT) and congenital Long QT Syndrome (LQTS) are the most significant diseases associated with mutations in both RyR2 and CaM. The molecular basis of CPVT and LQTS stemming from RyR2 and CaM dysfunction will be explored in detail in the following sections.

1.6.1 Catecholaminergic polymorphic ventricular tachycardia

CPVT is a rare inherited exercise- or stress-induced ventricular tachycardia found in children and young people with a structurally normal heart that can lead to a sudden cardiac death (Leenhardt et al. 1995; Priori et al. 2002). It affects approximately 1 in 10,000 people with the majority of patients having a history of arrhythmia or syncope in their families (Jabbari et al. 2013). The average age at onset of symptoms is between seven and 12 years, but later onset has also been reported (Napolitano et al. 2022). Patients with CPVT present a normal electrocardiogram (ECG) pattern under resting conditions, and symptoms only occur during β-adrenergic stimulation such as physical or emotional stress (Leenhardt et al. 1995; Scheinman and Lam 2006). Clinical electrophysiological studies have demonstrated that arrhythmias can be triggered in patients with CPVT through exercise testing or catecholamine infusion (Priori et al. 2002). CPVT is characterised by DADs and polymorphic or bidirectional ventricular tachycardia. Spontaneous recovery can occur when these arrhythmias self-terminate. However, in some cases, ventricular tachycardia may degenerate into ventricular fibrillation and causes sudden cardiac death, which is sadly often the first manifestation of the disease. The phenotypic presentation of the disorder is highly variable, with affected individuals within the same family often exhibiting differing symptoms (Priori et al. 2002; Sumitomo et al. 2003).

If left untreated, CPVT is extremely lethal, with roughly 30% of patients experiencing at least one cardiac arrest (Priori et al. 2002; Hayashi et al. 2009). Current treatment options for CPVT include β-blockers, which target the adrenergic drive of the disease. Studies have shown that non-selective β-blockers (nadolol and propranolol) are more effective than selective β-blockers in preventing recurrence of syncope in most CPVT patients. Since sudden death is often the first manifestation of the disease, β-blockers have also been used as a preventative treatment for carriers of a pathogenic variant of one of the CPVT-associated genes with negative exercise stress test. Flecainide, a Na^+ channel blocker, is also used alongside β-blockers in patients non-responsive to β-blockers alone who experience recurrent syncope, or have experienced a previous aborted sudden death. Implantable cardioverter defibrillator (ICD) treatment is indicated in patients in whom drug treatment is not effective in controlling their arrythmia. Finally, left cardiac sympathetic denervation (LCSD) is considered in patients who had several ICD shocks while on β-blockers and flecainide. However, a significant burden of life-threatening arrythmia remains even after LCSD (Priori et al. 2015; Al-Khatib et al. 2018; Napolitano et al. 2022).

Typically, CPVT phenotype is caused by the presence of pathogenic variants in *RyR2* or *CASQ2* genes, but it is also caused by mutations in *CALM1*, *CALM2*, *CALM3* and *TRDN* genes (Napolitano et al. 2022).

1.6.1.1 CPVT-linked RyR2 mutations

Linkage studies and genetic sequencing have revealed that mutations in the hRyR2 gene (located at chromosomal locus 1q42-q43) are directly associated with CPVT type 1 (CPVT1) (Swan et al. 1999; Priori et al. 2001). Around 70% of CPVT cases have an autosomal-dominant RyR2 mutation that leads to aberrant Ca^{2+} signalling in the heart, meaning that the inheritance of one allele is sufficient to cause the disease phenotype (Sleiman et al. 2021). While the majority of patients with CPVT have a family history of cardiac disorders, some patients have been found to be the only symptomatic family member with neither parent harbouring a mutant allele, indicating that CPVT-linked mutations can arise in a *de novo* manner (Priori et al. 2001; Postma et al. 2005). There are

>200 CPVT-linked RyR2 mutations, most of which (96%) are missense variations resulting in gain of function (Paludan-Müller et al. 2017; Wleklinski et al. 2020), and they cluster in four distinct hotspot regions in the N- and C-terminal domains, and the central domain (see **Figure 1.12**) (Thomas et al. 2006). Interestingly, *de novo* RyR2 mutations are more likely found in the C-terminal domain, unlike familial RyR2 mutations that are more likely located in the N-terminal domain (Shimamoto et al. 2022). Loss-of-function RyR2 mutations also exist but are less common and cause arrhythmias distinct from CPVT (Roston et al. 2017).

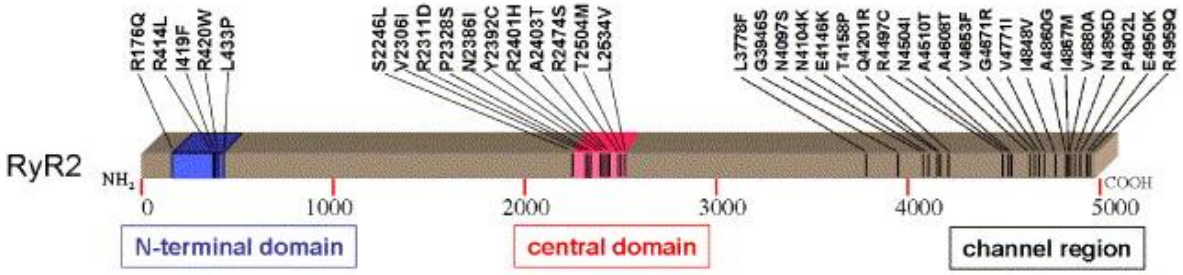

Figure 1.12 Schematic diagram illustrating the clustering of some CPVT mutations within the domains of RyR2 monomer. To date, Over 200 missense mutations have been identified (though not all are shown here), and these mutations cluster into four distinct hotspot regions in the N-terminal domain, the central domain, and the C-terminal region (referred to as the "channel region" in the figure). Figure adapted and modified from Yano et al. (2005).

Currently, there are multiple hypothesis on how gain-of-function RyR2 mutations cause aberrant RyR2 Ca^{2+} release that leads to CPVT. One proposed hypothesis is that CPVT-linked mutations of RyR2 increases the channel's sensitivity to luminal Ca^{2+} activation, decreasing the threshold of SR Ca^{2+} required to activate RyR2, leading to diastolic Ca^{2+} leak. This process is termed store overload-induced Ca^{2+} release (SOICR), which occurs when luminal SR Ca^{2+} concentration reaches a critical threshold, triggering spontaneous Ca^{2+} efflux through RyR2, often leading to a decrease in SR Ca^{2+} load (see **Figure 1.13**) (Jiang et al. 2004; Jiang et al. 2005; Jiang et al. 2007). Another hypothesis suggests that RyR2 mutations reduce FKBP12.6 binding affinity to RyR2, possibly via channel hyperphosphorylation by PKA, destabilising the channel and leading to diastolic Ca^{2+} leak evident in RyR2 mutants (Marx et al. 2000). However, this hypothesis was challenged by several research groups (as previously discussed in **Section 1.5**), demonstrating that

FKBP12.6 still binds to mutant RyR2 with comparable affinity to WT under both resting and catecholamine-stimulated conditions (George, Sorathia, et al., 2003; B. Xiao et al., 2007; J. Xiao et al., 2007). Instead, Zhang et al. (2016)) e reported that FKBP12.6 was incapable of facilitating SOICR termination in arrhythmogenic RyR2 variants compared to WT channels, potentially leading to diastolic leak (George et al. 2003a; Xiao et al. 2007; Zhang et al. 2016). This hypothesis can possibly extend to include impaired binding of mutant RyR2 to channel regulators, such as junctophilin-2 and CaM. CPVT-linked RyR2 mutants are also thought to disrupt the interaction between the N-terminal and central domains of RyR2 monomers which is critical for RyR2 autoregulation and for stabilising the closed state of the channel. Ikemoto and Yamamoto (2002) termed this disruption "domain unzipping" because it weakens the tight "zipping" of the domains, allowing the channel to open and leak Ca^{2+} under resting conditions (see **Figure 1.14**) (Ikemoto and Yamamoto 2002; George et al. 2004; George et al. 2006; Uchinoumi et al. 2010). Despite ongoing debate about the validity of each hypothesis, they all agree that CPVT-linked RyR2 mutations increase the probability of pathological Ca^{2+} leak during diastole. However, given the broad spectrum of clinical phenotypes and the diverse locations of mutations throughout the big RyR2 coding sequence, it is unlikely that a single mechanism of dysfunction explains all cases, but instead, different mutations likely produce pathological phenotypes via a combination of the proposed mechanisms. For instance, R420Q mutation of RyR2 was shown to have a weaker interaction with junctophilin-2 and cause domain unzipping of the N-terminal and central domains (Yin et al. 2021). Similarly, the R2474S mutation causes defective interdomain interaction facilitating unzipping in addition to reducing luminal Ca^{2+} activation threshold (Uchinoumi et al. 2010).

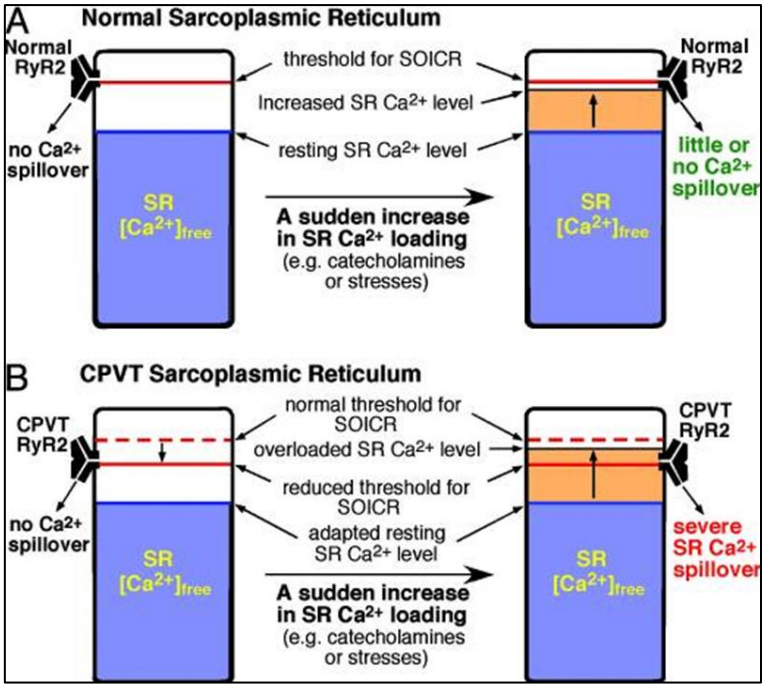

Figure 1.13. SOICR: a hypothesis on how RyR2 mutations can cause CPVT. The figure illustrates the relationship between the threshold for SOICR and the SR-free Ca^{2+} levels in **(A)** Normal, and **(B**) CPVT SR comparing resting conditions (left) with the stimulated state (right). SOICR threshold (represented by a red bar) is reduced in CPVT SR due to mutations in RyR2. The blue line depicts the level of free SR Ca^{2+}. The yellow area represents an increase in free SR Ca^{2+} triggered by catecholamine stimulation or stresses. When the SR-free Ca^{2+} level reaches the SOICR threshold, SOICR occurs, resulting in a significant Ca^{2+} spillover. This spillover can then lead to DADs and trigger arrhythmias. Figure adapted from Jiang et al. (2004).

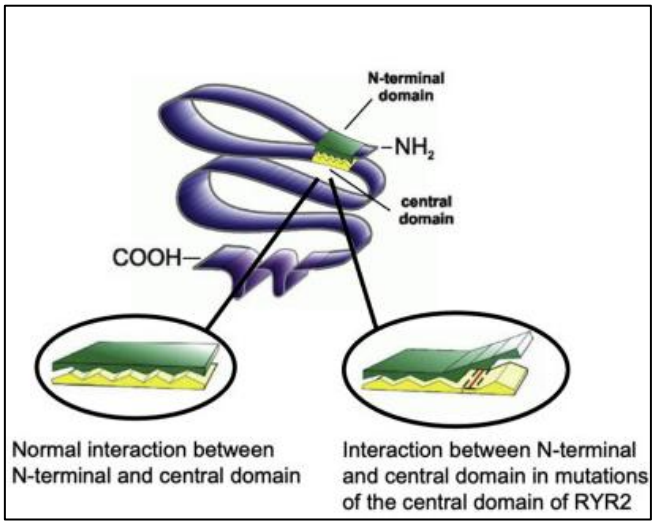

Figure 1.14. Zipping/unzipping hypothesis of RyR2 dysfunction caused by mutations in CPVT. The N-terminal and central domains of each RyR2 monomer interact to function as a regulatory switch for channel gating. The close interaction between these domains is crucial for stabilising the channel. A mutation in either domain disrupts this interdomain interaction, resulting in Ca^{2+} leak. Figure modified from Yang et al. (2006).

1.6.1.2 CPVT-linked CaM mutations

CaM mutations associated with CPVT were first discovered in 2012 by Nyegaard et al. in a Swedish family with CPVT-like symptoms despite lacking mutations in *RyR2* or *CASQ2* genes. Linkage analysis then identifies the first human CaM mutation in *CALM1* gene with dominance inheritance in that family. Subsequent studies that looked into CPVT patients who had previously tested negative for all CPVT-known gene mutations later revealed other CPVT CaM mutations in all three *CALM* genes in both N- and C-lobes.

CaM mutants exert their dysfunction via increased RyR2-mediated Ca^{2+} release from the SR. Some CaM mutations have been proposed to affect the affinity of CaM for the CaMBD of RyR2, while others are thought to affect Ca^{2+} -binding or kinase activation (Prakash et al. 2022). This could therefore lead to diastolic SR Ca^{2+} leak in CPVT patients. CaMKII activity level has been shown to be affected by several CPVT-linked CaM mutations (Chazin and Johnson 2020; Prakash et al. 2022).

1.6.2 Long QT Syndrome

Congenital LQTS is an inherited cardiac ion channelopathy with an estimated prevalence of 1 in 2000 (Roden et al., 1996; Schwartz et al., 2009; Wallace et al., 2019). LQTS can also be acquired because of drug administration (Kannankeril et al., 2010). The syndrome is characterised by delayed repolarisation of the cardiomyocyte AP, which manifests on the ECG as a prolongation of the QT interval. This extended AP duration predisposes individuals to malignant arrhythmia, including *torsade de pointes*, and rarely, sudden cardiac death (W. Zhu et al., 2024). The clinical symptoms of LQTS include palpitations, syncope and anoxic seizures (Wallace et al., 2019). Some carriers of the disease remain asymptomatic while others experience serious cardiac events at childhood (Wallace et al., 2019; W. Zhu et al., 2024). Interestingly, the disease phenotype is highly variable, even among family members carrying the same genetic mutation (Amin et al., 2013; Wallace et al., 2019). Management of LQTS patients involves the use of β-blockers (*e.g.,* nadolol or propranolol). Patients who are unresponsive to β- blockers are also offered Na^{+} channel blockers (*e.g.,* Mexiletine) (W. Zhu et al., 2024). K^{+} channel openers (*e.g.,* nicorandil) have been proposed as a promising future option for LQTS

treatment (W. Zhu et al., 2024). ICDs are indicated in LQTS patients who survived a cardiac arrest despite medical therapy. Finally, LCSD is reserved for high-risk patients who are intolerant or unresponsive to β-blockers (W. Zhu et al., 2024).

To date, There are 17 autosomal dominant gene mutations associated with LQTS which encode cardiac ion channels such as Na^+ and K^+ channels (Adler et al., 2020; W. Zhu et al., 2024). Genetic screening has revealed that mutations in *CALM1, CALM2* and *CALM3* genes are also associated with LQTS (Adler et al., 2020; Crotti et al., 2013; Makita et al., 2014; Reed et al., 2015), and will be discussed below.

1.6.2.1 LQTS-linked CaM mutations

Multiple mutations in CaM protein have recently been associated with LQTS (Crotti et al., 2023), but the underlying pathogenic mechanisms are still a topic of ongoing research, with disease mechanisms including dysregulated LTCCs and voltage-gated Na^+ and K^+ channels by mutant CaMs (Limpitikul et al., 2014). LQTS-linked CaM mutations have been shown to exert their dysfunction on LTCCs through decreasing their Ca^{2+}-dependent inactivation, thus increasing the Ca^{2+} current during phases 2 and 3 of the AP (Boczek et al., 2016; Gupta et al., 2025; Helassa et al., 2022; Limpitikul et al., 2014). LQTS CaM mutations have also been shown to affect CaM's binding affinity to LTCCs and Ca^{2+} in addition to affecting CaMKII activation and its downstream kinase activity (Gupta et al., 2025; Helassa et al., 2022; Limpitikul et al., 2014).

1.6.3 CPVT/LQTS mixed phenotype: D132E and Q136P variant CaM

A mixed phenotype of CPVT and LQTS was observed with some CaM mutations in the *CALM1* and *CALM2* genes, where patients present with a prolonged QT interval alongside exercise-induced ventricular ectopy (Crotti et al., 2023). These mutations are intriguing because their phenotypic presentation suggests that their underlying calmodulinopathy affects both RyR2 channels (CPVT component), as well as an LQTS-associated component, such as LTCCs. Five CaM mutations have been identified with this overlapping phenotype: E83K, E105A, D134N, D132E and Q136P (Crotti et al., 2023). This research project focuses on D132E and Q136P CaM variants, aiming to elucidate their

mechanism of dysfunction exerted on RyR2 channels.

Both D132E and Q136P CaM variants are located within the Ca^{2+}-coordinating residues of EF-hand 4 of CaM (Makita et al., 2014) (see **Figure 1.15**). D132E CaM variant was identified in a 29-year old German female diagnosed with neonatal LQTS. She remained asymptomatic on β-blocker therapy until age nine, when she experienced syncope while swimming. At age 22, she was diagnosed with exercise-induced polymorphic ventricular tachycardia. Genetic testing was negative for all known LQTS and CPVT mutations. The Q136P CaM mutation was identified in a Moroccan girl diagnosed with LQTS following a syncopal episode at age eight. Sadly, she died suddenly at age 11 while dancing, thus a later CPVT diagnosis was made given the clinical circumstances, although no prior exercise test was performed. Similar to the D132E case, genetic screening for established LQTS and CPVT mutations was negative (Makita et al., 2014).

Since 2019, multiple research groups have investigated the effects of D132E and Q136P CaM variants on LTCCs function and their Ca^{2+} and RyR2 binding affinities. However, little is known about their impact on RyR2 channel function, with only one study to date (Søndergaard et al., 2019). A summary of the literature on D132E and Q136P CaM is provided in **Table 1.1**.

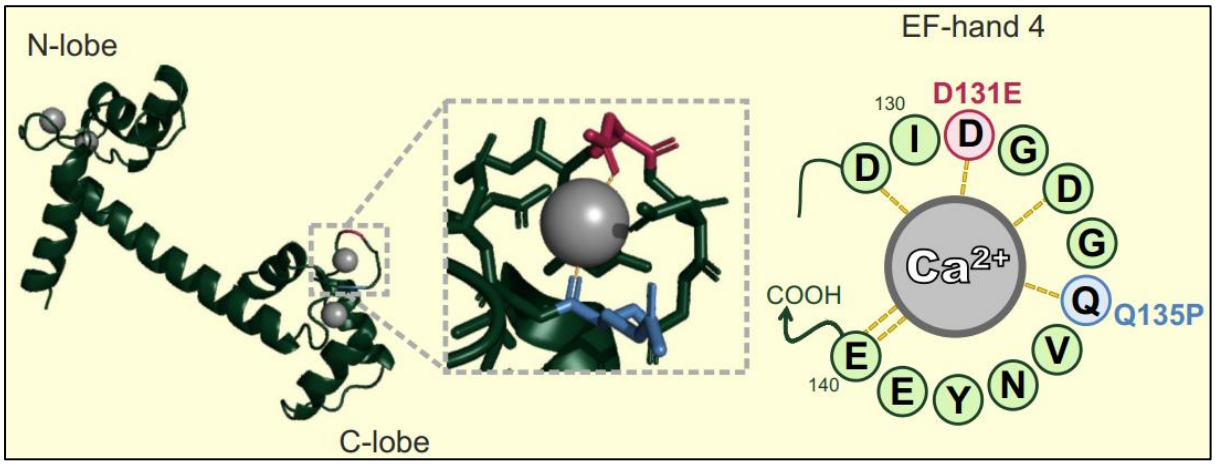

Figure 1.15. Representation of D132E and Q136P CaM position in the Ca^{2+}-coordinating region in EF-hand 4 of CaM. Figure adapted from Gupta et al. (2025)

Table 1.1. Summary of the effects of D132E and Q136P CaM variants on Ca^{2+} binding, LTCCs and RyR2.

CaM mutation	**Gene** (Makita et al., 2014)	**Patients** (Crotti et al., 2023; Makita et al., 2014)		**ACMG classification** (Crotti et al., 2023)	**Ca^{2+} binding affinity** (Da'as et al., 2024; Gupta et al., 2025)		**Effects on LTCCs** (Gupta et al., 2025)		**Effects on RyR2**					**Effects on heart beat**
		n of families	*n* of patients		N-lobe fold change	C-lobe fold change	Ca^{2+} dependent inhibition	Binding to IQ domain of LTCCs	Single channel P_o (Søndergaard et al., 2019)	CaM binding to RyR2- fold change (Thanassoulas et al., 2023)		SOICR (Søndergaard et al., 2019)		Zebrafish heart rate (Da'as et al., 2024)
										100 µM Ca^{2+}	0 µM Ca^{2+}	Activation threshold	Termination threshold	
D132E	*CALM 2*	1	1	Pathogenic	No change	↓ ~15	Completely abolished	↑ 2 fold		↓ ~1.8	No change	↓ 3%	↓ 25%	↓
Q136P	*CALM 2*	1	1	Pathogenic	No change	↓ ~5	↓	No change	↑	↓ ~2	No change	↓ 3%	↓ 19%	↑

1.7 Research project aim

This research aims to characterise two arrhythmia-linked CaM variants: D132E and Q136P (Makita et al. 2014), whose effect on RyR2 function is not yet fully understood. Given that individuals harbouring mutations D132E or Q136P CaM have been shown to have an overlapping CPVT and LQTS phenotype, it is hypothesised that both variants would alter RyR2-mediated Ca^{2+} release, leading to dysregulated RyR2-mediated Ca^{2+} leak, a potential mechanism in the CPVT component of their clinical presentation. To test this hypothesis, the main objectives of the project are to characterise the effect of these CaM mutants on local and global RyR2-mediated Ca^{2+} release in both recombinant and animal systems and further to assess their effects on CaMKII activation and thereafter the knock on effect on RyR2 phosphorylation and function. This will be done by:

- Co-expressing WT or mutant CaM with RyR2 in a human recombinant system (HEK293) and characterising the effect on global, synchronised RyR2-mediated Ca^{2+} release events at the whole cell level.
- Investigate the effects of mutant D132E and Q136P CaM on local Ca^{2+} release at the spark level in permeabilised mouse ventricular myocytes. Effects on RyR2 single channel gating will also be assessed, such that effects on channel P_o and open and closed dwell times can be measured.
- Use a kinase assay to determine the effects of mutant D132E and Q136P CaM on the activation of CaMKII and evaluate its subsequent phosphorylation of RyR2 at the S2814 site, which may explain effects on channel function.

Chapter 2: Materials and methods

2.1 Working in the laboratory

2.1.1 General laboratory equipment and reagents

- All chemicals and reagents were of analytical grade obtained from Sigma-Aldrich or Fisher Scientific, unless otherwise stated. All reagents were dissolved in autoclaved deionised water (dH_2O) and stored at room temperature (RT), unless manufacturer advises otherwise.
- Solution pH was measured using Mettler Toledo FiveEasy F20 pH Meter with LE438 Sensor , and adjusted using either 1M HCl, NaOH or KOH.
- Solutions were filter-sterilised when needed using 0.22 µM Millex® syringe filters (Millipore).
- Plastics and glassware were purchased from Greiner or Fisher Scientific. Prior to use, glassware was soaked in detergent and thoroughly washed.

2.1.2 Health and safety

Full general health and safety training was provided by my supervisor, Dr N. Lowri Thomas, and the Safety, Health, Environment and Welfare (SHEW) manager, Dr Bevan Cumbes prior to commencing any laboratory work. All experiments were conducted in accordance with COSHH regulations and after completion of relevant risk assessments.

2.1.3 Computer software and data analysis

- All data were analysed and plotted in GraphPad Prism® 10.4.2. Data normality was first tested to determine which statistical tests were appropriate to use. Normality was analysed using Shapiro Wilks test and plotted on QQ plots. Where data were normally distributed, t-test or one-way ANOVA test were used, whereas Kruskal-Wallis or Mann-Whitney U tests were used for non-parametric data.
- Western blots were analysed using Fiji ImageJ software.
- Spark Master 2 (SM2) software was used for the analysis of line-scan Ca^{2+} spark imaging data.
- Single channel data were analysed and modelled in QuB suite 2.0.0.32.

- NEBcutter® 3.0.19 was used to predict restriction enzyme sites within RyR2 sequence and produce a virtual restriction digest pattern to compare against experimental results.
- Chromas 2.5.0 was used to view sequencing electropherograms.
- MatLab R2023a was used to pre-process line-scans and a MatLab-based applet was used to analyse Ca^{2+} oscillations graphs from confocal microscopy.

2.2 Materials

2.2.1 hRyR2 and CaM plasmid expression vectors

eGFP-tagged human RyR2 was obtained from Dr N. Lowri Thomas in the mammalian expression vector pcDNA3 (Invitrogen) (pcDNA3-eGFP-hRyR2). The eGFP tag is placed at the N-terminus of hRyR2, separated by a four amino acid spacer (Thr-Ser-Gly-Ser).
The mammalian expression vectors pIRES containing WT or mutant (D132E, Q136P) human CaM with dTomato (pIRES-dTomato-CaM) were obtained from Dr Nordine Helassa (University of Liverpool). The IRES (internal ribosome entry site) element allows coordinated co-expression of the two genes from the same vector without one being tagged to the other, allowing us to track which cells are expressing CaM without affecting its normal function.

2.2.2 WT and variant CaM proteins

Purified WT, D132E and Q136P CaM constructs were obtained from Dr Nordine Helassa (University of Liverpool). The proteins were expressed in *Escherichia coli* (E-coli) BL21(DE3) STAR cells and purified using HisTrap™ HP column (GE Healthcare); as detailed in Prakash et al. (2022).

2.2.3 Site-directed mutagenesis

- pSL1180 plasmid (GE Healthcare) containing *KpnI/NdeI* fragment of hRyR2 (cassette) were obtained from Dr N Lowri Thomas.

- Forward and Reverse mutagenic primers (Eurofins) for the S2814A RyR2 mutation, as shown in **Table 4.1.**
- QuikChange II XL Site-Directed Mutagensis kit (Agilent)
    - PfuUltra High Fidelity DNA polymerase (2.5 U/µL).
    - 10x reaction buffer (proprietary formula).
    - QuickSolution reagent (proprietary formula).
    - dNTP mix (proprietary formula).
- *DpnI* methylation-sensitive restriction enzyme (10 U/µL)

2.2.4 Plasmid transformation and propagation

- XL10-Gold ultracompetent cells (Agilent).
- MAX Efficiency™ Stbl2™ competent cells (Thermo Fisher Scientific).
- Super optimal medium with catabolic repressor (SOC):
    - 2% tryptone; 0.5% yeast extract; 10 mM NaCl; 2.5 mM KCl; 10 mM $MgCl_2$; 10 mM $MgSO_4$ and 20 mM glucose.
- Luria Bertani (LB_{AMP}) broth:
    - 10 g/L tryptone; 5 g/L yeast extract; 5 g/L NaCl- prepared to 1 L with dH_2O. autoclaved and ampicillin added before use to reach a final concentration of 100 mg/L.
- LB_{AMP} agar plates:
    - Prepared using LB broth components with the addition of 15 g/L agar- autoclaved, and ampicillin added at 100 mg/L concentration before pouring into sterile petri dishes.
- Ampicillin 100 mg/ml stock: used at a working concentration 100 µg/mL and stored at -20°C.

2.2.5 Small- and large-scale plasmid isolation – Miniprep and maxiprep

- QIAprep® Spin Miniprep Kit (Qiagen)
    - Resuspension buffer (P1): 50 mM Tris-HCl (pH 8); 10 mM Ethylenediaminetetraacetic acid (EDTA) and 100 µg/mL RNase A.

    - Lysis buffer (P2): 200 mM NaOH and 1% (w/v) sodium dodecyl sulphate (SDS).
    - Neutralisation buffer (N3): 4.2 M Guanidine-HCl and 0.9 M potassium acetate (pH 4.8).
    - Spin column wash buffer (PE): 80 mM NaCl and 8 mM Tris-HCl (pH 7.5). Ethanol (96-100%) added 4:1 before use.
- HiSpeed® Plasmid Maxi Kit (Qiagen)
    - Resuspension buffer (P1): 50 mM Tris-HCl (pH 8); 10 mM EDTA and 100 µg/mL RNase A.
    - Lysis buffer (P2): 200 mM NaOH and 1% (w/v) SDS.
    - Neutralisation buffer (P3): 3 M potassium acetate (pH 5.5).
    - Equilibration solution (QBT): 750 mM NaCl; 50 mM MOPS (pH 7); 15% (v/v) isopropanol and 0.15% (v/v) Triton® X-100.
    - Wash buffer (QC): 1 M NaCl; 50 mM MOPS (pH 7) and 15% (v/v) isopropanol.
    - Elution buffer (QF): 1.25 M NaCl; 50 mM Tris-HCl (pH 8.5) and 15% (v/v) isopropanol).

2.2.6 Restriction digest for verification

All plasmid DNA digests were carried out using FastDigest restriction enzymes in their Universal FastDigest buffer system (Thermo Fisher Scientific).

2.2.7 Agarose gel electrophoresis

- Tris Acetate-EDTA (TAE) buffer, 50x stock: 2 M Tris; 2 M glacial acetic acid and 50mM EDTA.
- 1% agarose gels: 1% (w/v) high purity agarose (Bio-Rad) in 1x TAE buffer.
- UltraPure™ Ethidium Bromide (Invitrogen™; 10 mg/ml stock): used at 0.1 µg/mL concentration.
- DNA loading buffer: 50% 1x TAE buffer and 50% (v/v) glycerol. Orange G loading dye was added to achieve the required detection colour.

- 1 Kb Plus DNA ladder (Invitrogen™): 1 µg per lane.

2.2.8 DNA extraction and ligation

- GeneJET™ Gel Extraction Kit (Thermo Fisher Scientific)
    - Binding Buffer – contains guanidinium thiocyanate (proprietary formula)
    - Wash Buffer – diluted 1:5 with 96-100% ethanol (proprietary formula)
    - Elution Buffer – 10 mM Tris-HCl, pH 8.5
- Rapid DNA Ligation Kit (Roche Applied Science)
    - T4 DNA Ligation buffer, 2x concentrated.
    - DNA dilution buffer, 5x concentrated.
    - T4 DNA Ligase (5 U/µL)

2.2.9 HEK293 cell culture

- HEK293 cells (European Collection of Authenticated Cell Cultures (ECACC)).
- Dulbecco's Modified Eagle Medium (DMEM) (Gibco™; 11965092): containing 25 mM D-Glucose; 4 mM L-Glutamine and 1 mM sodium pyruvate, referred to as minimal DMEM (mDMEM). This was augmented with 10% (v/v) Fetal Bovine Serum (FBS) (Gibco™; A5256701) and 2% (v/v) 100 µg/mL Penicillin-Streptomycin-Glutamine (PSG) (Gibco™) to make complete DMEM (cDMEM).
- Phosphate buffered saline (PBS), pH 7.4 (Gibco™).
- Trypsin-EDTA (0.25%) phenol red (Gibco™).
- Cell freezing medium: 10% (v/v) dimethyl sulphoxide (DMSO) in FBS.
- Nunc™ EasYFlask™ Cell Culture Flasks.

2.2.10 Effectene® transfection of HEK293 cells

- Effectene® Transfection Reagent Kit (Qiagen)
    - Effectene® Transfection Reagent (1 mg/mL)
    - Enhancer (1 mg/mL)
    - Buffer EC
- 35 mm dishes with 10 mm glass diameter, poly-D-lysine coated (MatTek)

- CELLview™ tissue culture treated dishes, 35 mm, 4 compartments, glass bottom (Greiner Bio-One).
- 6-well cell culture plates (Thermo Fisher Scientific).

2.2.11 HEK293 cells loading and imaging

- Calbryte™ 520 AM dye (AAT Bioquest)
- Krebs-Ringer-HEPES (KRH) buffer: 9 g/L glucose; 7 g/L NaCl; 6 g/L HEPES; 0.35 g/L KCl; 0.16 g/L KH_2PO_4; 0.29 g/L $MgSO_4$ and 1.3 mM $CaCl_2$. pH adjusted to 7.4 and filter sterilised.

2.2.12 Immunofluorescence (IF)

- Paraformaldehyde (Sigma-Aldrich).
- Anti-CaM primary mouse antibody (Sigma-Aldrich C3545).
- chicken anti-mouse Alexa Fluor™ 647 cross-absorbed secondary antibody (Thermo Fisher Scientific A21463).
- FluorSave Reagent (Calbiochem®).

2.2.13 Calcium phosphate ($CaPO_4$) transfection of HEK293 cells

- Calcium chloride ($CaCl_2$) (Sigma-Aldrich); pH 7- supplied as 1 M stock and stored at -20 °C.
- 2x HEPES Buffered Saline (HBS): 280 mM NaCl; 10 mM NaCl; 10 mM KCl; 1.5 mM Na_2HPO_4;10 mM glucose and 50 mM HEPES- pH 7.05, solution was filter sterilised and stored in aliquots at -20 °C.
- Sodium butyrate (NaB) (Sigma-Aldrich): 1 M stock prepared with autoclaved dH_2O.
- 10 cm^2 tissue culture dishes.

2.2.14 Cell homogenate preparation

- Hypo-osmotic buffer: 20 mM Tris; 1 mM EDTA pH 7.4; Pierce Protease and

Phosphatase Inhibitor Mini Tablets (Thermo Fisher Scientific) (one tablet for every 10mL buffer) and 1% (v/v) Triton-X-100.

2.2.15 Protein assay for quantification

- Pierce™ BCA Assay Kit (Thermo Fisher Scientific)
    - BCA reagent A (proprietary formula).
    - BCA reagent B (proprietary formula).
    - Albumin Standard Ampules, 2 mg/mL.

2.2.16 Reagents and buffers for hRyR2 protein isolation and purification

- 3-[(3-cholamidopropyl) dimethylammonio]-1-propanesulfonate (CHAPS) (Thermo Fisher Scientific).
- L-α-Phosphatidylcholine (PC) (Merck).
- Hypo-osmotic lysis buffer: 20 mM Tris; 1 mM EDTA; pH to 7.4 and Pierce Protease and Phosphatase Inhibitor Mini Tablets (Thermo Scientific), one tablet for every 10 mL buffer.
- Cryoprotective buffer (resuspension buffer): 400 mM sucrose ;10 mM HEPES; pH to 7.4 and cOmplete™ Protease Inhibitor Cocktail tablets (Roche), one tablet for every 50mL buffer.
- Gradient buffer: 300 mM NaCl; 25 mM Tris-HCl; 50 mM HEPES buffer; 0.3 mM EGTA; 0.1 mM $CaCl_2$; 0.3% (w/v) CHAPS/PC; 2 mM dithiothreitol (DTT), made up with dH_2O, and cOmplete™ Protease Inhibitor Cocktail tablets (Roche), one tablet for every 50 mL buffer.
- Sucrose solutions: 5, 25 and 40% (w/w) sucrose in gradient buffer.
- High-salt solubilisation buffer: 1 M NaCl; 0.15 mM $CaCl_2$; 0.1 mM EGTA; 25 mM PIPES; 0.6% (w/v) CHAPS/PC and 2 mM DTT; made up with dH_2O and pH to 7.4 with NaOH, and 1:1000 protease inhibitor cocktail (Sigma-Aldrich).

2.2.17 Sodium Dodecyl Sulfate-Polyacrylamide Gel Electrophoresis (SDS-PAGE)

- 2x Laemmli sample buffer: 10% (w/v) SDS; 0.5 M Tris (pH 6.8); 10% (v/v) glycerol;

0.5% (w/v) bromophenol blue and 5% (v/v) β-mercaptoethanol.

- SDS-PAGE running buffer: 25 mM Tris; 250 mM Glycine and 0.1% (w/v) SDS.
- Kaleidoscope Precision Plus™ Protein Prestained Standards (Bio-Rad).
- Novex™ Tris-Glycine Mini Protein Gels, 1.0 mm, WedgeWell™ (Thermo Fisher Scientific).
- Invitrogen™ Mini Gel Tank (Thermo Fisher Scientific).

2.2.18 Transfer of protein onto polyvinylidene difluoride (PVDF) membrane

- Invitrogen™ iBlot™ 2 Gel Transfer Device (Thermo Fisher Scientific) for dry blotting.
- iBlot™ 2 Transfer Stacks (Thermo Fisher Scientific) : each stack includes a copper-coated electrode, along with the appropriate cathode and anode buffers embedded within the gel matrix, with an integrated pre-activated PVDF transfer membrane (pore size 0.2 µm) for dry blotting of proteins.

2.2.19 Western blot analysis by chemiluminescence

- Tris-buffered saline-tween (TBS-T): 20 mM Tris; 137 mM NaCl; pH adjusted to 7.6 before adding 0.1% (v/v) Tween-20.
- Blocking solution: 5% (w/v) low-fat dried milk powder in TBS-T.
- Wash buffer/blocking solution: 1% (w/v) low-fat dried milk powder in TBS-T.
- Stripping buffer: 50 mM Tris/HCl (pH 6.8); 2 % SDS and 0.1 M β-mercaptoethanol, made up with dH_2O
- Pierce™ ECL Western Blotting Substrate (Thermo Fisher Scientific):
    - Detection Reagent 1: peroxide solution
    - Detection Reagent 2: Luminol Enhancer Solution
- G:BOX Chemi XX6 (Syngene): a chemiluminescence imaging system.

2.2.20 Isolation of mouse ventricular myocytes

CPVT mice used were heterozygous RYR2-R420Q+/- on a C57BL/6 background originally generated by Ana-Maria Gomez at INSERM (Domingo et al. 2015; Wang et al. 2017). WT littermates were used as controls. Male and female mice were used for experiments.

Mouse Ventricular myocytes were isolated by enzymatic digestion of the heart as described in Zissimopoulos et al. (2025). All cells were obtained from Dr Ewan D. Fowler (School of Biosciences, Cardiff University).

2.2.21 Permeabilisation and preparation of mouse ventricular myocytes

- Permeabilisation solution: 0.05% (w/v) saponin (Sigma-Aldrich) in Milli-Q water.
- Mock intracellular solution: 0.1 M potassium aspartate; 20 mM HEPES; $MgCl_2$ (to attain 1 mM free [Mg^{2+}]); 0.35 mM EGTA; 5 mM Na_2ATP; 10 mM Na_2PCr; $CaCl_2$ (to attain 100 nM free [Ca^{2+}]); pH adjusted to 7.2 with KOH.
- Fluorescently-labelled CaM (F-CaM): labelled using Rhodamine Fast Conjugation kit- Lightning-Link® (Abcam ab188286) as per the manufacturer instructions. F-CaM was a gift from Dr Pavel Kirilenko (School of Biosciences, Cardiff University).
- Fluo-3 pentapotassium (Thermo Fisher Scientific): 5 mM stock stored at -20 °C and used at a concentration of 15 µM in mock intracellular solution.

2.2.22 Coomassie Blue Assay

Coomassie® Brilliant Blue G 250 (SERVA):

- Fixing solution: 10% (v/v) glacial acetic acid and 40% (v/v) EtOH.
- Stock solution I: 0.2% (w/v) Brilliant Blue G in 90% (v/v) EtOH.
- Stock solution II: 20% (v/v) acetic acid.
- Destainer I: same as the fixing solution.
- Destainer II: 10% (v/v) glacial acetic acid and 20% (v/v) EtOH.

2.3 Methods

2.3.1 Transformation and propagation of plasmid DNA:

Due to the large size and fragility of the hRyR2 plasmid DNA, it is prone to spontaneous rearrangements and deletions under nonoptimised conditions. thus, it is not possible to store the plasmids in glycerol stocks for extended period, therefore, fresh transformation and propagation must be carried out using stored plasmid stocks as needed. The bacterial transformation protocol was adjusted to overcome the challenges posed by the large hRyR2 plasmid. This includes the use of lower incubation temperature (≤30 °C), shorter culture duration (≤18 h), and the use of super-competent bacterial cell lines (George et al., 2005; Viero et al., 2012).

eGFP-hRyR2 plasmids were transformed into competent cells; XL10- Gold Ultracompetent Cells (Agilent) and MAX Efficiency Stbl2 Competent Cells (Invitrogen). XL10- Gold cells are designed for cloning large plasmids and ligated DNA with the highest transformation efficiency possible, and therefore were used here for mutant cassette propagation. The Stbl2 cell line, on the other hand, was used to transform WT hRyR2 plasmid at a high yield. The transformation protocol was as follows: plasmid DNA was diluted to 1-10 ng/µL and 2 µL was then added to 50 µL of Stbl2 cells or 45 µL of XL10-Gold cells (pre-treated with beta-mercaptoethanol). The cells were then incubated on ice for 30 mins before heat shocking them at 42 °C for 30 sec for XL10- Gold cells or 25 sec for Stbl2 cells, then returned on ice for 2.5 mins. Following this, 500 µL of SOC medium was added to the cells which were then left to grow in the shaking incubator (225 RPM) for 1 hr at 37 °C. After the incubation, around 150 µL of the solution was spread onto LB_{AMP} agar plates and incubated at 30 °C for at least 24 hrs. On the following day, multiple single colonies were picked using sterile plastic pipette tips and transferred into 5 ml LB_{AMP} broth and incubated in the shaking incubator (225 RPM) for another 18 hrs at 30 °C.

Half of the bacterial culture (~3mL) was centrifuged at 13,000 RPM (~17,900 x *g*) for 1 min to collect the bacterial pellet for use in small-scale plasmid DNA isolation (miniprep) (see **Section 2.3.2**). Meanwhile, the remaining culture was supplemented with 6 mL of LB_{AMP} broth and incubated at 30°C in the shaking incubator (225 RPM) for an additional 8

hrs to promote further growth before large-scale plasmid isolation (maxiprep) (see **Section 2.3.2**).

2.3.2 Small and large-scale plasmid isolation (Miniprep and maxiprep)

Plasmids were extracted from bacterial cultures using the QIAprep® Spin Miniprep Kit (Qiagen) according to manufacturer's instructions as follows:
(all centrifugation steps were carried out at 13,000 RPM (~17,900 x *g*)).

- Bacterial pellets were resuspended in 250 µL buffer P1
- Buffer P2 (250 µL) was added and mixed thoroughly by inverting the tube 4-6 times until the solution becomes clear.
- Buffer N3 (350 µL) was then added and mixed thoroughly by inverting the tube 4-6 times.
- The solution was then centrifuged for 10 mins at 4 °C.
- The supernatant was collected (~ 800 µL) and pipetted onto QIAprep 2.0 spin column and centrifuged for 1 min and the flow-through was discarded.
- The column was then washed by adding 500 µL buffer PB before centrifugation for 1 min and the flow-through was discarded.
- The column was washed again by adding 750 µL buffer PE before centrifugation for 1 min and the flow-through was discarded.
- The column was centrifuged for another 1 mins to remove any residual wash buffer and the flow-through was discarded.
- The DNA was then eluted by placing the column in a clean 1.5 mL Eppendorf and adding 50 µL dH_2O. the column was left to stand for 1 min before centrifugation for 1 min to collect the flow-through containing plasmid DNA.

Plasmids were verified by restriction digest (see **Section 2.3.3**), and chosen cultures were then seeded into 200-400 ml LB_{AMP} broth flasks at 1:200 dilution and incubated in the shaking incubator (225 RPM) for no longer than 18 hrs at 30 °C. The cultures were then pelleted at 6000 RPM, 4 °C for 15 mins using a JLA16.250 fixed-angle rotor (Avanti J-25, Beckman) and the plasmid DNA was then extracted and purified using the HiSpeed®

Plasmid Maxi Kit (Qiagen) according to manufacturer's instructions as follows:

- Bacterial pellets were resuspended in 10 mL buffer P1.
- Buffer P2 (10 mL) was then added and mixed by inverting 4-6 times. The mixture was incubated at room temperature for 5 mins
- After incubation, 10 mL pre-chilled buffer P3 was added and mixed thoroughly by inverting 4-6 times.
- The lysate was then transferred into QIAfilter cartridge (with the cap screwed onto the outlet nozzle) and left to incubate at room temperature for 10 mins.
- Meanwhile, the HiSpeed® Tip was equilibrated with 10 mL buffer QBT, allowing it to enter the resin.
- The cap was then removed from the QIAfilter cartridge outlet nozzle and the plunger was gently inserted into the cartridge and the cell lysate was filtered into the equilibrated HiSpeed® Tip using constant pressure.
- After the lysate has entered, the HiSpeed® Tip was washed with 60 mL buffer QC.
- The DNA was then eluted with 15 mL buffer QF in a sterile collection tube.
- The DNA was then precipitated by adding 10.5 mL isopropanol, mixing by inversion and leaving the mixture to incubate for 5 mins at toom temperature.
- Meanwhile, a QIAprecipitator Module was attached onto the outlet nozzle of a sterile 30 mL syringe (with the plunger removed).
- The QIAprecipitator was then placed over a waster bottle and the elute-isopropanol mixture was then transferred into the syringe. The plunger was then inserted and the mixture was filtered through the QIAprecipitator using constant pressure.
- The QIAprecipitator was then removed from the syringe and the plunger was pulled out before re-attaching the QIAprecipitator and adding 2 mL 70% (v/v) ethanol to the syringe to wash the DNA by inserting the plunger and pressing the ethanol through the QIAprecipitator.
- The QIAprecipitator was removed and the plunger removed before re-attaching the QIAprecipitator, inserting the plunger and pressing air through the QIAprecipitator forcefully to dry the membrane. (this step was repeated multiple times)

- The QIAprecipitator was removed and attached to a sterile 5 mL syringe (with the plunger removed) before adding 500 µL warm DNAse-free water to the 5 mL syringe and inserting the plunger to elute the DNA through into a clean Eppendorf using constant pressure.

The plasmid DNA was then quantified using the BioMate 3S Spectrophotometer (Thermo) and verified again by restriction digest. Sequence confirmation was carried out by Eurofins Genomics' TubeSeq service using 50-100 ng/µL of purified plasmid DNA from each construct, with oligonucleotide primers spanning the mutation site and restriction sites, as detailed in **Table 4.4**.

2.3.3 Restriction digest for verification and agarose gel electrophoresis

To verify WT and mutant hRyR2 plasmids, restriction enzymes were utilised to cleave the plasmid DNA, creating unique fragment patterns that served as molecular fingerprints for identification. Potential restriction sites within the hRyR2 sequence were identified using the NEBcutter® 3.0.19 tool, which produces a virtual restriction digest pattern to compare against experimental results (see **Figure 2.1**). Restriction digests were carried out at two check points during plasmid propagation; the first was to verify miniprep clones, and the second was to verify plasmids following maxiprep. Only plasmids that produced fragments of the correct molecular weight were selected for propagation.

For restriction digest, 1 µg of the DNA plasmid was treated with 0.5 µL (5 units) of the FastDigest enzyme (*EcoRI*, *BglII* or *HindIII*), and 2 µL of 10x Universal FastDigest buffer and made up to 20 µL with dH_2O. Following a 30-min incubation at 37 °C in a water bath, the digest products were mixed with 10 µL of 1x DNA loading buffer and loaded on 1% (w/v) agarose gel alongside 1 kb DNA marker and separated according to their molecular weight by electrophoresis.

A 1% (w/v) agarose gel was made by mixing agarose powder with 1x TAE buffer, then the mixture was heated in the microwave in short intervals (swirling in between), until the agarose is fully dissolved. Once dissolved, the agarose solution was cooled to ~50 °C before adding UltraPure™ Ethidium Bromide to achieve a final concentration of 0.1

µg/mL. the mixture was poured into a Bio-Rad Mini-Sub® gel tray with well comb. Once it solidifies, each gel was then placed in a Bio-Rad tank and covered with 1x TAE buffer.

Electrophoresis was carried out under a constant voltage of 100 V for 45 mins- 1 hour. The separated DNA fragments stained with ethidium bromide were visualized under UV light using the G:BOX Chemi XX6 (Syngene) chemiluminescence imaging system.

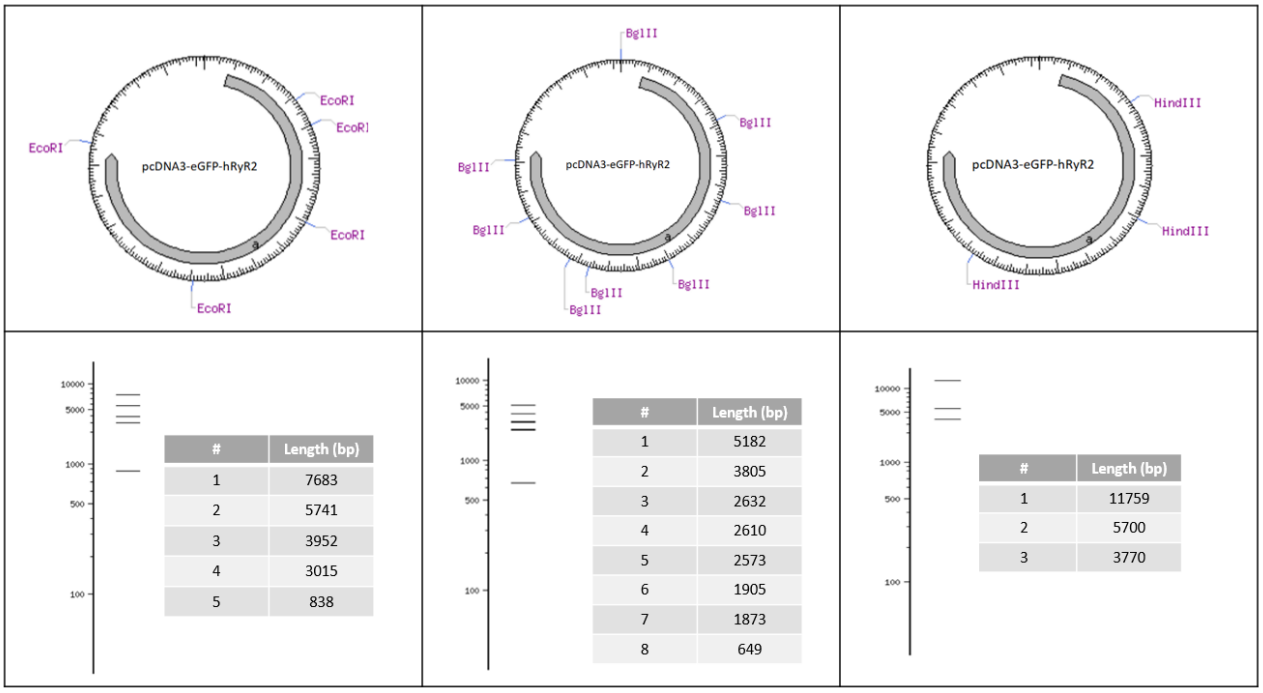

Figure 2.1. Representation of the expected hRyR2 cutting pattern and fragments length produced by *EcoRI*, *BglII* and *HindIII* restriction enzymes. The cutting pattern gives a "fingerprint" that distinguishes and identifies hRyR2. While *BglII* digest theoretically produces 8 fragments, only 5 distinct bands could be observed experimentally because fragment pairs 3/4 and 6/7 have very similar length, making them unresolvable by agarose gel electrophoresis. Digests obtained from NEBcutter® 3.0.19.

2.3.4 HEK293 cell culture and maintenance

HEK293 cell line was utilised to express hRyR2 plasmids. All cell culture work took place in HEPA-filtered, class II laminar flow containment hoods, in a tissue culture laboratory. The cells were grown in T75 culture flasks with filter caps in cDMEM and kept in a humid cell culture incubator at 37 °C and gassed with 5% CO_2.

Regular subculture (passaging) of HEK293 cells was necessary to sustain a viable

monolayer of cells and avoid over-confluency and subsequent cell death. Cells were passaged when the monolayer approached ~80 % confluency; typically twice weekly. In doing so, the cells were rinsed with 10mL of PBS solution and then detached from the culture flasks using 2 mL of trypsin. Once detached, enzyme activity was neutralised by adding 10 mL of cDMEM and cells were centrifuged at 1000 RPM for 5 mins. The supernatant was discarded and the pellet of cells was gently resuspended in 10mL cDMEM and seeded in an appropriate concentration into new flasks. If cell quantification was required, e.g., prior to transfection, cell numbers were calculated before centrifugation using a hemocytometer slide under light microscopy (Hawksley).

When cells were not required for further experiments, they could be cryopreserved at -80 °C for future use. For freezing, cells from a confluent flask were pelleted, resuspended in approximately 4.5 mL of freezing medium (10% (v/v) DMSO in FBS, filter-sterilised), and aliquoted into 1.5 mL tubes.

2.3.5 Effectene transfection of HEK293

Transfection with Effectene reagent transfection kit (Qiagen) was used to introduce the hRyR2 and CaM plasmids into the cells for live cell imaging and IF. This method of transfection was selected due to its reduced cytotoxicity and high efficiency. Its lipid-based formulation minimises cytotoxicity and cell death, offering a gentler alternative to harsher methods like $CaPO_4$ transfection. In addition, Effectene delivers consistently high transfection efficiency, as its standardized protocol eliminates variability associated with pH sensitivity, precipitate size, and timing; which are common limitations of $CaPO_4$ transfection.

For live-cell imaging, HEK293 cells ($1x10^5$) suspended in cDMEM (200 µL) were seeded, as a meniscus, onto 35mm poly-lysine coated glass-bottomed chambers, whereas for IF, cells were seeded in 6-well plates at a density of $8x10^5$ cells per well. Following this, cells were incubated for 4 hours at 37 °C and 5% CO_2 before flooding the coverslips/wells with 2 mL cDMEM before being returned to the incubator. After overnight incubation, Effectene transfection was carried out the next day for eight coverslips (live-cell) or one

well (IF) according to manufacturer's instructions as follows:

- Plasmid DNA (0.8 µg in total) was made up to 100 µL with buffer EC. For double transfection with both RyR2 and CaM, total DNA amount was 0.8 µg and a 1:2 molar ratio was used.
- Enhancer (6.4 µL) was then added to the solution (8 X 0.8 µg), mixed by vortex for 10 sec and then incubated at room temperature for 5 mins.
- Effectene (20 µL) was then added to the solution, mixed by vortex for 10 sec and then incubated at room temperature for 10 mins.
- In the meantime, the medium was removed from each coverslip/well, and the cells were washed with PBS and 200 µL of cDMEM was added to each coverslip meniscus/well.
- After the 10 mins, 600 µL of cDMEM was added to the solution and mixed by pipetting up and down twice and a 100 µL was then seeded into each coverslip drop by drop (live cell), or the whole reaction mixture was added to a single well (IF). The coverslips/plates were then returned to the incubator for 16 hours before flooding with 2 mL of cDMEM.

2.3.6 $CaPO_4$ transfection of HEK293

$CaPO_4$ transfection was used to introduce hRyR2 and CaM plasmids into HEK293 cells. $CaPO_4$ transfection gives a high level of protein expression suitable to quantify by Western Blot, which cannot be achieved by Effectene transfection which yields low protein expression that keeps the cells viable to allow us to image them. The cells were seeded on 10 cm^2 petri dishes at a $1.5x10^6$ cell/dish density and incubated for 24 hours in 10 mL cDMEM at 37 °C and 5% CO_2, to allow for growth to ~75% confluency. Plasmid DNA (12 µg/dish) was mixed with 124 mM $CaCl_2$ solution (pH 7) and dH_2O to a volume of 500 µL. the DNA solution was added dropwise to 500 µL of warmed 2x HBS (pH 7.05) with continuous vortexing. This was then incubated at RT for 20 mins to allow a fine precipitate to form, which is essential for DNA endocytosis. After this, the suspension was vortexed and 1mL added dropwise to each dish before incubation for 24 hours at 37 °C and 5% CO_2. Protein expression was upregulated using 2 mM NaB (Gorman et al. 1983) 24 hours prior to assessment of transfection efficiency using fluorescence microscopy and

collection by centrifugation at 1000 RPM for 5 mins before storage at -80 °C.

2.3.7 Cell homogenate preparation from transfected HEK293

Cell homogenate was used for western blotting to determine hRyR2 and CaM expression levels, and to ascertain hRyR2 phosphorylation levels in the presence of WT or mutant CaM. Transfected HEK293 cells (produced as described in **Section 2.3.6**) were thawed and resuspended in hypo-osmotic buffer (50 µL per 10^6 cells) containing 1 % (v/v) Triton-X-100 on ice to rupture the cells by osmotic stress. Cells were then passed through a 23G needle 25 times in order to homogenise them. After this, cells were subjected to 5 freeze-thaw-sonication cycles using liquid nitrogen and a sonicator waterbath (Decon F5100b sonicator, Decon laboratories Ltd) followed by centrifugation at 1000 xg for 5 mins at 4 °C to pellet cell nuclei and remove the supernatant which contains the cell homogenate. The cell homogenate was aliquoted into appropriate volumes, snap-frozen with liquid nitrogen before storing at -80 °C.

2.3.8 Protein assay for quantification

Protein concentration of each cell homogenate samples and microsomal fractions was estimated using Pierce™ BCA Assay Kit (Thermo Fisher Scientific) according to manufacturer's instructions. This method is based on the biuret reaction with enhanced sensitivity due to bicinchoninic acid (BCA). In an alkaline environment (provided by the BCA reagent), the peptide bonds in proteins reduce Cu^{2+} to Cu^{+}. BCA then binds to Cu^{+} forming a purple-coloured complex. The intensity of this colour is directly proportional to protein concentration, and its absorbance of light at wavelength of 562 nm was measured using Tecan Infinite 200 Pro Plate Reader following manufacturer's instructions.

Cell homogenate samples were diluted 1:50, 1:100 and 1:200 (in duplicates), and a set of albumin protein standards dilutions were prepared for the plotting of a standard curve of absorbance vs. protein concentration (µg/mL) (see **Figure 2.2**). Sample protein concentration could then be estimated from the standard curve, using the polynomial equation $y=ax^2+bx+c$ of the standard curve.

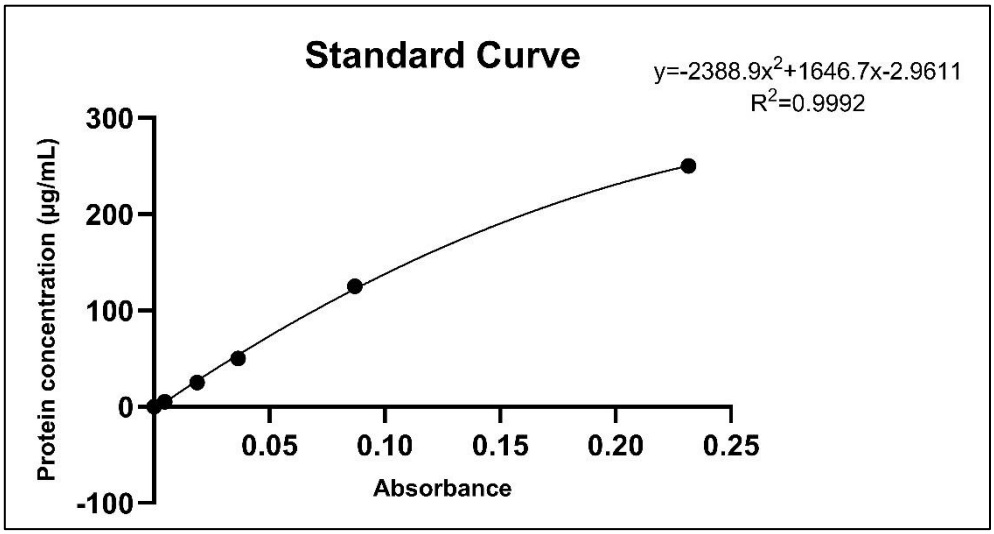

Figure 2.2. Example of a standard curve for protein assay. A set of six albumin protein standards were prepared and their measured absorbance at 562 nm was used to plot the standard curve. The polynomial equation of the standard curve was then used to measure sample protein concentration.

2.3.9 Preparation of mixed membranes from transfected HEK293 cells

As RyR2 is a membrane protein, initial isolation of the membrane fraction from cellular components is required before proceeding with solubilisation and subsequent purification of the channel. Transfected cell pellets (produced as described in **Section 2.3.6**) were thawed and resuspended in hypo-osmotic buffer on ice (1 mL for every 10^6 cells) to rupture the cells by osmotic pressure. Cells were then passed through a 23G needle 25 times on ice in order to disrupt the cells before low-speed centrifugation at 1500 xg for 10 mins at 4 °C to discard the pellets containing unbroken cells, cell debris and nuclei. A small known volume of the supernatant was taken out for use in protein assay to estimate protein concentration. Microsomal membranes were collected by high-speed centrifugation of the supernatant at 100,000 g (28,000 RPM) for 1 hour at 4 °C in a Beckman Optima Ultracentrifuge. The pellets, containing microsomal material, were kept on ice ready for solubilisation and purification (see **Section 2.3.10**), while the small pellet was resuspended in 500 µL resuspension buffer using a dounce homogeniser and used in BCA protein assay; as outlined in **Section 2.3.8**.

2.3.10 Purification of recombinant eGFP-hRyR2 from microsomal material

The hRyR2 channels were purified and isolated from the mixed membrane preparation (produced as described in **2.3.9**) by first solubilising the protein with detergent-lipid mixture, followed by separation of the solubilised membrane proteins using density gradient ultracentrifugation.

Following protein quantification, pellets containing microsomal material were resuspended at a concentration of 2.5 mg/mL in high-salt solubilisation buffer, and left to solubilise on ice for one hour while stirring before centrifugation at 16,000 g (11,500 RPM) for 30 mins at 4 °C to pellet any insoluble protein. The supernatant obtained after centrifugation was then gently loaded onto a continuous sucrose density gradient. To prepare the sucrose gradient, 5%, 25% and 40% (w/w) sucrose in gradient buffer were allowed to mix on rotary agitator for one hour at 4 °C. A sucrose density gradient was formed in centrifugation tubes using a gradient maker connected to a peristaltic pump. The gradient was made by gradually diluting the 25% sucrose solution with the 5% sucrose solution on a 5 mL cushion of 40% sucrose. The gradient tubes were gently placed inside a pre-chilled rotor without disturbing the gradient and centrifuged at 100,000 g for 18 hours at 4 °C.

On the following day, 1 mL fractions were carefully collected from the top of the gradient, and sucrose density of each fraction was measured using a refractometer to identify the fractions with 26-30% sucrose, which is where hRyR2 is expected to reside. All desired fraction were aliquoted into 5 µL and snap-frozen in liquid nitrogen before storing at -80 °C.

2.3.11 SDS/PAGE and western blotting

eGFP-hRyR2 and CaM expression and/or phosphorylation levels were assessed using Western blotting. Cell homogenate samples (prepared as described in **Section 2.3.7**) were run on an SDS-PAGE gels to separate proteins by molecular weight. Cell homogenate samples were prepared by mixing in a 1:1 ratio with 2x Laemmli sample buffer. Samples were then heated at 42 °C for 20 mins before loading into a precast Tris-glycine gel (Thermo Fisher Scientific) of appropriate fixed or gradient concentration,

along with Precision Plus Protein Kaleidoscope marker (Bio-Rad). The gel was run at 100 V in Invitrogen™ mini gel tank in SDS-PAGE running buffer for approximately 90 mins, or until the dye front reaches the bottom of the gel. Following SDS-PAGE, proteins were transferred onto PVDF membrane using the iBLOT™ 2 dry blotting system (Invitrogen) and specialised transfer stacks according to manufacturer's instructions. The blotting voltage and time were optomised for each protein according to their molecular weight as following:

- RyR2 probing: 25 V for 6 mins.
- CaM probing: 20 V for 1 min followed by 23 V for 3 mins, then 25 V for 1 min.
- CaMKII probing: 20 V for 1 min followed by 23 V for 4 mins, then 25 V for 2 mins.

PVDF membranes were blocked overnight at 4 °C with 5 % (w/v) blocking solution. Primary antibodies were prepared in 1% blocking solution at the appropriate dilution (as detailed in the methods section of relevant chapters) and incubated with the membrane for 2 hours at RT on a rocker. The membranes were then washed three times with 1% blocking solution for 5 mins each on the rocker to remove unbound primary antibodies before the addition of secondary antibodies at 1:10,000 dilution in 1% blocking solution, and incubation at RT for 90 mins on the rocker. Membranes were then washed five times with TBS-T for 5 mins each on the rocker to remove remaining antibody and blocking solution. ECL reagent (Pierce) was used according to manufacturer's instructions. Briefly, equal volumes of detection reagent 1 and detection reagent 2 (500 µL each per membrane) were combined before adding the mixture on the membrane. The mixture was applied evenly across the entire membrane surface. Following a 1-min incubation, excess solution was drained and immunoreactive protein bands were detected using a G-Box Chemi XX6 gel documentation system (Syngene).

When membrane stripping of antibodies was required, membranes were placed in a tube containing 50 mL pre-warmed stripping buffer and incubated in a water bath set at 50 °C for 10 mins in a fume cupboard. Following this, membranes were washed 3 times with excess TBS-T for 5 mins each, before blocking with 5% blocking solution overnight.

Densitometric analysis of Western blots was carried out in Fiji ImageJ software. For each sample lane, the raw value of the protein of interest was divided by the raw value of its

corresponding loading control. This corrected for any differences in protein loading or transfer. Information of densitometric analysis for each experiment are detailed in the methods section of each chapter.

2.3.12 Coomassie Brilliant Blue gel staining

In order to confirm the presence and purity of CaM mutant proteins obtained from our collaborators, Coomassie Brilliant Blue G (SERVA) was used according to manufacturer's instructions following SDS/PAGE as described in **Section 2.3.11**

Following electrophoresis, gels were fixed for 30 mins in 100 mL of fixing solution. Immediately before use, a staining solution was prepared by mixing 50 mL each of stock solutions I and II. Gels were then stained in this mixture for 20 mins. For destaining, gels were initially incubated in destainer I 5 mins for rapid background removal, followed by extended destaining in destainer II until optimal contrast was achieved (monitored visually). Finally, gels were rinsed twice with dH_2O (5 mins per wash) before imagine using a G-Box Chemi XX6 gel documentation system (Syngene).

Chapter 3: Characterisation of spontaneous global Ca^{2+} release in HEK293 co-expressing hRyR2 and variant CaM

3.1 Introduction

3.1.1 Recombinant co-expression of hRyR2 and CaM variants in HEK293 cells

To investigate the influence of CPVT-linked CaM mutants (D132E and Q136P) on RyR2 function, a recombinant approach was employed in which RyR2 was co-expressed with either WT or mutant CaM in a mammalian HEK293 cell system. This system was selected over cardiac myocytes, where the introduction of specific CaM variants is technically challenging, requiring viral transduction or permeabilisation. The HEK293 cell line was chosen for its well-established use in characterising RyR2 function because the cells do not endogenously express RyR2, but are capable of expressing functional RyR2 tetramers at high levels upon transfection. While HEK293 cells do express low levels of endogenous CaM, by transfecting the cells, the desired CaM variant (WT or mutant) is over-expressed, thus any observed change in function could be attributed to the introduced construct.

The use of a mammalian expression system also offers advantages for this work because they are capable of performing native post-translation modifications such as glycosylation which is essential for junctional SR trafficking. Additionally, mammalian cells provide a physiologically relevant environment for protein assembly, enabling proper subunit interactions, oligomerisation, and functional complex formation (Hopkins et al., 2012; Kiarash et al., 2004). While HEK293 cells lack certain cardiac-specific features such as contractile machinery, t-tubules and some RyR2 regulators (*e.g.,* FKBP12.6, junctin and calsequestrin), which may simplify the regulatory environment around recombinant RyR2, they express CaMKII endogenously; a key signalling component to our research. This would allow the study of CaMKII phosphorylation of RyR2 as well as the direct effect of CaM on channel function.

3.1.2 RyR2 expression levels and trafficking defects in arrhythmogenesis

Given the important role of RyR2 expression level in modulating Ca^{2+} release dynamics, it is essential to quantify and account for RyR2 abundance in all co-expression experiments. There is evidence suggesting that decreased expression of RyR2 is seen in

some forms of heart disease including heart failure and arrhythmia (Cerrone et al., 2017; Houser et al., 2000). For instance, previous work by Y. Liu et al. (2017)demonstrated that the CPVT-linked G357S mutation of RyR2 reduced RyR2 protein expression in HEK293 cells. Similarly, Tester et al. (2020) reported that loss-of-function RyR2 mutations leading to lower RyR2 expression diminished cardiomyocyte responsiveness to caffeine and β-adrenergic stimulation in induced pluripotent stem cell-derived cardiomyocytes (iPSC-CMs). Additionally, Ai et al. (2005) observed a 30% decrease in RyR2 protein and a 50% reduction in RyR2-mRNA levels in failing hearts. More recently, Nikolaienko et al. (2024) showed that RyR2 density within release clusters impacts CICR dynamics, with higher expression levels increasing the probability of Ca^{2+} sparks and waves. Together, these findings highlight the importance of assessing RyR2 expression level following transfection, not only because it is a key variable in experimental models, but also a potential modulator of disease.

Proper intracellular trafficking of recombinant hRyR2 tetramers to the ER is another important factor to assess post-transfection, as defective protein trafficking is a well-documented mechanism underlying aberrant ion channel function in inherited arrhythmia syndromes. For instance, in LQTS, certain K^+ channel mutations interfere with membrane localisation rather than channel gating or conductance, a behaviour termed “defective intracellular trafficking” (Delisle et al., 2004; Ruan et al., 2008). Similarly, in Brugada syndrome, some trafficking-defective Na^+ channel mutations have been reported (Pérez-Hernández et al., 2018).

CaM has been shown to regulate the intracellular trafficking of various ion channels, including trafficking of $Ca_V1.2$ Ca^{2+} channels in neuronal tissue (H. G. Wang et al., 2007), the trafficking of the renal Ca^{2+} channel, TRPV5, to the ER (Zuidscherwoude et al., 2024), and the membrane trafficking of small-conductance Ca^{2+}-activated K^+ (SK) channels (Heijman et al., 2023; Maylie et al., 2003). Notably, the CPVT-linked N54I CaM variant was shown to cause incorrect membrane trafficking of SK3 channels in Madin-Darby canine kidney (MDCK) cells co-expressing SK3 and N54I CaM, leading to a significant reduction in channel current (Saljic et al., 2019). Therefore, the potential impact of D132E and Q136P CaM mutants on RyR2 channel trafficking to the ER will be investigated in HEK293

cells as a possible disease mechanism.

3.1.3 Live-cell Ca^{2+} imaging in HEK293

HEK293 cells provide a physiologically relevant environment for recombinant expression of hRyR2 and CaM for functional studies. Although lacking the contractile machinery, HEK293 expressing recombinant RyR2 will exhibit SOICR (Jiang et al., 2004; Xiao et al., 2007). When the ER Ca^{2+} content reaches an activation threshold, SOICR is triggered in HEK293 cells, the same way observed in cardiomyocytes, and spontaneous Ca^{2+} release in the form of oscillations occurs in the absence of membrane depolarisation. Ca^{2+} release is stopped when ER Ca^{2+} content reaches a termination threshold (Jiang et al., 2004, 2005). These Ca^{2+} oscillations could therefore be analysed to provide valuable information on RyR2 channel function.

This technique has been employed in the literature to characterise the functional impact of CaM mutations on RyR2-mediated Ca^{2+} release. In permeabilised HEK293 cells expressing murine RyR2, mutant D132E and Q136P CaM have been shown to decrease activation and termination thresholds during SOICR using the genetically encoded D1ER ER luminal Ca^{2+} indicator (Søndergaard et al., 2019). Additionally, previous work with our collaborators showed that two CPVT-linked CaM mutants A103V and N54I affected Ca^{2+} oscillations in HEK293 co-expressing hRyR2 and these variant CaMs. These CaM mutants showed a loss of inhibitory action on RyR2 channels, causing changes in the Ca^{2+} release dynamics (significantly increasing Ca^{2+} release duration and thus decreasing frequency of release) (Prakash et al., 2022). The effect of D132E and Q136P CaM mutations on spontaneous RyR2-mediated Ca^{2+} oscillation dynamics has not been investigated before, thus live-cell Ca^{2+} imaging in transfected HEK293 cells was carried out to characterise the functional impact of these mutations on RyR2. In these experiments, a cytosolic acetoxymethyl (AM)-conjugated CalBryte 520 Ca^{2+} indicator was selected for its high sensitivity and temporal resolution, which is ideal for detecting small, rapid calcium transients. CalBryte 520 also shows low resting fluorescence and high signal-to-noise ratio. Once inside the cell, intracellular esterases cleave the AM group of the dye, converting the non-fluorescent, lipophilic AM ester into a charged,

fluorescent indicator (Lock et al., 2015).

3.1.4 Chapter aims and objectives

There is growing evidence to suggest that pathogenic CaM variants are associated with arrhythmogenic Ca^{2+} release through dysregulation of RyR2 function (Hwang et al., 2014). This chapter aims to characterise the functional impact of D132E and Q136P variant CaM on spontaneous global Ca^{2+} fluxes using confocal live-cell Ca^{2+} imaging in a mammalian cell system. Using the same system, the impact of variant CaM on RyR2 expression level and channel intracellular trafficking to the ER will be assessed.

Key objectives:

- Establish a heterologous expression system by co-expressing hRyR2 with either WT or mutant D132E or Q136P CaM proteins in HEK293 cells using transient transfection.
- Assess hRyR2 and CaM transfection efficiencies in HEK293 cells to confirm consistent expression level between experiments.
- Estimate hRyR2 and CaM protein expression levels by western blotting cell homogenates of HEK293 cells co-transfected with hRyR2 and WT or variant CaM to assess potential effects of co-transfection on protein expression level which could have an impact on function.
- Assess hRyR2 channels' intracellular localisation in HEK293 cells co-expressing WT or variant CaM in IF experiments to determine whether CaM variants affect RyR2 channel intracellular trafficking to the ER, which could affect function.
- Assess the effect of D132E and Q136P CaM mutants on global Ca^{2+} release dynamics using live-cell Ca^{2+} imaging of HEK293 co-transfected with hRyR2 and mutant CaMs in comparison to those co-expressing WT CaM.
- Evaluate the impact of variant CaM on ER Ca^{2+} content of HEK293 co-expressing hRyR2 and D132E or Q136P CaM compared to those co-expressing WT CaM using the amplitude of Ca^{2+} release in response to a maximal caffeine concentration (10 mM) as an indicator of ER store load, thereby determining if any functional effects of these mutants are linked to altered ER Ca^{2+} content.

3.2 Methods

3.2.1 HEK293 cell transfection and loading for Ca^{2+} imaging

Effectene-mediated HEK293 cell transfection with eGFP-RyR2 and dTomato-CaM (WT or mutant D132E or Q136P) plasmid DNA was carried out as described in **Section 2.3.5**. Standard HEK293 cell culture and maintenance protocols were followed (see **Section 2.3.4**). On the day of imaging (48 hours post-transfection), transfected cells were first imaged using confocal microscopy to calculate transfection efficiencies prior to dye loading for Ca^{2+} imaging experiments. The Ca^{2+}-sensitive dye CalBryte™ 520 AM was prepared by resuspending the lyophilised indicator (50 µg) in 20% (w/v) Pluronic F-127 in DMSO. This stock solution was then diluted 1:300 in minimal DMEM and added to the culture media to achieve a 10 µM final concentration.

To load the cells, the culture media was first removed from the Mattek dishes and the edges were wiped with clean tissue to ensure a good meniscus formation during subsequent steps. A 200 µL volume of the dye mix was added to each Mattek dish and incubated at 30 °C for 45-60 mins. After this, the Mattek dishes were gently flooded with 2 mL of minimal DMEM and allowed to de-esterify in the incubator for 10 mins. Following de-esterification, the media surrounding the cells was removed, and 200 µL meniscus of KRH buffer containing 1.3 mM Ca^{2+} was added to each Mattek dish ready for imaging. The cells were loaded in batches of two-three dishes at a time as dye compartmentalisation typically occurs approximately one hour after de-esterification.

The ER Ca^{2+} load in transfected HEK293 cells was measured by the careful addition of a caffeine bolus (50 mM stock in KRH) to the cell medium during recording to achieve a final concentration of 10 mM around the cells, thus achieving maximal activation of all expressed RyR2 channels without disturbing the meniscus.

3.2.2 Calculation of transfection efficiency

HEK293 cells expressing hRyR2 were identified by visualisation of eGFP fluorescence, while cells expressing CaM were detected by visualisation of the dTomato fluorescence. Transfection efficiency in a field of view (FoV) was calculated by counting the total

number of cells in the bright-field image, and then quantifying the green (hRyR2-expressing) and red (CaM-expressing) cells within the same FoV. To assess co-expression in a FoV, fluorescence images were overlaid, and cells exhibiting both eGFP and dTomato signals (appearing yellow) were counted. The percentage of co-transfected cells was then calculated relative to the total cell count in the FoV.

3.2.3 Confocal microscopy for live-cell HEK293 imaging

Live-cell HEK293 cell imaging was carried out using the Leica SP5 laser scanning confocal microscope with a 20x objective lens. Data were acquired and analysed using the Leica LAS-AF software at 512 x 512 pixel resolution and at a rate of 5 frames per second for 360 seconds, with the addition of 10 mM caffeine in the final 60 seconds to measure ER Ca^{2+} load.

The CalBryte 520 dye is excited by argon laser line at 488 nm and emitted fluorescence was detected at 500-550 nm range. Due to spectral overlap between CalBryte 520 and dTomato, which is excited by helium-neon (HeNe) laser line at 543 nm with an emission range of 560-600 nm, fluorescence bleed-through was an issue when trying to identify CaM-expressing cells. A specific protocol was implemented to overcome this in co-transfection experiments:

1. A FoV was selected.
2. With the argon laser (488 nm) turned off, the HeNe (543 nm) laser was used to excite dTomato and identify CaM-expressing cells.
3. Regions of interest (ROIs) were drawn around these CaM-expressing cells and saved within the software.
4. The HeNe laser was then turned down to 0 V, and the argon laser was turned on to excite CalBryte 520, and the 360-second Ca^{2+} recording was initiated.
5. The pre-defined ROIs were then applied to the recording to exclusively analyse Ca^{2+} signals from the identified CaM-expressing cells (see **Figure 3.1**).

HEK293 cells expressing CaM but not RyR2 do not exhibit Ca^{2+} oscillations. Notably, some HEK293 cells that co-express CaM and RyR2 would not spontaneously oscillate. However, in these cells, the presence of functional RyR2 channels was confirmed via

their caffeine-induced Ca^{2+} release (see **Figure 3.1**)

For experiments involving transfection with RyR2 alone, ROIs were selected based on functional activity. This is because the eGFP fluorescence of RyR2 cannot be seen when the cells are loaded with CalBryte 520 (*i.e.,* all cells in the FoV appear green). Therefore, RyR2-expressing cells could only be identified by their spontaneous Ca^{2+} oscillations or their caffeine-induced Ca^{2+} release.

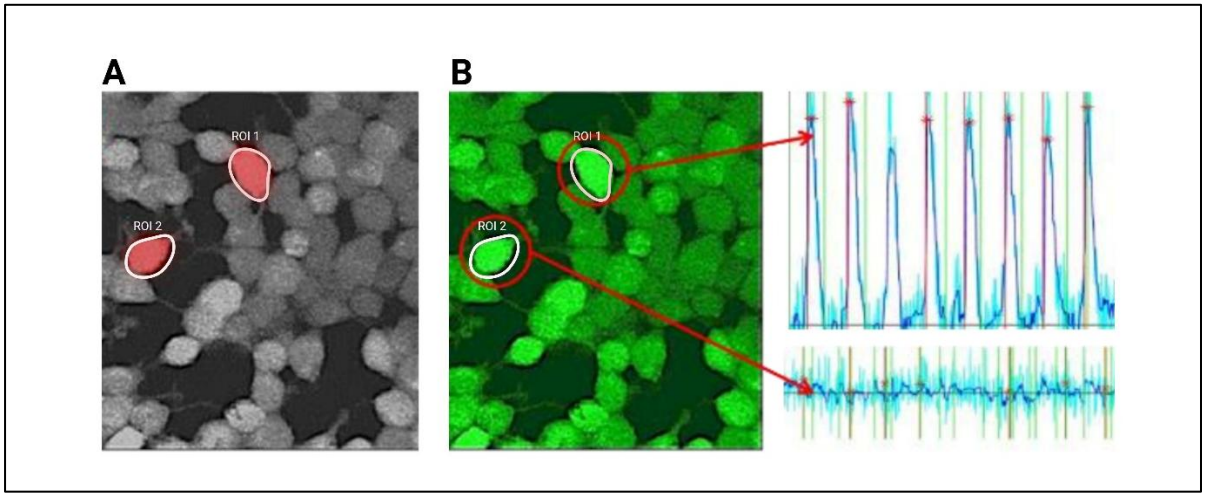

Figure 3.1. Illustration of how Ca^{2+} imaging results were acquired from HEK293 cells co-transfected with CaM and RyR2. (A) Shows two ROIs identified in a FoV as CaM-expressing cells via HeNe laser excitation of dTomato fluorescence, while argon laser was switched off to prevent bleed-through fluorescence. **(B)** Shows the same FoV imaged with argon laser switched on to excite the Ca^{2+} indicator Calbryte 520. Fluorescence was collected at 500-550 nm to detect Ca^{2+} oscillation in HEK293 cells. The pre-defined ROIs from A were then applied to the recording to analyse Ca^{2+} signals from CaM-expressing cells. ROI 1 exhibits spontaneous Ca^{2+} oscillations, indicating the presence of RyR2 channels, while ROI 2 did not oscillate suggesting either lack of RyR2 expression, or expression RyR2 channels that do not spontaneously oscillate.

3.2.4 Data processing and analysis

Analysis of the live-cell Ca^{2+} imaging results was carried out using AnalyseSpikes MatLab applet (created by Dr Aled Jones, Queen Mary University of London (Prakash et al., 2022) and GraphPad Prism 10.4.2. Different parameters were measured to characterise spatiotemporal patterns of Ca^{2+} release including transient amplitude, rise and fall rates, signal duration and inter-transient interval, as illustrated in **Figure 3.2**.

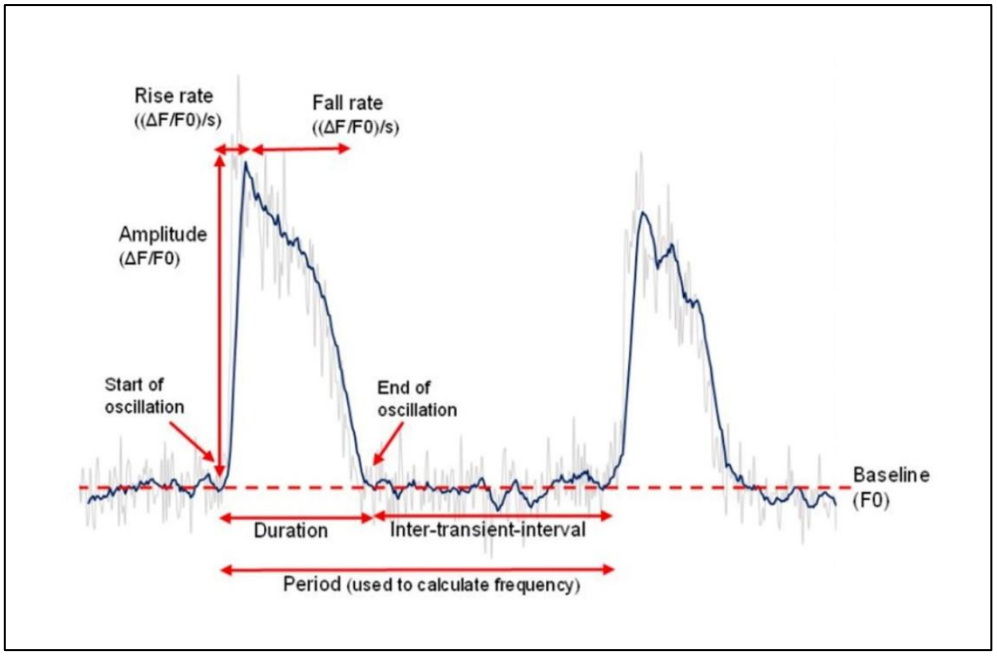

Figure 3.2. Parameters used to characterise Ca^{2+} release events in RyR2-transfected HEK293 cells. Analysis of the results was carried out using AnalyseSpikes Matlab-based applet (Prakash et al., 2022).

The parameters used in Ca^{2+} release characterisation are as follows:

- Baseline (F_0): represents the basal signal intensity measured by calculating the average of fluorescence intensities between Ca^{2+} release events; shown as dashed line in **Figure 3.2**.
- Amplitude ($\Delta F/F_0$): represents the amplitude of a Ca^{2+} release event following RyR2 activation, measure by subtracting the basal signal intensity (F_0) from the peak signal intensity (F), and expressed as a proportion of the basal signal intensity.
- Duration (seconds): represents the duration of each Ca^{2+} oscillation, measured by calculating the difference between the time at which the Ca^{2+} oscillation was initiated and the time at which the signal intensity returned to basal level (F_0).
- Inter-transient interval (seconds): represents the time duration between the end of a Ca^{2+} release oscillation event and the start of a new oscillation.
- Frequency (events/min): represents the number of "periods" per minute, where a period represents the Ca^{2+} release event duration and the inter-transient duration added together.
- Rise rate ($(\Delta F/F_0)/s$): represents the rate of Ca^{2+} release, measured as the change

in signal intensity from the baseline (F_0) to peak signal intensity (F) divided by the time duration at which this occurred.

- Fall rate (($\Delta F/F_0$)/s): represents the rate of Ca^{2+} signal decay, measured as the change in signal intensity from the peak (F) to baseline signal intensity (F_0) divided by the time duration at which this occurred.

3.2.5 Fixing and preparation of cells for IF

IF imaging was used to investigate the effect of WT or mutant CaM co-expression on RyR2 intracellular localisation. HEK293 cells were first co-transfected with hRyR2 and CaM plasmids using Effectene transfection reagent, as described in **Section 2.3.5**. All further incubations were done at room temperature under a foil wrapper to prevent fluorescence bleaching, and all washes were done on a rocker. The cells were washed three times with PBS and fixed with 4% (v/v) paraformaldehyde in PBS for 15 mins. Cells were then washed and rehydrated with PBS for at least 1 hour. Following rehydration, cells were washed with PBS and permeabilised with 0.1% (v/v) Triton® X-100 in PBS for 30 mins at room temperature in the dark before washing again with PBS. After this, cells were blocked with 10% (v/v) FBS in PBS for another 30 mins to prevent non-specific immune-reactivity, then washed with PBS. The cells were then incubated with Anti-CaM primary mouse antibody (Sigma-Aldrich C3545, 1:150) in 150 µL meniscus for 90 mins. Following this, cells were washed three times, 10 mins each, with PBS before incubation with chicken anti-mouse Alexa Fluor™ 647 cross-absorbed secondary antibody (Thermo Fisher Scientific A21463, 1:1,000) for a further 90 mins. The cells were then washed three times, 10 mins each, with PBS in the dark. Coverslips were then washed with dH_2O and mounted on glass slides with one drop of FluorSave Reagent and left to dry for 30 mins. The slides were stored at 4 °C until viewing.

IF cell imaging was carried out using a Leica SP5 laser scanning confocal microscope with 100x oil immersion objective lens. eGFP was excited at 488 nm with an argon laser and emission was collected at 500-550 nm. dTomato was excited at 543 nm with a HeNe laser and emission was collected at 560-600 nm. Alexa Fluor™ 647 was excited at 633 nm with a HeNe laser, and emission was detected at 647 nm. Images were acquired at a resolution of 512 x 512 pixels using Leica LAS-AF software.

3.2.6 $CaPO_4$ co-transfection of HEK293 and preparation of cell homogenate for western blot

HEK293 cells were co-transfected with RyR2 and CaM plasmids using the $CaPO_4$ method as detailed in **Section 2.3.6**. This approach was selected for its ability to achieve high protein expression levels, which are necessary for reliable detection and quantification by western blotting. HEK293 cell homogenates were then produced as outlined in **Section 2.3.7**, and the protein concentration of each cell homogenate sample was estimated using Pierce™ BCA Assay Kit (Thermo Fisher Scientific), as detailed in **Section 2.3.8**. The expression level of RyR2 and CaM proteins was then assessed using SDS/PAGE and western blotting. Details of methodology can be found in **Section 2.3.11**. Antibodies used in western blotting are:

- GFP (B-2) mouse monoclonal antibody (Santa Cruz Biotechnology, sc-9996): used at 1:5,000 dilution.
- Calmodulin rabbit monoclonal antibody (Cell Signaling, D1F7J): used at 1:1,000 dilution.
- α-tubulin mouse monoclonal antibody (Proteintech, 66031-1-Ig): used at 1:20,000 dilution.
- Rabbit anti-mouse secondary antibody (Abcam, ab6728): used at 1:10,000 dilution.
- Goat anti-rabbit secondary antibody (Cell Signaling, 7074): used at 1:10,000 dilution.

3.3 Results

3.3.1 Transfection efficiencies of hRyR2, WT, D132E and Q136P CaM in HEK293

Using a 1:2 molar ratio of RyR2 to CaM in Effectene-mediated transfection, the average transfection efficiency of RyR2 and CaM constructs are shown in **Table 3.1**. RyR2 transfection efficiency was not affected significantly by CaM co-expression (p>0.05). Additionally, Q136P CaM showed comparable transfection efficiency to WT CaM when co-expressed with RyR2, whereas D132E CaM transfection efficiency was lower than WT CaM with RyR2 co-transfection, though not statistically significant (p>0.05).

The average percentage of cells that co-express RyR2 and Q136P was higher than those co-expressing RyR2 and D132E, although not statistically significant compared to WT CaM co-transfection (see **Figure 3.3**). In co-transfections, 85.1% of cells expressing WT CaM also expressed RyR2. Similarly, 92.8% and 96.6% of cells expressing D132E and Q136P CaM, respectively, also expressed RyR2. A representative FoV showing HEK293 cells transfected with RyR2 and Q136P CaM is shown in **Figure 3.4**.

Table 3.1. Average transfection efficiencies of RyR2 and WT or mutant CaM. n= 5 FoVs for each construct. Data shown as average ± standard error.

Construct	Transfection efficiency (%)
RyR2 alone	43.9 ± 2.5
RyR2 (with WT CaM co-transfection)	34.5 ± 2.8
RyR2 (with D132E CaM co-transfection)	32.95 ± 4.1
RyR2 (with Q136P CaM co-transfection)	40.09 ± 9.1
WT CaM (with RyR2 co-transfection)	23.9 ± 2.6
D132E CaM (with RyR2 co-transfection)	13.2 ± 3.8
Q136P CaM (with RyR2 co-transfection)	26.9 ± 7.2
RyR2 **and** WT CaM	20.3 ± 2.4
RyR2 **and** D132E CaM	12.0 ± 3.3
RyR2 **and** Q136P CaM	26.1 ± 7.1

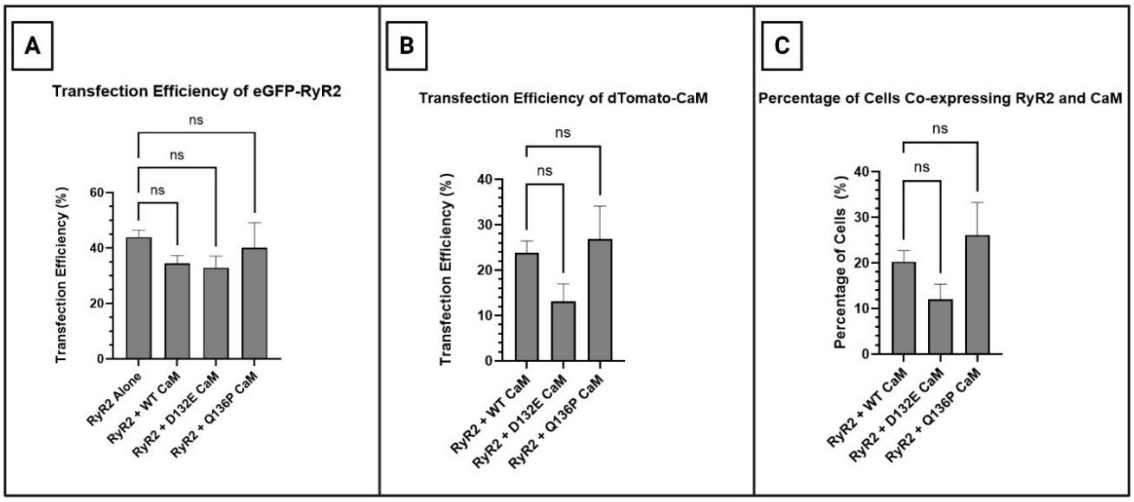

Figure 3.3. Average transfection efficiencies of RyR2 and CaM in HEK293 cell following Effectene-mediated transfection. (A) Shows RyR2 transfection efficiency, either alone or with CaM co-expression. Co-expression of CaM did not significantly alter RyR2 transfection efficiency. **(B)** Shows transfection efficiencies of WT and mutant CaM variants with RyR2 co-expression. No significant difference was observed between WT and mutant CaMs when co-expressed with RyR2. **(C)** Percentage of cells co-expressing both RyR2 and CaM. A lower proportion of cells co-expressed RyR2 with D132E CaM compared to WT CaM co-transfection, though this difference was not statistically significant. Data are displayed as mean ± SEM and were analysed using One-Way ANOVA test followed by Šídák's multiple comparisons post hoc test. *n*= 5 FoVs for each construct.

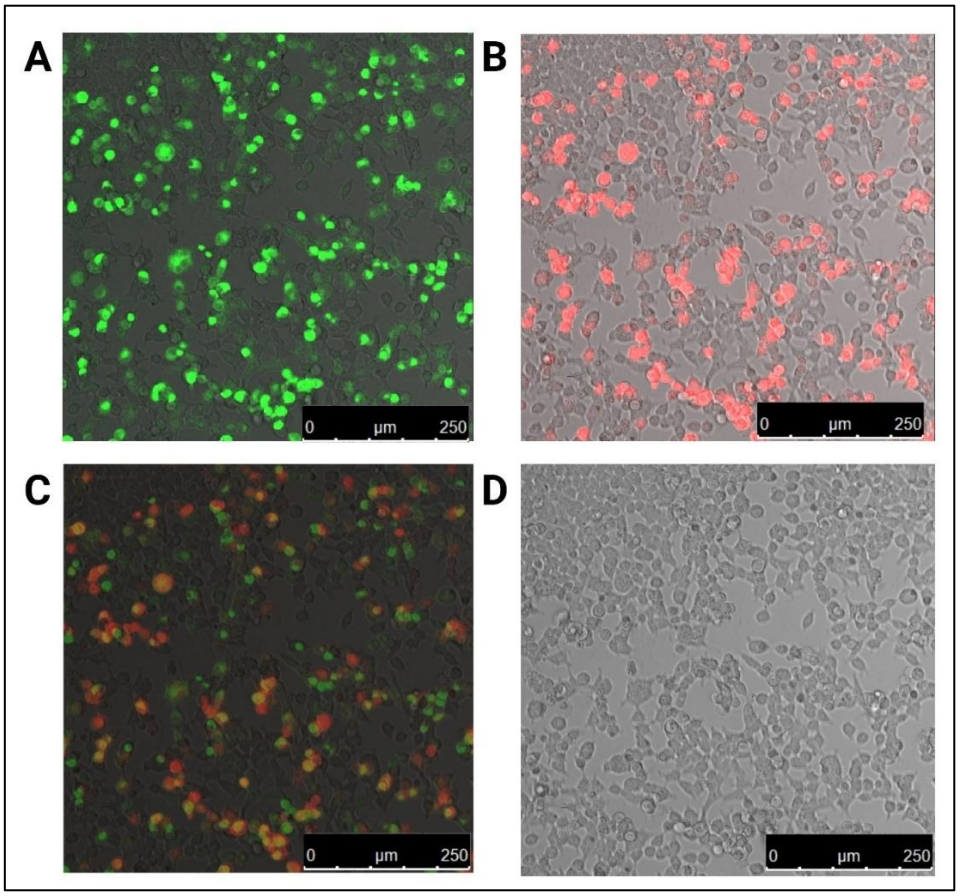

Figure 3.4. Sample FoV used for estimating Effectene-mediated transfection efficiencies for RyR2, WT, D132E and Q136P CaMs. Green fluorescence indicates eGFP-RyR2-expressing cells, whereas red fluorescence indicates dTomato-CaM-expressing cells. **(A)** Shows green fluorescence of cells transfected with RyR2, with a transfection efficiency of ~53.4%. **(B)** Shows red fluorescence of cells transfected with Q136P CaM, with a transfection efficiency of ~31.1%. **(C)** Represents figures A and B overlaid. Cells co-expressing RyR2 and CaM appear to be yellow, with a co-transfection efficiency of ~23%. **(D)** Shows the bright-field image of all cells in the FoV.

3.3.2 Mutant CaM co-expression does not affect RyR2 expression level in HEK293

Some CPVT-linked RyR2 mutations have been shown to alter RyR2 expression level which could affect Ca^{2+} release (Liu et al.. 2017). However, this mechanism of pathogenesis has not been explored for CPVT-linked CaM mutants. To investigate whether a similar mechanism could underly the pathogenicity of CaM variants (D132E and Q136P), RyR2 protein expression levels in HEK293 were assessed in the presence of WT or mutant CaM. Additionally, CaM expression level in co-transfections was also assessed to investigate whether CaM mutations alter CaM's expression level. This initial

analysis of recombinant protein expression level was nevertheless essential to carry out prior to detailed kinetic studies of Ca^{2+} release events (as shown in **Section 3.3.5**) as RyR2 and CaM expression level can affect Ca^{2+} release dynamics.

Cell homogenates of HEK293 cells transfected with RyR2 alone or in combination with WT or mutant CaM were analysed using western blotting. Untransfected HEK293 cell homogenate was used as a negative control because RyR2 is not expressed endogenously in this cell line. RyR2 was detected using anti-GFP antibody and the intensity of the signal at the expected molecular weight of 565 kDa was estimated using densitometric analysis. The signal was corrected for loading error using α-tubulin antibody (50 kDa). Results were normalised to RyR2 expression with WT CaM. **Figure 3.5.A** shows an example of a western blot. All original western blots used in the analysis can be seen in **Appendix I**. Densitometric analysis revealed that RyR2 expression level did not significantly change with WT CaM co-expression compared to RyR2-alone transfection. Similarly, D132E or Q136P CaM co-expression did not significantly alter RyR2 expression level compared to WT CaM co-expression ($p>0.05$) (see **Figure 3.5 B-C**).

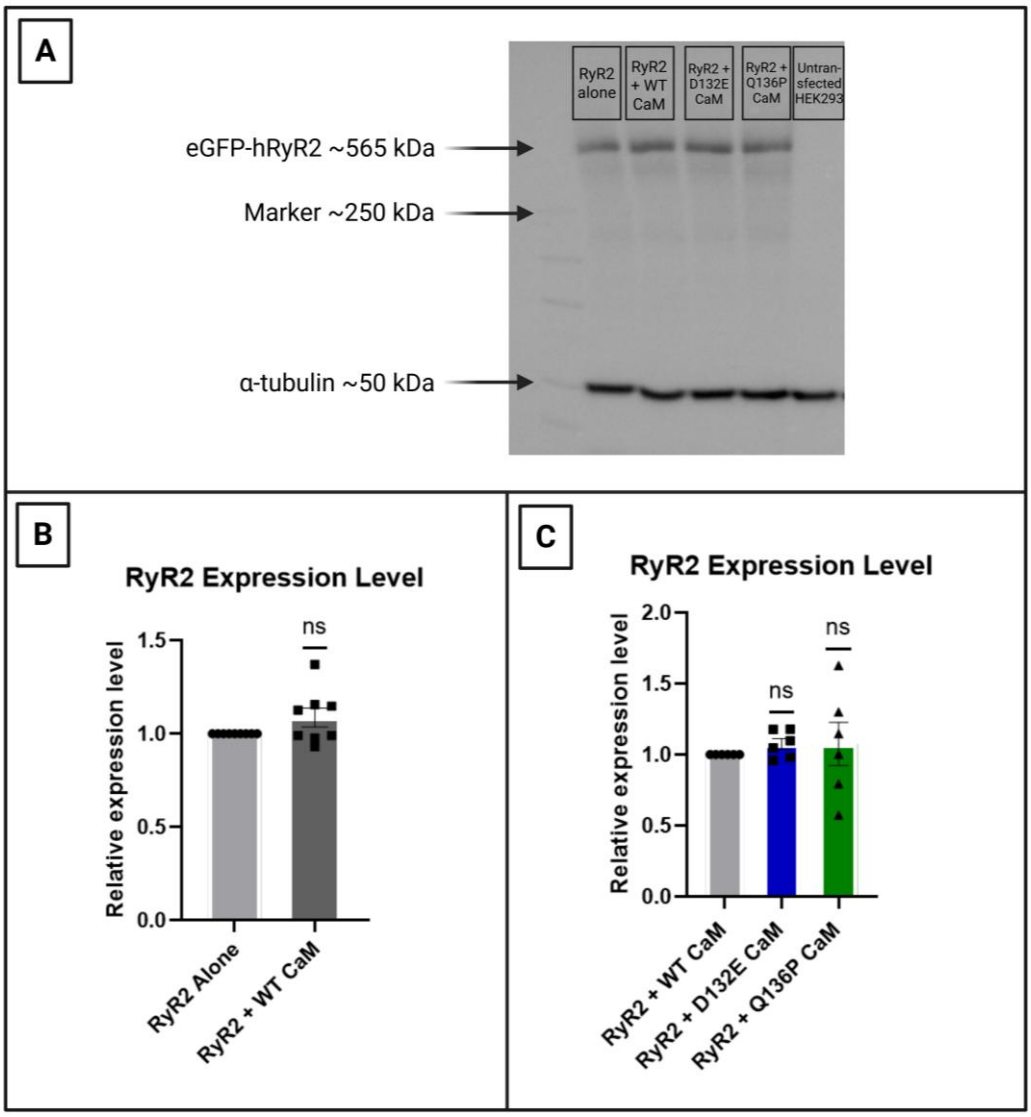

Figure 3.5. Western blot analysis of HEK293 co-expressing RyR2 and either WT or mutant CaMs revealed that RyR2 expression level was not affected by D132E or Q136P mutant CaMs co-expression compared to WT CaM. (A) Shows a representative western blot. A total of 100 µg protein homogenate sample was loaded for each well. Anti-GFP signal was normalised to the equivalent α-tubulin signal (loading control). Untransfected HEK293 cell homogenate does not show a band corresponding to RyR2 but shows α-tubulin expression. **(B)** Shows comparison of RyR2 expression level with and without WT CaM expression. **(C)** There was no significant change in RyR2 expression level in cells expressing mutant CaMs compared to WT CaM. Estimation of RyR2 expression level was normalised to RyR2 expression with WT CaM. Data are displayed as mean ± SEM, with individual data points blotted and analysed by one sample Wilcoxon test. *n*= 6 blots.

To assess CaM constructs expression level in RyR2 co-transfections, cell homogenates of HEK293 transfected with RyR2 and WT or variant CaM were also analysed using western blotting. Untransfected HEK293 cell homogenate was used as a baseline control

because HEK293 cells express CaM at a low level. Results were normalised to transfected WT CaM expression. Densitometric analysis revealed that D132E CaM showed higher expression level compared to WT CaM in HEK293 cells co-transfected with RyR2. However, these results should be interpreted cautiously due to small sample size (*n*=2 blots) (see **Figure 3.6** and **Appendix II**).

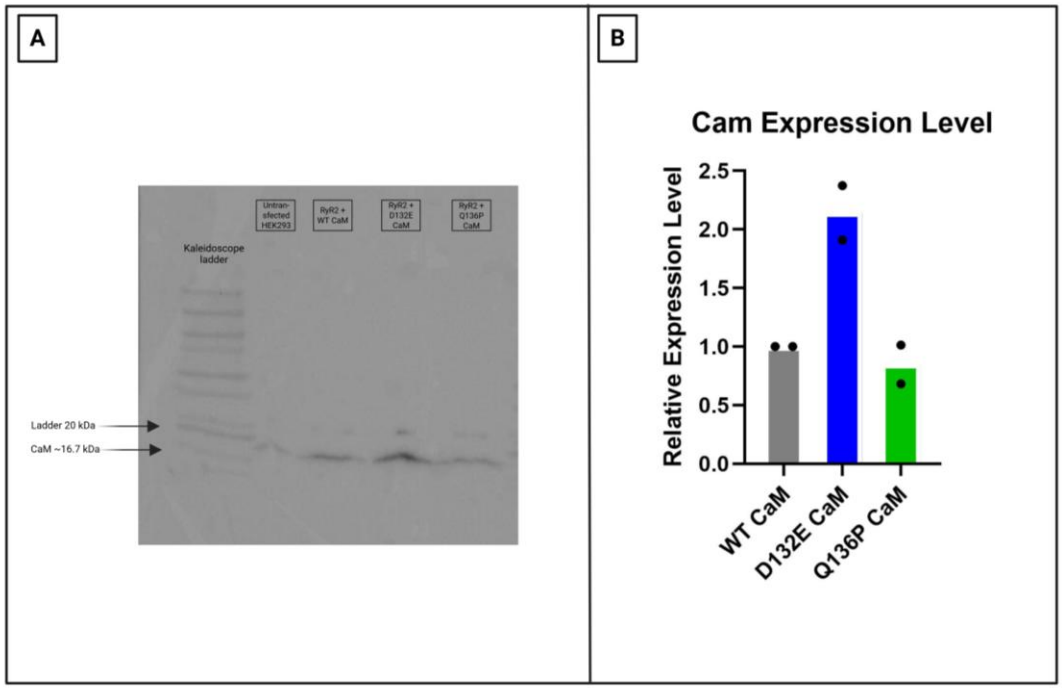

Figure 3.6. Western blot analysis of CaM constructs expression in HEK293 cells co-transfected with RyR2. D132E CaM showed higher expression level compared to WT CaM (A) Shows a representative western blot. A total of 50 µg cell homogenate sample was loaded for each well. Untransfected HEK293 cell homogenate was used as a positive control. **(B)** There was no difference in variant CaM expression level in HEK293 cells co-expressing RyR2 compared to WT CaM. Estimation of CaM expression level was normalised to WT CaM expression with RyR2. Bar charts represent the mean value of 2 blots, with individual data points blotted.

3.3.3 D132E and Q136P mutant CaMs do not appear to affect RyR2 intracellular trafficking

Defective intracellular trafficking is a trademark for some arrhythmia-linked channelopathies such as Brugada and LQTS, with mis-trafficking of K^+ and Na^+ channels

as the causative mechanism (Delisle et al., 2004; Pérez-Hernández et al., 2018; Ruan et al., 2008). Additionally, the CPVT-linked N54I CaM variant was shown to cause defective trafficking of SK3 channels, leading to a reduction in channel current (Saljic et al., 2019). Therefore, to investigate whether RyR2 intracellular trafficking to the ER is affected by variant D132E or Q136P CaM co-expression, fluorescence microscopy was used to compare the reticular pattern of eGFP-RyR2 distribution in HEK293 cells with and without mutant CaM expression. A reticular pattern of fluorescence was observed denoting RyR2 trafficking to the ER. There was no recognisable difference in the reticular distribution of RyR2 with D132E CaM and Q136P CaM co-expression in HEK293 cells (see **Figure 3.7**). dTomato fluorescence is seen distributed evenly throughout the cell as this tag is not attached to CaM, but is an indication of successful CaM transfection. Alexa647 immunofluorescence, on the other hand, is indicative of where CaM really is in the cell. CaM staining does not follow RyR2 staining completely, but some areas of CaM staining look reticular which increases the validity of the imaging as CaM can be found bound to RyR2 (hence the reticular appearance), or unbound and free in the cell.

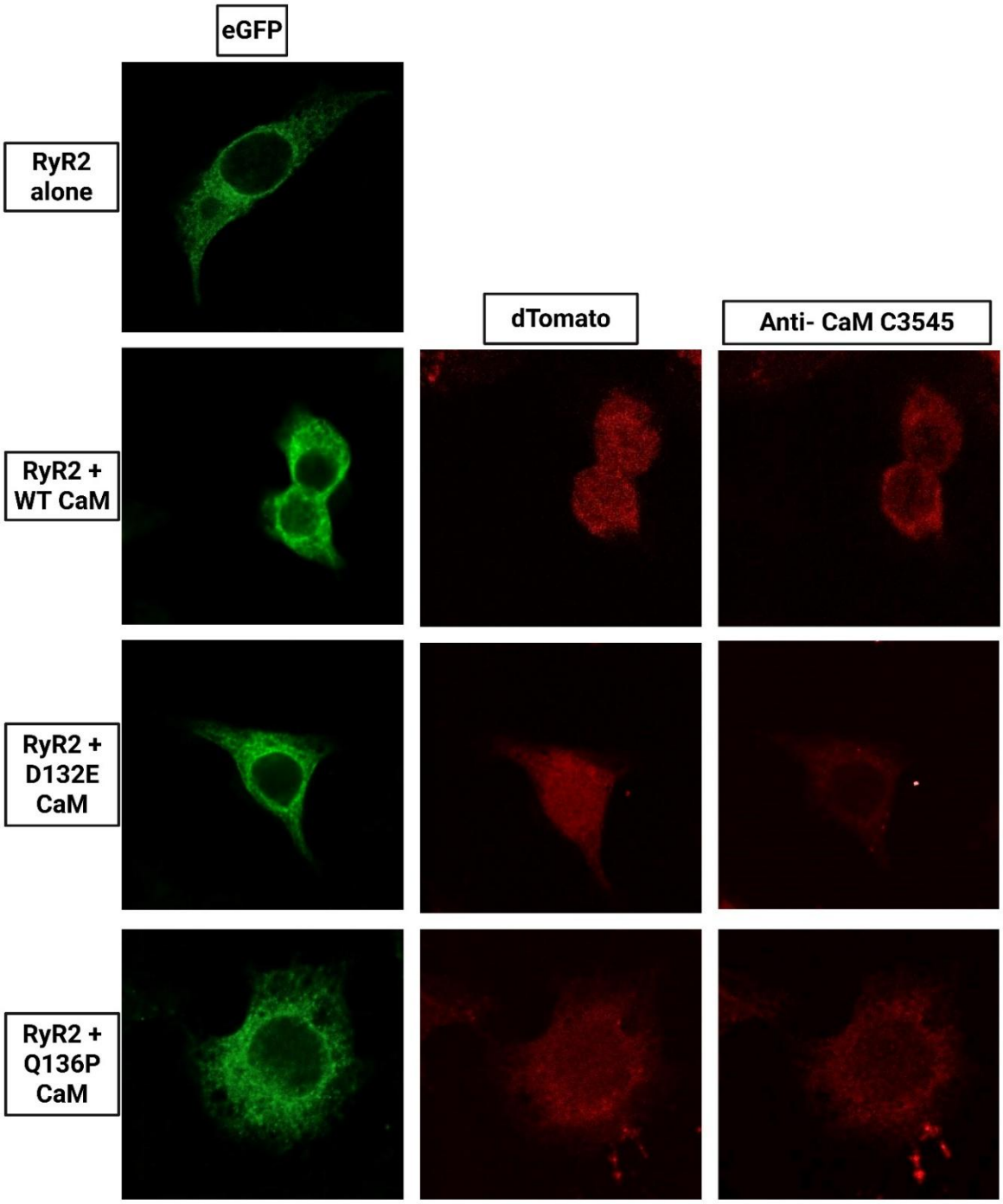

Figure 3.7. Reticular pattern of HEK293 cells expressing RyR2 on its own, or in combination with WT or mutant CaM is comparable. HEK293 cells were examined for eGFP fluorescence (ex. 488nm, em. 525nm), dTomato fluorescence (ex.554nm, em.581nm) and immunofluorescence of Alexa647 chicken anti-mouse secondary antibody targeted to calmodulin primary antibody (sigma C3545) (ex. 633nm, em. 647nm). Imaging was carried out using confocal microscopy with a 100x oil immersion objective lens.

3.3.4 RyR2 spontaneous Ca^{2+} release efficiency is altered with WT and mutant CaM co-expression

Some RyR2-expressing HEK293 cells exhibit spontaneous Ca^{2+} oscillations (indicating that they are being expressed at the correct density in those cells for the initiation of spontaneous Ca^{2+}release), while others do not; the reason for this is not fully understood and will be discussed in **Section 3.4.3**. Spontaneous Ca^{2+} release efficiency refers to the proportion of RyR2-expressing cells that displays recursive, spontaneous Ca^{2+} release. To assess whether CaM (WT and variant) affects the spontaneous Ca^{2+} release efficiency of RyR2 in HEK293, all CaM-expressing cells in a FoV were identified via dTomato fluorescence and circled as ROIs. Following a 5-minute recording, caffeine (RyR2 agonist) was then applied at a high concentration. Cells that co-express RyR2 produced a characteristic caffeine-induced Ca^{2+} transient. The ROIs were then categorised as either (oscillating before caffeine application) or (non-oscillating before caffeine application). The cells that did not produce a caffeine-induced peak were identified as expressing CaM only (without RyR2), and were excluded from the analysis. The spontaneous Ca^{2+} release efficiency was calculated as the percentage of cells that co-express RyR2 and CaM and exhibit Ca^{2+} oscillation before caffeine application, relative to the total number of cells the co-express RyR2 and CaM.

Data analysis revealed that RyR2 has a spontaneous Ca^{2+} release efficiency of 12% when expressed alone in HEK293. Co-expression with WT CaM increased the spontaneous Ca^{2+} release efficiency to 17.3%. Co-expression with D132E CaM yielded a spontaneous Ca^{2+} release efficiency equivalent to that of WT CaM. In contrast, co-expression with Q136P CaM was associated with a modest decrease in spontaneous Ca^{2+} release efficiency to 14% (n=150 cells for each transfection; pooled from 6-9 FoVs each).

3.3.5 D132E and Q136P CaM variants alter spontaneous RyR2-mediated Ca^{2+} release signalling events

Representative traces of spontaneous Ca^{2+} release events are shown in **Figure 3.8**. The effect of WT CaM co-expression on RyR2 is inhibitory – significantly decreasing the amplitude and duration of Ca^{2+} release events and thereby increasing the frequency of

release (p<0.05). Additionally, WT CaM significantly slows down the rise and fall rates of Ca^{2+} transients compared to RyR2 on its own.

Co-expression of D132E or Q136P CaM was shown to significantly increase the duration of Ca^{2+} release compared to WT CaM, leading to a decrease in the frequency of spontaneous Ca^{2+} release events. Transient fall rate was also significantly reduced by D132E and Q136P CaM co-expression compared to WT CaM. Inter-transient interval was also significantly increased by Q136P CaM co-expression (see **Figure 3.9**). Summary of the differences in Ca^{2+} release parameters between HEK293 transfections with RyR2 alone or in combination with WT or mutant CaMs is shown in **Table 3.2.**

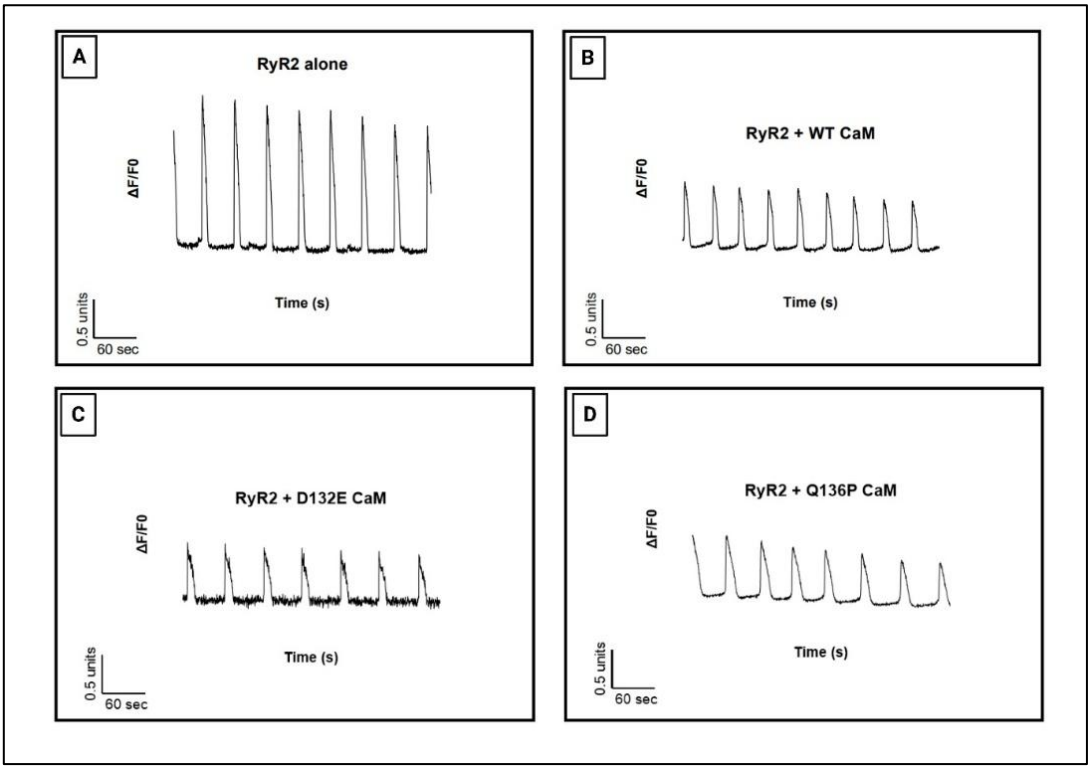

Figure 3.8. Representative traces of spontaneous Ca^{2+} release events in HEK293 cells transfected with (A) RyR2 only, (**B)** RyR2 + WT CaM, **(C)** RyR2 + D132E CaM, **(D)** RyR2 + Q136P CaM; measured by changes in CalBryte 520 dye fluorescence.

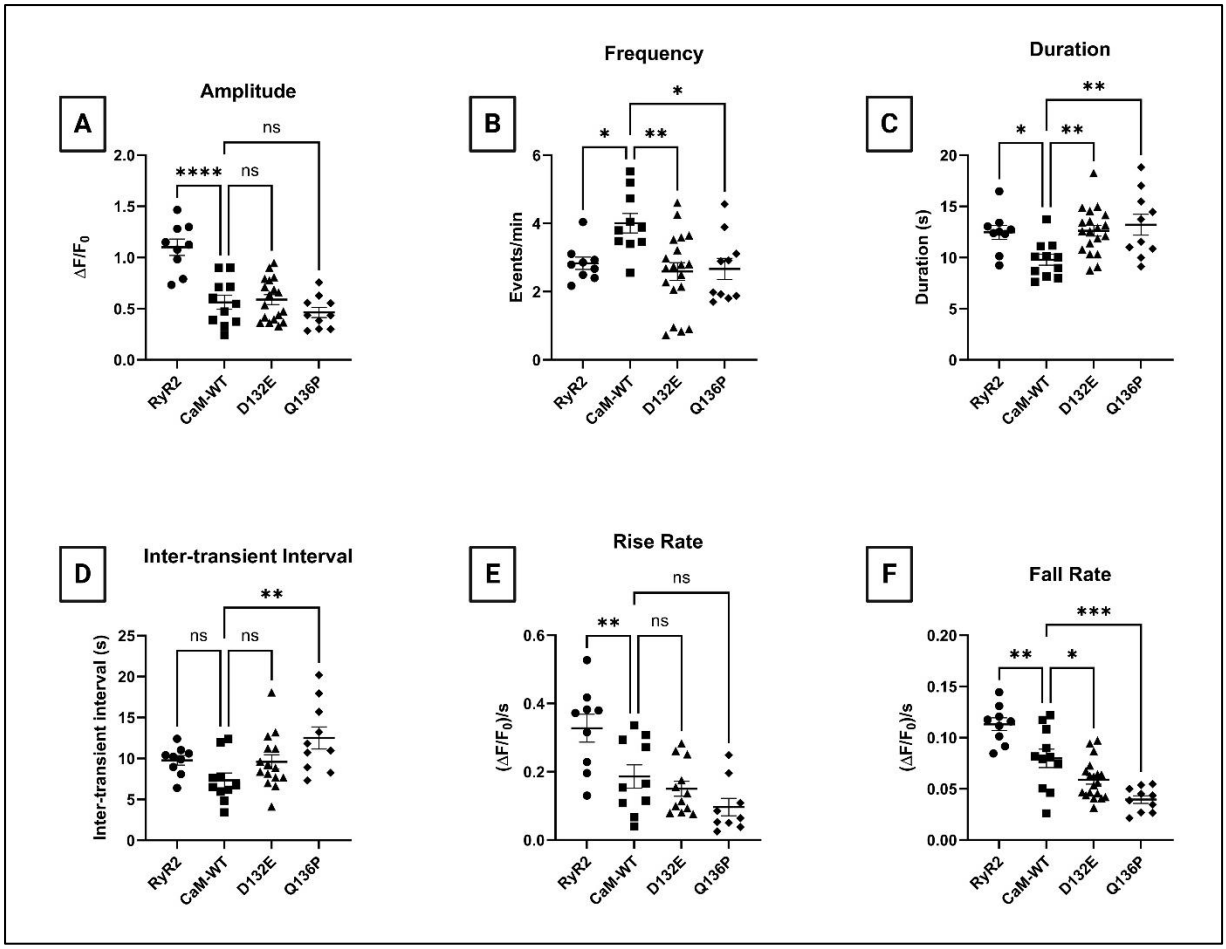

Figure 3.9. Analysis of Ca^{2+} release events produced in HEK293 cells transfected with either RyR2 on its own or RyR2 with WT or variant CaM. WT CaM significantly decreases the amplitude and duration of Ca^{2+} release events, and thus significantly increases signal frequency. WT CaM also significantly slows down the rise and fall rates of Ca^{2+} transients compared to RyR2 on its own. Co-expression of D132E and Q136P variant CaMs significantly reduced the frequency of release and increased the duration of Ca^{2+} release transients compared to WT CaM. Fall rate significantly slowed down with mutant CaMs co-expression, and Q136P CaM co-expression significantly increased the inter-transient interval duration compared to WT CaM co-expression. Each data point represents the mean of a FoV. Error bars indicate SEM. Significance, as indicated by *, was determined using one-way ANOVA test followed by Šídák's multiple comparisons post hoc test. *n* RyR2 alone= 9, RyR2 + WT CaM=11, RyR2 + D132E CaM= 19, RyR2 + Q136P CaM= 10, where *n* is the number of FoVs containing typically 15-20 cells. A total of 5 transfections were conducted to produce this data.

Table 3.2. Summary of Ca^{2+} release parameters in HEK293 transfected with RyR2 on its own, or in combination with WT or variant D132E or Q136P CaM. Values are shown as mean ± SEM. Yellow and Blue indicate a significant increase or decrease, respectively, compared to equivalent parameter in RyR2 alone expression. Purple and green indicate a significant increase or decrease, respectively, compared to RyR2 + WT CaM co-transfection. Significance, as indicated by *, was determined using one-way ANOVA test followed by Šídák's multiple comparisons post hoc test. *n* RyR2 alone= 9, RyR2 + WT CaM=11, RyR2 + D132E CaM= 19, RyR2 + Q136P CaM= 10, where *n* is the number of FoVs containing typically 15-20 cells. A total of 5 transfections were conducted to produce this data.

	RyR2 alone	RyR2 + WT CaM	RyR2 + D132E CaM	RyR2 + Q136P CaM
Amplitude	1.1±0.08	0.56±0.07 ****	0.59±0.05	0.46±0.05
Frequency	2.8±0.18	4.0±0.29 *	2.6±0.26 **	2.7±0.31 *
Duration	12±0.68	9.8±0.54 *	13±0.52 **	13±1.0 **
Inter-transient interval	9.8±0.58	7.3±0.9	9.6±0.86	13±1.3 **
Rise rate	0.33±0.04	0.19±0.03 **	0.15±0.02	0.1±0.03
Fall rate	0.11±0.006	0.08±0.009 **	0.06±0.004 *	0.04±0.004 ***

3.3.6 D132E and Q136P variant CaMs alter ER Ca^{2+} load

The RyR2 agonist, caffeine, was used at a very high dose (10 mM) to maximally activate all RyR2 channels expressed in HEK293 cells in order that the ER store level could be assessed. This was done by measuring the amplitude of the Ca^{2+} transient elicited by caffeine application. Emptying of the ER store halted any further spontaneous Ca^{2+} release as expected. This method of measuring ER load has been used widely (George et al., 2006; Jiang et al., 2005, 2007; Loaiza et al., 2013). However, it should be noted that it is an indirect measurement and potentially inaccurate because it does not take into account Ca^{2+} release events occurring before the addition of caffeine. While caffeine was added at a consistent time point in each live-cell recording, it was applied at a random and unpredictable phase of the cell's Ca^{2+} oscillation cycle which introduces variability. A proportion of RyR2 transfected cells exhibited spontaneous oscillations before

caffeine addition, whereas some did not, but all RyR2-expressing cells underwent caffeine-mediated Ca^{2+} release. Representative caffeine-induced Ca^{2+} release traces in oscillating and non-oscillating HEK293 cells are shown in **Figure 3.10**.

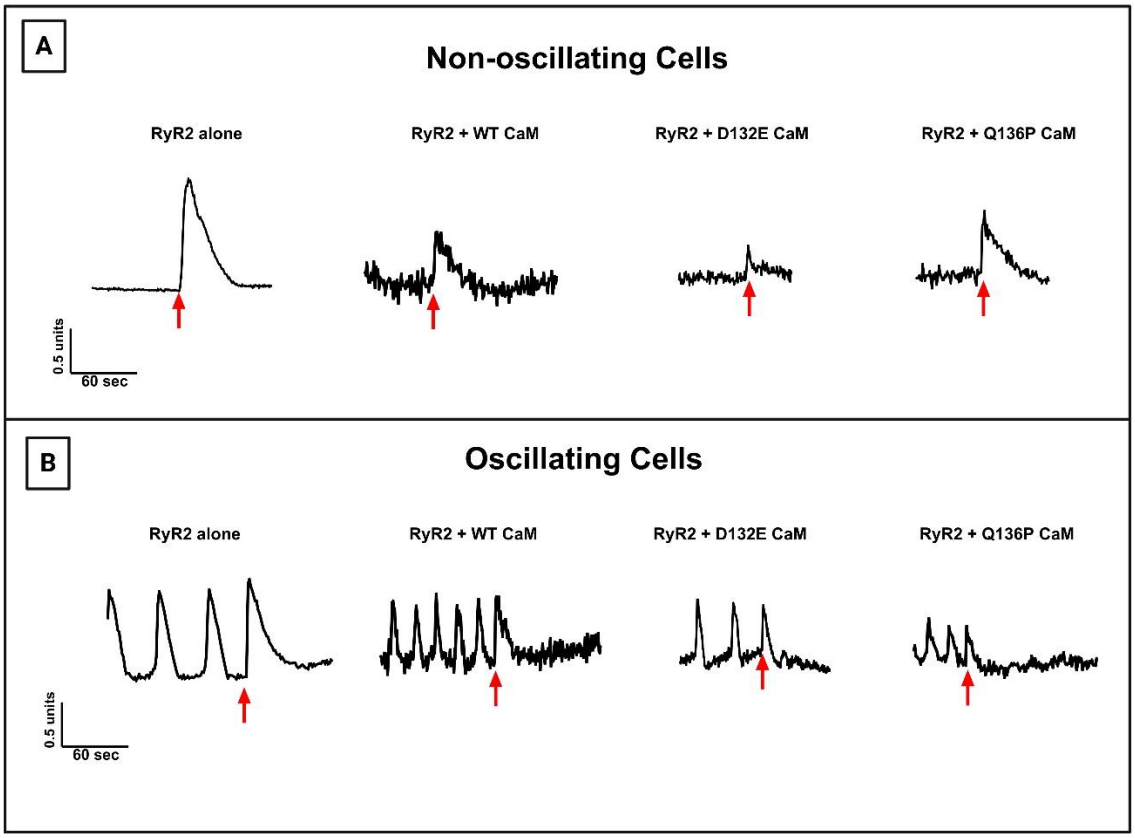

Figure 3.10. Representative traces of caffeine-induced Ca^{2+} release events in HEK293 cells transfected with RyR2 on its own, or in combination with WT or mutant CaMs (D132E or Q136P), in (A) non-oscillating and **(B)** oscillating cells. Red arrows indicate the point at which 10 mM caffeine was added to the cell media.

Co-expression of D132E and Q136P CaM in HEK293 cells produced a caffeine-induced peak of significantly smaller amplitude than those co-expressing WT CaM in oscillating cells, indicating that mutant D132E and Q136P CaMs have significantly reduced ER Ca^{2+} store load compared to WT CaM. In most of those oscillating cells expressing D132E and Q136P CaM, the caffeine-induced Ca^{2+} peak is often of a similar amplitude to the normal Ca^{2+} transient that precedes, followed by a steady return to the baseline. This finding could suggest that mutant CaMs promote ER Ca^{2+} leak during spontaneous Ca^{2+} release events. Interestingly, in non-oscillating cells, only D132E CaM co-expression produced caffeine-induced Ca^{2+} peaks of significantly smaller amplitude compared to WT CaM co-

expression. This means that D132E CaM diminishes ER Ca^{2+} store load in both oscillating and non-oscillating cells (see **Figure 3.11**).

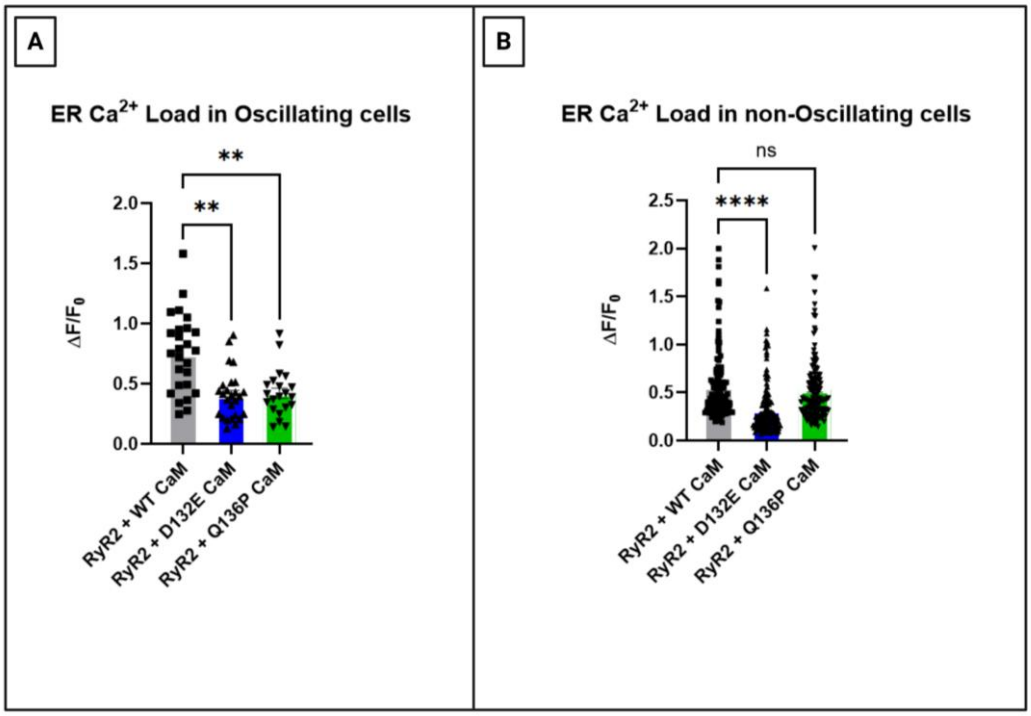

Figure 3.11. Q136P CaM significantly reduces ER Ca^{2+} load compared to WT CaM in oscillating HEK293 cells only, whereas D132E CaM significantly reduces ER Ca^{2+} load in comparison to WT CaM in both oscillating and non-oscillating cells as determined by the addition of 10 mM caffeine. Data are displayed as mean ± SEM with individual data points blotted. Significance, as indicated by *, was calculated using Kruskal-Wallis test followed by Dunn's multiple comparisons post hoc test. *n* = 124, 124, 129 non-oscillating cells and 26, 26, 21 oscillating cells for RyR2 + WT CaM, RyR2 + D132E CaM and RyR2 + Q136P CaM respectively, where *n* is the number of cells; pooled from 6-9 FoVs for each co-transfection.

3.3.7 Differential effects of WT and mutant CaM on Ca^{2+} release patterns

For characterisation of Ca^{2+} release in transfected HEK293 (shown in **Section 3.3.5**), only cells exhibiting recursive, regular Ca^{2+} oscillations were included in the analysis. Selection required a stable baseline (F_0) and at least three consecutive transient events. However, not all initially selected ROIs met these criteria. Excluded ROIs displayed heterogeneous behaviours and were categorised as follows:

- Recursive irregular: includes cells that show disorganised Ca^{2+} release or an unstable baseline.
- Single event: cells exhibiting only one Ca^{2+} release event.
- Noise: includes undefinable traces.

The percentage of cells displaying each behaviour per FoV was recorded to identify potential trends. CaM co-expression (both WT and variants D132E and Q136P) significantly reduced the proportion of cells with co-ordinated recursive Ca^{2+} release events. The proportion of cells exhibiting irregular, recursive Ca^{2+} release events was comparable amongst all transfections. However, CaM co-expression (whether mutant or WT) led to a significantly higher percentage of cells producing noise signals compared to RyR2 alone, though no statistically significant difference in noisy traces frequency was observed between WT and mutant CaMs. Single Ca^{2+} release peaks were more common with WT CaM co-expression than RyR2 alone, and most frequent with Q136P CaM co-expression (see **Figure 3.12**).

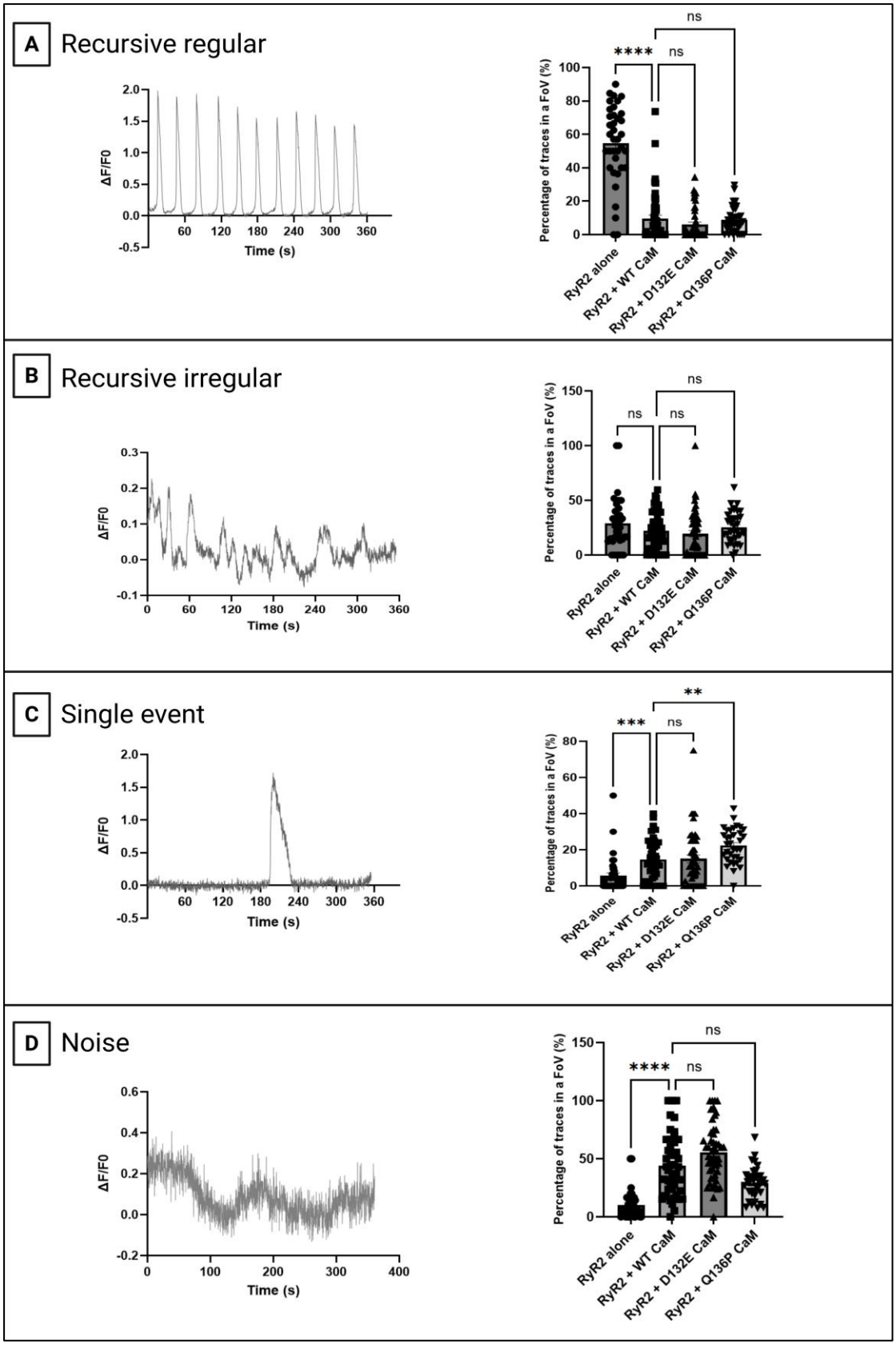

<u>Figure 3.12.</u> Categorisation of Ca^{2+} release traces in HEK293 cells transfected with RyR2 alone or in combination with WT or variant D132E or Q136P CaM. Data are displayed as mean ± SEM. Significance, as indicates by *, was determined using Kruskal-Wallis test followed by Dunn's multiple comparisons post hoc test. *n* = 37, 48, 49 and 35 for RyR2 alone, RyR2 + WT CaM, RyR2 + D132E CaM and RyR2 + Q136P CaM respectively, where *n* is the number of FoVs, containing typically 15-20 cells.

3.4 Discussion

3.4.1 Co-expression of WT and mutant D132E and Q136P CaMs does not alter recombinant RyR2 expression level, nor RyR2 intracellular trafficking in HEK293

CPVT-linked RyR2 mutations have recently been associated with altered RyR2 expression level which could plausibly contribute to dysregulated RyR2-mediated Ca^{2+} release (Y. Liu et al., 2017). To determine whether a similar mechanism could underlie the pathogenicity of CaM variants (D132E and Q136P)- despite no prior reports of such effect of CaM mutants- RyR2 expression level was assessed. Additionally, controlling for RyR2 expression was essential in all Ca^{2+} release experiments, as variations in RyR2 levels could independently influence Ca^{2+} release dynamics.

Although the transfection efficiencies of RyR2 were reproducible and not statistically different in all co-transfections, it was still important to assess RyR2 expression level with WT or mutant CaMs co-expression in HEK293 cells because transfection efficiency does not take into account any changes in expression level per cell. HEK293 cells are widely used for studying RyR2 function because they do not express RyR2 endogenously. Hence, any RyR2 detected from cell homogenates is a result of the transfection. Western blot analysis revealed that WT, D132E and Q136P CaM co-expression did not change RyR2 expression level. Therefore, RyR2 expression level is comparable in all experiments. D132E variant CaM's expression level with RyR2-co-expression, however, was higher compared to WT CaM. This increase in expression level should be interpreted with caution due to the small sample size (n=2 blots). This small n was a consequence of significant challenges in identifying a suitable CaM antibody with sufficient specificity.

IF imaging allowed us to investigate the intracellular localisation of RyR2 in HEK293 with and without WT/mutant CaMs co-expression. Forward trafficking of channels to their correct position on membranes is also an important regulator of channel function (Smyth & Shaw, 2010). Defective K^+ and Na^+ channel trafficking has been linked to Long QT and Brugada syndromes (Delisle et al., 2004; Pérez-Hernández et al., 2018). In IF experiments, RyR2 localisation in HEK293 cells was determined using endogenous eGFP fluorescence, whereas mutant CaM expression was determined using endogenous dTomato expression or via immunofluorescent detection using anti-CaM antibody. The

characteristic reticular fluorescence observed indicated that mutant CaM co-expression had no obvious effect on RyR2 intracellular trafficking.

3.4.2 D132E and Q136P CaM mutations exert a slightly weaker inhibitory effect on RyR2-mediated Ca^{2+} release compared to WT CaM

CPVT-linked CaM mutations have been shown to alter Ca^{2+} release dynamics at the cellular level by increasing the duration of Ca^{2+} oscillation in HEK293 cells transfected with RyR2 and N53I or A102V CaM variants (Prakash et al., 2022). Furthermore, a study by Søndergaard et al. (2019) investigated the effect of 14 arrhythmogenic CaM mutations on ER Ca^{2+} concentration during SOICR showed that D132E and Q136P CaM mutations significantly decreased RyR2 termination threshold by 25% and 19% respectively during SOICR in permeabilised HEK293 cells, (*i.e.*, the channel continues to release Ca^{2+} at a store level at which a WT CaM-regulated channel would be closed), and slightly decreased the activation threshold by 3% on average (*i.e.,* the channel is activated at a lower Ca^{2+} store load).

Our detailed analysis of global Ca^{2+} release traces from HEK293 cells co-expressing hRyR2 and WT CaM revealed that CaM co-expression significantly decreased the amplitude and duration of Ca^{2+} release events compared to RyR2 expression alone, which resulted in increased frequency of oscillations. These results are similar to those reported in the literature in HEK293 cells transfected with RyR2 and WT CaM (Prakash et al., 2022; Søndergaard et al., 2019), which reflect WT CaM's well-documented inhibitory function on RyR2.

Here, we present novel data showing that D132E and Q136P CaMs co-expression with RyR2 significantly increases the duration of spontaneous Ca^{2+} release events in HEK293 cells compared to WT CaM (which could be an indication of Ca^{2+} leak), and thus decreasing the frequency of release. The increase in global Ca^{2+} release duration with D132E and Q136P variant CaM were consistent with the fact that both variants were found to have lower Ca^{2+} affinity to the C-terminal domain. Da'as et al. (2024) and Gupta et al. (2025) found that the Ca^{2+} dissociation constant with Q136P CaM was found to be

~ seven times higher than WT CaM, whilst with D132E CaM it was ~15 fold higher. No change in Ca^{2+} binding affinity was reported in the N-terminal domain of D132E and Q136P CaM, which is consistent with the location of these mutants. Therefore, Ca^{2+}-dependent activation and inhibition of RyR2 could be impaired with these mutants. Interestingly, the frequency and duration of Ca^{2+} transients with D132E and Q136P CaM co-transfections were not statistically different from those observed where RyR2 was expressed alone (p>0.05). The Ca^{2+} release traces more closely resembled traces from cells where there is no overexpression of CaM, albeit with a smaller amplitude. Since HEK293 cells express a small amount of endogenous WT CaM, these results suggest that mutant D132E and Q136P CaMs may be exerting a dominant-negative effect on RyR2-mediated Ca^{2+} release.

D132E and Q136P CaMs' divergent regulation of RyR2 channels might also be caused by their reduced binding affinity to RyR2. In a recent study by Thanassoulas et al. (2023), the binding affinity of D132E and Q136P CaMs to RyR2 has been shown to be Ca^{2+}-dependent. Co-immunoprecipitation assays to investigate these mutant CaMs binding to native RyR2 from pig cardiac SR revealed that both D132E and Q136P CaMs showed significantly reduced binding to RyR2 at 100 μM Ca^{2+} concentration, but no statistically significant reduction in binding in the absence of Ca^{2+}.

Collectively, D132E and Q136P CaM were found to cause changes in RyR2-mediated Ca^{2+} release dynamics at the cellular level in HEK293. While this could be due to defective RyR2 or Ca^{2+} binding to variant CaM, function may also be impaired by changes in CaM-dependant CaMKII autophosphorylation, which leads to changes in RyR2 phosphorylation levels at the CaMKII phosphorylation site (S2814). Given that HEK293 express CaMKII endogenously, a possible way to dissect these mechanisms would be by engineering a phosphoablative form of RyR2 at the CaMKII phosphorylation site (attempted in **Chapter 4**), which would allow the study of -only- direct CaM binding effect on RyR2 function.

3.4.3 Co-expression of D132E and Q136P CaM variants alters ER Ca^{2+} load

The amplitude of Ca^{2+} transients elicited by 10 mM caffeine was taken as a measure of total ER load, since this concentration ensured maximal activation of RyR2 ensuring total depletion of the releasable store. The amplitude of the caffeine response fluorescence peak therefore represents the amount of Ca^{2+} stored in the ER. Some RyR2-transfected cells would not exhibit spontaneous Ca^{2+} oscillations but did produce a caffeine response peak. The reason for this is not fully understood but may be a result of inter-cellular variations in RyR2 expression level due to variable levels of plasmid uptake. Consequently, a sub-optimal channel density may prevent the co-operative behaviour that is required for RyR2-mediated Ca^{2+} oscillations (Chen-Izu et al., 2006).

CaM co-expression (WT or variant) was found to increase the spontaneous Ca^{2+} release efficiency of RyR2 compared to when RyR2 was expressed alone (see **Section 3.3.4**). The reason for this is unknown, although it is not unreasonable to suggest that CaM co-expression may have an effect on the co-ordination of RyR2 cluster function, given that this regulatory protein is known to facilitate coupling of other ion channels (Dixon et al., 2015).

HEK293 cells co-expressing Q136P CaM variant showed similar caffeine responses in non-oscillating cells compared to WT CaM. However, they demonstrated impaired caffeine response in oscillating cells where the caffeine-induced peaks produced were significantly smaller compared to WT CaM. Given that Q136P decreases termination threshold by ~20% during SOICR (Søndergaard et al., 2019) and was shown to significantly increase the duration and slow down the fall rate of Ca^{2+} transients in HEK293, the observed reduction in ER load could mean that Q136P CaM is causing greater fractional Ca^{2+} leakage when RyR2 channels are releasing Ca^{2+} and initiating transients.

Cells co-expressing RyR2 and the D132E CaM variant, on the other hand, showed an impaired caffeine response, producing a significantly smaller peak compared to those co-expressing RyR2 and WT CaM in both oscillating and non-oscillating cells. Knowing that D132E CaM also decreased termination threshold by ~25% during SOICR (Søndergaard et al., 2019) and significantly increased the duration of Ca^{2+} release and

slowed down transients fall rate in HEK293, it is likely that D132E is causing greater fractional Ca^{2+} release resulting in smaller Ca^{2+} stores. However, it is also suspected that D132E is causing Ca^{2+} leak under low Ca^{2+} (diastolic) conditions because the reduction in ER load is seen even in non-oscillating cells. Alternatively, this observation could be due to the higher D132E CaM expression level observed in HEK293 cells (as shown in **Section 3.3.2**), resulting in potential buffering of cytosolic Ca^{2+}. However, the reported ~15-fold reduction in Ca^{2+} binding affinity of this mutant's C-terminal domain (Da'as et al., 2024; Gupta et al., 2025) argues against this being an efficient buffer. These findings are consistent with those of Søndergaard et al. (2019) who also reported significant reduction in ER Ca^{2+} load with D132E and Q136P CaM variants in permeabilised HEK293 cells compared to WT CaM.

3.4.4 WT and variant CaM co-expression affects Ca^{2+} release patterns

The co-expression of either WT or variant CaM with RyR2 significantly reduced the proportion of HEK293 cells exhibiting recursive, regular Ca^{2+} transients and increased the percentage of cells displaying noise signals. This is likely caused by CaM's inhibitory effect on RyR2, or it could be due to cytosolic Ca^{2+} buffering caused by CaM overexpression, which potentially lowers the level of free Ca^{2+} for RyR2 activation. Even though D132E and Q136P CaM are known to have lower Ca^{2+} binding affinity (Da'as et al., 2024; Gupta et al., 2025), overexpression of the proteins would likely produce a buffering effect to some extent.

WT CaM co-expression significantly increased the proportion of cells that exhibit a single Ca^{2+} release peak during the 5-min recording period. This observation could also be due to the inhibitory effect of CaM on RyR2 channels, supressing oscillations, which causes ER Ca^{2+} overload until a single, often large, release event is triggered to maintain Ca^{2+} homeostasis. Interestingly, even though mutant D132E and Q136P CaM show a diminished inhibitory effect on RyR2, their co-expression also increased the chance of single Ca^{2+} release event, with Q136P to a higher extent. This finding could be due to the fact that D132E and Q136P CaM reduce ER Ca^{2+} load in oscillating cell, thus the single observed transient may represent an initial, spontaneous Ca^{2+} release event that could

not be sustained due to low ER Ca^{2+} load.

Chapter 4: Attempts to clone a CaMKII phosphoablative mutant (S2814A) of hRyR2

4.1 Introduction

Phosphorylation is a major regulator of RyR2 function (and multiple other ECC proteins) during β-adrenergic stimulation of the heart, for example, during "fight-or-flight" response. The S2814 site of RyR2 is one of its main phosphorylation sites that is primarily phosphorylated by CaMKII, see **Section 1.5.2.3**.

The fact that CaM can regulate RyR2 through activating CaMKII adds an extra layer of complexity when it comes to trying to understand the mechanism by which mutant CaMs cause RyR2 dysfunction. This is because the measured effect of mutant CaMs on RyR2 function could be through; 1) direct effect on the channel alone, i.e., binding affinity, 2) Changes in CaMKII phosphorylation level of RyR2, or 3) both, as detailed in **Section 1.4.2.2**. Therefore, engineering a phosphoablative S2814 recombinant hRyR2 that cannot be phosphorylated by CaMKII would be useful in investigating the functional effects of -only- direct binding of CaM mutants with RyR2. Additionally, it would allow the study of the significance of CaMKII phosphorylation of RyR2 by studying the function of phosphoablative-RyR2 mutant channel.

While current research has focused on RyR2 phosphorylation and its pathological overactivation (hyper-phosphorylation), the functional effects of RyR2 dephosphorylation have been less thoroughly explored. However, several studies have examined acute RyR2 dephosphorylation using phosphatases, primarily in experiments using RyR2 reconstituted in a lipid bilayer or Ca^{2+} spark analysis in permeabilised cardiomyocytes (e.g., Lokuta et al. 1995; Terentyev et al. 2003; Li et al. 2013; Terentyev and Hamilton 2016; Potenza et al. 2020). Transgenic animal models were also developed to study RyR2 that is constitutively dephosphorylated and cannot be phosphorylated (Dobrev & Wehrens, 2014).

RyR2-S2814A knock-in mouse model was first generated by the Wehrens group in 2009 (Chelu et al., 2009). There was no significant change reported in Ca^{2+} spark frequency, amplitude and duration in the S2814 phosphoablative mouse model compared to WT (Van Oort et al., 2010). The S2814A mouse model also demonstrated enhanced cardiac resilience, showing protection against catecholaminergic and pacing-induced arrhythmias following transverse aortic constriction surgery (Van Oort et al., 2010).

Additionally, Ather et al. (2013)found that genetic crossing of S2814A mice with a DMD model resulted in significant suppression of the arrhythmogenic spontaneous Ca^{2+} sparks and waves observed in DMD mice. Similarly, crossbreeding RyR2-S2814A knock-in mice with CaMKIIδ_C-overexpressing transgenic mice completely prevented the SR Ca^{2+} leak observed in CaMKIIδ_C transgenic mouse model, reducing Ca^{2+} spark frequency and size, which indicates that SR Ca^{2+} leak induced by CaMKIIδ_C is dependent on RyR2-S2814 phosphorylation by CaMKII (Dewenter et al., 2024). S2814A knock-in has also been shown to protect against atrial fibrillation in FKBP12.6 knockout mice by suppressing RyR2-mediated Ca^{2+} leak (N. Li et al., 2012) and reverse atrial ectopy observed in spinophilin knockout mice where loss of PP1 regulation destabilised the RyR2 complex (Chiang et al., 2014).

Notably, no studies to date have looked into the functional effects of S2814A phosphoablation in a recombinant human RyR2 system. This chapter will present attempts to introduce a S2814A point mutation in the human sequence of RyR2 using site-directed mutagenesis, intended to be used in studies to investigate WT and mutant CaM binding to RyR2, and to investigate Ca^{2+} release dynamics in HEK293 co-expressing S2814A-RyR2 and WT or mutant CaM.

4.1.1 Chapter aims and objectives

The aim of this chapter is to engineer a phosphoablative form of hRyR2 at the CaMKII phosphorylation site, changing serine 2814 to alanine to prevent channel phosphorylation. This would mean that any observed effect of mutant CaM on RyR2 channel function would likely be down to direct CaM interaction with RyR2.

Key objectives:

- Use a cassette-based site-directed mutagenesis method to engineer a phosphoablative mutant of eGFP-hRyR2 channel at the CaMKII phosphorylation site (S2814) where the target serine is mutated to an alanine (S2814A), thereby preventing phosphorylation.
- Transform and propagate WT and mutant hRyR2 plasmid DNA in super-competent bacterial cells lines.
- Use restriction digest and DNA sequencing to verify plasmids.

4.2 Methods

4.2.1 Generation of S2814A phosphoablative construct of eGFP-hRyR2

The S2814A mutation of hRyR2 was attempted using an *in vitro* site-directed mutagenesis technique. Due to the large size of the pcDNA3-eGFP-hRyR2 plasmid (~21kb), a cassette-based mutagenesis strategy was employed where the mutation was introduced to a segment of RyR2 (*KpnI*/*NdeI* cassette) that had previously been cloned into a smaller intermediate plasmid (pSL1180). This cassette contained the hRyR2 coding sequence 7553 bp (2518aa) to 11,857 bp (3953aa), which encompasses the target amino acid S2814.

To introduce the point mutation into the cassette, oligonucleotide primers for site-directed mutagenesis were designed with the following criteria:

- Forward and reverse primers contained the desired mutation, annealing to the same sequence on opposite strands of the DNA plasmid.
- The desired mutation positioned in the middle of the primer, surrounded by at least 10–15 complementary base pairs on each side.
- The melting temperature of primers (T_m) should be above 78°C.
- The primers have at least 40% GC content and end with one or more G or C bases.

The primers, sequences for which are shown in **Table 4.1**, were ordered from Eurofins and were used with the QuikChange II XL Site-Directed Mutagenesis Kit (Agilent) to introduce the mutation into the pSL1180 intermediate plasmid vector according to manufacturer's instructions (see **Figure 4.1**). The reaction mixture was prepared as shown in **Table 4.2**, and the thermal cycling conditions are shown in **Table 4.3.**

Table 4.1. Oligonucleotide primers designed for site-directed mutagenesis used to insert the S2814A mutation in the *KpnI/NdeI* cassette of hRyR2. Sequences are given in the 5' to 3' direction. The nucleotides in red indicate those that were changed.

Description	Sequence	Length (bp)	T_m (°C)	GC content (%)
Forward mutagenic primer of hRyR2 (S2814A)	GACAAGCCAGGTTGCTGTGGACGCTGCCC	29	83.8	65.5
Reverse mutagenic primer of hRyR2 (S2814A)	GGGCAGCGTCCACAGCAACCTGGCTTGTC	29	83.8	65.5

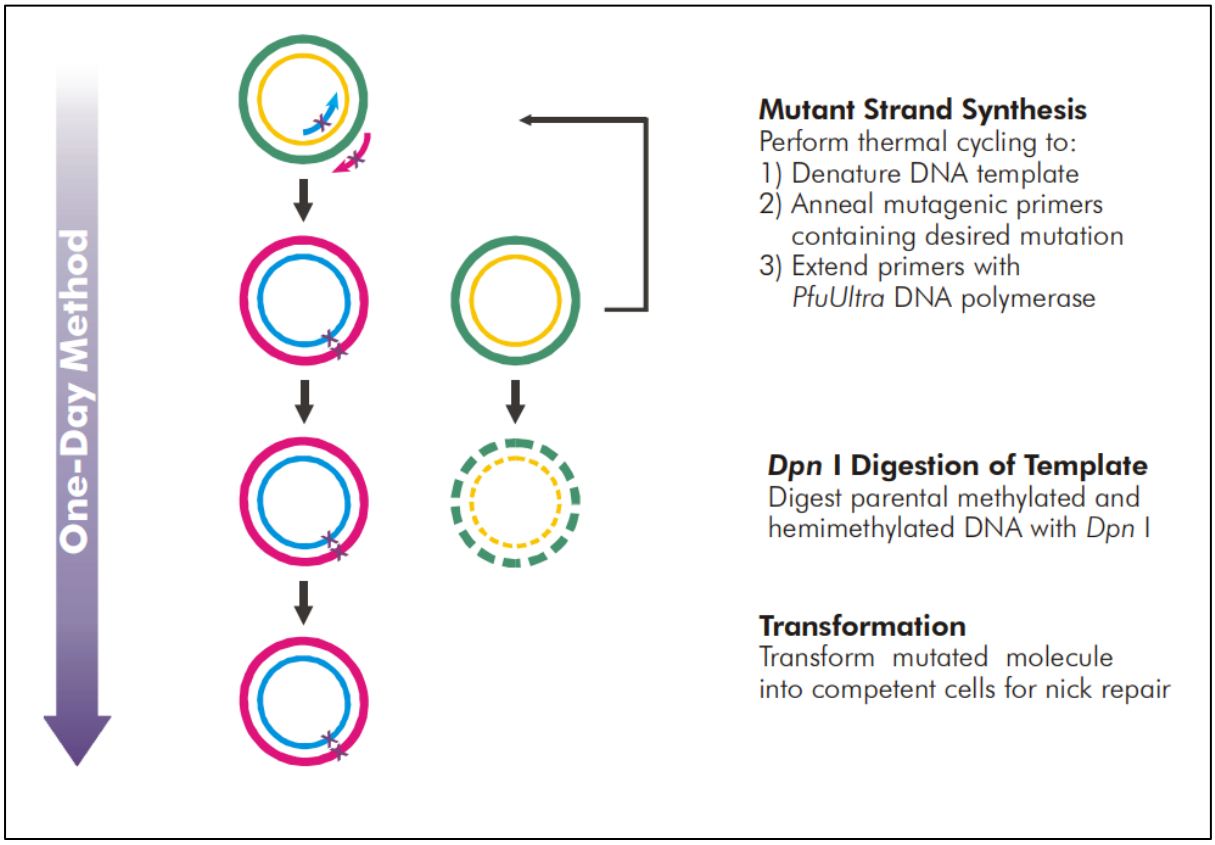

Figure 4.1. Overview of the QuickChange II XL site-directed mutagenesis method. The method was used to introduce a point mutation (S2814A) into the *KpnI/NdeI* cassette of hRyR2. Figure adapted from Agilent product manual.

Table 4.2. The reaction mixture for site-directed mutagenesis.

Reagent	Volume
10x buffer	5 µL
QuikSolution reagent	3 µL
dNTP mix	1 µL
Forward mutagenic primer (150 ng/µL)	1.5 µL
Reverse mutagenic primer (150 ng/µL)	1.5 µL
dsDNA template (*KpnI*/*NdeI* Cassette)	1.5 µL
PfuUltra HF DNA polymerase	1 µL
Deionized dH_2O	Up to 50 µL

Table 4.3. Thermal cycling conditions for site-directed mutagenesis using the QuikChange II XL site-directed mutagenesis kit (Agilent).

Segment	cycle	Stage	Temperature	Time
1	1	Initial denaturation	95 °C	1 min
2	18	Denaturation	95 °C	50 sec
		Annealing	60 °C	50 sec
		Extension	68 °C	8 min (1min/kb of plasmid length)
3	1	Final extension	68 °C	7 min

Following this, the product was treated with 1 µL *DpnI* enzyme and incubated for 1 hour at 37 °C. *DpnI* is an endonuclease enzyme that is specific for methylated and hemi-methylated DNA. Given that DNA isolated from E. coli strains is methylated by deoxyadenosine methylase, *DpnI* would only digest the parental template DNA leaving just the mutated DNA cassette that can then be transformed into competent cells and propagate.

4.2.2 Incorporating the S2814A-mutant cassette into full-length hRyR2 plasmid

The RyR2 sequence in the *KpnI/NdeI* cassette is bordered by *KpnI* and *NdeI* restriction sites. Following mutagenesis, cleavage with *KpnI* and *FseI* (a site internal to the *NdeI* site) restriction enzymes releases the correct fragment for re-ligation into full-length hRyR2.

The hRyR2 plasmid (pcDNA3- eGFP-hRyR2) and the mutated *KpnI/NdeI* cassette were both cut with *FseI* and *KpnI* enzymes to obtain fragments for ligation. The *KpnI/NdeI* cassette was also cut with an additional enzyme, *XhoI*, which is located outside of the coding sequence, *i.e.,* triple digest. This is because double digest of the cassette produces two bands with similar molecular weights that cannot be resolved using gel electrophoresis (3839 bp and 3827 bp). Upon triple digest, three bands (3827 bp, 3291 bp and 548 bp) are produced, which make it easier to identify and cut the desired 3827 bp fragment containing the S2814A point mutation (see **Figure 4.2**).

The digest reactions were optimised for enzyme-buffer compatibility and plasmid concentration. The reactions were incubated overnight to try and ensure that the reaction ran to completion. The cleaved plasmids were then run on a 1% (w/v) agarose electrophoresis gel. The desired bands (17.4 kb for pcDNA3-eGFP-hRyR2 and 3.8 kb for S2814A-*KpnI/NdeI* cassette) were then identified and removed quickly under an Ultraviolet (UV) transilluminator using a scalpel. The gel slices were then treated with the GeneJet™ Gel extraction kit (Thermo Fisher Scientific) to extract and purify the plasmid fragments according to manufacturer's instructions.

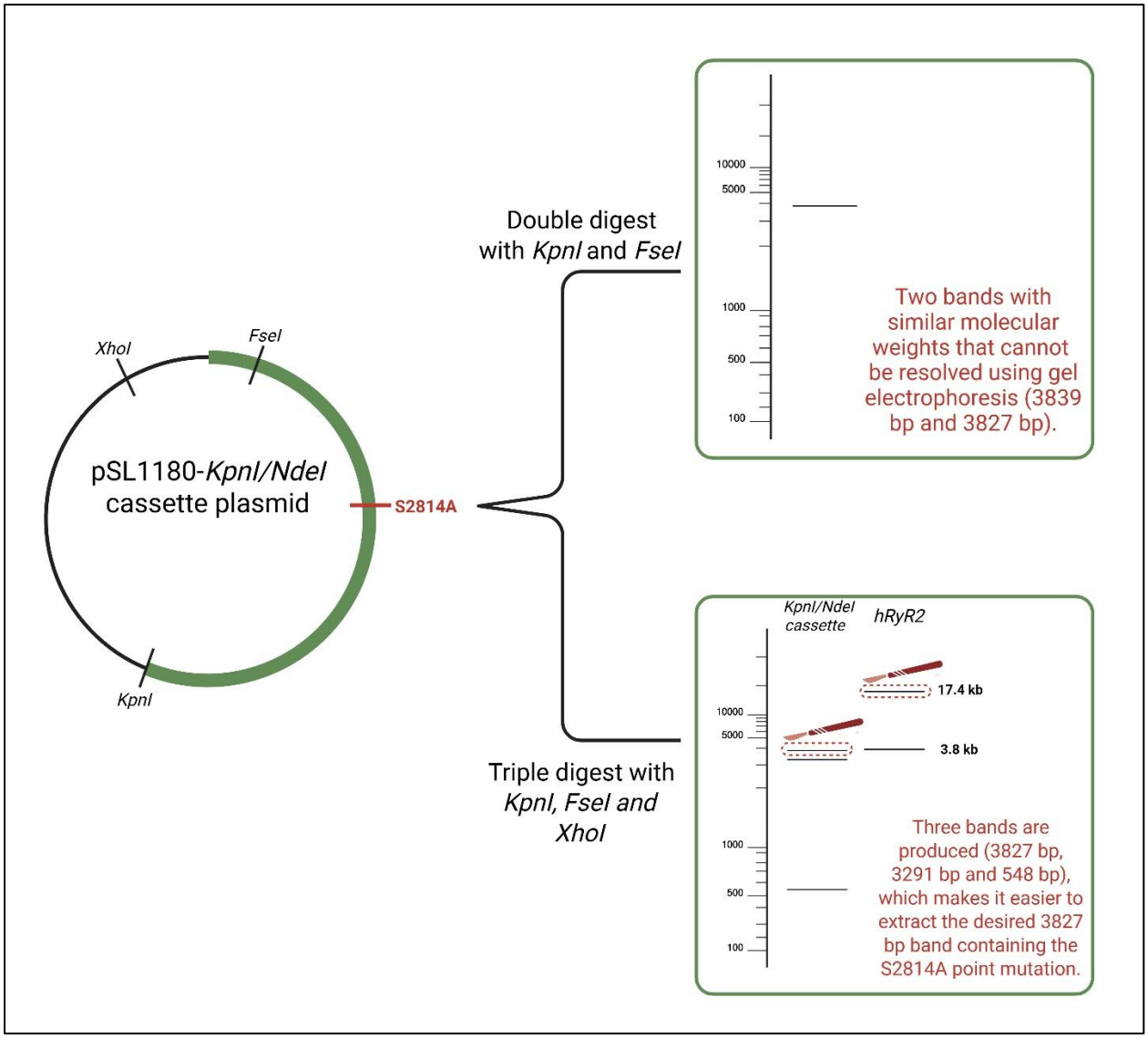

Figure 4.2. Triple digest of mutagenic *KpnI/NdeI* cassette to obtain fragments for ligation. Figure shows a schematic representation of the *KpnI/NdeI* cassette and its restriction sites, with hRyR2 coding sequence shown in green. Upon double digest with *KpnI* and *FseI,* the fragments produced have very similar molecular weights, and thus cannot be resolved by gel electrophoresis Upon triple digest with *KpnI, FseI* and *XhoI,* three fragments are produced (3827 bp, 3291 bp and 548 bp), which make it easier to identify and cut the desired 3.8 kb band containing S2814A mutation for ligation into hRyR2 plasmid. Virtual restriction digests were created using the NEBcutter® 3.0.19 tool.

A proportion of the extracted DNA fragments (5 µL) were then run on a 1% (w/v) agarose electrophoresis gel (see **Figure 4.3**) to estimate the concentration before using the Rapid DNA ligation kit (Roche) according to manufacturer's instructions to ligate the vector (RyR2 fragment) with the insert (mutated cassette). A 1:3 molar ratio of vector to insert was initially attempted (50 ng of the 17,400 bp vector and 33 ng of the 3800 bp insert), then the reaction was optimised by using a 1:5 ratio instead (50 ng of vector and 55 ng of

insert) (see **Figure 4.4)**. The reaction was incubated at 4°C for 16 hours before transforming into Stbl2 cells as detailed in **Section 2.3.1**. Successful ligation was checked for using plasmid restriction digest with *EcoRI* as detailed in **Section 2.3.3**.

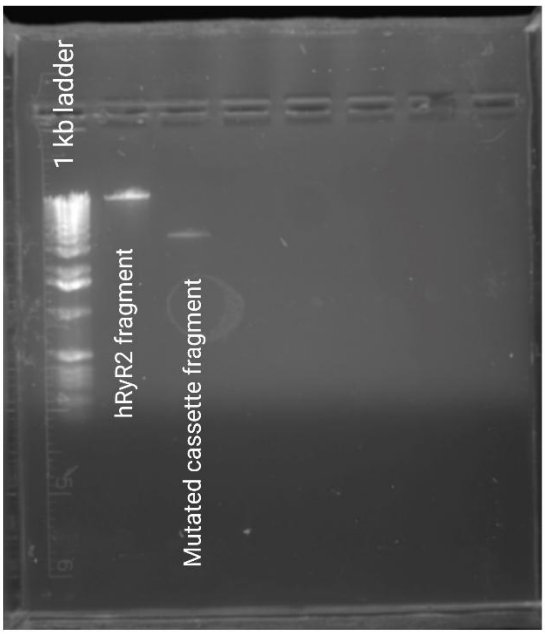

Figure 4.3. Gel electrophoresis image of extracted DNA fragments from pcDNA3-eGFP-hRyR2 and S2814A-*KpnI/NdeI* plasmids respectively. The fragments concentration was estimated and then used in Rapid DNA ligation kit (Roche) to ligate the vector (RyR2 fragment) with the insert (mutated cassette) in a 1:5 molar ratio.

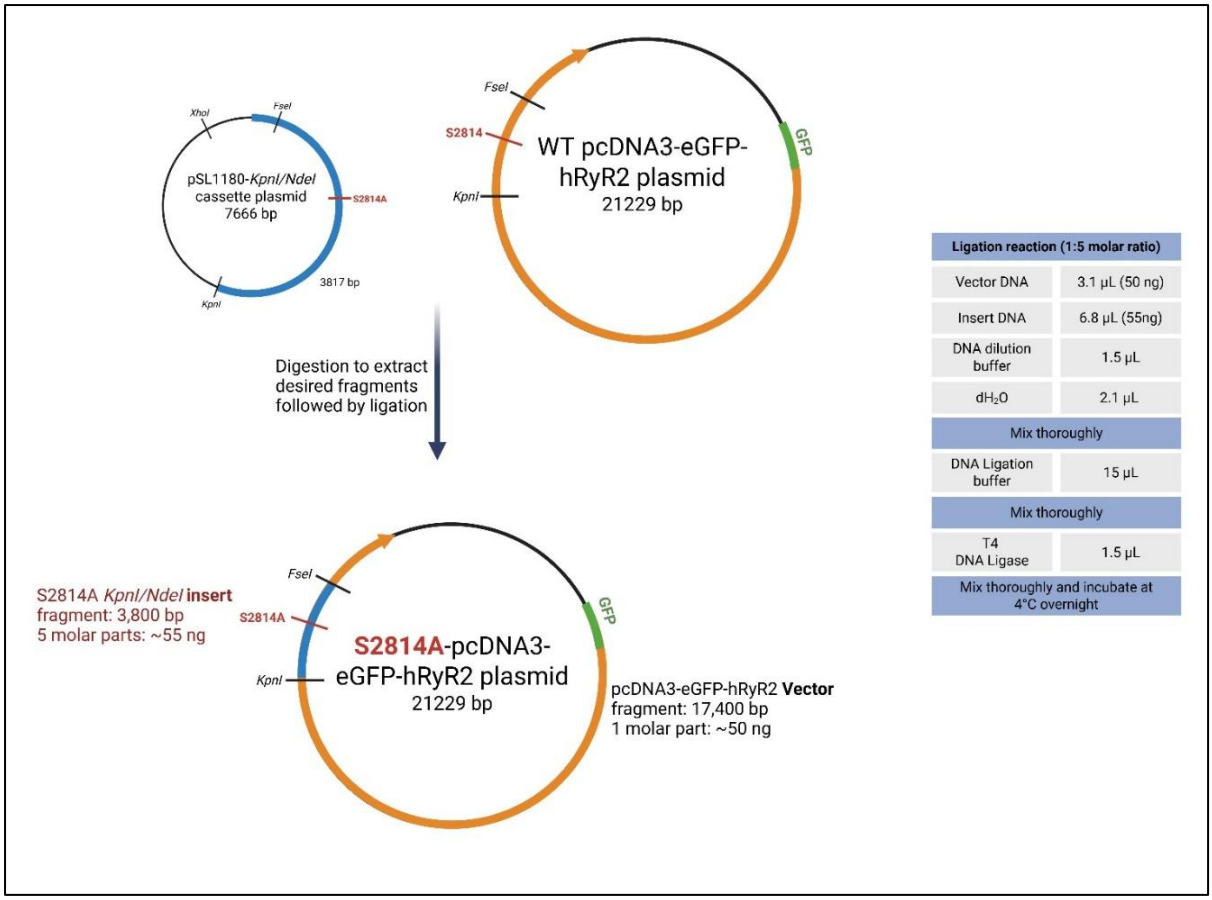

Figure 4.4. A Schematic representation of the S2814A-hRyR2 construct generated by cloning the mutated *KpnI/FseI* fragment into the pcDNA3-eGFP-hRyR2 plasmid. *(Top left)* The *KpnI/NdeI*-mutated cassette containing *KpnI*, *FseI*, and *XhoI* restriction sites. The blue line represents the coding part of the hRyR2 sequence. *(Top right)* The WT eGFP-hRyR2 plasmid with *KpnI* and *FseI* restriction sites; the orange line represents the hRyR2 coding region. *(Bottom)* Final S2814A-hRyR2 plasmid after ligation of the S2814A-*KpnI/NdeI* cassette into the full-length hRyR2 plasmid. A 1:5 molar ratio of vector to insert was used. The ligation reaction was catalysed by T4 ligase using the Rapid DNA ligation kit (Roche) according to manufacturer's instructions.

4.2.3 Colony screening for ligation products

Ligation products were transformed into XL-10 Gold cells. Bacterial colonies were then picked and plasmids were extracted from bacterial cultures using the QIAprep® Spin Miniprep Kit (Qiagen) according to manufacturer's instructions as detailed in **Section 2.3.2**. Once plasmids were verified as eGFP-hRyR2 by restriction digest, cultures were then allowed to grow overnight before large-scale plasmid extraction using the HiSpeed Plasmid Maxi Kit (Qiagen) according to manufacturer's instructions as detailed in **Section 2.3.2**. The plasmid DNA was then quantified and verified again by restriction

digest.

Plasmid restriction digest was carried out as described in **Section 2.3.3** and served as a check-point to confirm that correct ligation of the plasmid fragments had occurred, giving an RyR2 "fingerprint" pattern in the digest. Digest with one enzyme (*BglII* or *EcoRI*) was used to verify plasmids after miniprep, whereas separate digests with *BglII*, *EcoRI* and *HindIII* enzymes was used for verification of plasmids after maxiprep.

Full-length S2814A-hRyR2 and the mutated cassette were sent for Sanger sequencing by Eurofins Genomics' TubeSeq service using 50-100 ng/µL of purified plasmid DNA from each construct. Three primers were used to sequence the mutation site, *FseI* restriction site and *KpnI* restriction site (See **Table 4.4)**. The sequencing electropherograms were viewed on Chromas 2.5.0 and DNA sequences were aligned using BLAST 2 Sequences tool on the National Centre for Biotechnology Information (NCBI) website.

Table 4.4. Sequencing primers used to verify the mutation site and enzyme restriction sites following cassette-based site-directed mutagenesis and ligation. Sequences are given in the 5' to 3' direction.

Primer	Description	Direction	Sequence	GC content (%)	Start nucleotide
SPFOR8305-22	Verification of S2814A mutation site	Forward	CCATGACAAATGGTCAAT	39	C8184
24F	Verification of *FseI* restriction site	Forward	GGCACTAAGAGAGTTGATCCTC	50	G10969
AGKPN	Verification of *KpnI* restriction site	Reverse	GGATAGAAGCCATTGTAGCC	50	G5883

4.3 Results

4.3.1 Propagation of WT hRyR2 plasmid

After transforming Stbl2 cells with the WT hRyR2 plasmid, six bacterial colonies were selected for screening. All colonies showed the correct *BglII* digest pattern after the miniprep stage (see **Appendix III**). Four colonies were then cultured for 18 hours, followed by large-scale plasmid extraction, yielding plasmid concentrations of 585, 245, 129, and 200 µg/mL. Digests with *EcoRI*, *BglII*, and *HindIII* respectively confirmed that all four colonies displayed the expected pattern for pcDNA3-eGFP-hRyR2 plasmid (see **Figure 4.5** and **Appendix IV**). Plasmids were stored at -20 °C until used.

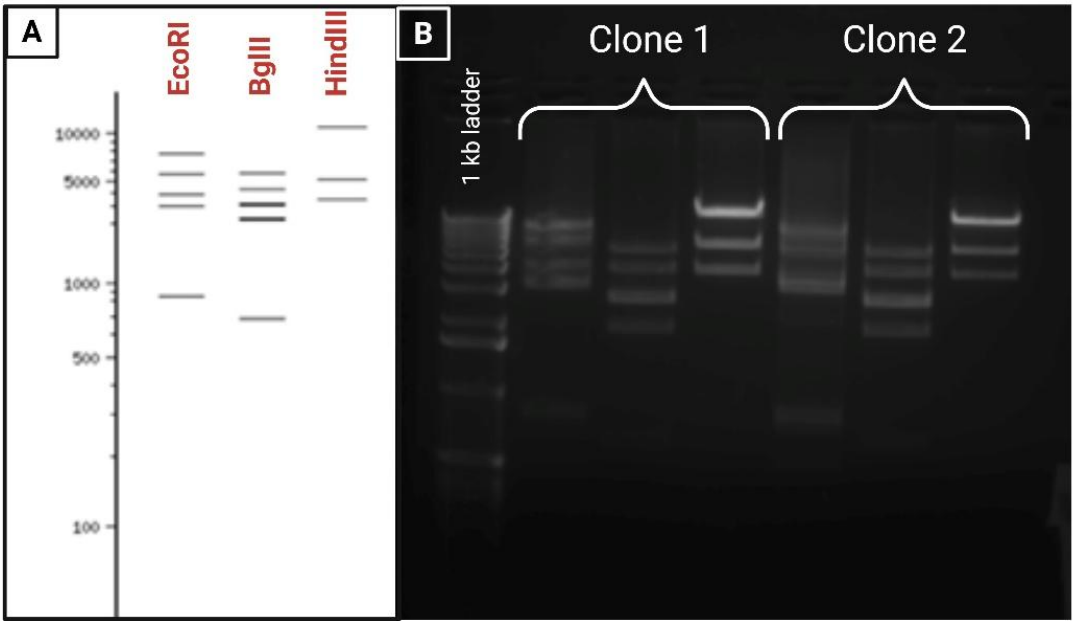

Figure 4.5. Successful propagation of WT pcDNA3-eGFP-hRyR2 plasmid. (A) Shows illustration of expected digest patters with *EcoRI*, *BglII*, and *HindIII* restriction enzymes indicative of positive clones. Digests obtained from NEBcutter® 3.0.19 tool **(B)** A representative gel electrophoresis image of two clones digested with *EcoRI*, *BglII*, and *HindIII* respectively following large-scale plasmid extraction which yielded concentration of 585 and 245 µg/mL for clone 1 and 2 respectively. Both clones show correct digest pattern.

4.3.2 hRyR2-S2814A ligation challenges

In order to construct the phosphoablative form of hRyR2 (S2814A), the mutation was inserted into the *KpnI/NdeI* cassette of hRyR2 using site-directed mutagenesis. Mutagenesis of the cassette was then confirmed by Sanger sequencing before ligating into full-length hRyR2 plasmid (see **Figure 4.8.C**). Two ligation attempts were carried out. For each attempt, at least 20 bacterial colonies were picked and screened using *EcoRI* digest to identify positive clones that show the digest pattern characteristic of pcDNA3-eGFP-hRyR2 and exclude those clones which underwent recombination.

Following the first ligation attempt of the *KpnI/NdeI* cassette in the 1:3 vector:insert ratio, gel electrophoresis revealed that none of the 20 clones screened showed the correct digest pattern, denoting recombination (see **Appendix V**). The ligation process was thus repeated using a molar ratio of 1:5 because increasing the insert abundance in the reaction mixture is sometimes required for smaller inserts and could increase the chance of successful cloning. Out of 23 colonies that were picked, 7 colonies showed correct digest pattern of full-length hRyR2 with *EcoRI* (*i.e.*, ligation efficacy of ~30 %) (see **Figure 4.6**).

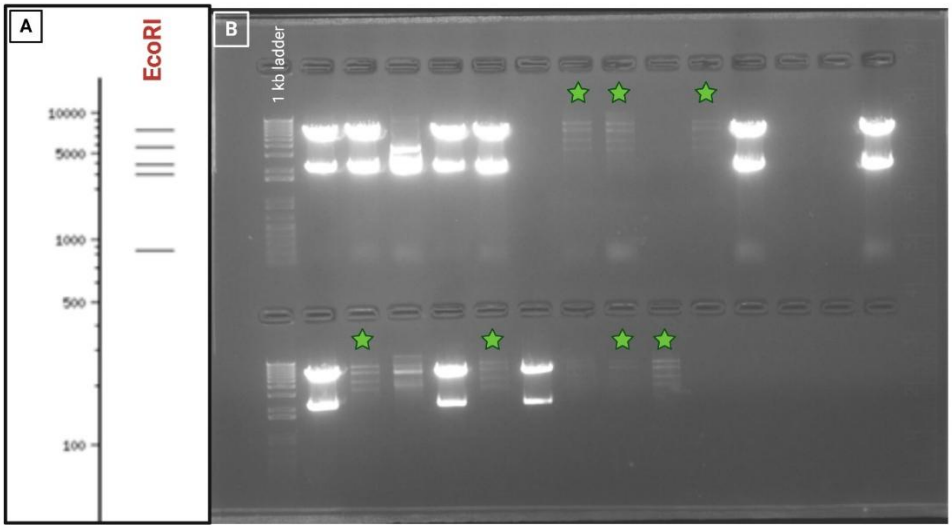

Figure 4.6. Attempts to ligate mutated S2814A *KpnI/NdeI* cassette into full length hRyR2 plasmid. (A) Shows illustration of expected digest pattern with *EcoRI* restriction enzyme, obtained from NEBcutter® 3.0.19 tool, indicative of positive clones. The cutting pattern gives a "fingerprint" that distinguishes and identifies hRyR2 plasmids. **(B)** Represents gel electrophoresis image of 23 colonies obtained from XL10-Gold transformation from the 2nd ligation attempt using 1:5 insert: vector ratio. Seven colonies showed the correct RyR2 digest pattern (marked with green stars) with *EcoRI*.

4.3.3 Instability of hRyR2-S2814A construct during plasmid propagation

In our laboratory's experience, scaling up of mutated hRyR2 plasmid cultures in XL-10 Gold can lead to plasmid recombination, particularly with mutations that render the plasmid more fragile than usual. It was found that re-transforming of mini-prep plasmid DNA from XL10-Gold cells into Stbl2 cells aids the stability of some recombination-prone constructs (Hamilton, 2017). Therefore, Stbl2 cells were used to re-transform positive ligation clones identified by *EcoRI* digest, as shown in **Figure 4.6**. However, the clones recombined either at the mini-prep stage or in the process of scaling up from mini to maxi cultures, which reflected the instability of the mutant construct. Two out of seven colonies recombined at the mini-prep stage. The remaining four positive clones recombined following large-scale plasmid extraction (see **Figure 4.7**).

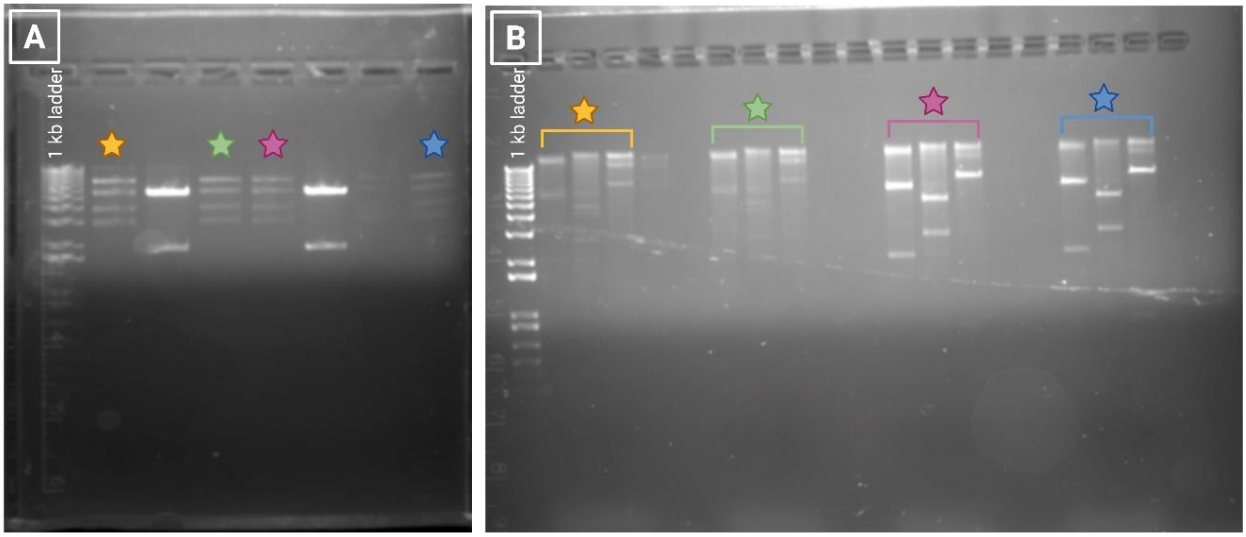

Figure 4.7. S2184A-hRyR2 clones do not easily propagate in E.coli. Gel electrophoresis images of mini- and maxi-prep plasmids obtained from Stbl2 cells transformation of positive ligation clones shown in Figure 4.6. **(A)** Shows *EcoRI* digest of mini-prep plasmids. Two out of 7 colonies had already recombined at this stage. **(B)** Shows cutting pattern of four verified maxi-prep plasmids with *EcoRI*, *BglII* and *HindIII*, respectively. Coloured stars represent the same colony culture at the mini and maxi-prep stages. At the maxi-prep stage, all colonies had recombined.

To address the issue of recombination, both XL10-Gold and Stbl2 cells were used to re-transform the positive ligation clones to test whether the mutated plasmid was more stable in one type of cells than the other. Also, different experimental conditions were optimised to reduce the chance of recombination at the large-scale culture stage as

follows: The maxi-prep flasks were seeded with cells at a 1:400 concentration rather than 1:200. Additionally, the incubation time was reduced to 16 hours rather than 18 hours to reduce the chance of recombination. Four retransformation attempts (using two different positive ligation clones) were carried out under the above-mentioned conditions using XL10-Gold and Stbl2 summarised in **Table 4.5.** Gel electrophoresis of mini-prep plasmids digest can be seen in **Appendix VI** and **Appendix VII**.

Two colonies from one positive ligation clone (attempts no. 4 and 5) displayed correct RyR2 restriction digest pattern when cut with *EcoRI*, *BglII* and *HindIII* enzymes following maxi-prep (see **Figure 4.8.B**). The propagation yielded concentrations of 360 µg/ml and 230 µg/ml. However, alignment with the hRyR2 coding sequence revealed these plasmids to be WT hRyR2. This prompted some confusion as the mutant sequence of the cassette used for ligation had been confirmed (see **Figure 4.8.C**). The possible reasons for this result are discussed below.

In summary, while cassette mutagenesis was confirmed by sequencing, ligation of the mutated fragment into full-length hRyR2 produced an unstable construct prone to recombination, with very few clones surviving large-scale propagation. Notably, the two clones that did withstand large-scale propagation were sequenced as WT hRyR2- reasons for this will be explored in the discussion.

Table 4.5. Attempts to retransform and propagate S2814 phosphoablative hRyR2 construct in super-competent E.coli cells.

Ligation clone transformation attempt number	Type of cell line used	Conditions of the large-scale culture	Number of clones picked	Number of positive clones	Number of maxipreps	Digest result at maxiprep
1	Stbl2	18 hrs incubation. Seeded at 1:200	7	5	4	**Negative**
2	Stbl2	16 hrs incubation. Seeded at 1:400	6	1	0 - due to inability to access the lab.	
3	XL10-Gold	16 hrs incubation. Seeded at 1:400	6	0		
4	Stbl2	16 hrs incubation. Seeded at 1:400	6	4	1	**Positive**
5	XL10-Gold	16 hrs incubation. Seeded at 1:400	6	1	1	**Positive**

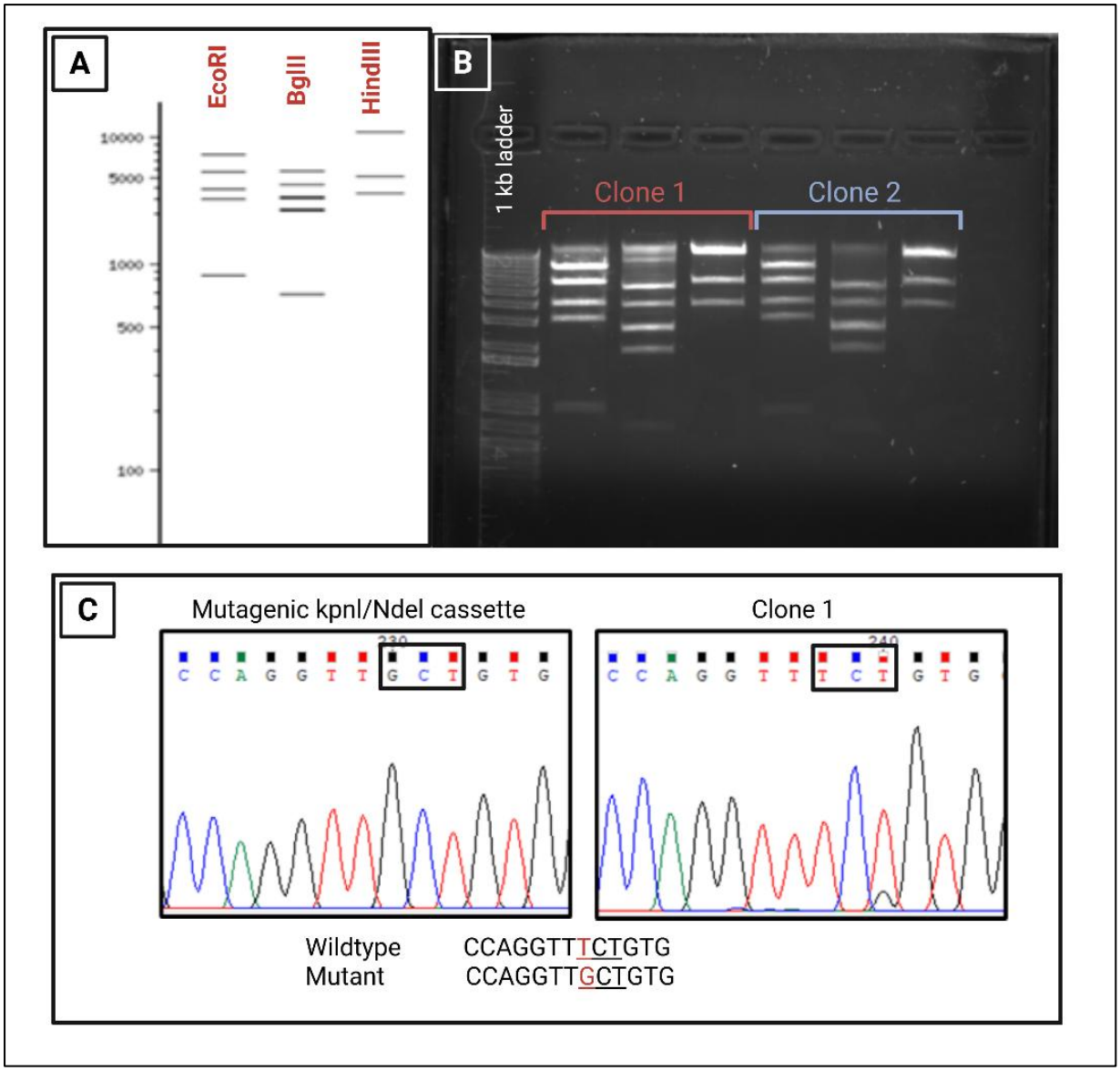

Figure 4.8. Attempts to propagate the S2814A phosphoablative mutant of hRyR2. (A) Represents the expected hRyR2 plasmid cutting pattern and fragments length produced by *EcoRI*, *BglII* and *HindIII* restriction enzymes. The cutting pattern gives a "fingerprint" that distinguishes and identifies hRyR2. Digests obtained from NEBcutter® 3.0.19 tool. **(B)** Shows gel electrophoresis image of the maxi-prep plasmids of two colonies obtained from Stbl2 (clone 1) and XL10-Gold (clone 2) transformation of one positive ligation mini-prep. The two colonies show correct cutting patterns for all three restriction enzymes: *EcoRI*, *BglII* and *HindIII* respectively. **(C)** Electropherogram generated from sequencing *KpnI*/*NdeI* cassette following site-directed mutagenesis verifies the desired point of mutation. However, sequencing (clone 1) hRyR2 plasmid shows that the construct has WT hRyR2 sequence.

4.4 Discussion

The S2814A construct has shown to be very fragile and difficult to propagate in super-competent *E.coli* cells. Although site-directed mutagenesis and cassette ligation into the full length hRyR2 plasmid was successful, plasmid recombination was a major issue. The mutant construct recombined at the mini-prep stage or in the process of scaling up from mini to maxi cultures which reflects the instability of the structure. This could not be overcome by optimising the incubation conditions of the large-scale culture (*e.g.,* lower temperature and reduced seeding concentration), nor by retransformation of positive ligation clones in XL-10 gold cells (see **Table 4.5**). The only clone that survived the process and did not recombine was shown to be WT hRyR2 by sequencing.

Given that cassette mutagenesis had been verified by sequencing, it is possible that a miniscule amount of WT hRyR2 that was only cut once rather than twice (*i.e.*, linearised), was extracted during gel extraction, and later re-ligated itself in the ligation process (see **Figure 4.9**). This is possible due to the difficulty getting double digests reaction to be complete, even when incubating overnight. Additionally, separating high molecular weight bands (18 kb and 21 kb) by agarose gel electrophoresis is very difficult, and given the fact that the gel slice was cut quickly to prevent DNA damage by prolonged exposure to UV light, it is therefore possible that a very small amount of higher molecular weight fragment that had been cut once was extracted along with the desired band.

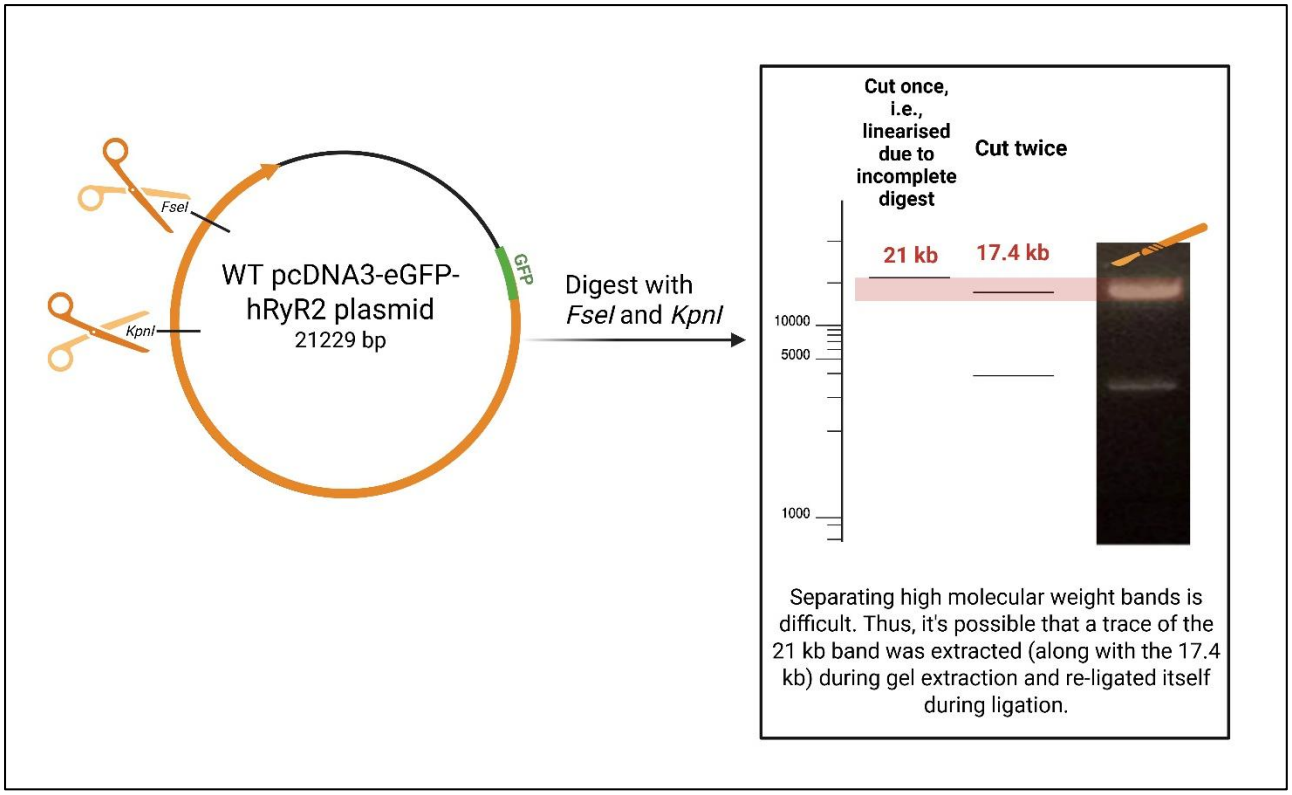

Figure 4.9. Illustration of the potential source of WT hRyR2 contamination during cassette mutagenesis. Incomplete double digest reaction could leave a small amount of linearised hRyR2 plasmids. Due to the difficulty of resolving high molecular weight fragments by gel electrophoresis, this linearised plasmid may have been co-extracted with the desired 17.4 kb band during the rapid excision of the gel slice.

The observed instability of the S2814A hRyR2 mutant construct also means that it would likely be extremely difficult to express in HEK293, if at all possible. Previous work in our laboratory by Hamilton (2017) showed that some phosphomimetic RyR2 mutants that were exceptionally difficult to generate, requiring numerous ligation and transformation attempts, were also unstable at the protein level when expressed in HEK293 cells. These mutants exhibited significantly lower transfection efficiencies compared to WT hRyR2, and visualisation of their intracellular localisation in IF experiments denoted a “granular” appearance. This appearance is suggestive of protein mislocalisation to lysosomes or aggregates that are consistent with protein misfolding, defective channel assembly and degradation.

The failure to generate a stable S2814A RyR2 mutant highlights a critical limitation in the molecular engineering of large ion channels. The instability of the construct in bacterial

systems suggests that either the point mutation induces structural perturbations that impair DNA replication or that the hRyR2 sequence surrounding S2814 is inherently prone to recombination.

All previous research on RyR2 phosphorylation by CaMKII at S2814 has been carried out in knock-in mice, and there are no studies in the literature that used *in vitro* methods of S2814A cloning. An alternative method to study the role of CaMKII phosphorylation of RyR2 is the use kinase inhibitors, *e.g.,* KN-93 (Wong et al., 2019) if this direction were to be taken. However, the poor selectivity and potential off-target binding of kinase inhibitors is sometimes unavoidable.

On the basis of these results, it was decided not to further pursue making the S2814A-RyR2 mutant construct, as even if a positive DNA sequence was achieved, it would likely produce an unstable protein that would be difficult to express in a mammalian cell system. Therefore, the focus was shifted to studying the effects of mutant CaMs on CaMKII activation and investigating RyR2 phosphorylation level at S2814 in the presence of mutant D132E and Q136P CaMs, in addition to investigating the direct effect of mutant CaMs on RyR2 channel gating in response to cytosolic and luminal Ca^{2+} using single channel recording technique.

Chapter 5: Understanding the mechanism of calmodulinopathy: Investigating the effects of variant CaM on CaMKII phosphorylation of RyR2 and single-channel gating

5.1 Introduction

5.1.1 The role of CaMKII phosphorylation in arrhythmogenesis and CPVT

CaMKII is a critical regulator of RyR2 function, particularly during β-adrenergic stimulation (**see Section 1.4.2.2**). Its activation directly enhances RyR2 function, promoting SR Ca^{2+} release and ensuring adequate contractile force (Kushnir et al., 2010; Wehrens, 2011; Y. Wu et al., 2009). However, evidence suggests that CaMKII is the principal mediator of SR Ca^{2+} leak induced by β-adrenergic stimulation (Anderson et al., 2011; Baier et al., 2021). Aberrant CaMKII signalling is a well-established arrhythmogenic mechanism implicated in various cardiac pathologies, including dilated cardiomyopathy, cardiac hypertrophy, and arrhythmias (Anderson et al., 2011; Berchtold et al., 2016; Zhang et al., 2003). This is thought to be driven by CaMKII-mediated hyperphosphorylation of key targets, such as RyR2, leading to pathological SR Ca^{2+} release events (Van Oort et al., 2010). In a study by Ai et al. (2005), abnormal SR Ca^{2+} leak in a rabbit model of arrhythmogenic heart failure was mitigated by CaMKII inhibition with KN-93 but remained unaltered by PKA inhibition. Similarly, CaMKII inhibition with KN-93 completely prevented catecholamine-induced ventricular sustained tachyarrhythmia in RyR2-mutant mice (N. Liu et al., 2011).

Little is known about the direct effects of CPVT-associated CaM mutants on CaMKII activation and kinase activity. Prakash et al. (2022) and Hwang et al. (2014) reported no difference in CaM-dependent CaMKII activation level between WT and CPVT-linked N54I, N98S and A103V CaM variants. There is no data currently available on the effects of D132E and Q136P mutant CaMs on CaMKII activation and its subsequent phosphorylation of RyR2 at the S2814 site. Elucidating how these mutants alter CaMKII signalling is a critical step in understanding the pathogenesis of CaM-linked CPVT and could reveal novel therapeutic targets.

5.1.2 Variant CaM effect on RyR2 single channel gating

Looking at RyR2 channel function at the single-channel level provides valuable data on the direct effect of variant CaM on RyR2 channel gating kinetics. Being an intracellular

channel protein, it is not possible to study single channel properties of RyR2 with traditional patch-clamp techniques. Instead, purified RyR2 channels could be incorporated in an artificial lipid bilayer to measure ionic flux in real time. The use of solubilised and purified RyR2 channels offers the advantage of studying the effect of -only- direct binding of CaM on channel function in the absence of CaMKII and other channel regulators. Although the use of a detergent-based purification process has inherent limitations, the experimental procedure applied here used the lowest possible detergent concentration, thereby preserving channel function and Ca^{2+} sensitivity.

In single channel experiments by Søndergaard et al. (2019) and Hwang et al. (2014), WT CaM has been shown to decrease P_o of canine and sheep RyR2 channels, aligning with its well-established inhibitory role on RyR2 function. Looking at the effect of CPVT-linked CaM mutations on RyR2 function at the single-channel level, A103V, N54I and N98S CaM have been shown to increase RyR2 channel P_o at activating Ca^{2+} concentrations compared to WT CaM, denoting loss of CaM inhibition of RyR2 (Hwang et al., 2014; Søndergaard et al., 2019). N54I was also shown to increase RyR2 channel P_o at diastolic Ca^{2+} concentration, which may indicate Ca^{2+} leak at the channel level caused by this mutant (Hwang et al., 2014). In contrast, D96V CaM variant that is associated with LQTS showed no difference in RyR2 single channel regulation compared to WT CaM (Hwang et al., 2014).

While Q136P CaM variant has been reported to increase P_o in canine RyR2 channels (Søndergaard et al., 2019), the effect of D132E and Q136P CaM on human RyR2 single channel function remains to be investigated. Characterising the direct effect of D132E and Q136P CaM on recombinant hRyR2 channels would help identify the molecular mechanisms underlying CPVT pathogenesis.

5.1.3 Chapter aims and objectives

The aim of this chapter is to determine whether the CPVT-linked CaM variants D132E and Q136P impair CaMKII regulation of RyR2 function either by affecting CaM-dependent CaMKII autophosphorylation or by altering CaMKII-mediated phosphorylation level of RyR2 at the S2814 site. Furthermore, the functional impact of these variants will be directly evaluated by examining single-channel gating of RyR2 in the presence of WT or mutant CaM. This work aims to establish whether the aberrant Ca^{2+} release that was observed in **Chapter 3** is caused by dysfunctional CaMKII signalling and/or direct alterations to single-channel function.

Key objectives:

- Assess WT and variant D132E and Q136P CaM activation of CaMKII by measuring CaMKII autophosphorylation level over time in the presence of WT or mutant CaM using an *in vitro* autophosphorylation assay and western blotting.
- Assess RyR2 phosphorylation level at the S2814 CaMKII phosphorylation site by western blotting cell homogenates of HEK293 cells co-transfected with hRyR2 and WT or variant CaM.
- Incorporate purified recombinant hRyR2 channels in an artificial lipid bilayer and assess channel gating at an activating Ca^{2+} concentration of 100 μM in the presence of WT or variant D132E and Q136P CaM.

5.2 Methods

5.2.1 Coomassie Brilliant Blue Gel Staining

In order to confirm the presence and purity of CaM proteins obtained from our collaborators (see **Section 2.2.2**), Coomassie Brilliant Blue G (SERVA) staining was used according to manufacturer's instructions following SDS/PAGE as described in **Section 2.3.12.** The protein concentrations, as quantified by our collaborators, were 10.50 mg/mL, 13.94 mg/mL and 11.41 mg/mL for WT, D132E and Q136P CaM, respectively. A total of 5 µL of each protein sample were loaded, corresponding to approximately 55-65 µg of protein.

5.2.2 *In vitro* CaMKII autophosphorylation assay

An *in vitro* kinase assay was carried out to assess CaMKII autophosphorylation levels in the presence of WT or mutant CaMs (D132E or Q136P). For each reaction, recombinant GST-tagged human CaMKIIδ protein (300 nM; Abcam, ab84552) and 1 µM CaM protein were incubated at room temperature (23 °C) with 2x reaction buffer (100 mM HEPES, 200 mM KCl, 4 mM $MgCl_2$, pH adjusted to 7.5 with KOH before adding 200 µM $CaCl_2$) and 5 mM DTT in an Eppendorf ThermoMixer at 1200 RPM speed. The reaction was started by adding Na_2ATP (150 µM; Fisher Scientific, 15450177). Immediately following ATP addition, a 10 µL aliquot was removed and defined as the 0-second time point. Subsequent 10 µL samples were taken at 30, 60, 120, and 300 seconds. Each sample was immediately transferred to a tube containing SDS-Laemmli buffer to terminate the phosphorylation reaction.

Samples were then heated at 40 °C for 20 mins before loading onto 4-12% Tris-Glycine gel and SDS/PAGE. Following this, the proteins were transferred onto PVDF membrane using the iBLOT™ 2 dry blotting system as detailed in **Section 2.3.11**. The blots were then blocked and then probed for phosphorylated CaMKII using the following antibodies:

- Anti-CaMKII (phospho T287) rabbit polyclonal primary antibody (Abcam, ab182647): used at 1:1,000 dilution.
- Goat anti-rabbit secondary antibody (Cell Signalling, 7074): used at 1:10,000

dilution.

To probe for total CaMKII protein (to serve as a loading control), membranes were then stripped of all antibodies (as described in **Section 2.3.11**) and reprobed using the following antibodies:

- Anti-GST mouse monoclonal primary antibody (Sigma-Aldrich, G1160): used at 1:1,000 dilution
- Rabbit anti-mouse secondary antibody (Abcam, ab6728): used at 1:10,000 dilution.

5.2.3 Measuring RyR2 phosphorylation at S2814 site

PVDF membranes previously probed for eGFP-RyR2 expression levels in **Section 3.1.1** were stripped of all antibodies as described in **Section 2.3.11**, and reprobed for S2814-phosphorylated RyR2. This was to investigate the effect of mutant CaMs on RyR2 phosphorylation level at the S2814 CaMKII phosphorylation site. Antibodies used in reprobing are:

- RyR2 pSER2814 rabbit primary antibody (Badrilla, A010-31): used at 1:500 dilution.
- Goat anti-rabbit secondary antibody (Abcam, ab6721): used at 1:10,000 dilution.

5.2.4 RyR2 Single channel recording

5.2.4.1 Experimental setup

Lipid bilayers were established in a two-chamber system consisting of a cup (corresponding to the cytosolic chamber (cis)) and a block (corresponding to the luminal chamber (trans)) (see **Figure 5.1**). The cup-block system and the electronic head-stage connections are fixed on a heavy lead block placed on a vibration isolation table to reduce mechanical noise distortion of the bilayers. The setup is also placed in an aluminium box with a lid which acts as a Faraday cage to minimise ambient electromagnetic interference from other surrounding devices. The cup is made of a styrene copolymer with a cylindrical cavity that forms a think septum with a small hole of

200 µm diameter at the centre of the septum, which connects the cis and trans chambers. A small magnetic stirrer is incorporated in the lead block under the cup-block system to allow for solutions to be mixed when needed. The block, which is made of Perspex, is rectangular in shape and has a circular cavity in the middle where the cup can tightly fit in with the hole facing towards the front facing a rectangular cavity which forms the trans chamber. The front face of the block is made of clear glass to allow for clear view of the trans chamber and the front of the cis chamber bearing the hole. The cis and trans chambers are filled with 500 µL and 1000 µL of the recording solution, respectively (consists of 210 mM KCl and 20 mM HEPES; pH 7.4). The recording solutions are connected to two cylindrical wells in the block filled with 3 M LiCl using agar salt bridges. The bridges are made of thin glass capillaries filled with 2% (w/v) agar in 3 M LiCl. The electronic system is connected to the cup and block via silver wire electrodes coated with AgCl and placed in the two cylindrical wells in the block. The electronic components used in the bilayer setup were designed and custom-built by R.A. Montgomery (National Heart and Lung Institute, Imperial College, UK).

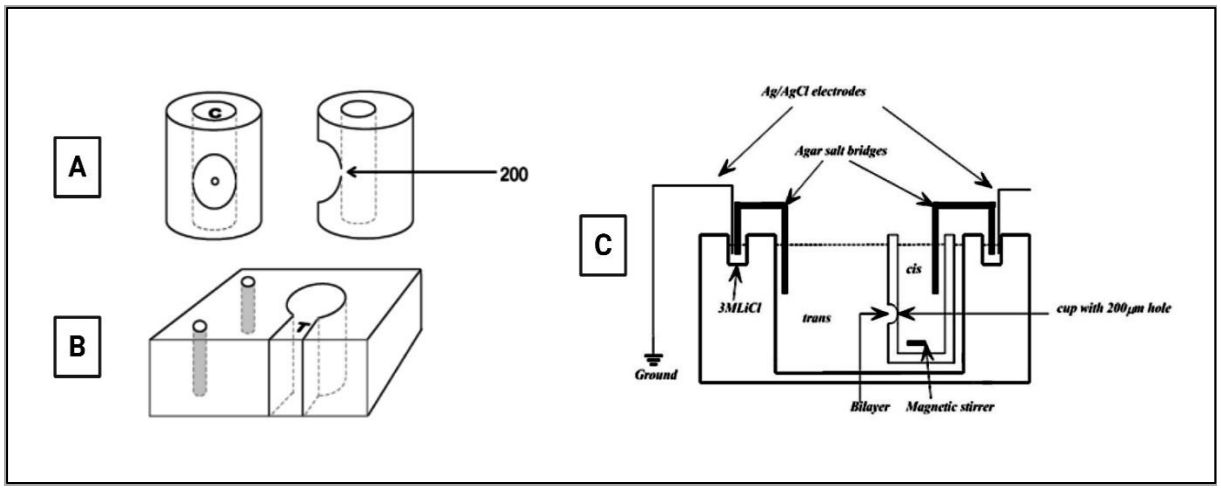

Figure 5.1. Schematic representation of the cup and block experimental setup used for RyR2 single channel recording. (A) Shows the cup (cis chamber) with a cylindrical cavity that forms a think septum with a small hole of 200 µm diameter at the centre of the septum where the channel incorporate within an artificial bilayer. **(B)** Shows the block and the circular cavity in the middle where the cup can tightly fit in with the hole facing towards the front facing a rectangular cavity which forms the trans chamber. The two cylindrical wells in the block contain 3 M LiCl. **(C)** Diagram of the bilayer recording chambers and its associated electronics. AgCl-coated silver electrodes connect the electronic system to the cup and block in order to measure channel gating. Figure adapted from Mukherjee (2014).

5.2.4.2 Bilayer formation and hRyR2 channel incorporation

During single channel experiments, the trans chamber is always held at virtual ground, while the cis chamber can be held at different voltages relative to the ground. The phospholipid phosphatidylethanolamine (PE) (Avanti) was used to create artificial lipid bilayers for RyR2 channels to incorporate in. PE was stored as 50 mg/mL stocks in chloroform in -20 °C. An aliquot of the lipid is prepared on the day by evaporating the chloroform under a stream of N_2 before resuspending the lipid in n-Decane to a final concentration of 35 mg/mL. Before starting the experiment, the 200 µm hole of the cup was 'primed' by painting a small amount of the lipid across the inside of the hole using a 'painting stick', and allowing it to dry (repeated 3 times), which helps in formation of planar lipid bilayers. Following hole priming, assembly of the cup and block and addition of the recording solutions, an artificial lipid bilayer is formed by spreading the PE lipid upwards across the hole inside the cup, which occurs spontaneously due to the nature of the lipid (Laver, 2001; White, 1986).

During the formation of a lipid bilayer, its thickness decreases, a change that can be tracked electrically. Because the bilayer acts as an insulating capacitor situated between two conductive ionic solutions, its capacitance increases as it becomes thinner. By applying a small, alternating square wave pulse (oscillating between ± 4 mV) across the membrane, the thinning process can be monitored in real-time using the Acquire 5.0.1 software (Bruxton). The growing capacitance spikes observed in response to this pulse directly signal the thinning of the lipid film into a stable bilayer (~200 pA).

Once a planar bilayer was established, an osmotic gradient was created by the addition of two 100 µL aliquots of 3 M KCl to the cis chamber and stirring before the addition of a small volume of 1-3 µL of recombinant hRyR2 channels from microsomal material (for purification method, see **Section 2.3.10**), to the cis chamber to facilitate channel incorporation. Due to the unique structure of RyR2, the channel would always incorporate in a fixed orientation, with its large cytosolic domain facing the cis chamber, and the luminal domain facing the trans chamber (Laver, 2001; Sitsapesan & Williams, 1994). A magnetic reed switch was used to isolate the electric set up every time something is added to the cis chamber to prevent breaking of the bilayer. Channel

incorporation was monitored using the Acquire software.

5.2.4.3 hRyR2 channel activation and CaM addition

Once a channel had incorporated, the cis chamber was perfused with the recording solution supplemented with 1 mM nitrilotriacetic acid (NTA) and 510 mM $CaCl_2$ to achieve free Ca^{2+} concentration of 100 µM for maximal activation of hRyR2; as calculated using the MaxChelator software. The channels were recorded at +30 mV for ~1-2 mins before adding 1 µM CaM protein and recording for ~ 5 mins. EMD-41000 was then added at the end of the recording at a concentration of 150 µM to confirm the number of channels in the bilayer.

5.2.4.4 Single channel gating analysis

Single channel recordings were analysed using the QuB analysis suite 2.0.032 (Milescu et al., 2000). After cleaning the recording by removing any areas of excessive noise, the baseline, open and closed states of the channel recording were assigned in QuB. The data were then idealised using the *idl/base* function in QuB. The dead time (T_d); defined as the minimum length of an event to be detected, was set to 50 µs. The analysis generates several parameters including P_o, median open time (T_o) and median closed time (T_C).

5.3 Results

5.3.1 Coomassie Blue Assay confirmed CaM proteins presence and purity

To study the direct effect of variant CaM on CaMKII autophosphorylation, Ca^{2+} spark generation and RyR2 channel recording, purified CaM proteins were needed. Coomassie Brilliant Blue dye was used to confirm the presence and purity of the CaM mutant constructs obtained from our collaborators prior to use in experiments. All CaM constructs were visualised at the expected molecular weight (17.6 kDa) following SDS-PAGE. A couple of lower molecular weight bands were observed with D132E and Q136P CaM, which suggests a negligible degree of protein degradation (see **Figure 5.2)**

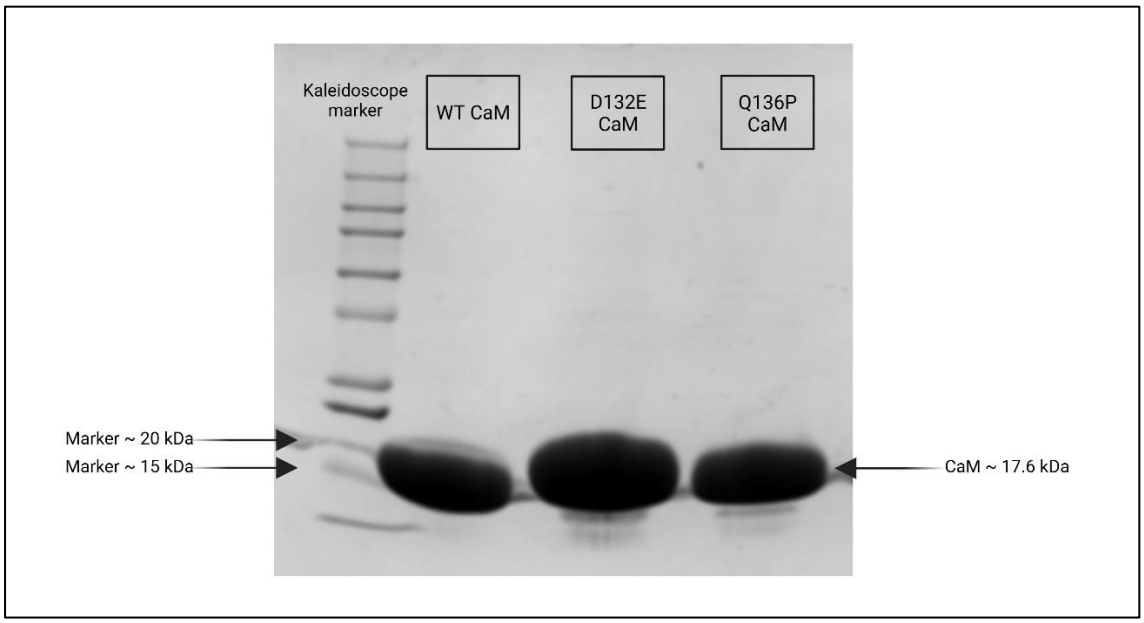

Figure 5.2. Coomassie Brilliant Blue assay to confirm presence and purity of mutant CaM proteins constructs. A 5 µL sample of each CaM construct (corresponding to ~55-65 µg of protein) was loaded into 4-20% Tris-Glycine gel and separated through electrophoresis. All constructs were visualised at the expected molecular weight of 17.6 kDa.

5.3.2 CaMKII autophosphorylation levels were significantly reduced by Q136P CaM

CaM binding to CaMKII at elevated Ca^{2+} concentrations leads to a conformational change in CaMKII which triggers CaMKII autophosphorylation at T287 site. This CaM-activated CaMKII then phosphorylates RyR2 at the S2814 site during β-adrenergic activation. To investigate whether mutant D132E and Q136P CaM alter CaMKII activation as a

mechanism of pathogenesis, a time course of CaMKII autophosphorylation level was measured. The detected signal for phosphorylated CaMKII was normalised to CaMKII total protein level.

CaMKII autophosphorylation was significantly reduced in the presence of Q136P CaM compared to WT CaM for each time point (p<0.05). CaMKII autophosphorylation levels were similar in the presence of D132E CaM compared to WT (see **Figure 5.3B**). **Figure 5.3A** shows an example of a western blot. All original blots used in the analysis can be seen in **Appendix VIII**, **Appendix IX** and **Appendix X**.

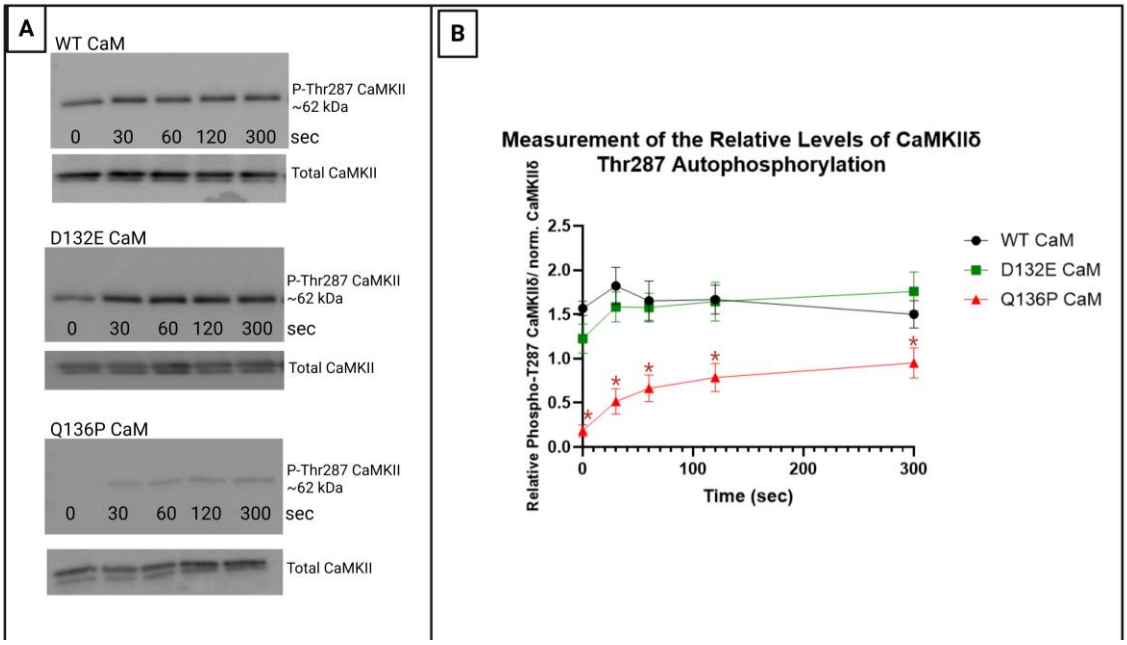

Figure 5.3. Q136P variant CaM significantly reduces CaMKII autophosphorylation. (A) Shows representative western blot of the time course of CaMKII autophosphorylation in the presence of WT, D132E or Q136P CaM. **(B)** Shows densitometric analysis of CaMKII autophosphorylation level with WT or variant CaM relative to total CaMKII total protein level. Each point represents the mean ± SEM. Significance for each time point, indicated by *, was calculated using a Multiple unpaired t-test. n = 4, 5 and 5 blots for WT, D132E and Q136P CaM, respectively.

5.3.3 Q136P CaM variant significantly reduced RyR2 basal phosphorylation level at S2814 CaMKII phosphorylation site

Membranes previously used to estimate RyR2 expression level in HEK293 (see **Figure 3.5** and **Appendix I**) were stripped of all antibodies and reprobed for S2814-phosphorylated RyR2. This was to investigate the effect of mutant CaMs on RyR2 phosphorylation level

at the S2814 CaMKII phosphorylation site.

Densitometric analysis revealed that basal phosphorylation at the S2814 site of RyR2 was comparable in cells co-expressing WT CaM and those expressing RyR2 alone. Cells expressing RyR2 alone show levels of CaMKII phosphorylation because HEK293 cells express CaM endogenously at low levels. Q136P CaM co-expression significantly decreased RyR2 phosphorylation at S2814 compared to WT CaM co-expression (p<0.05). RyR2 phosphorylation level at S2814 with D132E CaM was comparable to that observed with WT CaM (see **Figure 5.4**). All original blots used in the analysis can be seen in **Appendix XI**.

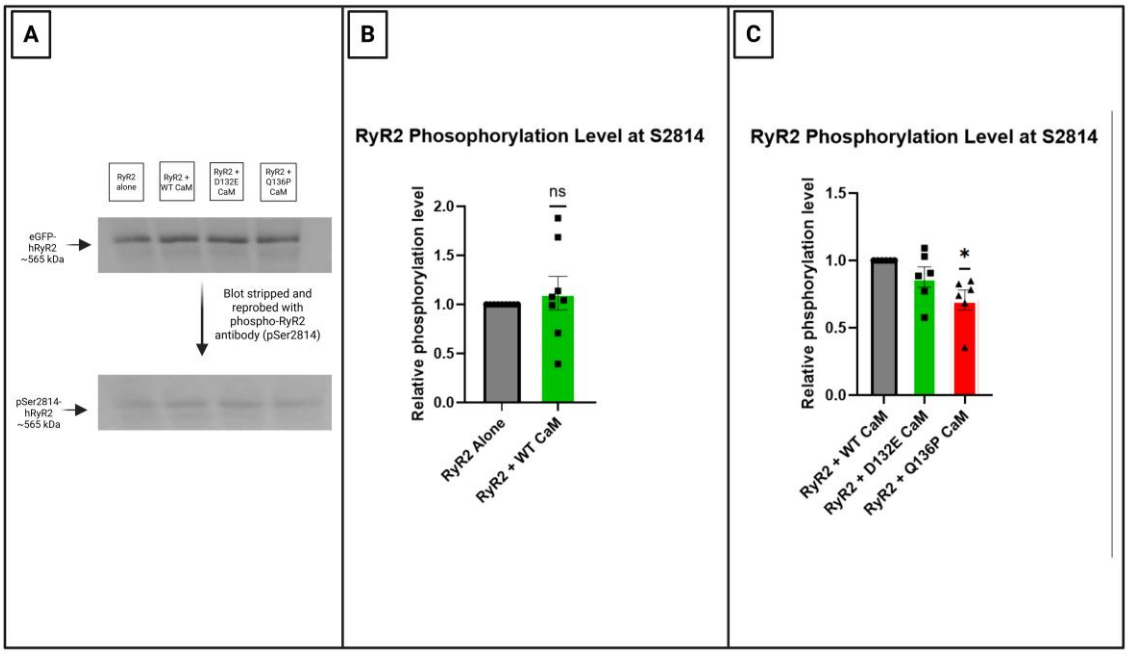

Figure 5.4. Western blot analysis of HEK293 cells co-transfected RyR2 and WT or mutant CaM revealed that basal phosphorylation level at the S2814 is significantly reduced in cells co-expressing Q136P CaM compared to WT CaM. (A) Shows a representative Western blot. 100µg protein homogenate was loaded for each well. Blots were first probed with eGFP antibody before membrane stripping and reprobing with phospho-RyR2 antibody (S2814). **(B)** Shows phosphorylation level of RyR2 at S2814 in the presence of WT CaM relative to S2184 phosphorylation level without CaM expression. **(C)** Shows phosphorylation level of RyR2 when co-expressed with D132E or Q136P CaMs. Levels were normalised to RyR2 phosphorylation with WT CaM. Data are shown as mean ± SEM with individual data points blotted. Significance, as indicated by *, was determined using one sample Wilcoxon test. n =6 blots.

5.3.4 Preliminary single-channel experiments suggest D132E and Q136P CaM reduce RyR2 channel P_o

hRyR2 channel recording was carried out in order to investigate the direct effect of variant D132E and Q136P CaM on channel gating kinetics. However, single channel recording is technically difficult, conditions that favour channel incorporation into the bilayer are tricky to achieve with any consistency and the subsequent perfusion of cis chamber can easily lead to bilayer rupture (Williams & Thomas, 2019). Due to the technical challenges of perfusing the bilayers, multiple attempts to record perfused channels at 100 µM activating Ca^{2+} concentration failed. Thus, preliminary single channel recordings were recorded before and after CaM addition without perfusion. This meant that channel activity was recorded at contaminant Ca^{2+} concentrations (estimated to be ~1 µM (Mukherjee, 2014), and with a chemical gradient present (~800 mM cis/210 mM KCl trans). These sub-optimal conditions do not allow a fair comparison of channel gating between CaM variants, though a comparison of gating before vs after CaM addition can be made. Representative single channel recordings and summary of the findings are shown in **Figure 5.5**.

Addition of WT CaM to RyR2 channel was found to cause a slight decrease in channel P_o from 0.02 to 0.01 and increased the T_C of the channel. Similarly, D132E CaM decreased channel P_o from 0.01 to 0.007 via an increase in channel T_C. The RyR2 channel recorded with Q136P had a high P_o of 0.78 to begin with, and Q136P addition reduced that to 0.51. Channel T_C was not affected by Q136P CaM, but T_o decreased by ~5 ms.

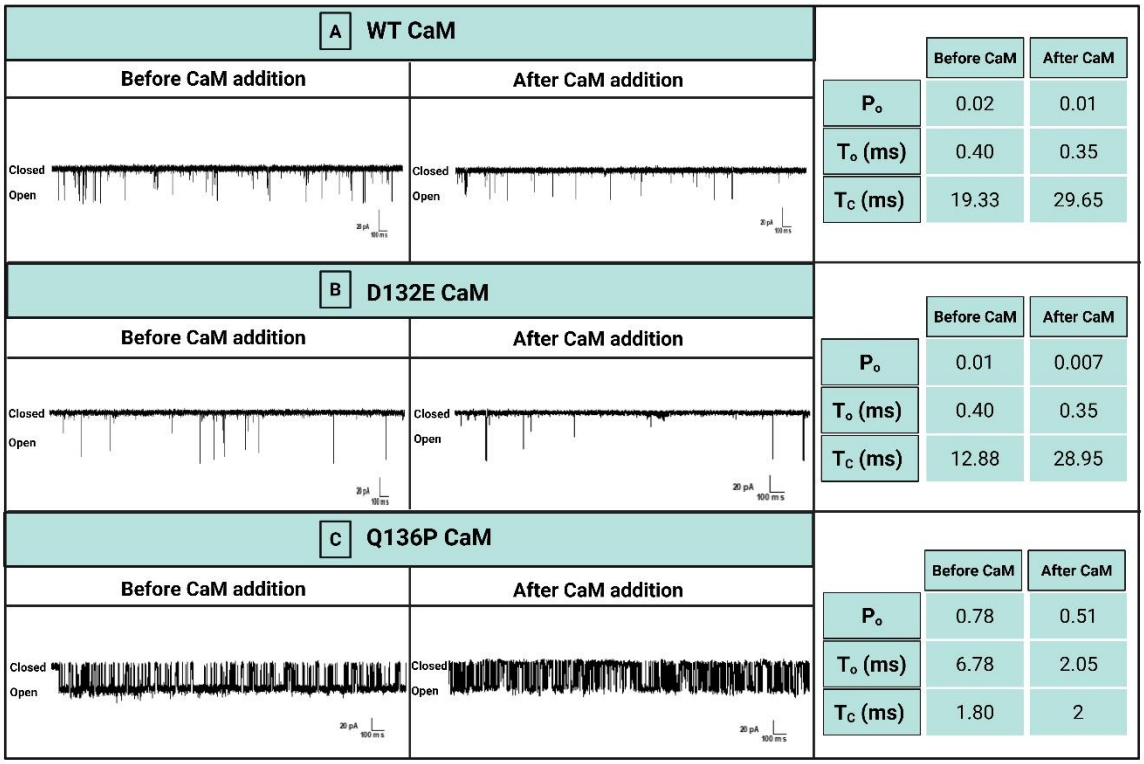

	Before CaM	After CaM
P_o	0.02	0.01
T_o (ms)	0.40	0.35
T_C (ms)	19.33	29.65

	Before CaM	After CaM
P_o	0.01	0.007
T_o (ms)	0.40	0.35
T_C (ms)	12.88	28.95

	Before CaM	After CaM
P_o	0.78	0.51
T_o (ms)	6.78	2.05
T_C (ms)	1.80	2

Figure 5.5. Representative traces of hRyR2 channel activity and parameters describing the idealisation of the traces before and after the addition of 1 µM (A) WT**, (B)** D132E or **(C**) Q136P CaM. Channel openings are represented by downward deflections from the closed state. Channel P_o was decreased with WT or variant CaM addition. *n*= 1 channel each.

5.4 Discussion

5.4.1 S2814-phosphorylated RyR2 level decreased with Q136P CaM co-expression

CaMKII is an important CaM target and aberrant CaMKII phosphorylation of RyR2 has been linked to SR Ca^{2+} leak and CPVT pathogenesis (Hwang et al., 2014; N. Liu et al., 2011). Once bound to CaCaM, the kinase first autophosphorylates itself at Thr287, and then proceeds to phosphorylate target proteins, such as RyR2. Under conditions of β-adrenergic activation, the basal phosphorylation level of RyR2 at the CaMKII-specific site S2814 is elevated, resulting in channel activation characterised by an increased P_o and frequency of Ca^{2+} release (Baier et al., 2021; Guo et al., 2006; Hwang et al., 2014). Western analysis has revealed that Q136P CaM significantly reduced RyR2 phosphorylation at S2814 compared to WT CaM (via impaired CaMKII autophosphorylation), whereas D132E CaM did not. This finding suggests that Q136P CaM is not as effective as WT CaM in facilitating CaMKII-mediated RyR2 activation which could lead to the dysregulated Ca^{2+} handling observed in CPVT.

Our results contribute to a growing but still limited body of literature on the effects of CPVT-associated CaM mutants on CaMKII activity. Similar to our findings on D132E CaM, Prakash et al. (2022) showed that the N54I and A103V CPVT-linked CaM mutants showed no significant difference from WT CaM in activating CaMKII in a similar autophosphorylation assay. However, A103V CaM significantly increased the phosphorylation level of syntide-2 (a model of CaMKII substrate) by over 60%. Likewise, Hwang et al. (2014) found that the CPVT-associated N54I and N98S CaM mutations did not alter CaM-dependent activation of CaMKII using the genetically encoded sensor "Camui", which detects conformational changes in CaMKII upon CaCaM binding.

In contrast, the inhibitory effect of Q136P CaM on CaMKII activation and RyR2 phosphorylation at S2814 is a novel finding for CPVT-linked CaM mutants, but has been documented for LQTS-associated CaM mutants (D130G and E141G), which could be due to the fact that Q136P CaM has been identified in cases with overlapping phenotypes of CPVT and long QT syndrome. Similar to Q136P CaM, a study using Camui has showed that D130G CaM significantly reduces CaMKII activation, exhibiting a dominant-negative effect even in the presence of WT CaM (Berchtold et al., 2016). In addition, D130G and

E141G CaM variants significantly reduced CaMKII autophosphorylation at Thr287 and significantly reduced its kinase activity compared to WT CaM (Berchtold et al., 2016; Prakash et al., 2023). The mechanism for D130G dysfunction is thought to involve a premature phosphorylation of the regulatory T306/T307 sites of CaMKII, which prevents CaCaM binding and inhibits kinase activity (Berchtold et al., 2016, 2021).

Collectively, our data suggest that D132E and Q136P CaM mutants drive calmodulinopathy through distinct mechanisms: D132E likely acts via a CaMKII-independent pathway, while Q136P affects RyR2 channel function by impairing CaMKII activation.

5.4.2 Both D132E and Q136P variant CaM reduce RyR2 channel P_o

Recombinant hRyR2 channel recording was carried out in order to characterise the direct functional impact of D132E and Q136P CaM mutants on single channel activity. The single-channel recordings provide preliminary data that contribute to unravelling the mechanistic basis of this mechanistically complex effect of D132E and Q136P on RyR2.

A significant technical challenge was encountered during single channel experiments which was the consistent loss of RyR2 channels and/or breakage of bilayers during the perfusion process which is required to establish a defined cytosolic Ca^{2+} concentration of 100 µM and ensure a symmetrical ion concentration on both sides of the bilayer. Consequently, the presented recordings were obtained without perfusion, meaning the Ca^{2+} concentration at the time of recording is unbuffered. The unbuffered recording solution (210 mM KCl) contains ~1 µM contaminant Ca^{2+}, which is within the channel's activating range that is sufficient to elicit RyR2 channel openings (Mukherjee, 2014; Mukherjee et al., 2012). However, because this contaminant level varies between experiments and lies on the steep, logarithmic phase of the RyR2 activation curve (Mukherjee et al., 2012), the resulting P_o is highly sensitive to minor concentration changes. Consequently, a direct quantitative comparison of P_o between different channels is not possible. Nevertheless, the relative change in P_o and gating kinetics (T_o and T_C) for a given channel before and after the addition of a specific CaM variant remains an informative measure of CaM's direct regulatory effect on that channel.

Both WT and mutant CaMs were shown to exert an inhibitory effect on RyR2 channel activity under the experimental conditions. The addition of WT CaM decreased RyR2 channel P_o via an increase in T_C, which is similar to results reported with RyR2 channels from canine and sheep hearts at 1 μM and 10 μM Ca^{2+} concentration, respectively (Hwang et al., 2014; Søndergaard et al., 2019), consistent with WT CaM's established role as a RyR2 inhibitor. D132E mutant CaM produced a similar effect, reducing P_o via an increase in T_C. Q136P CaM also decreased RyR2 channel's P_o, primarily through a reduction in T_o, with no significant change in T_C. This gating profile is distinct from that of WT and D132E CaM and suggests a possible difference in gating mechanism. However, this difference could be influenced by the high starting P_o in the channel recording with Q136P. Unfortunately, modelling of channel recordings was not possible due to low *n* size.

RyR2 channel inhibition by Q136P observed here appears to contradict the findings by Søndergaard et al. (2019), who found that Q136P CaM and the CPVT-linked A103V CaM both significantly increased channel P_o and decreased mean closed time at 10 μM Ca^{2+} using canine RyR2 channels. Similarly, Hwang et al. (2014) found that RyR2 channels from sheep heart showed an increase in channel P_o following the addition of the CPVT-linked N54I and N98S CaM variants compared to WT CaM, whereas the LQTS-associated D96V CaM did not alter channel P_o compared to WT CaM. Using hRyR2 channels from human left ventricular tissue preincubated with PKA to mimic β-adrenergic stress, Walweel et al. (2017) showed that N54I and N98S failed to inhibit RyR2 activity compared to WT CaM which reduced channel P_o by ~40% in response to β-adrenergic stimulation of the channels.

In summary, our findings hint towards inhibition of hRyR2 channels activity by reducing channel P_o with D132E and Q136P CaM variants. However, because the channels are not directly comparable due to varying Ca^{2+} concentrations between recordings, it is not possible to compare the level of inhibition caused by these variants to that of WT CaM.

Chapter 6: Investigating the effects of variant CaM on spontaneous Ca^{2+} spark generation in permeabilised mouse ventricular myocytes

6.1 Introduction

6.1.1 Functional characterisation of D132E and Q136P variant CaM

While global Ca^{2+} release analysis in HEK293 cells (**Chapter 3**) revealed RyR2 dysregulation by D132E and Q136P CaM variants, the distinct functional impacts of these mutants may have been masked in the global Ca^{2+} release events. Additionally, this heterologous system lacks the specialised machinery of cardiac myocytes. Therefore, a more physiologically-relevant cardiac model was employed in this chapter to examine the fundamental unit of SR Ca^{2+} release: the Ca^{2+} spark.

6.1.2 Calcium sparks: fundamental units of cardiac Ca^{2+} signalling

Ca^{2+} sparks are localised, transient microscopic releases of Ca^{2+} through RyR2 from the SR that directly contribute to global Ca^{2+} release. Ca^{2+} sparks constitute the fundamental units of Ca^{2+} release in a cardiomyocyte, and the spatiotemporal summation of these events triggers cellular contraction. During ECC, Ca^{2+} sparks are evoked by Ca^{2+} entry through LTCCs. Evoked sparks account for Ca^{2+} release flux in cardiomyocytes which triggers cardiac muscle contraction. The generation of Ca^{2+} sparks through RyR2 and their characteristics are modulated by the same factors that regulate global Ca^{2+} release including phosphorylation, interaction with accessory proteins such as CaM and FKBP12.6, and with ions and small molecules, such as caffeine (Cheng et al., 1993; Cheng & Lederer, 2008; Hoang-Trong et al., 2015; Shirokova et al., 1999).

Ca^{2+} sparks can also occur spontaneously in unstimulated cardiac myocytes under resting potential (-80 mV), known as spontaneous sparks. They are the result of the small but finite opening of RyR2 channels that depends on intracellular and SR Ca^{2+} concentration. Spontaneous sparks usually remain solitary and local within 300 nm of the releasing RyR2 cluster, whereas some sparks can jump to neighbouring clusters (that is “travelling sparks”) (Hou et al., 2023). The occurrence of spontaneous sparks does not require Ca^{2+} entry into the cells through LTCCs and can continue to be seen when all extracellular Ca^{2+} is removed for a short period of time. Spontaneous sparks could also be detected when LTCCs had been blocked pharmacologically (Bers, 2002; Cannell et al., 1994; Cheng et al., 1993; Cheng & Lederer, 2008).

Historically, estimates of the number of RyR2 channels involved in the generation of a Ca^{2+} spark varied widely, from a single channel to over 100 channels (Cheng et al., 1993; Franzini-Armstrong et al., 1999). A recent study by Hou et al. (2023) that used super-resolution photoactivated localisation microscopy and high-speed imaging of transgenic mouse cardiomyocytes with photoactivated label on RyR2 estimated that for the majority of sparks, between one and five RyR2 channels in a cluster are simultaneously open at the spark peak.

6.1.3 Calcium sparks and heart disease

Spatial and temporal characteristics of Ca^{2+} sparks, such as their location, duration, rise and fall rates are critical for their physiological impact, and are tightly regulated under normal physiological conditions (Jafri et al., 2015). Being the elementary unit of Ca^{2+} release in cardiomyocytes, abnormalities in sparks' spatial and temporal characteristics can disrupt the process of ECC, leading to impaired cardiac output and arrhythmias (Shirokova et al., 1999). Studies have shown that spark duration can be influenced by factors such as Ca^{2+} reuptake into the SR, local depletion of SR Ca^{2+} store and the gating kinetics of RyR2 channels (Gómez et al., 1996; Hou et al., 2023b; Tarifa et al., 2023). An example of a condition in which aberrant Ca^{2+} sparks occur is AF. The spatial distribution of Ca^{2+} sparks was found to show a preferential localisation near the sarcolemma in atrial myocytes of patients suffering from AF. These sparks were also typically smaller, wider and decay more slowly in AF cardiomyocytes, which may facilitate the fusion of neighbouring sparks into Ca^{2+} waves or transients near the sarcolemma and increasing the incidence of afterdepolarization in AF (Tarifa et al., 2023). Dyssynchrony of Ca^{2+} sparks has also been observed in myocardial infarction models of heart failure. The sparks were not synchronised with cellular depolarisation in these models and 'late' sparks were observed, slowing the decline in Ca^{2+} transient (Litwin et al., 2000).

Abnormal Ca^{2+} sparks are also implicated in the development of cardiac arrhythmias. Abnormal Ca^{2+} release events can lead to DADs, which are a significant trigger for arrhythmias. These abnormal sparks result from dysregulated RyR2 activity, often due to post-translational modifications or genetic mutations affecting the RyR2 channel (H.

Cheng & Lederer, 2008; Jafri et al., 2015). One example of the latter is the CPVT-linked CaM mutants.

6.1.4 CaM regulation of RyR2-mediated Ca^{2+} spark release

Changes in CaM's regulation of RyR2 has been linked to cardiac disease, including CPVT. Mutations in CaM that affect CaM-mediated RyR2 inhibition can lead to SR Ca^{2+} leakage through RyR2, promoting higher spontaneous Ca^{2+} wave and spark activity. Recent studies have found that the A103V, N54I and N98S CaM mutants significantly increased spark frequency in permeabilised mouse cardiomyocytes compared to WT CaM, with N54I and N98S CaM variant also reducing spark amplitude and increasing spark duration and width. Interestingly, A103V promoted wave and spark activity even when expressed at a ratio of 1:3 of A103V to WT CaM, demonstrating functional dominance even in the presence of WT CaM. The observed increased frequency of Ca^{2+} sparks was also found to significantly reduce SR Ca^{2+} content as a result of Ca^{2+} leak (Gomez-Hurtado et al., 2016; Hwang et al., 2014).

The functional effects of D132E and Q136P CaM variants on RyR2 Ca^{2+} release at the spark level have not yet been investigated. Characterising their impact on spark generation and spatiotemporal dynamics would help identify their mechanisms of dysfunction and pathogenesis.

6.1.5 Chapter aims and objectives

CPVT-linked CaM mutations reportedly increased spark activity due to loss of RyR2 regulation by CaM (Gomez-Hurtado et al., 2016; Hwang et al., 2014). Being the elementary unit of Ca^{2+} release, spark frequency and characteristics directly affect global Ca^{2+} release dynamics and any abnormal spark activity could therefore contribute to pro-arrhythmic electrophysiological effects on the heart. This chapter aims to investigate whether D132E and Q136P CaM variants can induce CPVT-like changes in spontaneous spark generation and characteristics in normal permeabilised mouse ventricular cardiomyocytes using confocal microscopy.

Key objectives:

- Analyse the frequency and other spatiotemporal characteristics of spontaneous Ca^{2+} sparks generated in saponin-permeabilised mouse ventricular myocytes incubated with D132E and Q136P CaM variants in comparison to those incubated with WT CaM.
- Measure Ca^{2+} spark activity in saponin-permeabilised mouse ventricular myocytes of CPVT knock-in mouse model harbouring the heterozygous RyR2-R420Q$^{+/-}$ (R420Q) gain-of-function mutation to serve as a model of SR pathological Ca^{2+} leak.

6.2 Methods

6.2.1 Cardiomyocyte permeabilisation and preparation

Mouse ventricular myocytes were isolated as previously outlined in **2.2.20**. The isolated cells were permeabilised by a 30-second incubation with 0.05% (w/v) saponin, which selectively permeabilises the sarcolemma due to its higher cholesterol-to-phospholipid ratio compared to intracellular membranes (Korn, 1969). This approach leaves internal organelles such as the SR and mitochondria intact. The permeabilised cells were then immediately transferred to a mock intracellular solution containing 100 nM free [Ca^{2+}] (for composition, see **Section 2.2.21**).

Preliminary experiments with fluorescently labelled CaM (F-CaM) were conducted to determine CaM's binding time to cellular sites. Purified F-CaM protein was a gift from Dr Pavel Kirilenko (School of Biosciences, Cardiff University). The protein was expressed in Rosetta™ E-coli BL21(DE3) cells and purified using Ni-NTA resin and subsequently labelled using Lightning-Rhodamine labelling kit (Abcam, ab188286), as per the manufacturer's instructions.

Following permeabilisation, isolated mouse ventricular myocytes were first incubated with 1 µM CaM protein (WT, D132E or Q136P; see **Section 2.2.2**) in mock intracellular solution for 20 mins. After this, 2-3 drops of the solution containing cells were placed in a cylindrical bath (~5 mm diameter) in a plastic block (see **Figure 6.1**). The bottom of the bath was formed by attaching a coverslip to the bottom of the block. A tightly fitting perfusion column was inserted into the bath until the lower surface was close to myocytes that had rested on the coverslip. Perfusion was achieved by pumping the perfusion solution (consists of mock intracellular solution supplemented with 15 µM Fluo-3 (pentapotassium salt) fluorescent Ca^{2+} indicator and 200 nM CaM to replace any CaM that may dissociate during the experiment) at ~20 µL/min rate, down a narrow pore running longitudinally through the centre of the column. Excess solution in the bath flowed continuously up the side of the column, where it was collected and taken to waste via a waste line. The experimental setup was developed based on Duke & Steele (1998) and Z. Yang & Steele (2002). WT mouse ventricular myocytes sparks were measured under the same conditions 20 mins after permeabilisation (without CaM incubation) to

be used as a control. Similarly, sparks in myocytes from CPVT mouse model (harbouring the R420Q RyR2 mutation) were measured to serve as a model of Ca^{2+} leak (Domingo et al., 2015; Fowler et al., 2025; Zissimopoulos et al., 2025).

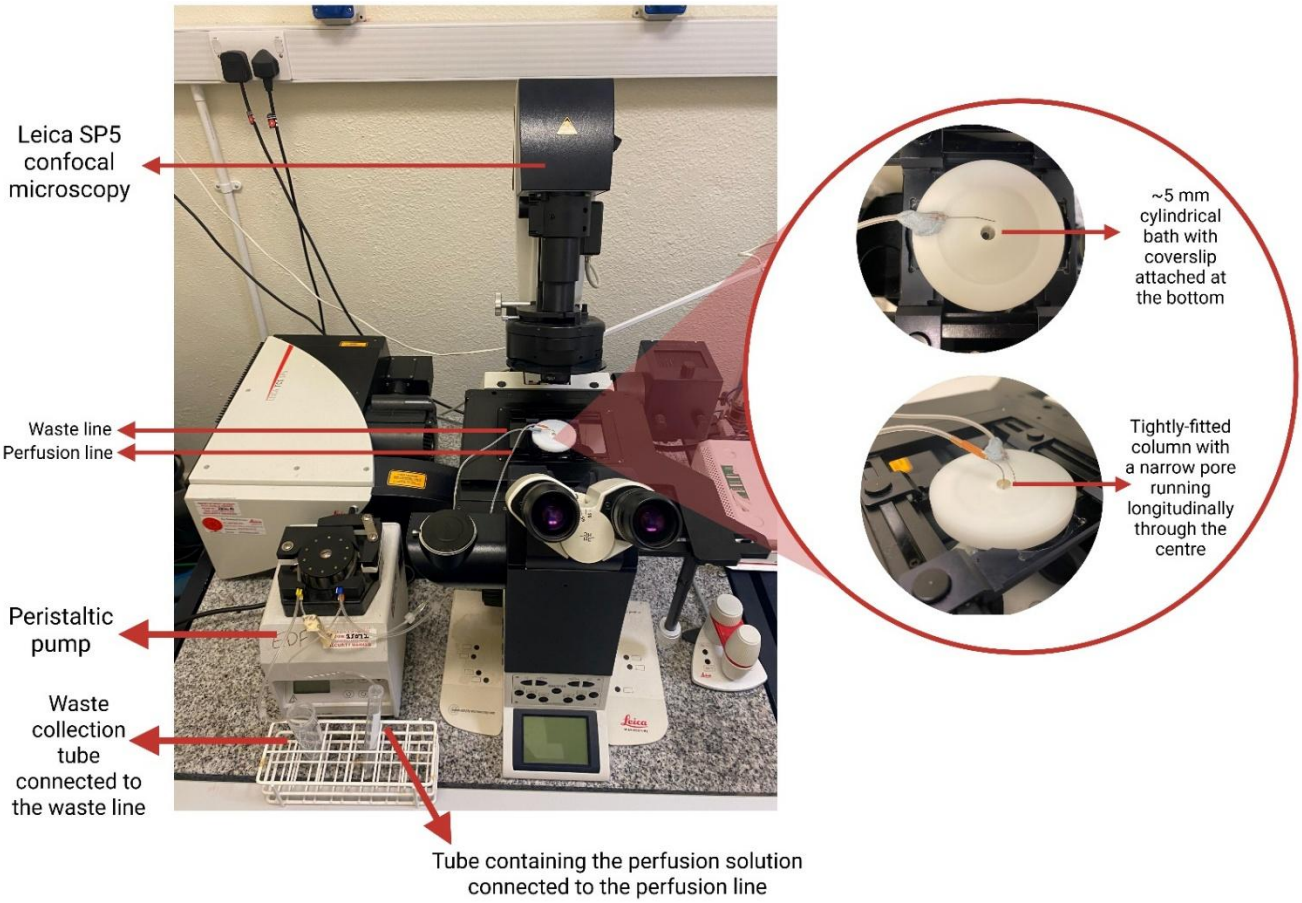

Figure 6.1. Experimental setup for measuring sparks in saponin-permeabilised mouse ventricular myocytes in the presence of WT or variant D132E or Q136P CaM using confocal microscopy. Following a 20-min incubation with CaM, the permeabilised cells were placed in a cylindrical bath with a coverslip attached at the bottom. A tightly-fitted column was then inserted in the bath. Slow perfusion of intracellular solution containing 200 nM CaM and 15 µM Fluo-3 was achieved by pumping the solution down a narrow pore running longitudinally through the centre of the column. Excess solution in the bath flowed continuously up the side of the column, where it was collected through a waste line and taken to waste.

6.2.2 Confocal imaging

Imaging was carried out using a Leica SP5 laser scanning confocal microscopy with a 40x oil-immersion lens. Fluo-3 fluorescence was excited by an argon laser line at 488 nm and emitted fluorescence was collected at 500-600 nm. Images were acquired in line-

scanning mode. In this mode, the laser repeatedly scans a single line positioned along the longitudinal axis of the cardiomyocyte 2000 times at a high frequency of 1 ms/line. These sequential lines are then stacked vertically over time, creating a spatiotemporal image where the x-axis represents distance along the line, and the y-axis represents time. This provides the high millisecond-scale temporal resolution necessary to resolve Ca^{2+} sparks. Line scans were then analysed using SparkMaster 2 software (see **Figure 6.2**) (Tomek et al., 2023). Different parameters were measured to characterise the spatiotemporal properties of Ca^{2+} sparks including spark frequency, amplitude, width, duration, time to peak and tau of decay (i.e., the time constant of decay) (see **Figure 6.3**).

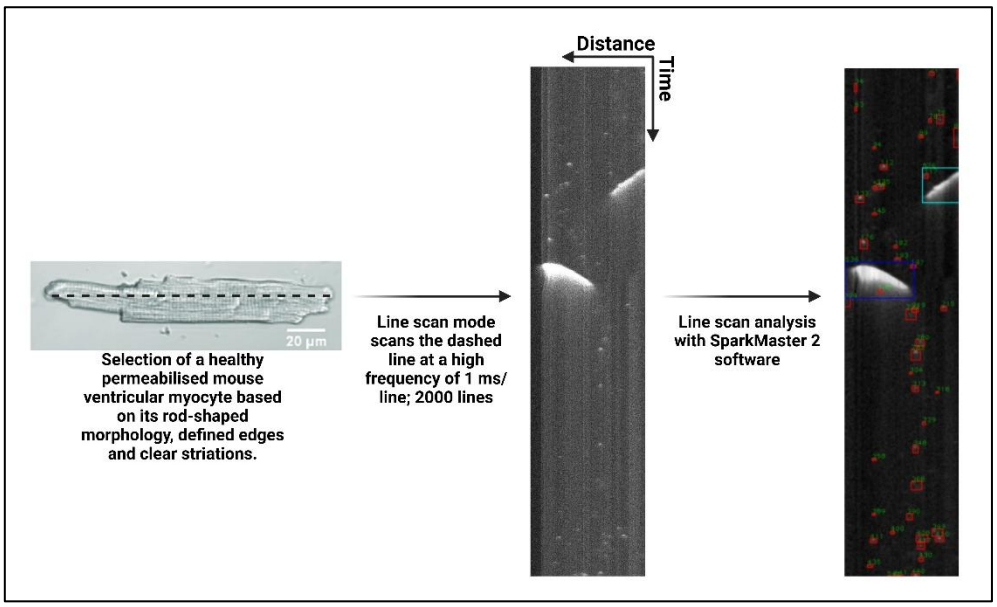

Figure 6.2. Confocal line-scan imaging and analysis of Ca^{2+} sparks in a permeabilized mouse ventricular myocyte. A line is positioned along the longitudinal axis of a healthy-looking myocyte. The line is then scanned by argon laser 2000 times at a high frequency creating a spatiotemporal image that is then analysed using the SparkMaster 2 software (Tomek et al., 2023). Detected events are classified as: sparks (red boxes), waves (blue boxes) and miniwaves (cyan boxes).

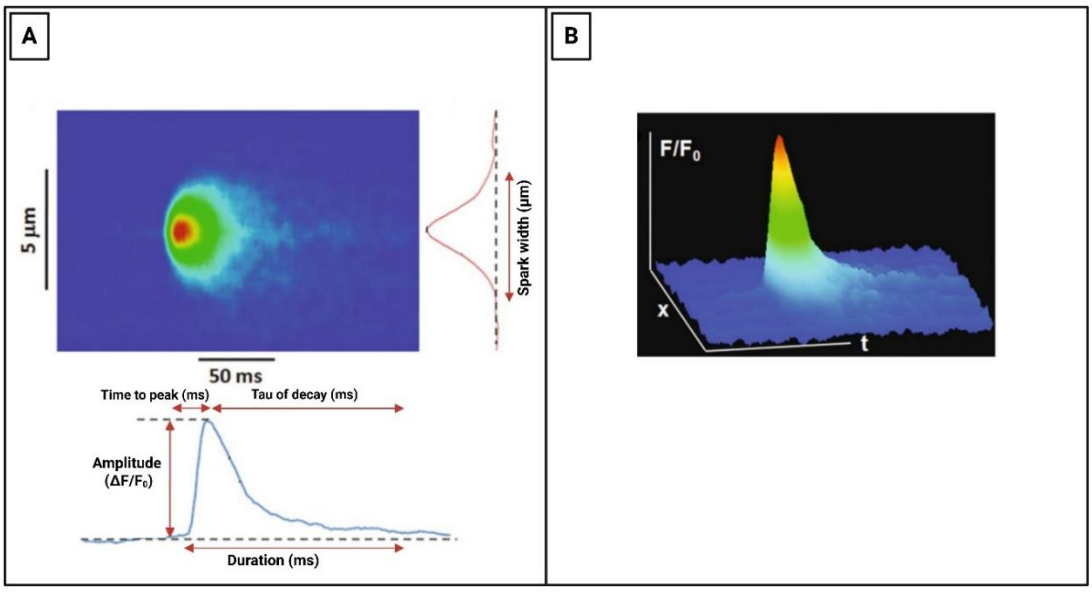

Figure 6.3. Illustration of a typical Ca^{2+} spark captured in a rat ventricular myocyte. (A) Shows parameters used to characterise Ca^{2+} sparks. Analysis was carried out using the SparkMaster 2 software (Tomek et al., 2023). **(B)** Shows surface blot of the Ca^{2+} spark shown in A. Figure adapted and modified from Chiarini-Garcia & Melo (2011).

6.3 Results

6.3.1 CaM binding in permeabilised mouse ventricular myocytes

Preliminary experiments with F-CaM were carried out to determine the time taken for the endogenous intracellular CaM to be replaced by exogenous F-CaM in permeabilised cells. This was used to establish an appropriate CaM incubation time required before imaging sparks in myocytes. Saponin-permeabilised myocytes were resuspended in 1 µM F-CaM in intracellular solution and change in fluorescence intensity over time inside the cells was recorded using confocal microscopy. Background fluorescence was subtracted from the F-CaM signal inside the myocyte. The time taken for F-CaM to enter and bind to its targets within the cells was ~ 3.7 mins, and the fluorescence intensity plateaued at ~15 mins (see **Figure 6.4A**). After 20 mins incubation, F-CaM localisation showed a clear striated pattern in myocytes, an indication of CaM binding to z-lines (X. Wu & Bers, 2007). Permeabilised cardiomyocytes were recorded for 20 mins without CaM addition and imaged to serve as a control. No cellular striated pattern was observed in these cells (see **Figure 6.4B-C**).

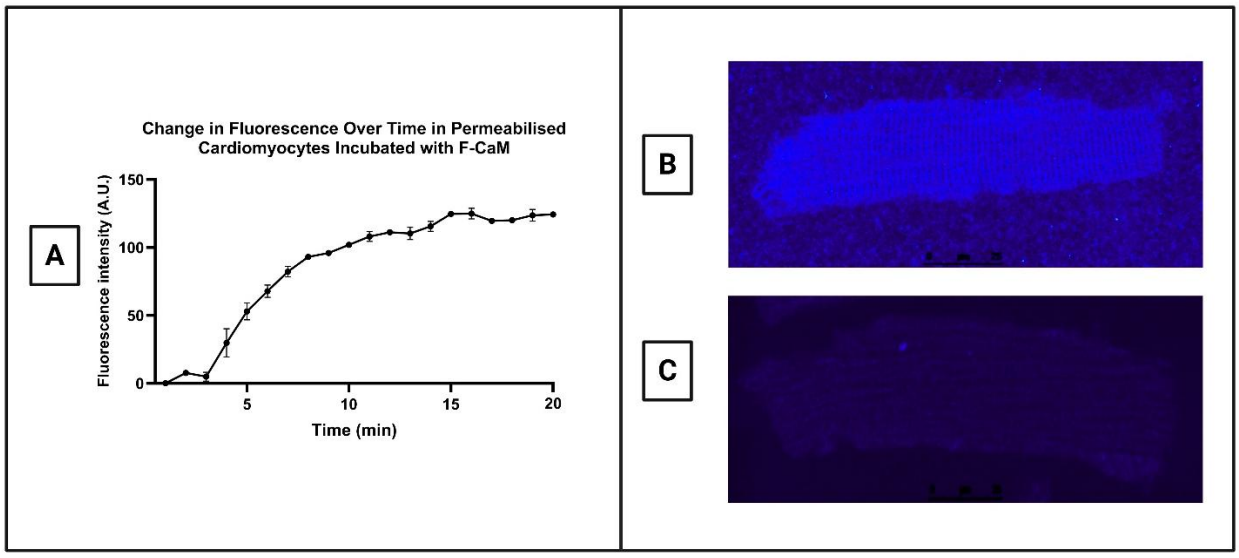

Figure 6.4. Lightning-Rhodamine labelled CaM binding in saponin-permeabilised mouse ventricular myocytes. (A) A graph of average change in fluorescence intensity over time in saponin-permeabilised mouse ventricular myocytes incubated with 1 µM F- CaM at 100nM [Ca^{2+}]. Background fluorescence was subtracted from the myocyte F-CaM signal. Each data point represents the mean of 3 myocytes and error bars indicate SD. **(B)** Shows an example of a permeabilised mouse ventricular myocyte after 20 mins incubation with F-CaM at 100nM [Ca^{2+}]. F-CaM localisation presents a clear striated pattern in myocytes, an indication of CaM binding to z-lines. **(C**) Shows an example of a permeabilised mouse ventricular myocyte at 100nM [Ca^{2+}]; 20 mins after saponin permeabilisation without CaM incubation. No cellular striated pattern was observed.

6.3.2 R420Q-RyR2 mutation alters Ca^{2+} spark frequency and characteristics in permeabilised mouse cardiomyocytes

Sparks in myocytes from a knock-in mouse model harbouring the CPVT-linked RyR2 mutation R420Q were investigated to serve as a model of pathological Ca^{2+} leak. This was used to establish a reference Ca^{2+} release phenotype without additional exogenous CaM for subsequent comparison with sparks generated in the presence of variant CaM. Spark and wave frequency was significantly higher in CPVT mice cardiomyocytes compared to WT mice. Additionally, spark amplitude was found to be significantly reduced in CPVT mice compared to WT mice, and time for sparks to peak was significantly longer in CPVT mice (p<0.01) (see **Figure 6.5**).

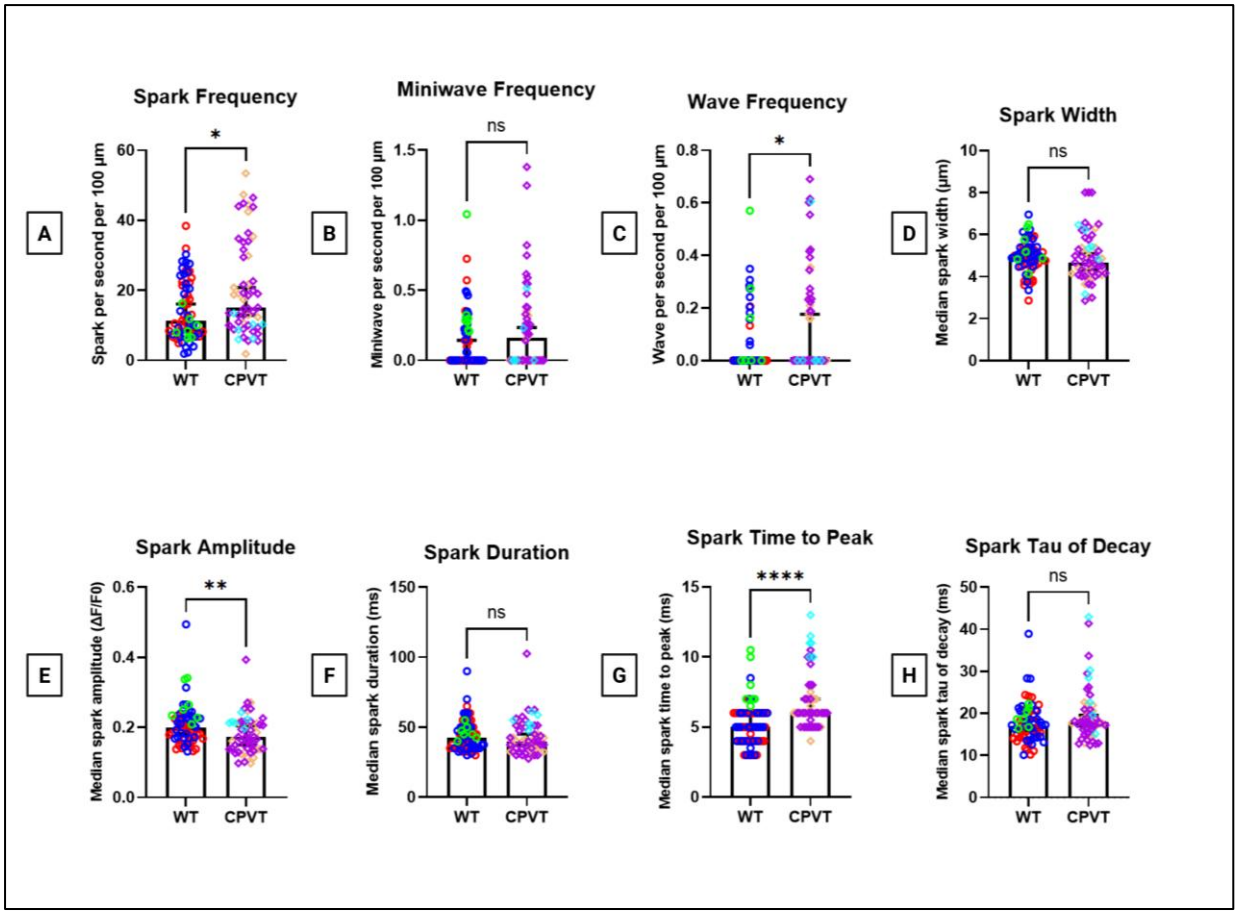

Figure 6.5. R420Q RyR2 mutation promotes Ca^{2+} spark activity and alters some sparks characteristics in permeabilised mouse ventricular myocytes. Each point represents a median of a line scan from one cell. Data are shown as median with 95% CI. Significance, as indicated by *, was determined using Mann-Whitney U test. *n*= 65 and 55 cells for WT and CPVT mice respectively; obtained from 3 mice each. Each point colour represents data obtained from the same mouse.

6.3.3 D132E and Q136P CPVT-linked CaM variants reduce spark frequency in permeabilised mouse cardiac myocytes without altering other spark characteristics

Spark frequency and other spatiotemporal characteristics were measured in saponin-permeabilised WT mouse ventricular myocytes incubated with WT or mutant CaM (D132E or Q136P) to investigate the effect that variant CaM might have on Ca^{2+} release at the spark level (see **Figure 6.6**). Incubation with WT CaM was found to reduce spark frequency compared to the control myocytes (without CaM incubation); although this reduction was not statistically significant (control 11.37 spark/sec/100 µm, 95% CI [8.5,16.2] vs with CaM 8.54 spark/sec/100 µm, 95% CI [7.5, 10.1]). Additionally, WT CaM incubation significantly increased miniwave and wave frequency compared to the

control. Spark amplitude and duration were also significantly increased with WT CaM incubation, and time for sparks to peak and tau of decay were found to be higher with WT CaM compared to the control (see **Figure 6.6**).

Both D132E and Q136P CaM mutants significantly reduced Ca^{2+} spark frequency in permeabilised cardiac myocytes compared to WT CaM ($p \leq 0.0001$). Furthermore, Q136P CaM significantly decreased the frequency of miniwave propagation compared to WT CaM. Neither mutant significantly altered other spatiotemporal spark properties when compared to WT CaM. **Table 6.1** summarises parameters used to characterise Ca^{2+} sparks reported in this chapter.

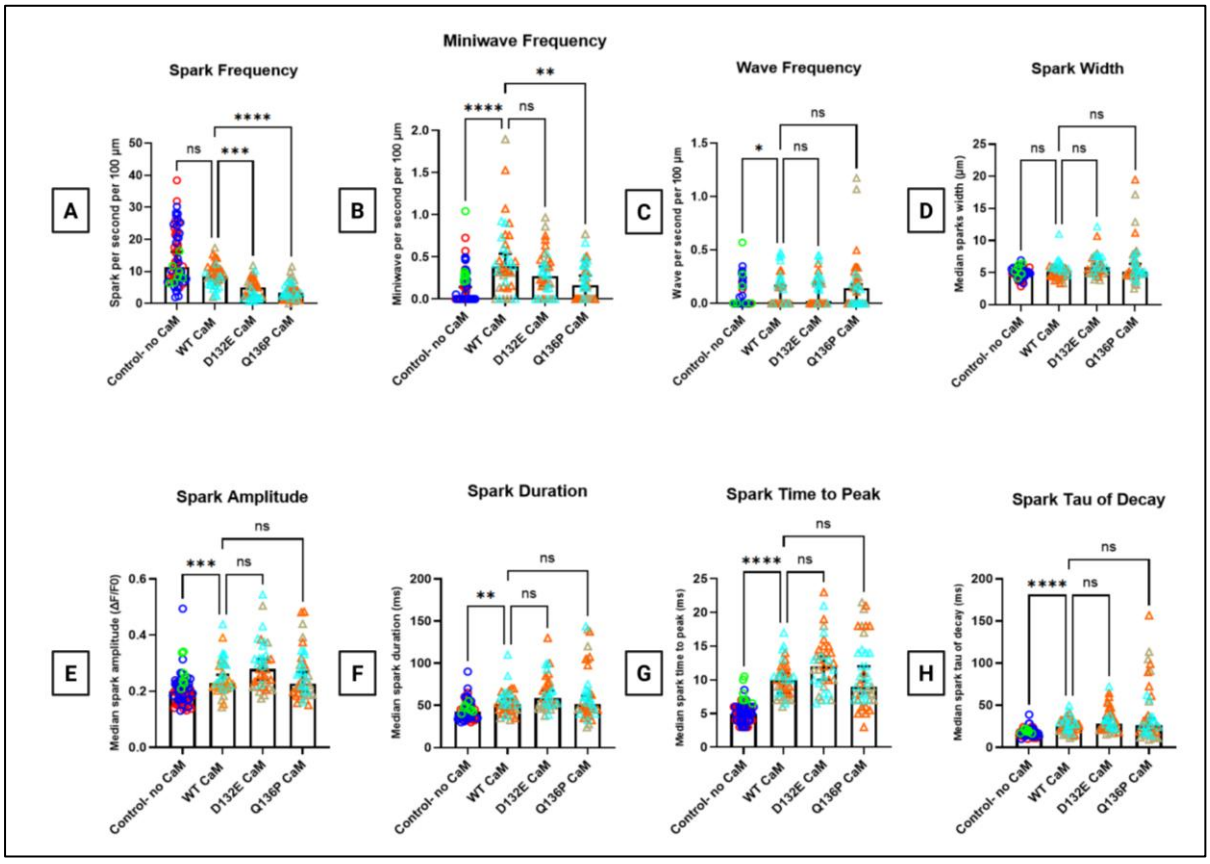

<u>Figure 6.6.</u> D132E and Q136P CPVT-linked CaM mutations reduce spark frequency without altering spark characteristics in permeabilised mouse ventricular myocytes compared to WT CaM. Each point represents a median of a line scan from one cell. Data are shown as median with 95% CI. Significance, as indicated by *, was determined using Kruskal-Wallis test followed by Dunn's multiple comparisons post hoc test. Sample sizes (cells/mice): control (no CaM), *n* = 65/3; WT CaM, *n* = 39/3; D132E CaM, *n* = 37/3; Q136P CaM, *n* = 42/3. Each point colour represents cells obtained from the same mouse.

Table 6.1. Summary of parameters used to characterise Ca^{2+} sparks obtained from saponin-permeabilised mouse ventricular myocytes. The mouse harbouring the CPVT-linked mutation R420Q was used as a CPVT model of Ca^{2+} leak. Values are shown as median, 95% CI [lower confidence limit, upper confidence limit], *n* WT mouse without CaM=65, CPVT mouse= 55, WT mouse with WT CaM= 39. WT mouse with D132E CaM= 37, WT mouse with Q136P CaM=42, where *n* is the number of cells; obtained from 3 different mice each.

	WT mouse - no CaM	**WT mouse + WT CaM**	**WT mouse + D132E CaM**	**WT mouse + Q136P CaM**	**CPVT mouse - no CaM**
Spark frequency (Spark/sec/100 µm)	11 [8.5, 16]	8.5 [7.5, 10]	5.0 [2.4, 5.7]	3.3 [2.3, 4.3]	15 [13, 21]
Miniwaves frequency	0.0 [0,0.14]	0.39 [0.31, 0.54]	0.27 [0.15, 0.39]	0.16 [0.0, 0.28]	0 [0. 0.23]
Wave frequency	0.0 [0, 0]	0.0 [0.0, 0.16]	0.0 [0.0, 0.18]	0.14 [0.0, 0.18]	0 [0, 0.18]
Spark amplitude	0.2 [0.18, 0.21]	0.23 [0.22, 0.26]	0.28 [0.24, 0.31]	0.23 [0.20, 0.27]	0.17 [0.15, 0.2]
Spark width	4.9 [4.8, 5.1]	5.3 [4.6, 5.8]	5.8 [5.2, 6.4]	5.2 [4.8, 6.4]	4.7 [4.3, 5.1]
Spark duration	43 [38, 45]	51 [45, 58]	59 [53, 68]	51 [46, 61]	40 [38, 45]
Spark time to peak	5 [5, 6]	10 [8, 11]	12 [10, 14]	9 [8, 12]	6 [6, 7]
Spark tau of decay	17 [16, 19]	26 [22, 29]	29 [23, 34]	26 [20, 34]	18 [17, 20]

6.4 Discussion

6.4.1 CaM binding time in permeabilised mouse ventricular myocytes

The binding time of F-CaM (1 μM) in permeabilised myocytes was investigated to determine an appropriate CaM incubation period for subsequent experiments with WT and mutant CaM. The selection of a 1 μM CaM concentration was based on the findings by Y. Yang et al. (2013) that the maximum concentration of bound CaM at the z-lines is 1.17±0.1 μM in mouse ventricular myocytes. Since 90-95% of CaM in myocytes is found in a bound state (X. Wu & Bers, 2007; Y. Yang et al., 2013), it was reasoned that a 1 μM CaM concentration would be sufficient to ensure all endogenous bound CaM is replaced by exogenous CaM with which the cells are incubated.

Incubation of saponin-permeabilised mouse ventricular myocytes with F-CaM (1 μM) resulted in its distinct localisation to the z-lines, giving the myocytes a characteristic striated pattern. This pattern is consistent with the established distribution of endogenous CaM in cardiac myocytes, where Y. Yang et al. (2013) found that bound CaM is relatively concentrated at the z-lines and over 90% of this z-line associated CaM was found to be bound to RyR2 in mouse ventricular myocytes. This is also consistent with findings from X. Wu & Bers (2007)where over 95% of CaM in rabbit cardiac myocytes was found in a bound state and only a small concentration of 50-100 nM is found free.

Timeseries of F-CaM binding to permeabilised mouse ventricular myocytes at 100 nM free [Ca^{2+}] showed that the time taken for F-CaM to enter cells was ~ 3.7 mins and cellular binding at z-lines saturated with CaM at ~15 mins. This process represents F-CaM replacing endogenous RyR2-bound CaM in permeabilised myocytes. This is faster than previously reported values where X. Wu & Bers (2007) reported a F-CaM binding time constant of ~ 11.1 mins in rabbit myocytes, and Y. Yang et al. (2013)reported a similar binding time constant of ~ 11.5 mins in mouse myocytes at 100nM free [Ca^{2+}], but both experiments used a lower concentration of F-CaM (60 nM). Additionally, X. Wu & Bers (2007) found that at the same free [Ca^{2+}] of 100nM, there was F-CaM dissociation at a time constant of ~11.7 mins (X. Wu & Bers, 2007).

Based on these findings, a 20-min incubation period with CaM prior to spark imaging was

implemented to ensure complete replacement of endogenous CaM and saturation of all cellular binding sites. Furthermore, a slow perfusion of 200 nM CaM during imaging ensured that CaM binding sites remained saturated throughout the experiment.

6.4.2 CPVT-linked RyR2 mutation (R420Q) affects Ca^{2+} release at the spark level

The R420Q RyR2 mutation was first identified in a highly symptomatic Spanish family with several sudden deaths (Domingo et al., 2015). It has since been documented in 52 patients and is recognised to arise through both autosomal dominant inheritance and *de novo* mutation (Chang et al., 2025). Remarkably, this mutation was associated not only with CPVT under stress, but also sinus bradycardia, atrial and junctional arrhythmias (Domingo et al., 2015; Fowler et al., 2025). The R420Q RyR2 mutation is located in the N-terminus of the RyR2 gene and was found to alter the interdomain interaction within the RyR2 channel and weaken its binding to junctophilin-2, a protein that anchors the SR to the plasma membrane in cardiomyocytes and plays an important role in regulating Ca^{2+} signalling through inhibition of RyR2 Ca^{2+} leak in cardiomyocytes (Luo et al., 2022; Yin et al., 2021). A heterozygous R420Q mouse model exhibited a pro-arrhythmic phenotype, including stress-induced ventricular arrhythmias (Domingo et al., 2015; Yin et al., 2021) and increased spontaneous diastolic Ca^{2+} release in the form of Ca^{2+} sparks and waves (Fowler et al., 2025; Yin et al., 2021). The R420Q mouse model was employed in this chapter as an established model of clinical CPVT, providing a positive control for pathological Ca^{2+} release for comparison with CPVT-linked CaM variants.

The effect of R420Q mutation on RyR2-mediated Ca^{2+} release at the spark level and its contribution to arrhythmogenic Ca^{2+} signalling were investigated. A significant increase in spontaneous Ca^{2+} spark and wave frequency was observed with the R420Q RyR2 mutation in permeabilised mouse ventricular myocytes. Spark amplitude was found to be significantly decreased, and the time-to-peak was longer in CPVT myocytes compared to WT. Multiple studies using different CPVT-linked RyR2 mouse models have reported similar findings (for instance: Okabe et al., 2024; Qian et al., 2023; Savio-Galimberti & Knollmann, 2015; Uchinoumi et al., 2010).

The increased frequency of Ca^{2+} sparks and subsequent wave propagation are consistent

with increased SR leak in this disease model (Yin et al., 2021). The prolonged duration of release and the low spark amplitude could be explained by a decrease in SR Ca^{2+} load. Reduced SR Ca^{2+} content has been reported in the R420Q model (Fowler et al., 2025), as well as other models of CPVT (Kashimura et al., 2010; Uchinoumi et al., 2010). The increased spark frequency was also reported by Yin et al. (2021)in intact quiescent cardiomyocytes from R420Q knock-in mice model (the same model used in our experiments); electrically stimulated at 2 or 4 Hz. Our findings here are consistent with R420Q being a gain-of-function mutation of RyR2 that is causing SR Ca^{2+} leak due to RyR2 channel dysfunction which leads to arrhythmogenic Ca^{2+} release events.

6.4.3 WT CaM inhibits Ca^{2+} spark generation and alters spark characteristics in permeabilised mouse ventricular myocytes

Spark frequency and other spatiotemporal characteristics were investigated in order to find out the effect of WT CaM on microscopic Ca^{2+} release in saponin-permeabilised mouse cardiomyocytes. Spark frequency was reduced (though not statistically significant) in the presence of CaM compared to the control; which reflects CaM-dependent RyR2 inhibition, reducing channel P_o (Sorensen et al., 2013). Spark frequency in the presence of CaM ranged from 2 to17.4 spark/sec/100 µm; with a median of 8.5, whereas in the control, it ranged from 1.9 to 38.4; with a median of 11.4 event/sec/100 µm. Therefore, CaM did not only reduce the frequency of spark, but also lowered the variability in distribution, denoting regulated Ca^{2+} release. Consistent with this observation, Guo et al. (2006), found that CaM decreased Ca^{2+} spark frequency in permeabilised mice myocytes in a dose dependent manner; with maximal inhibition at ~1 µM CaM. Similarly, Hwang et al. (2014) reported that the addition of CaM caused a significant reduction of ~30% in spark frequency in permeabilised rat myocytes. On the contrary, Sigalas et al. (2009) showed that 100 nM CaM significantly increases Ca^{2+} spark frequency in permeabilised rat cardiomyocytes. This finding, however, is questionable for two reasons. First, the experimental protocol used suramin as a pre-treatment for cells to displace endogenous CaM bound to RyR2. As suramin is known to increase P_o and conductance of RyR2 channels (Hill et al., 2004; Santonastasi & Wehrens, 2007), the

observed increase in spark frequency could be due to incomplete washout of suramin prior to imaging. Second, the 100 nM CaM concentration may have been insufficient to fully occupy RyR2 binding sites, given that the concentration of bound CaM at the z-lines is estimated to be ~ 1 μM (Y. Yang et al., 2013).

Guo et al. (2006) did not observe changes in spark properties of permeabilised mouse cardiomyocytes in the presence of CaM. However, in our experiments exogenous WT CaM significantly increased spark amplitude, duration, and time-to-peak. The increase in spark amplitude is potentially due to enhanced SR Ca^{2+} content (which may be a consequence of the decreased spark frequency) and prolonged spark release duration. Additionally, the Tau of decay of sparks was significantly higher with CaM compared to the control, *i.e.*, the sparks decay more slowly. This finding could be explained by the potential increase in SR Ca^{2+} content, which reduces the rate of Ca^{2+} uptake by SERCA pumps on the SR.

At physiological free Ca^{2+} concentration of 100 nM, Ca^{2+} waves were not expected to be seen. However, miniwave and wave propagation were observed in some cells. The frequency of these miniwaves and waves was significantly increased with CaM incubation. Miniwaves occurred in 84.6% of cells that were incubated with CaM, compared to 46.1% in the control group. Similarly, 48.7% of cardiomyocytes incubated with CaM generated wave(s), compared to only 23% in the control group. This increase is likely attributed to CaM's inhibition of RyR2. As CaM inhibits spontaneous spark generation, this presumably leads to a build up of SR Ca^{2+} that would get released as odd miniwaves/waves. Alternatively, CaM activation of endogenous CaMKII might result in occasional miniwave/wave propagation, although CaMKII activation is not expected at such low free Ca^{2+} concentration (Guo et al., 2006).

6.4.4 D132E and Q136P CaM further reduce spark frequency without altering spark spatiotemporal characteristics

To investigate the effect of CPVT-linked variant CaMs on spark generation, permeabilised WT mouse ventricular myocytes were incubated with CaM (WT, D132E or Q136P) for 20 mins before imaging with confocal microscopy. Surprisingly, both mutant CaMs

significantly reduced spark frequency compared to WT CaM, and Q136P CaM also significantly reduced miniwave frequency. Wave frequency was increased with Q136P CaM, although the increase was not statistically significant. Spark characteristics were not significantly altered by D132E or Q136P CaM compared to WT CaM. These results diverge from those observed in RyR2 CPVT-mouse model (R420Q) (see **Section 6.3.2**) and from previous reports on other CPVT-linked CaM mutations; A103V, N54I and N98S. Those studies reported a significant increase in spark frequency in permeabilised mouse cardiomyocytes, and a significant reduction in SR Ca^{2+} content compared to WT CaM (indicative of SR Ca^{2+} leak); with N54I and N98S CaM variant also reducing spark amplitude and increasing spark duration and width (Gomez-Hurtado et al., 2016; Hwang et al., 2014). A103V also demonstrated functional dominance even when expressed at a ratio of 1:3 of A103V to WT CaM; promoting wave and spark activity (Gomez-Hurtado et al., 2016). The reduced spark frequency with D132E and Q136P CaM may result from their lower Ca^{2+} binding affinity (Da'as et al., 2024; Gupta et al., 2025), which could impair Ca^{2+} sensitisation because spontaneous Ca^{2+} spark generation is dependent on intracellular and SR Ca^{2+} concentration. However, the A103V and N98S CaM mutants also have a similarly lower Ca^{2+} binding affinity yet show an increase in spark frequency (Gomez-Hurtado et al., 2016; Hwang et al., 2014). Notably, the LQTS-associated CaM mutants E141G did not alter spontaneous Ca^{2+} spark frequency, amplitude or SR Ca^{2+} content in permeabilised mouse ventricular myocytes (Boczek et al., 2016). There are no data currently available in the literature on the effect of D132E and Q136P CaM variants on SR Ca^{2+} content in animal studies. Therefore, it is difficult to interpret the observed reduction in spark frequency with these mutants in relation to SR Ca^{2+} load.

These findings align with the atypical phenotype and the unique clinical presentation of D132E and Q136P CaMs as those variants, unlike the aforementioned CaM mutations, were associated with mixed clinical features of both CPVT and LQTS. This positions D132E and Q136P not as typical CPVT mutants, but as dysfunctional regulators that disrupt Ca^{2+} homeostasis in a distinct, and potentially more complex mechanism.

Chapter 7: General discussion

The principal aim of this research was to investigate the effects of variant D132E and Q136P CaM on hRyR2 function. These two CaM mutants have been linked to overlapping clinical phenotypes of CPVT and LQTS (Makita et al., 2014). It was thus hypothesised that their pathophysiological mechanism would involve dysregulation of RyR2 channels, resulting in aberrant Ca^{2+} release. RyR2-mediated Ca^{2+} release was examined in the presence of mutant D132E and Q136P CaMs at the global cellular, spark, and single-channel levels. Additionally, the contribution of phosphorylation by CaMKII in the generation of arrhythmogenic Ca^{2+} release was investigated.

7.1 Dysfunctional RyR2-mediated Ca^{2+} release with D132E and Q136P CaM

Patients harbouring the D132E or Q136P CaM mutations present with overlapping LQTS and CPVT symptoms, characterised by a prolonged QT interval and exercise-induced polymorphic ventricular ectopy. To date, the International Calmodulinopathy Registry (ICalmR) has identified five CaM mutations associated with this mixed phenotype: E83K, E105A, D134N, D132E and Q136P (Crotti et al., 2023). While the Ca^{2+} and RyR2 binding affinity of some mutants and their effects on LTCCs have been investigated (Da'as et al., 2019, 2024; Gupta et al., 2025; Thanassoulas et al., 2023), their direct impact on RyR2 function remains largely unexplored, with only one study to date (Søndergaard et al., 2019). This thesis provides novel data on how D132E and Q136P CaM affect RyR2-mediated Ca^{2+} release, offering a potential mechanism for the CPVT component of their clinical presentation.

RyR2-mediated Ca^{2+} release was assessed at the global, cellular level in HEK293 cells co-transfected with hRyR2 and WT or mutant CaM using live-cell Ca^{2+} imaging. Spontaneous Ca^{2+} release profiles with D132E and Q136P CaMs were found to be very similar to each other, but were significantly different from that of WT CaM. Compared to WT CaM, the Ca^{2+} transients were characterised by a prolonged duration of release, reduced frequency, and a slower decay rate, which is suggestive of aberrant Ca^{2+} release behaviour that could be arrhythmogenic. The functional impact of D132E and Q136P CaM on spontaneous spark propagation and characteristics was also investigated. In permeabilised mouse ventricular myocytes, a significant reduction in Ca^{2+} spark

frequency was observed with D132E and Q136P CaM variants compared to WT CaM, while other spark characteristics were not significantly affected. In cardiomyocytes, Q136P CaM appeared to increase both Ca^{2+} wave frequency and spark tau of decay, although these effects did not reach statistical significance. Notably, in both HEK293 cells Ca^{2+} imaging and spark experiments, the contribution of LTCCs was excluded, thus any observed changes in Ca^{2+} release are attributed to RyR2 channels. In the HEK293 model, LTCCs are not endogenously expressed (di Silvio et al., 2016; Xia et al., 2004), while in the spark experiments, membrane permeabilisation with saponin and absence of voltage-activation prevented LTCCs involvement. Single-channel recording with purified recombinant hRyR2 showed a reduction in P_o after the addition of D132E and Q136P variant CaM. However, the extent of channel inhibition by mutants could not be quantitatively compared to that of WT CaM, as the channels were recorded at an unbuffered Ca^{2+} concentration due to technical difficulties.

The Ca^{2+} imaging data from HEK293 cells suggest that D132E and Q136P CaM may result in a loss of RyR2 inhibition as indicated by prolonged Ca^{2+} transient durations. This is consistent with the CPVT phenotype associated with these mutants. However, the observed reduction in Ca^{2+} spark frequency contrasts with the increased frequency reported with multiple CPVT-linked CaM mutants (Gomez-Hurtado et al., 2016; Hwang et al., 2014), and diverges from LQTS-linked CaM variants, which show no effect on spark generation (Boczek et al., 2016). A limitation of the Ca^{2+} spark experiments conducted in this thesis is that SR Ca^{2+} load was not assessed in cardiomyocytes following incubation with WT or mutant CaM. Thus, the spark results could not be interpreted relative to potential changes in SR content. Collectively, these results suggest that D132E and Q136P CaM promote aberrant regulation of RyR2 Ca^{2+} release channels at the whole cell and spark level.

One limitation of the HEK293 and permeabilised myocyte models is that the concentration of mutant CaM likely does not accurately replicate the heterozygous 5:1 WT-to-mutant allelic stoichiometry found in patients (Badone et al., 2018). In HEK293 transfections, achieving this ratio is unreliable, as a 5:1 plasmid DNA ratio does not guarantee equivalent protein expression. While permeabilised myocytes can be

incubated with a precisely controlled ratio of WT and mutant proteins, the only methods to guarantee expression at the correct allelic stoichiometry are the generation of transgenic mouse models or the use of patient-derived iPSC-CMs.

7.2 Do D132E and Q136P CaM cause RyR2 dysfunction by different mechanisms?

Despite D132E and Q136P CaM variants demonstrating similar Ca^{2+} release profiles at the cellular, spark and singe-channel level, it is likely that they exert their dysfunction through different mechanisms of action. Based on results presented here, it is proposed that Q136P CaM exerts dysfunction through altered CaMKII signalling. Specifically, it has been shown to reduce CaMKII autophosphorylation and subsequently reduce S2814 phosphorylation of RyR2, a phenomenon that had been observed with LQTS-linked CaM mutants (Berchtold et al., 2016, 2021). CPVT CaM mutations, in contrast, are linked to either no change or an increase in CaMKII activation (Hwang et al., 2014; Prakash et al., 2022).

Although D132E CaM did not affect CaMKII activation, evidence from HEK293 cells transfected with RyR2 and this variant suggests that D132E promotes diastolic Ca^{2+} release, as indicated by lower ER Ca^{2+} load in non-oscillating cells. Lower SR/ER Ca^{2+} stores is a recognised hallmark of CPVT due to Ca^{2+} leak through RyR2 channels, that leads to arrhythmogenic Ca^{2+} release. In contrast, Q136P CaM did not alter ER load under diastolic conditions in non-oscillating cells.

Both D132E and Q136P CaM showed evidence of reduced ER Ca^{2+} load in oscillating HEK293 cells, which is consistent with their Ca^{2+} imaging profiles suggestive of Ca^{2+} leak. While spark experiments suggest that there is no Ca^{2+} leak at the spark level with D132E and Q136P CaM, it is now recognised that Ca^{2+} leak could be “silent” at a sub-spark level, termed “quarky Ca^{2+} leak” (Brochet et al., 2011), in which case the intracellular stores of Ca^{2+} are persistently depleted by Ca^{2+} leak.

Collectively, this research reveals that D132E and Q136P CaM drive CPVT pathogenesis via overlapping yet distinct mechanisms. Both mutants cause aberrant Ca^{2+} leak and

store depletion, but D132E seems to have a greater Ca^{2+} leak under diastolic conditions. Q136P CaM's weaker CaMKII activation may attenuate its associated leak, though its altered spark properties and increased wave propagation in cardiomyocytes suggest a loss in RyR2 channel regulation, suggesting that calmodulinopathy in CPVT is likely mechanistically complex.

7.3 Therapeutic strategies for patients with D132E or Q136P mutations

The ICalmR has documented a significant shift in the perceived clinical spectrum of calmodulinopathy, moving beyond the "grim picture" of almost invariably lethal, early-onset arrhythmias described in initial reports (Crotti et al., 2023). The expansion of the registry now suggests a clinically relevant changing pattern, characterised by increased phenotypic variety and decreased apparent extreme severity. This is reflected in a growing number of familial cases and a reduced frequency of *de novo* genetic variants. The increasing identification of milder and even asymptomatic *CALM* variant-positive individuals, some of whom reach adulthood and reproduce, is attributed to the recent, more widespread use of *CALM* gene screening in commercial genetic panels. Evidence also suggests that some patients may experience a spontaneous improvement in cardiac electrical stability over time (Badone et al., 2018; Crotti et al., 2023).

Conventional anti-arrhythmic therapies

The therapeutic strategy for patients presenting with calmodulinopathy remains challenging as definitive evidence-based recommendations are not yet available. However, the current recommended clinically reasonable strategy is full-dose triple therapy for all phenotypic variants. This regimen combines high-dose β-blockers (*e.g.,* propranolol or nadolol), Na^+ channel blockers (*e.g.,* mexiletine or flecainide), and LCSD (Crotti et al., 2023). Furthermore, due to the inherent severity, an ICD typically accompanies these therapeutic measures. Notably, registry data suggest that this intensive combination therapy is correlated with improved outcomes, as none of the reported sudden cardiac deaths occurred in patients receiving this full-dose, triple treatment (Crotti et al., 2023).

Genetically modified CaM

A Novel therapeutic strategy for CPVT with potential application in calmodulinopathy involves the use of genetically engineered CaM that can modify and correct aberrant Ca^{2+} release. One example Gly-Ser-His-CaM (GSH-CaM), also known as High Affinity-CaM (HA-CaM), which was engineered to have a higher binding affinity to RyR2 than WT CaM (Hino et al. 2012). This design aims to compensate for the reduced binding caused by pathogenic CaM variants, thereby stabilising RyR2 function. Studies have shown that HA-CaM successfully restored normal CaM binding, corrected elevated Ca^{2+} spark frequency, and prevented spontaneous arrhythmogenic transients in mouse cardiomyocytes from failing hearts (Hino et al., 2012; Kato et al., 2017). However, B. Liu et al. (2018) found that HA-CaM failed to prevent adverse Ca^{2+} waves in cardiomyocytes of CPVT mouse model (CASQ2 R33Q). To address this, a further modification was made, creating a therapeutic CaM (TCaM) by introducing a point mutation (M37Q) into the HA-CaM backbone. This M37Q mutation dramatically slows Ca^{2+} dissociation from the N-terminal domain, which aims to stabilise the ability of RyR2 channels to stay closed after activation (i.e., refractoriness). TCaM was found to reduce the frequency of diastolic Ca^{2+} waves in the same CPVT mouse model (B. Liu et al., 2018). These promising findings suggest that TCaM approach could be a potential novel therapeutic path for CPVT and LQTS linked to CaM mutations.

7.4 Future work

While this thesis has provided key insights into the effects of variant D132E and Q136P CaM on generating arrhythmogenic Ca^{2+} release, the findings open new questions and reveal several promising research avenues that warrant further investigation to fully elucidate the underlying mechanism of calmodulinopathy, the following research directions are proposed:

- Single-channel recordings of hRyR2 with D132E or Q136P CaM at diastolic (100 nM) and activating (100 μM) Ca^{2+} concentrations would elucidate variant CaM's direct effect on channel gating. Furthermore, hRyR2 channels could be pre-incubated with CaMKII and variant CaM to induce β-adrenergic phosphorylation to assess the direct impact of variant CaM on S2814-phosphorylated channels.

- Further Ca^{2+} spark experiments using caffeine conducted on mouse ventricular myocytes incubated with D132E or Q136P CaM variants would provide valuable data for assessing potential SR Ca^{2+} leak and would also aid in the interpretation of the spark data presented in this thesis. Additionally, spark experiments could be repeated with activation of PKA signalling to investigate if the arrhythmogenic effect of D132E and Q136P CaM would more pronounce under stress.
- Generation of transgenic mouse models harbouring the D132E and Q136P CaM mutations would allow to test the potential therapeutic benefits of TCaM in correcting abnormal Ca^{2+} transients.
- Research using human-derived iPSC-CMs would provide a physiologically relevant platform for studying D132E and Q136P CaM calmodulinopathy in a native cellular environment (Gomez-Hurtado et al., 2017). This model also provides the unique 5:1 WT-to-mutant protein stoichiometry, thereby enabling a more valid assessment of the mutant's functional impact.

Appendix

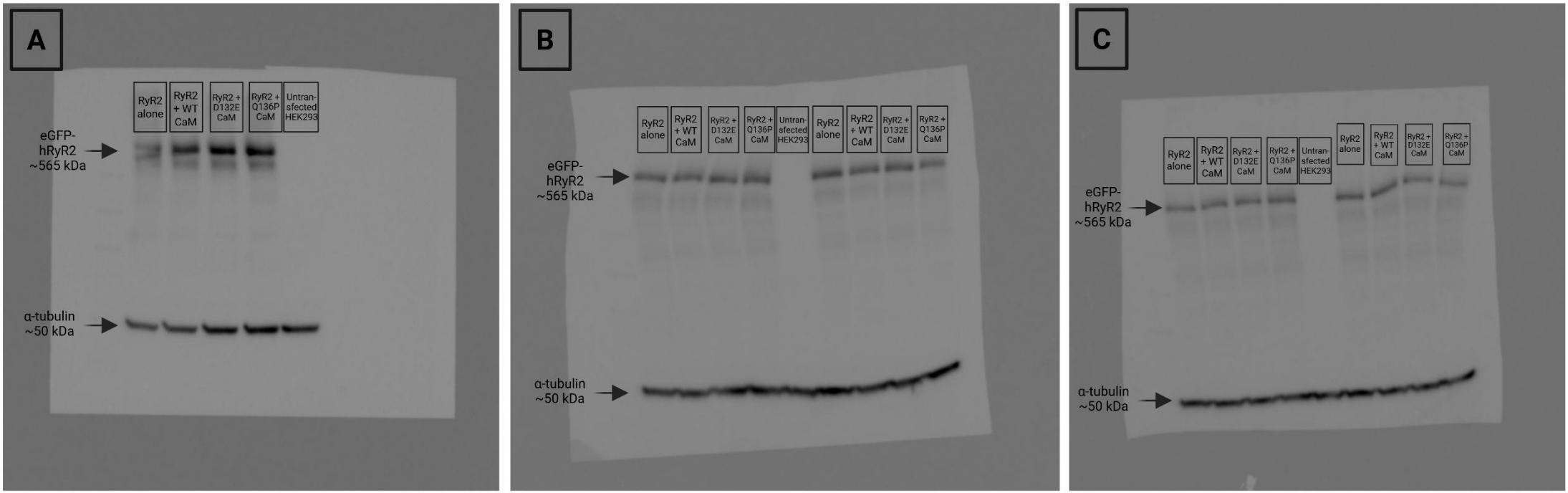

<u>Appendix I.</u> Western blots of cell homogenate of HEK293 co-expressing RyR2 and WT or variant CaM (D132E or Q136P). The expression level of RyR2 was not affected by mutant CaM co-expression compared to WT CaM. **(A)**, **(B)** and **(C)** shows five western blots used for densitometric analysis of RyR2 expression level. A total of 100 µg protein homogenate was loaded in each well. α-tubulin was used as a loading control and untransfected HEK293 cells homogenate was used as a negative control that does not show a band for RyR2 but shows a band corresponding to α-tubulin.

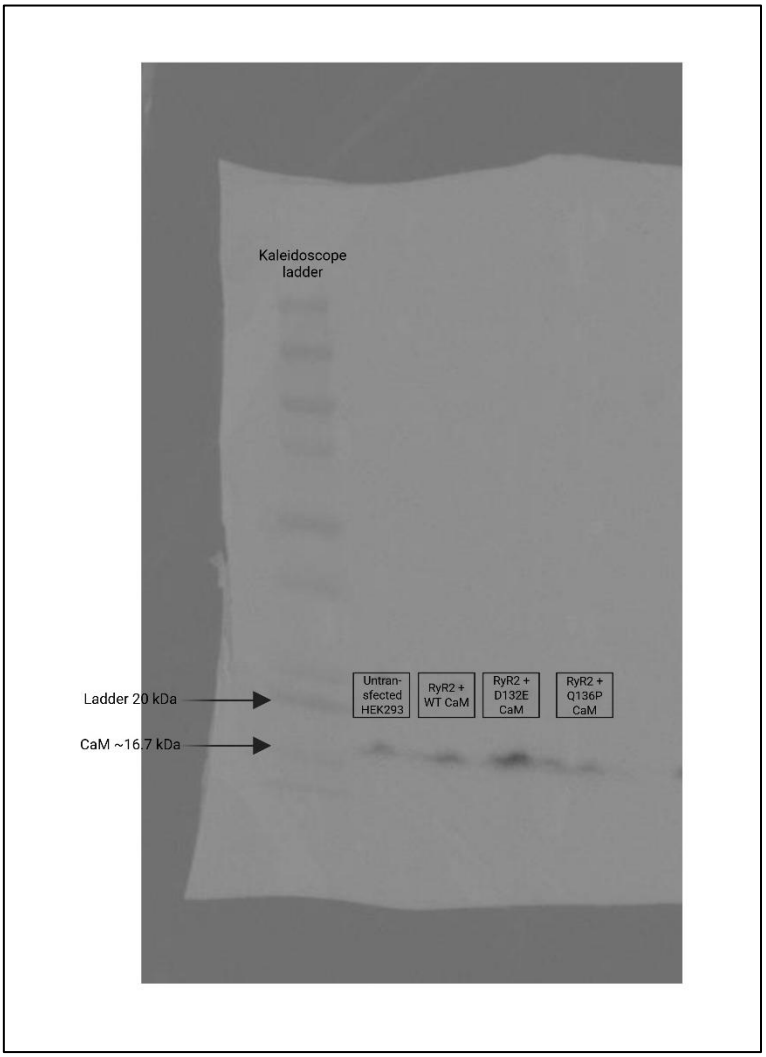

Appendix II. **Western blot of CaM constructs in HEK293 co-expressing RyR2 and WT or variant D132E or Q136P CaM. D132E CaM showed higher expression level compared to WT CaM.** A total of 50 µg cell homogenate sample was loaded for each well. Untransfected HEK293 cell homogenate was used as a positive control.

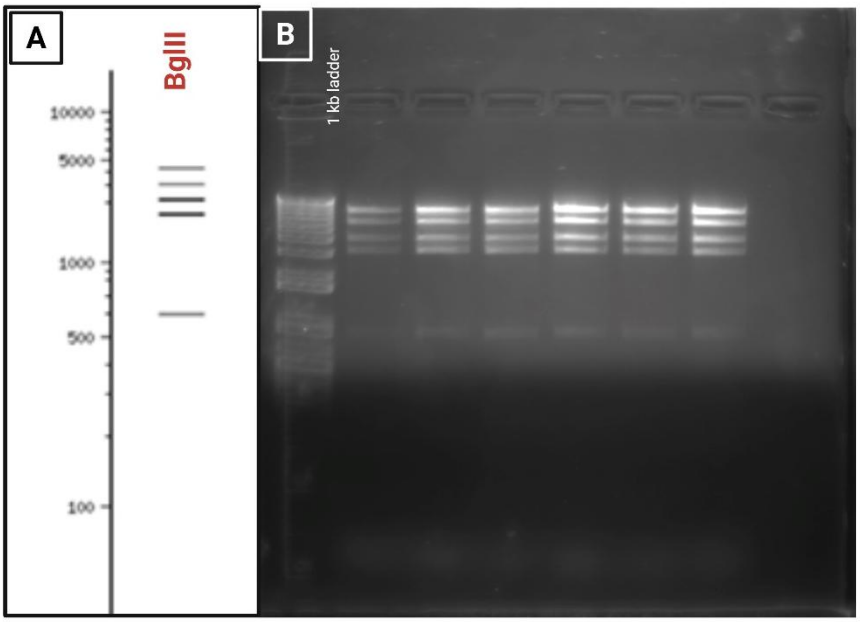

<u>Appendix III</u>. Successful transformation, propagation and small-scale extraction of WT pcDNA3-eGFP-hRyR2 plasmid. (A) Shows illustration of expected digest pattern with *BglII* restriction enzyme indicative of positive clones obtained using NEBcutter® 3.0.19 tool **(B)** Shows gel electrophoresis image of seven clones digested with *BglII* following small-scale plasmid extraction. All clones showed correct digest pattern and four clones were chosen for large-scale plasmid extraction.

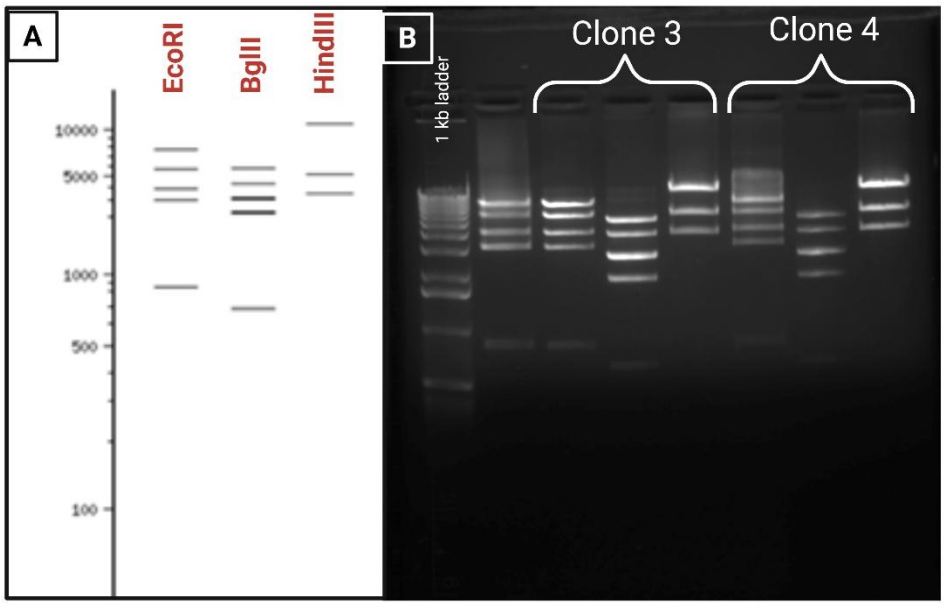

<u>Appendix IV</u>. Successful transformation, propagation and large-scale extraction of WT pcDNA3-eGFP-hRyR2 plasmid. (A) Shows illustration of expected digest patterns with *EcoRI*, *BglII*, and *HinDIII* restriction enzymes indicative of positive clones obtained using NEBcutter® 3.0.19 tool. **(B)** Shows gel electrophoresis image of two clones digested with *EcoRI*, *BglII*, and *HinDIII* respectively following large-scale plasmid extraction which yielded concentration of 129 and 200 µg/mL for clone 3 and 4 respectively. Both clones show correct digest pattern. The first well is a duplicate of the second well made in error (*i.e.*, clone 3 digested with *EcoRI*).

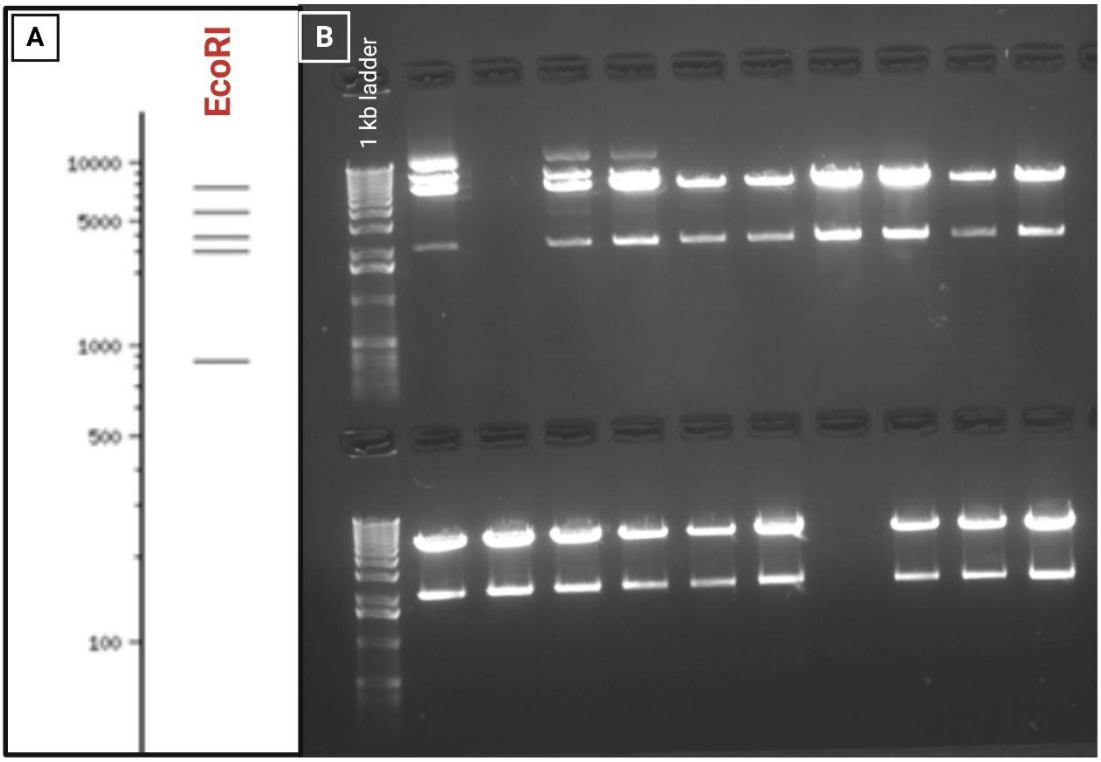

Appendix V. Unsuccessful ligation attempt of S2814A mutated *kpnI/FseI* cassette into full length hRyR2 plasmid. (A) Shows illustration of expected digest patters with *EcoRI* restriction enzyme indicative of positive clones. The cutting pattern gives a "fingerprint" that distinguishes and identifies hRyR2. Digests obtained from NEBcutter® 3.0.19 tool **(B)** Shows gel electrophoresis image of 20 colonies obtained from XL10-Gold transformation from the 1st ligation attempt using 1:3 insert: vector ratio. Digest of the colonies with *EcoRI* showed incorrect cutting pattern as all colonies recombined.

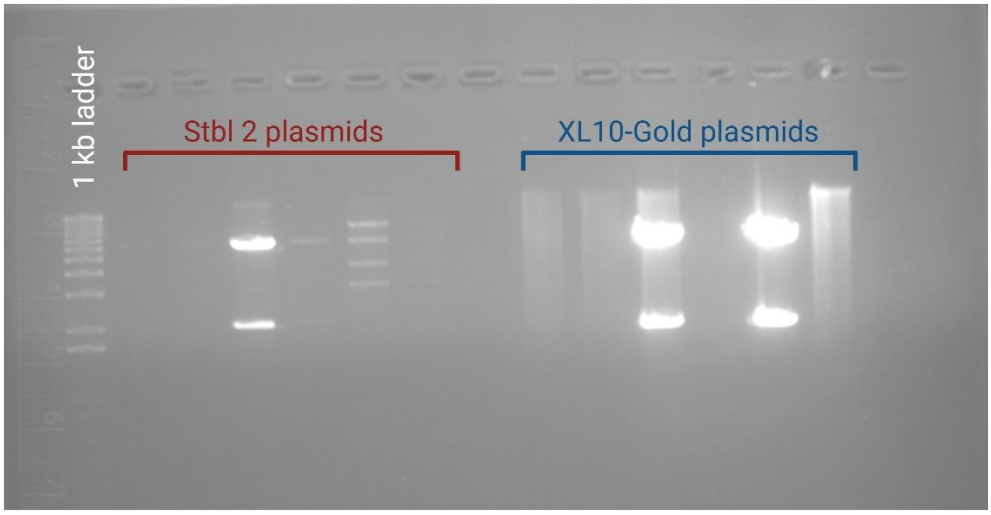

<u>Appendix VI.</u> Gel electrophoresis image of mini-prep plasmids digested with *EcoRI*. The plasmids were obtained from Stbl2 and XL10-Gold retransformations of two positive ligation clones (attempts *no*. 2 and 3 respectively). Only one out of 12 colonies picked shows correct RyR2 digest pattern. The colony was not maxi-prepped due to inability to access the lab the following day.

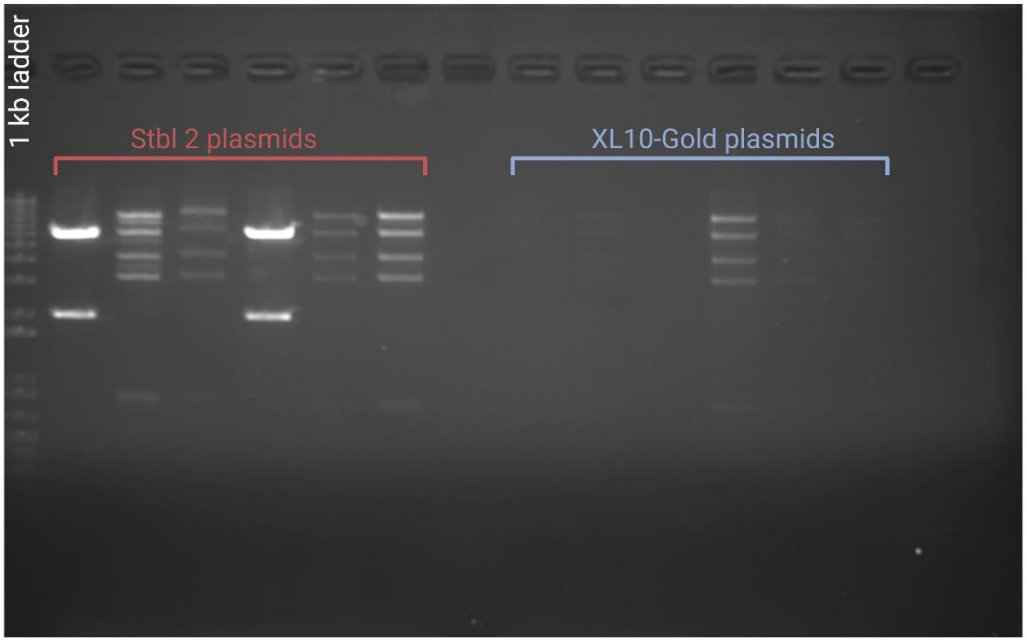

<u>Appendix VII.</u> Gel electrophoresis image of mini-prep plasmids digested with EcoRI. The plasmids were obtained from Stbl2 and XL10-Gold retransformations of two positive ligation clones (attempts *no*. 4 and 5 respectively). A positive colony from each cell type was chosen for large-scale propagation.

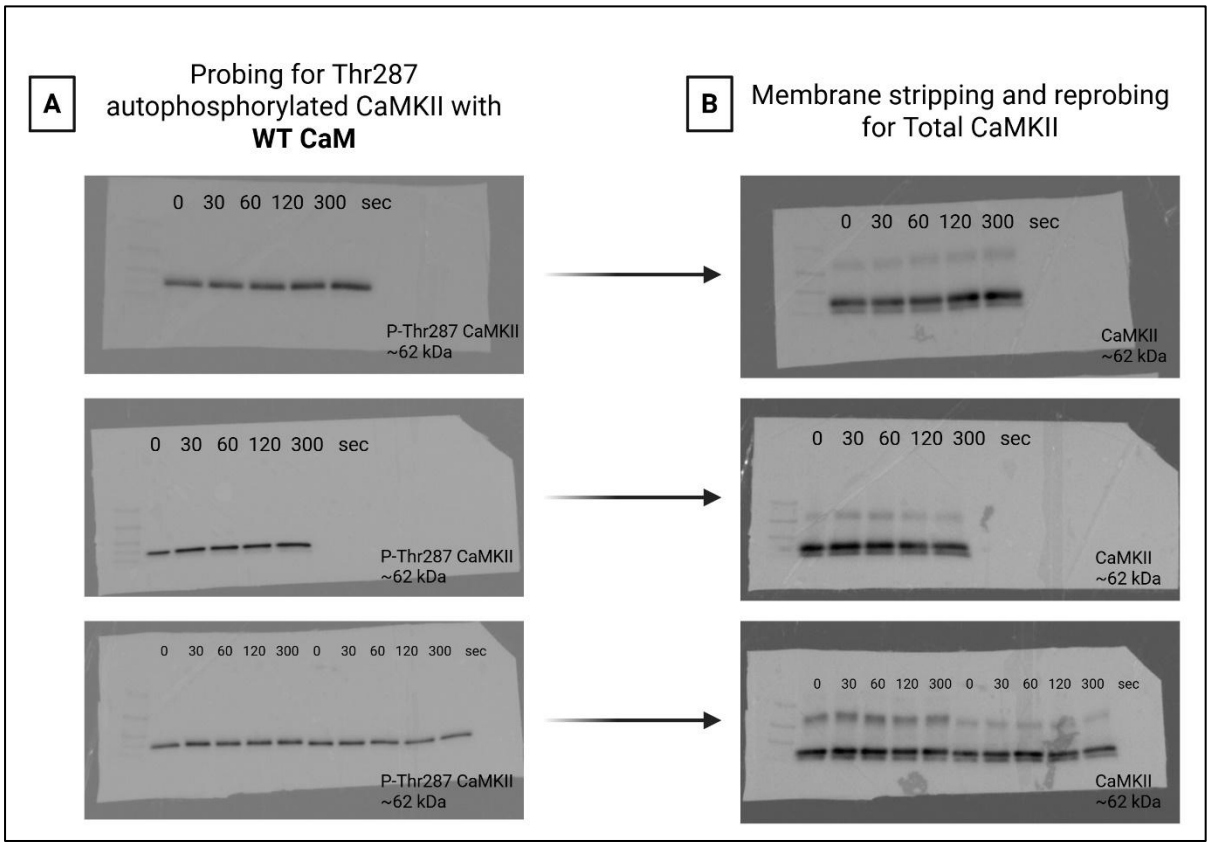

Appendix VIII. Western blots of CaMKII autophosphorylation assay with WT CaM incubation. (A) Shows four western blots used for densitometric analysis of Thr287-CaMKII autophosphorylation level in the presence of WT CaM over time. **(B)** Shows blots after stripping and reprobing for total CaMKII level used to normalise data.

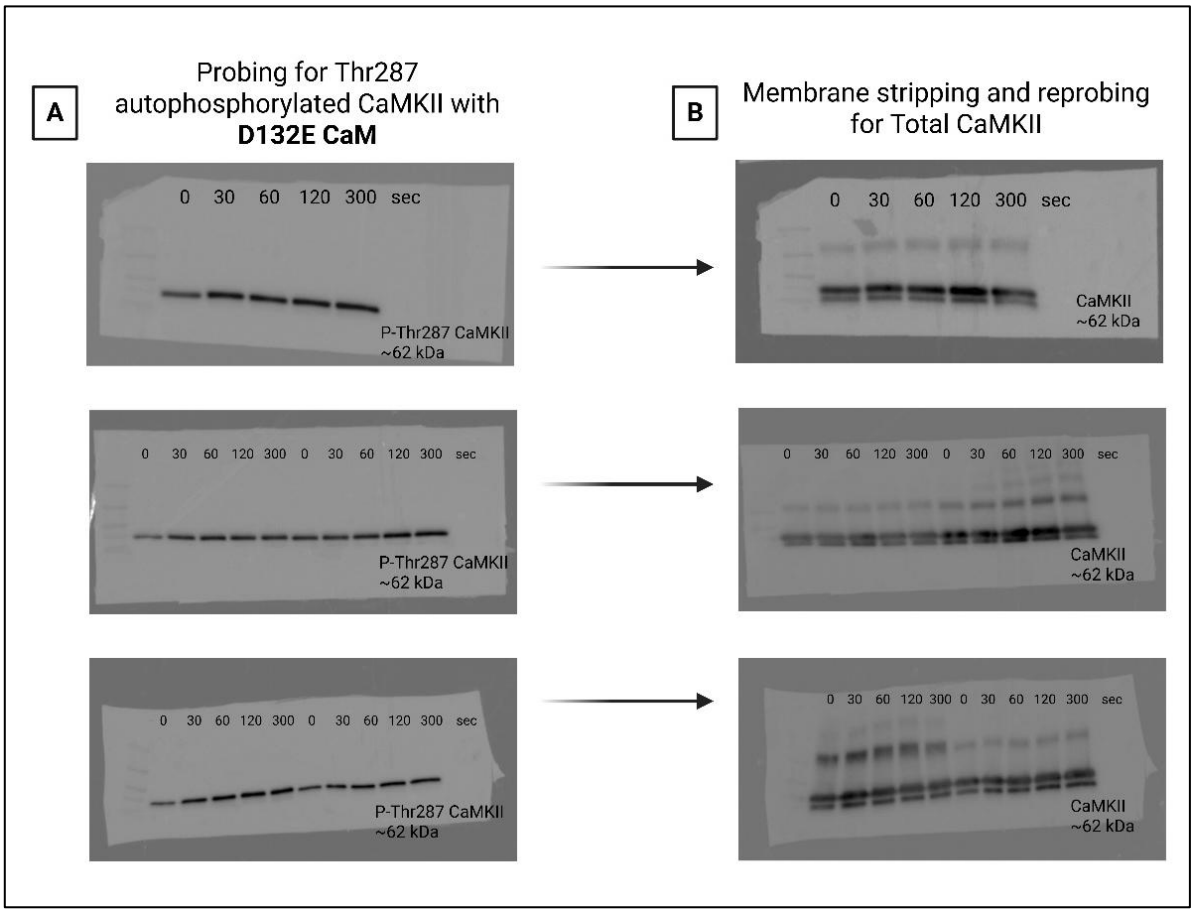

Appendix IX. Western blots of CaMKII autophosphorylation assay with D132E CaM incubation. (A) Shows five western blots used for densitometric analysis of Thr287-CaMKII autophosphorylation level in the presence of D132E CaM over time. **(B)** Shows blots after stripping and reprobing for total CaMKII level used to normalise data.

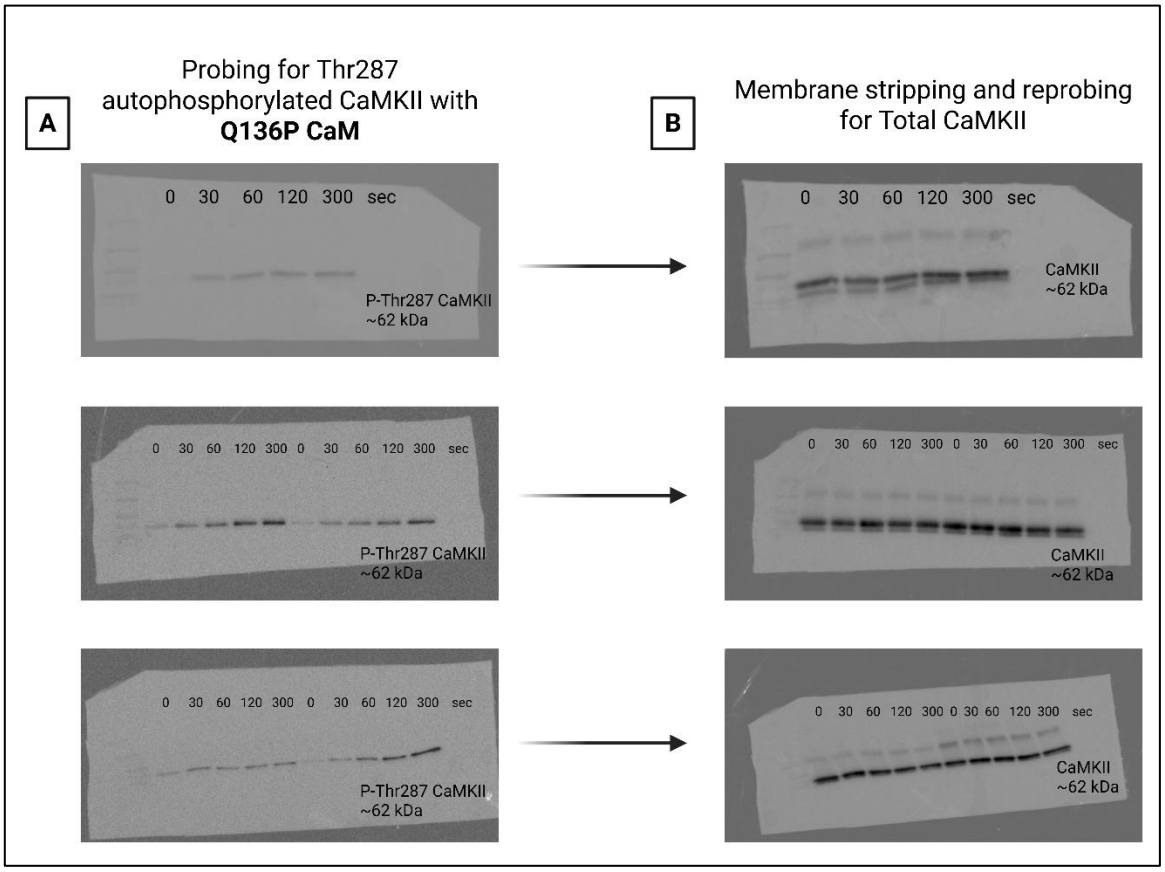

<u>Appendix X.</u> Western blots of CaMKII autophosphorylation assay with Q136P CaM incubation. (A) Shows five western blots used for densitometric analysis of Thr287-CaMKII autophosphorylation level in the presence of Q136P CaM over time. **(B)** Shows blots after stripping and reprobing for total CaMKII level used to normalise data.

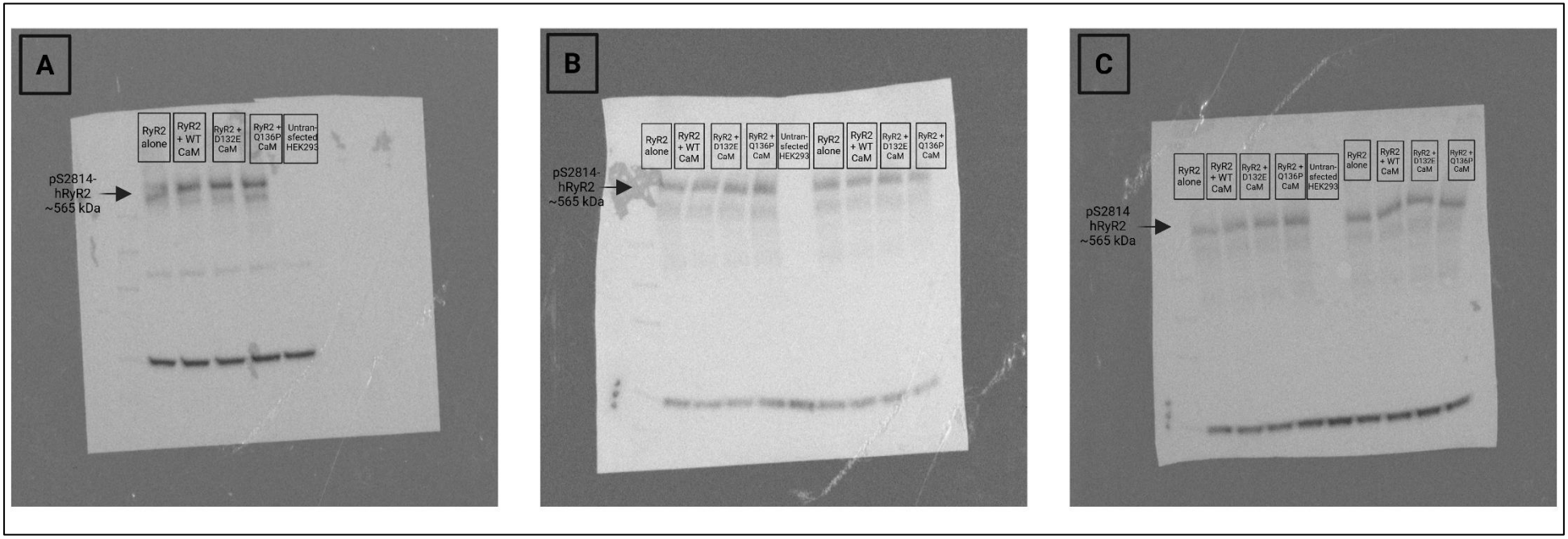

<u>Appendix XI.</u> Western blots of cell homogenate of HEK293 co-expressing RyR2 and WT or variant CaM (D132E or Q136P). After probing for hRyR2 expression level as shown in **Appendix I**, the blots were stripped of all antibodies and then checked using ECL to confirm successful stripping before reprobing to assess pS2814-hRyR2 level. **(A)**, **(B)** and **(C)** shows five western blots used for densitometric analysis of S2814 phosphorylated RyR2 level. A total of 100 µg protein homogenate was loaded in each well. HEK293 cells homogenate was used as a negative control.

References

Adler, A. et al. 2020. An International, Multicentered, Evidence-Based Reappraisal of Genes Reported to Cause Congenital Long QT Syndrome. *Circulation* 141(6), pp. 418–428. Available at: /doi/pdf/10.1161/CIRCULATIONAHA.119.043132?download=true [Accessed: 12 December 2025].

Ai, X., Curran, J.W., Shannon, T.R., Bers, D.M. and Pogwizd, S.M. 2005. Ca2+/calmodulin-dependent protein kinase modulates cardiac ryanodine receptor phosphorylation and sarcoplasmic reticulum Ca2+ leak in heart failure. *Circulation research* 97(12), pp. 1314–1322. Available at: https://pubmed.ncbi.nlm.nih.gov/16269653/ [Accessed: 19 February 2025].

Al-Khatib, S. et al. 2018. 2017 AHA/ACC/HRS guideline for management of patients with ventricular arrhythmias and the prevention of sudden cardiac death: a report of the American College of Cardiology/American Heart Association Task Force on Clinical Practice Guidelines and the Heart Rhythm Society. *J Am Coll Cardiol* 72, pp. e91–e220.

Amin, A.S., Pinto, Y.M. and Wilde, A.A.M. 2013. Long QT syndrome: beyond the causal mutation. *The Journal of Physiology* 591(Pt 17), p. 4125. Available at: https://pmc.ncbi.nlm.nih.gov/articles/PMC3779107/ [Accessed: 12 December 2025].

Anderson, M.E., Brown, J.H. and Bers, D.M. 2011. CaMKII in myocardial hypertrophy and heart failure. *Journal of molecular and cellular cardiology* 51(4), pp. 468–473. Available at: https://pubmed.ncbi.nlm.nih.gov/21276796/ [Accessed: 12 February 2025].

Anthony, D.F., Beattie, J., Paul, A. and Currie, S. 2007. Interaction of calcium/calmodulin-dependent protein kinase IIdeltaC with sorcin indirectly modulates ryanodine receptor function in cardiac myocytes. *Journal of molecular and cellular cardiology* 43(4), pp. 492–503. Available at: https://pubmed.ncbi.nlm.nih.gov/17707398/ [Accessed: 2 February 2025].

Asghari, P. et al. 2024. Phosphorylation of RyR2 simultaneously expands the dyad and rearranges the tetramers. *The Journal of general physiology* 156(4). Available at: https://pubmed.ncbi.nlm.nih.gov/38385988/ [Accessed: 21 February 2025].

Asghari, P., Scriven, D.R.L., Hoskins, J., Fameli, N., van Breemen, C. and Moore, E.D.W. 2012.

The structure and functioning of the couplon in the mammalian cardiomyocyte. *Protoplasma* 249 Suppl 1(SUPPL. 1), pp. 31–38. Available at: https://pubmed.ncbi.nlm.nih.gov/22057630/ [Accessed: 18 April 2022].

Asghari, P., Scriven, D.R.L., Ng, M., Panwar, P., Chou, K.C., van Petegem, F. and Moore, E.D.W. 2020. Cardiac ryanodine receptor distribution is dynamic and changed by auxiliary proteins and post-translational modification. *eLife* 9. Available at: https://pubmed.ncbi.nlm.nih.gov/31916935/ [Accessed: 24 February 2025].

Asghari, P., Scriven, D.R.L., Sanatani, S., Gandhi, S.K., Campbell, A.I.M. and Moore, E.D.W. 2014. Nonuniform and variable arrangements of ryanodine receptors within mammalian ventricular couplons. *Circulation Research* 115(2), pp. 252–262. Available at: https://www.ahajournals.org/doi/abs/10.1161/CIRCRESAHA.115.303897 [Accessed: 18 April 2022].

Ather, S., Wang, W., Wang, Q., Li, N., Anderson, M.E. and Wehrens, X.H.T. 2013. Inhibition of CaMKII phosphorylation of RyR2 prevents inducible ventricular arrhythmias in mice with Duchenne muscular dystrophy. *Heart rhythm* 10(4), pp. 592–599. Available at: https://pubmed.ncbi.nlm.nih.gov/23246599/ [Accessed: 24 February 2025].

Badone, B., Ronchi, C., Kotta, M.C., Sala, L., Ghidoni, A., Crotti, L. and Zaza, A. 2018. Calmodulinopathy: Functional Effects of CALM Mutations and Their Relationship With Clinical Phenotypes. *Frontiers in Cardiovascular Medicine* 5, p. 176. doi: 10.3389/FCVM.2018.00176/BIBTEX.

Baier, M.J., Noack, J., Seitz, M.T., Maier, L.S. and Neef, S. 2021. Phosphorylation of RyR2 Ser-2814 by CaMKII mediates β1-adrenergic stress induced Ca2+-leak from the sarcoplasmic reticulum. *FEBS Open Bio* 11(10), p. 2756. Available at: /pmc/articles/PMC8487045/ [Accessed: 31 May 2023].

Baine, S. et al. 2020. Muscarinic-dependent phosphorylation of the cardiac ryanodine receptor by protein kinase G is mediated by PI3K–AKT–nNOS signaling. *The Journal of Biological Chemistry* 295(33), p. 11720. Available at: https://pmc.ncbi.nlm.nih.gov/articles/PMC7450129/ [Accessed: 13 February 2025].

Balshaw, D.M., Xu, L., Yamaguchi, N., Pasek, D.A. and Meissner, G. 2001. Calmodulin Binding and Inhibition of Cardiac Muscle Calcium Release Channel (Ryanodine Receptor). *Journal of Biological Chemistry* 276(23), pp. 20144–20153. doi: 10.1074/JBC.M010771200.

Beard, N.A., Casarotto, M.G., Wei, L., Varsányi, M., Laver, D.R. and Dulhunty, A.F. 2005. Regulation of Ryanodine Receptors by Calsequestrin: Effect of High Luminal Ca2+ and Phosphorylation. *Biophysical Journal* 88(5), p. 3444. Available at: https://pmc.ncbi.nlm.nih.gov/articles/PMC1305491/ [Accessed: 31 January 2025].

Bellinger, A.M. et al. 2008. Remodeling of ryanodine receptor complex causes "leaky" channels: A molecular mechanism for decreased exercise capacity. *Proceedings of the National Academy of Sciences of the United States of America* 105(6), p. 2198. Available at: https://pmc.ncbi.nlm.nih.gov/articles/PMC2538898/ [Accessed: 19 February 2025].

Benkusky, N.A. et al. 2007. Intact beta-adrenergic response and unmodified progression toward heart failure in mice with genetic ablation of a major protein kinase A phosphorylation site in the cardiac ryanodine receptor. *Circulation research* 101(8), pp. 819–829. Available at: https://pubmed.ncbi.nlm.nih.gov/17717301/ [Accessed: 19 February 2025].

Berchtold, M.W. et al. 2016. The Arrhythmogenic Calmodulin Mutation D129G Dysregulates Cell Growth, Calmodulin-dependent Kinase II Activity, and Cardiac Function in Zebrafish. *Journal of Biological Chemistry* 291(52), pp. 26636–26646. Available at: https://www.sciencedirect.com/science/article/pii/S0021925820344185 [Accessed: 28 August 2025].

Berchtold, M.W. et al. 2021. The heart arrhythmia-linked D130G calmodulin mutation causes premature inhibitory autophosphorylation of CaMKII. *Biochimica et Biophysica Acta (BBA) - Molecular Cell Research* 1868(12), p. 119119. Available at: https://www.sciencedirect.com/science/article/pii/S0167488921001737 [Accessed: 28 August 2025].

Berridge, M.J., Lipp, P. and Bootman, M.D. 2000. The versatility and universality of calcium signalling. *Nature reviews. Molecular cell biology* 1(1), pp. 11–21. Available at: https://pubmed.ncbi.nlm.nih.gov/11413485/ [Accessed: 7 January 2025].

Bers, D.M. 2002. Cardiac excitation-contraction coupling. *Nature* 415(6868), pp. 198–205. Available at: https://pubmed.ncbi.nlm.nih.gov/11805843/ [Accessed: 21 May 2024].

Bers, D.M. 2006. Altered cardiac myocyte Ca regulation in heart failure. *Physiology (Bethesda, Md.)* 21(6), pp. 380–387. Available at: https://pubmed.ncbi.nlm.nih.gov/17119150/ [Accessed: 25 February 2025].

Bers, D.M. 2007. Going to cAMP just got more complicated. *The Journal of Physiology* 583(Pt 2), p. 415. Available at: https://pmc.ncbi.nlm.nih.gov/articles/PMC2277018/ [Accessed: 13 February 2025].

Black, D.J., Tikunova, S.B., David Johnson, J. and Davis, J.P. 2000. Acid Pairs Increase the N-Terminal Ca 2+ Affinity of CaM by Increasing the Rate of Ca 2+ Association. Available at: https://pubs.acs.org/journals/bichaw/index.html [Accessed: 6 February 2025].

Boczek, N.J. et al. 2016. Spectrum and prevalence of CALM1-, CALM2-, and CALM3-encoded calmodulin variants in long QT syndrome and functional characterization of a novel long QT syndrome-associated calmodulin missense variant, E141G. *Circulation: Cardiovascular Genetics* 9(2), pp. 136–146. Available at: https://www.ahajournals.org/doi/abs/10.1161/CIRCGENETICS.115.001323 [Accessed: 12 May 2022].

Bootman, M.D. et al. 2001. Calcium signalling--an overview. *Seminars in cell & developmental biology* 12(1), pp. 3–10. Available at: https://pubmed.ncbi.nlm.nih.gov/11162741/ [Accessed: 9 January 2025].

Braun, A.P. and Schulman, H. 1995. The multifunctional calcium/calmodulin-dependent protein kinase: from form to function. *Annual review of physiology* 57, pp. 417–445. Available at: https://pubmed.ncbi.nlm.nih.gov/7778873/ [Accessed: 11 February 2025].

Brillantes, A.M.B. et al. 1994. Stabilization of calcium release channel (ryanodine receptor) function by FK506-binding protein. *Cell* 77(4), pp. 513–523. Available at: https://pubmed.ncbi.nlm.nih.gov/7514503/ [Accessed: 31 January 2025].

Brochet, D.X.P., Xie, W., Yang, D., Cheng, H. and Lederer, W.J. 2011. Quarky calcium release

in the heart. *Circulation research* 108(2), pp. 210–218. Available at: https://pubmed.ncbi.nlm.nih.gov/21148431/ [Accessed: 9 October 2025].

Brochet, D.X.P., Yang, D., Di Maio, A., Lederer, W.J., Franzini-Armstrong, C. and Cheng, H. 2005. Ca2+ blinks: rapid nanoscopic store calcium signaling. *Proceedings of the National Academy of Sciences of the United States of America* 102(8), pp. 3099–3104. Available at: https://pubmed.ncbi.nlm.nih.gov/15710901/ [Accessed: 24 January 2025].

Brostrom, C.O. and Wolff, D.J. 1981. Properties and functions of calmodulin. *Biochemical pharmacology* 30(12), pp. 1395–1405. Available at: https://pubmed.ncbi.nlm.nih.gov/6268098/ [Accessed: 7 February 2025].

Buard, I., Coultrap, S.J., Freund, R.K., Lee, Y.S., Dell'Acqua, M.L., Silva, A.J. and Bayer, K.U. 2010. CaMKII "autonomy" is required for initiating but not for maintaining neuronal long-term information storage. *The Journal of neuroscience : the official journal of the Society for Neuroscience* 30(24), pp. 8214–8220. Available at: https://pubmed.ncbi.nlm.nih.gov/20554872/ [Accessed: 11 February 2025].

Calver, B. 2019. *The role of calmodulin in the regulation of calcium signalling proteins in health and disease*. Cardiff: Cardiff University.

Camors, E. and Valdivia, H.H. 2014. CaMKII regulation of cardiac ryanodine receptors and inositol triphosphate receptors. *Frontiers in Pharmacology* 5 MAY, p. 90897. doi: 10.3389/FPHAR.2014.00101/PDF.

Campbell, H.M. et al. 2020. Loss of SPEG Inhibitory Phosphorylation of Ryanodine Receptor Type-2 Promotes Atrial Fibrillation. *Circulation* 142(12), pp. 1159–1172. Available at: https://pubmed.ncbi.nlm.nih.gov/32683896/ [Accessed: 24 February 2025].

Cannell, M.B., Cheng, H. and Lederer, W.J. 1994. Spatial non-uniformities in [Ca2+]i during excitation-contraction coupling in cardiac myocytes. *Biophysical Journal* 67(5), p. 1942. Available at: /pmc/articles/PMC1225569/?report=abstract [Accessed: 21 May 2024].

Carter, S., Colyer, J. and Sitsapesan, R. 2006. Maximum Phosphorylation of the Cardiac Ryanodine Receptor at Serine-2809 by Protein Kinase A Produces Unique Modifications to

Channel Gating and Conductance Not Observed at Lower Levels of Phosphorylation. Available at: http://circres.ahajournals.org [Accessed: 19 February 2025].

Carter, S., Pitt, S.J., Colyer, J. and Sitsapesan, R. 2011. Ca^2+-dependent phosphorylation of RyR2 can uncouple channel gating from direct cytosolic Ca^2+ regulation. *The Journal of membrane biology* 240(1), pp. 21–33. Available at: https://pubmed.ncbi.nlm.nih.gov/21274522/ [Accessed: 25 February 2025].

Cerrone, M. et al. 2017a. Plakophilin-2 is required for transcription of genes that control calcium cycling and cardiac rhythm. *Nature Communications* 8(1), pp. 1–16. Available at: https://www.nature.com/articles/s41467-017-00127-0 [Accessed: 6 August 2025].

Cerrone, M., Agullo-Pascual, E. and Delmar, M. 2017b. The Intercalated Disc: A Molecular Network That Integrates Electrical Coupling, Intercellular Adhesion, and Cell Excitability. *Cardiac Electrophysiology: From Cell to Bedside: Seventh Edition*, pp. 198–211. doi: 10.1016/B978-0-323-44733-1.00022-5.

Chang, A. et al. 2025. RYR2 Variants in Catecholaminergic Polymorphic Ventricular Tachycardia Patients: Insights From Protein Structure and Clinical Data. *Circulation: Arrhythmia and Electrophysiology* 18, p. 13757. Available at: /doi/pdf/10.1161/CIRCEP.124.013757?download=true [Accessed: 16 November 2025].

Chao, L.H. et al. 2011. A mechanism for tunable autoinhibition in the structure of a human Ca2+/calmodulin- dependent kinase II holoenzyme. *Cell* 146(5), pp. 732–745. Available at: https://pubmed.ncbi.nlm.nih.gov/21884935/ [Accessed: 11 February 2025].

Chazin, W.J. and Johnson, C.N. 2020. Calmodulin Mutations Associated with Heart Arrhythmia: A Status Report. *International Journal of Molecular Sciences* 21(4). Available at: /pmc/articles/PMC7073091/ [Accessed: 30 April 2022].

Chelu, M.G. et al. 2009. Calmodulin kinase II-mediated sarcoplasmic reticulum Ca2+ leak promotes atrial fibrillation in mice. *Journal of Clinical Investigation* 119(7), pp. 1940–1951. Available at: https://pubmed.ncbi.nlm.nih.gov/19603549/ [Accessed: 3 July 2025].

Cheng, H. and Lederer, W.J. 2008. Calcium sparks. *Physiological Reviews* 88(4), pp. 1491–

1545. Available at: https://journals.physiology.org/doi/10.1152/physrev.00030.2007 [Accessed: 21 May 2024].

Cheng, H., Lederer, W.J. and Cannell, M.B. 1993a. Calcium sparks: elementary events underlying excitation-contraction coupling in heart muscle. *Science (New York, N.Y.)* 262(5134), pp. 740–744. Available at: https://pubmed.ncbi.nlm.nih.gov/8235594/ [Accessed: 9 January 2025].

Cheng, X., Phelps, C. and Taylor, S.S. 2001. Differential binding of cAMP-dependent protein kinase regulatory subunit isoforms Ialpha and IIbeta to the catalytic subunit. *The Journal of biological chemistry* 276(6), pp. 4102–4108. Available at: https://pubmed.ncbi.nlm.nih.gov/11110787/ [Accessed: 12 February 2025].

Chen-Izu, Y. et al. 2006. Three-dimensional distribution of ryanodine receptor clusters in cardiac myocytes. *Biophysical journal* 91(1), pp. 1–13. Available at: https://pubmed.ncbi.nlm.nih.gov/16603500/ [Accessed: 16 May 2023].

Chiang, D.Y. et al. 2014. Impaired local regulation of ryanodine receptor type 2 by protein phosphatase 1 promotes atrial fibrillation. *Cardiovascular Research* 103(1), p. 178. Available at: https://pmc.ncbi.nlm.nih.gov/articles/PMC4133595/ [Accessed: 5 July 2025].

Chiarini-Garcia, H. and Melo, R.C.N. eds. 2011. *Light Microscopy*. Totowa, NJ: Humana Press. Available at: http://link.springer.com/10.1007/978-1-60761-950-5 [Accessed: 16 September 2025].

Ching, L.L., Williams, A.J. and Sitsapesan, R. 2000. Evidence for Ca(2+) activation and inactivation sites on the luminal side of the cardiac ryanodine receptor complex. *Circulation research* 87(3), pp. 201–206. Available at: https://pubmed.ncbi.nlm.nih.gov/10926870/ [Accessed: 23 January 2025].

Chugun, A., Sato, O., Takeshima, H. and Ogawa, Y. 2007. Mg2+ activates the ryanodine receptor type 2 (RyR2) at intermediate Ca2+ concentrations. *American journal of physiology. Cell physiology* 292(1). Available at: https://pubmed.ncbi.nlm.nih.gov/16971497/ [Accessed: 25 January 2025].

Colbran, R.J. and Soderling, T.R. 1990. Calcium/calmodulin-independent autophosphorylation sites of calcium/calmodulin-dependent protein kinase II. Studies on the effect of phosphorylation of threonine 305/306 and serine 314 on calmodulin binding using synthetic peptides. *Journal of Biological Chemistry* 265(19), pp. 11213–11219. doi: 10.1016/S0021-9258(19)38578-3.

Crotti, L. et al. 2013. Calmodulin mutations associated with recurrent cardiac arrest in infants. *Circulation* 127(9), pp. 1009–1017. Available at: https://www.ahajournals.org/doi/pdf/10.1161/CIRCULATIONAHA.112.001216?download=true [Accessed: 13 December 2025].

Crotti, L. et al. 2023. Clinical presentation of calmodulin mutations: the International Calmodulinopathy Registry. *European Heart Journal* 44(35), p. 3357. Available at: https://pmc.ncbi.nlm.nih.gov/articles/PMC10499544/ [Accessed: 8 October 2025].

Crouchl, T.H. and Klee, C.B. 1980. Positive cooperative binding of calcium to bovine brain calmodulin. *Biochemistry* 19(16), pp. 3692–3698. Available at: https://pubmed.ncbi.nlm.nih.gov/7407067/ [Accessed: 7 February 2025].

Currie, S., Loughrey, C.M., Craig, M.A. and Smith, G.L. 2004. Calcium/calmodulin-dependent protein kinase IIdelta associates with the ryanodine receptor complex and regulates channel function in rabbit heart. *The Biochemical journal* 377(Pt 2), pp. 357–366. Available at: https://pubmed.ncbi.nlm.nih.gov/14556649/ [Accessed: 19 February 2025].

Da'as, S.I. et al. 2019. Arrhythmogenic calmodulin E105A mutation alters cardiac RyR2 regulation leading to cardiac dysfunction in zebrafish. *Annals of the New York Academy of Sciences* 1448(1), pp. 19–29. Available at: /doi/pdf/10.1111/nyas.14033 [Accessed: 9 October 2025].

Da'as, S.I. et al. 2024. Divergent Biochemical Properties and Disparate Impact of Arrhythmogenic Calmodulin Mutations on Zebrafish Cardiac Function. *Journal of Cellular Biochemistry* 125(8), p. e30619. Available at: /doi/pdf/10.1002/jcb.30619 [Accessed: 21 August 2025].

Delisle, B.P., Anson, B.D., Rajamani, S. and January, C.T. 2004. Biology of cardiac arrhythmias:

ion channel protein trafficking. *Circulation research* 94(11), pp. 1418–1428. Available at: https://pubmed.ncbi.nlm.nih.gov/15192037/ [Accessed: 31 May 2023].

Despa, S. et al. 2005. Phospholemman-phosphorylation mediates the β-adrenergic effects on Na/K pump function in cardiac myocytes. *Circulation Research* 97(3), pp. 252–259. Available at: https://www.ahajournals.org/doi/10.1161/01.RES.0000176532.97731.e5 [Accessed: 15 January 2025].

Dewenter, M. et al. 2024. Ca2+/calmodulin-dependent kinase IIδC-induced chronic heart failure does not depend on sarcoplasmic reticulum Ca2+ leak. *ESC Heart Failure* 11(4), pp. 2191–2199. Available at: https://pubmed.ncbi.nlm.nih.gov/38616546/ [Accessed: 3 July 2025].

Dixon, R.E., Moreno, C.M., Yuan, C., Opitz-Araya, X., Binder, M.D., Navedo, M.F. and Santana, L.F. 2015. Graded Ca2+/calmodulin-dependent coupling of voltage-gated CaV1.2 channels. *eLife* 2015(4). doi: 10.7554/ELIFE.05608.

Dobrev, D. and Wehrens, X.H.T. 2014. Role of RyR2 phosphorylation in heart failure and arrhythmias: Controversies around ryanodine receptor phosphorylation in cardiac disease. *Circulation Research* 114(8), pp. 1311–1319. Available at: https://www.ahajournals.org/doi/abs/10.1161/circresaha.114.300568 [Accessed: 25 April 2022].

Domingo, D. et al. 2015. Non-ventricular, Clinical, and Functional Features of the RyR2(R420Q) Mutation Causing Catecholaminergic Polymorphic Ventricular Tachycardia. *Revista espanola de cardiologia (English ed.)* 68(5), pp. 398–407. Available at: https://pubmed.ncbi.nlm.nih.gov/25440180/ [Accessed: 28 May 2024].

Duke, A.M. and Steele, D.S. 1998. Effects of cyclopiazonic acid on Ca2+ regulation by the sarcoplasmic reticulum in saponin-permeabilized skeletal muscle fibres. *Pflugers Archiv European Journal of Physiology* 436(1), pp. 104–111. Available at: https://link.springer.com/article/10.1007/s004240050610 [Accessed: 16 November 2025].

Eisner, D.A., Caldwell, J.L., Kistamás, K. and Trafford, A.W. 2017. Calcium and Excitation-Contraction Coupling in the Heart. *Circulation Research* 121(2), p. 181. Available at:

/pmc/articles/PMC5497788/ [Accessed: 12 April 2022].

Erickson, J.R., Herren, A.W., Wang, Y. and Bayer, K.U. 2014. Mechanisms of CaMKII activation in the heart. Available at: www.frontiersin.org [Accessed: 11 February 2025].

Erickson, J.R., Patel, R., Ferguson, A., Bossuyt, J. and Bers, D.M. 2011. Fluorescence resonance energy transfer-based sensor camui provides new insight into mechanisms of calcium/calmodulin-dependent protein kinase II activation in intact cardiomyocytes. *Circulation Research* 109(7), pp. 729–738. Available at: https://www.ahajournals.org/doi/10.1161/CIRCRESAHA.111.247148 [Accessed: 11 February 2025].

Eschenhagen, T. 2010. Is ryanodine receptor phosphorylation key to the fight or flight response and heart failure? *The Journal of clinical investigation* 120(12), pp. 4197–4203. Available at: https://pubmed.ncbi.nlm.nih.gov/21099119/ [Accessed: 12 February 2025].

Fabiato, A. 1985. Effects of ryanodine in skinned cardiac cells. *Federation proceedings* 44(15), pp. 2970–2976. Available at: https://pubmed.ncbi.nlm.nih.gov/2415405/ [Accessed: 20 January 2025].

Fan, J., Shuba, Y.M. and Morad, M. 1996. Regulation of cardiac sodium-calcium exchanger by beta-adrenergic agonists. *Proceedings of the National Academy of Sciences of the United States of America* 93(11), pp. 5527–5532. Available at: https://pubmed.ncbi.nlm.nih.gov/8643609/ [Accessed: 15 January 2025].

Farrell, E.F., Antaramian, A., Rueda, A., Gómez, A.M. and Valdivia, H.H. 2003. Sorcin inhibits calcium release and modulates excitation-contraction coupling in the heart. *The Journal of biological chemistry* 278(36), pp. 34660–34666. Available at: https://pubmed.ncbi.nlm.nih.gov/12824171/ [Accessed: 2 February 2025].

Fearnley, C.J., Llewelyn Roderick, H. and Bootman, M.D. 2011. Calcium Signaling in Cardiac Myocytes. *Cold Spring Harbor Perspectives in Biology* 3(11). Available at: /pmc/articles/PMC3220352/ [Accessed: 6 April 2022].

Fischer, R. et al. 1988. Multiple divergent mRNAs code for a single human calmodulin. *Journal*

of Biological Chemistry 263(32), pp. 17055–17062. doi: 10.1016/S0021-9258(18)37497-0.

Fischer, T.H. et al. 2013. Ca2+/calmodulin-dependent protein kinase II and protein kinase A differentially regulate sarcoplasmic reticulum Ca2+ leak in human cardiac pathology. *Circulation* 128(9), pp. 970–981. Available at: https://pubmed.ncbi.nlm.nih.gov/23877259/ [Accessed: 19 February 2025].

Fischer, T.H. et al. 2014. Ca(2+) /calmodulin-dependent protein kinase II equally induces sarcoplasmic reticulum Ca(2+) leak in human ischaemic and dilated cardiomyopathy. *European journal of heart failure* 16(12), pp. 1292–1300. Available at: https://pubmed.ncbi.nlm.nih.gov/25201344/ [Accessed: 24 February 2025].

Fowler, E.D., Diakite, S.L., Gomez, A.M. and Colman, M.A. 2025. Disruption of ventricular activation by subthreshold delayed afterdepolarizations in RyR2-R420Q catecholaminergic polymorphic ventricular tachycardia. *Journal of molecular and cellular cardiology plus* 13. Available at: https://pubmed.ncbi.nlm.nih.gov/40612651/ [Accessed: 28 September 2025].

Frank, D. and Frey, N. 2011. Cardiac Z-disc Signaling Network. *The Journal of Biological Chemistry* 286(12), p. 9897. Available at: https://pmc.ncbi.nlm.nih.gov/articles/PMC3060542/ [Accessed: 17 January 2025].

Franzini-Armstrong, C., Protasi, F. and Ramesh, V. 1999a. Shape, size, and distribution of Ca(2+) release units and couplons in skeletal and cardiac muscles. *Biophysical journal* 77(3), pp. 1528–1539. Available at: https://pubmed.ncbi.nlm.nih.gov/10465763/ [Accessed: 20 January 2025].

Fruen, B.R., Black, D.J., Bloomquist, R.A., Bardy, J.M., Johnson, J.D., Louis, C.F. and Balog, E.M. 2003. Regulation of the RYR1 and RYR2 Ca 2+ Release Channel Isoforms by Ca 2+-Insensitive Mutants of Calmodulin †. Available at: https://pubs.acs.org/sharingguidelines [Accessed: 24 April 2022].

Furuichi, T., Furutama, D., Hakamata, Y., Nakai, J., Takeshima, H. and Mikoshiba, K. 1994. Multiple types of ryanodine receptor/Ca2+ release channels are differentially expressed in rabbit brain. *The Journal of neuroscience : the official journal of the Society for Neuroscience* 14(8), pp. 4794–4805. Available at: https://pubmed.ncbi.nlm.nih.gov/8046450/ [Accessed:

13 April 2022].

Gaertner, T.R., Kolodziej, S.J., Wang, D., Kobayashi, R., Koomen, J.M., Stoops, J.K. and Waxham, M.N. 2004. Comparative analyses of the three-dimensional structures and enzymatic properties of alpha, beta, gamma and delta isoforms of Ca2+-calmodulin-dependent protein kinase II. *The Journal of biological chemistry* 279(13), pp. 12484–12494. Available at: https://pubmed.ncbi.nlm.nih.gov/14722083/ [Accessed: 11 February 2025].

Galfré, E. et al. 2012. FKBP12 activates the cardiac ryanodine receptor Ca2+-release channel and is antagonised by FKBP12.6. *PloS one* 7(2). Available at: https://pubmed.ncbi.nlm.nih.gov/22363773/ [Accessed: 31 January 2025].

Gautel, M. and Djinović-Carugo, K. 2016. The sarcomeric cytoskeleton: from molecules to motion. *The Journal of experimental biology* 219(Pt 2), pp. 135–145. Available at: https://pubmed.ncbi.nlm.nih.gov/26792323/ [Accessed: 24 February 2025].

Gellen, B. et al. 2008. Conditional FKBP12.6 overexpression in mouse cardiac myocytes prevents triggered ventricular tachycardia through specific alterations in excitation-contraction coupling. *Circulation* 117(14), pp. 1778–1786. Available at: https://pubmed.ncbi.nlm.nih.gov/18378612/ [Accessed: 31 January 2025].

George, C.H., Chang, C.Y. and Lai, F.A. 2005. Toward a molecular understanding of the structure-function of ryanodine receptor Ca2+ release channels: Perspectives from recombinant expression systems. *Cell Biochemistry and Biophysics* 42(2), pp. 197–222. Available at: https://link.springer.com/article/10.1385/CBB:42:2:197 [Accessed: 16 June 2025].

George, C.H., Higgs, G. V., Mackrill, J.J. and Anthony Lai, F. 2003a. Dysregulated ryanodine receptors mediate cellular toxicity: restoration of normal phenotype by FKBP12.6. *The Journal of biological chemistry* 278(31), pp. 28856–28864. Available at: https://pubmed.ncbi.nlm.nih.gov/12754204/ [Accessed: 26 February 2025].

George, C.H., Jundi, H., Thomas, N.L., Scoote, M., Walters, N., Williams, A.J. and Lai, F.A. 2004. Ryanodine receptor regulation by intramolecular interaction between cytoplasmic and transmembrane domains. *Molecular biology of the cell* 15(6), pp. 2627–2638. Available at:

https://pubmed.ncbi.nlm.nih.gov/15047862/ [Accessed: 26 February 2025].

George, C.H., Jundi, H., Walters, N., Thomas, N.L., West, R.R. and Lai, F.A. 2006. Arrhythmogenic mutation-linked defects in ryanodine receptor autoregulation reveal a novel mechanism of Ca2+ release channel dysfunction. *Circulation research* 98(1), pp. 88–97. Available at: https://pubmed.ncbi.nlm.nih.gov/16339485/ [Accessed: 26 February 2025].

George, C.H., Sorathia, R., Bertrand, B.M.A. and Lai, F.A. 2003b. In situ modulation of the human cardiac ryanodine receptor (hRyR2) by FKBP12.6. *The Biochemical journal* 370(Pt 2), pp. 579–589. Available at: https://pubmed.ncbi.nlm.nih.gov/12443530/ [Accessed: 31 January 2025].

Ginsburg, K.S. and Bers, D.M. 2005. Isoproterenol does not enhance Ca-dependent Na/Ca exchange current in intact rabbit ventricular myocytes. *Journal of molecular and cellular cardiology* 39(6), pp. 972–981. Available at: https://pubmed.ncbi.nlm.nih.gov/16242149/ [Accessed: 15 January 2025].

Gómez, A.M., Cheng, H., Lederer, W.J. and Bers, D.M. 1996. Ca2+ diffusion and sarcoplasmic reticulum transport both contribute to [Ca2+]i decline during Ca2+ sparks in rat ventricular myocytes. *The Journal of physiology* 496 (Pt 2)(Pt 2), pp. 575–581. Available at: https://pubmed.ncbi.nlm.nih.gov/8910239/ [Accessed: 16 November 2025].

Gomez-Hurtado, N. et al. 2016. Novel CPVT-Associated Calmodulin Mutation in CALM3 (CALM3-A103V) Activates Arrhythmogenic Ca Waves and Sparks. *Circulation. Arrhythmia and electrophysiology* 9(8). Available at: https://pubmed.ncbi.nlm.nih.gov/27516456/ [Accessed: 21 May 2024].

Gomez-Hurtado, N., Blackwell, D.J. and Knollmann, B.C. 2017. Modelling human calmodulinopathies with induced pluripotent stem cells: progress and challenges. *Cardiovascular Research* 113(5), p. 437. Available at: https://pmc.ncbi.nlm.nih.gov/articles/PMC5852527/ [Accessed: 8 October 2025].

Gong, D. et al. 2019. Modulation of cardiac ryanodine receptor 2 by calmodulin. *Nature 2019 572:7769* 572(7769), pp. 347–351. Available at: https://www.nature.com/articles/s41586-019-1377-y [Accessed: 30 April 2022].

Gong, D., Yan, N. and Ledford, H.A. 2021. Structural Basis for the Modulation of Ryanodine Receptors. *Trends in Biochemical Sciences* 46(6), pp. 489–501. doi: 10.1016/J.TIBS.2020.11.009.

Goonasekera, S.A., Chen, S.R.W. and Dirksen, R.T. 2005. Reconstitution of local Ca2+ signaling between cardiac L-type Ca2+ channels and ryanodine receptors: insights into regulation by FKBP12.6. *American journal of physiology. Cell physiology* 289(6). Available at: https://pubmed.ncbi.nlm.nih.gov/16049053/ [Accessed: 31 January 2025].

Gorman, C.M., Howard, B.H. and Reeves, R. 1983. Expression of recombinant plasmids in mammalian cells is enhanced by sodium butyrate. *Nucleic Acids Research* 11(21), p. 7631. Available at: https://pmc.ncbi.nlm.nih.gov/articles/PMC326508/ [Accessed: 18 June 2025].

Grimm, M. and Brown, J.H. 2009. β-Adrenergic receptor signaling in the heart: Role of CaMKII. *Journal of molecular and cellular cardiology* 48(2), p. 322. Available at: https://pmc.ncbi.nlm.nih.gov/articles/PMC2896283/ [Accessed: 11 February 2025].

Guo, T. et al. 2010. Kinetics of FKBP12.6 binding to ryanodine receptors in permeabilized cardiac myocytes and effects on Ca sparks. *Circulation Research* 106(11), pp. 1743–1752. Available at: https://www.ahajournals.org/doi/10.1161/CIRCRESAHA.110.219816 [Accessed: 31 January 2025].

Guo, T., Zhang, T., Mestril, R. and Bers, D.M. 2006a. Ca2+/Calmodulin-dependent protein kinase II phosphorylation of ryanodine receptor does affect calcium sparks in mouse ventricular myocytes. *Circulation research* 99(4), pp. 398–406. Available at: https://pubmed.ncbi.nlm.nih.gov/16840718/ [Accessed: 12 February 2025].

Guo, T., Zhang, T., Mestril, R. and Bers, D.M. 2006b. Ca2+/calmodulin-dependent protein kinase II phosphorylation of ryanodine receptor does affect calcium sparks in mouse ventricular myocytes. *Circulation Research* 99(4), pp. 398–406. Available at: http://circres.ahajournals.org [Accessed: 29 May 2024].

Gupta, N. et al. 2025. Arrhythmogenic calmodulin variants D131E and Q135P disrupt interaction with the L-type voltage-gated Ca 2+ channel (Ca v 1.2) and reduce Ca 2+-dependent inactivation. *Acta Physiologica* 241, p. 14276. Available at:

https://doi.org/10.1111/apha.14276wileyonlinelibrary.com/journal/apha [Accessed: 16 September 2025].

Györke, I. and Györke, S. 1998. Regulation of the cardiac ryanodine receptor channel by luminal Ca2+ involves luminal Ca2+ sensing sites. *Biophysical journal* 75(6), pp. 2801–2810. Available at: https://pubmed.ncbi.nlm.nih.gov/9826602/ [Accessed: 23 January 2025].

Györke, S., Stevens, S.C.W. and Terentyev, D. 2009. Cardiac calsequestrin: quest inside the SR. *The Journal of Physiology* 587(Pt 13), p. 3091. Available at: https://pmc.ncbi.nlm.nih.gov/articles/PMC2727018/ [Accessed: 23 January 2025].

Hamilton, S. 2017. *Functional heterogeneity of CPVT-mutant human cardiac ryanodine receptors: evaluation of the influence of S2031 and S2808 phosphorylation sites*. Cardiff University.

Hamilton, S. and Terentyev, D. 2024. The yellow brick road to understanding the RyR2 signalosome. *J Physiol* 602, pp. 5135–5136. Available at: https://physoc.onlinelibrary.wiley.com/doi/10.1113/JP287538 [Accessed: 14 February 2025].

Hamilton, S.L., Serysheva, I. and Strasburg, G.M. 2000. Calmodulin and Excitation-Contraction Coupling. *News in physiological sciences : an international journal of physiology produced jointly by the International Union of Physiological Sciences and the American Physiological Society* 15(6), pp. 281–284. Available at: https://pubmed.ncbi.nlm.nih.gov/11390927/ [Accessed: 6 February 2025].

Han, F., Bossuyt, J., Martin, J.L., Despa, S. and Bers, D.M. 2010. Role of phospholemman phosphorylation sites in mediating kinase-dependent regulation of the Na+-K+-ATPase. *American journal of physiology. Cell physiology* 299(6). Available at: https://pubmed.ncbi.nlm.nih.gov/20861470/ [Accessed: 15 January 2025].

Han, X. and Ferrier, G.R. 1995. Contribution of Na(+)-Ca2+ exchange to stimulation of transient inward current by isoproterenol in rabbit cardiac Purkinje fibers. *Circulation research* 76(4), pp. 664–674. Available at: https://pubmed.ncbi.nlm.nih.gov/7895340/ [Accessed: 15 January 2025].

Hanson, P.I., Meyer, T., Stryer, L. and Schulman, H. 1994. Dual role of calmodulin in autophosphorylation of multifunctional cam kinase may underlie decoding of calcium signals. *Neuron* 12(5), pp. 943–956. doi: 10.1016/0896-6273(94)90306-9.

Hanson, P.I. and Schulman, H. 1992. Inhibitory autophosphorylation of multifunctional Ca2+/calmodulin-dependent protein kinase analyzed by site-directed mutagenesis. *Journal of Biological Chemistry* 267(24), pp. 17216–17224. doi: 10.1016/S0021-9258(18)41915-1.

Hayashi, M. et al. 2009. Incidence and risk factors of arrhythmic events in catecholaminergic polymorphic ventricular tachycardia. *Circulation* 119(18), pp. 2426–2434. Available at: https://pubmed.ncbi.nlm.nih.gov/19398665/ [Accessed: 26 February 2025].

Heijman, J. et al. 2023. Enhanced Ca2+-Dependent SK-Channel Gating and Membrane Trafficking in Human Atrial Fibrillation. *Circulation Research* 132(9), pp. E116–E133. Available at: /doi/pdf/10.1161/CIRCRESAHA.122.321858?download=true [Accessed: 13 November 2025].

Helassa, N., Prakash, O., Gupta, N., McCormick, L.F., Antonyuk, S. and Dart, C. 2022. Disease-associated calmodulin mutations disrupt L-type Ca2+ channel (Cav1.2) activity and CaMKIIdelta phosphorylation in long QT syndrome. *European Heart Journal* 43(Supplement_2). Available at: https://dx.doi.org/10.1093/eurheartj/ehac544.2982 [Accessed: 13 December 2025].

Hidalgo, C. et al. 2009. PKC phosphorylation of titin's PEVK element-- a novel and conserved pathway for modulating myocardial stiffness. *Circulation research* 105(7), p. 631. Available at: https://pmc.ncbi.nlm.nih.gov/articles/PMC2764991/ [Accessed: 13 February 2025].

Hiess, F. et al. 2018. Dynamic and Irregular Distribution of RyR2 Clusters in the Periphery of Live Ventricular Myocytes. *Biophysical journal* 114(2), pp. 343–354. Available at: https://pubmed.ncbi.nlm.nih.gov/29401432/ [Accessed: 16 May 2023].

Hill, A.P., Kingston, O. and Sitsapesan, R. 2004. Functional regulation of the cardiac ryanodine receptor by suramin and calmodulin involves multiple binding sites. *Molecular pharmacology* 65(5), pp. 1258–1268. Available at: https://pubmed.ncbi.nlm.nih.gov/15102954/ [Accessed: 29 May 2024].

Hino, A. et al. 2012. Enhanced binding of calmodulin to the ryanodine receptor corrects contractile dysfunction in failing hearts. *Cardiovascular research* 96(3), pp. 433–443. Available at: https://pubmed.ncbi.nlm.nih.gov/22893680/ [Accessed: 8 October 2025].

Ho, H.T. et al. 2016. Muscarinic Stimulation Facilitates Sarcoplasmic Reticulum Ca Release by Modulating Ryanodine Receptor 2 Phosphorylation Through Protein Kinase G and Ca/Calmodulin-Dependent Protein Kinase II. *Hypertension (Dallas, Tex. : 1979)* 68(5), pp. 1171–1178. Available at: https://pubmed.ncbi.nlm.nih.gov/27647848/ [Accessed: 13 February 2025].

Hoang-Trong, T.M., Ullah, A. and Jafri, M.S. 2015. Calcium Sparks in the Heart: Dynamics and Regulation. *Research and reports in biology* 6, p. 203. Available at: https://pmc.ncbi.nlm.nih.gov/articles/PMC4871623/ [Accessed: 28 September 2025].

Hoch, B., Meyer, R., Hetzer, R., Krause, E.G. and Karczewski, P. 1999. Identification and expression of delta-isoforms of the multifunctional Ca2+/calmodulin-dependent protein kinase in failing and nonfailing human myocardium. *Circulation research* 84(6), pp. 713–721. Available at: https://pubmed.ncbi.nlm.nih.gov/10189359/ [Accessed: 11 February 2025].

Hoelz, A., Nairn, A.C. and Kuriyan, J. 2003. Crystal structure of a tetradecameric assembly of the association domain of Ca2+/calmodulin-dependent kinase II. *Molecular cell* 11(5), pp. 1241–1251. Available at: https://pubmed.ncbi.nlm.nih.gov/12769848/ [Accessed: 11 February 2025].

Holmberg, S.R.M. and Williams, A.J. 1989. Single channel recordings from human cardiac sarcoplasmic reticulum. *Circulation Research* 65(5), pp. 1445–1449. Available at: https://www.ahajournals.org/doi/10.1161/01.RES.65.5.1445 [Accessed: 22 January 2025].

Hopkins, R.F., Wall, V.E. and Esposito, D. 2012. Optimizing transient recombinant protein expression in mammalian cells. *Methods in Molecular Biology* 801, pp. 251–268. Available at: https://pubmed.ncbi.nlm.nih.gov/21987258/ [Accessed: 6 August 2025].

Hou, Y. et al. 2023a. Live-cell photoactivated localization microscopy correlates nanoscale ryanodine receptor configuration to calcium sparks in cardiomyocytes. *Nature Cardiovascular Research* 2, pp. 251–267. Available at: https://doi.org/10.1038/s44161-022-00199-2

[Accessed: 1 June 2024].

Hou, Y. et al. 2023b. Live-cell photoactivated localization microscopy correlates nanoscale ryanodine receptor configuration to calcium sparks in cardiomyocytes. *Nature Cardiovascular Research* 2(3), pp. 251–267. doi: 10.1038/s44161-022-00199-2.

Houser, S.R., Piacentino, V. and Weisser, J. 2000. Abnormalities of Calcium Cycling in the Hypertrophied and Failing Heart. *Journal of Molecular and Cellular Cardiology* 32(9), pp. 1595–1607. Available at: https://www.sciencedirect.com/science/article/pii/S0022282800912069 [Accessed: 6 August 2025].

Huang, F., Shan, J., Reiken, S., Wehrens, X.H.T. and Marks, A.R. 2006. Analysis of calstabin2 (FKBP12.6)-ryanodine receptor interactions: Rescue of heart failure by calstabin2 in mice. *Proceedings of the National Academy of Sciences of the United States of America* 103(9), pp. 3456–3461. Available at: https://www.pnas.org/doi/abs/10.1073/pnas.0511282103 [Accessed: 31 January 2025].

Huke, S. and Bers, D.M. 2008. Ryanodine receptor phosphorylation at Serine 2030, 2808 and 2814 in rat cardiomyocytes. *Biochemical and biophysical research communications* 376(1), pp. 80–85. Available at: https://pubmed.ncbi.nlm.nih.gov/18755143/ [Accessed: 19 February 2025].

Huttlin, E.L. et al. 2010. A tissue-specific atlas of mouse protein phosphorylation and expression. *Cell* 143(7), pp. 1174–1189. Available at: https://pubmed.ncbi.nlm.nih.gov/21183079/ [Accessed: 24 February 2025].

Hwang, H.S. et al. 2014. Divergent regulation of ryanodine receptor 2 calcium release channels by arrhythmogenic human calmodulin missense mutants. *Circulation Research* 114(7), pp. 1114–1124. Available at: https://www.ahajournals.org/doi/abs/10.1161/CIRCRESAHA.114.303391 [Accessed: 19 May 2023].

Ikemoto, N. and Yamamoto, T. 2002. Regulation of calcium release by interdomain interaction within ryanodine receptors. *Frontiers in bioscience : a journal and virtual library* 7(5), pp. 671–

683. Available at: https://pubmed.ncbi.nlm.nih.gov/11861212/ [Accessed: 26 February 2025].

Inui, M., Saito, A. and Fleischer, S. 1987. Isolation of the ryanodine receptor from cardiac sarcoplasmic reticulum and identity with the feet structures. *Journal of Biological Chemistry* 262(32), pp. 15637–15642. doi: 10.1016/S0021-9258(18)47774-5.

Jabbari, J. et al. 2013. New exome data question the pathogenicity of genetic variants previously associated with catecholaminergic polymorphic ventricular tachycardia. *Circulation. Cardiovascular genetics* 6(5), pp. 481–489. Available at: https://pubmed.ncbi.nlm.nih.gov/24025405/ [Accessed: 26 February 2025].

Jafri, M.S., Ullah, A. and Hoang-Trong, T. 2015. Calcium sparks in the heart: dynamics and regulation. *Research and Reports in Biology*, p. 203. doi: 10.2147/rrb.s61495.

Janicek, R. et al. 2024. Dual ablation of the RyR2-Ser2808 and RyR2-Ser2814 sites increases propensity for pro-arrhythmic spontaneous Ca2+ releases. *The Journal of physiology* 602(20). Available at: https://pubmed.ncbi.nlm.nih.gov/39316734/ [Accessed: 21 February 2025].

Jayasinghe, I. et al. 2018. True Molecular Scale Visualization of Variable Clustering Properties of Ryanodine Receptors. *Cell reports* 22(2), pp. 557–567. Available at: https://pubmed.ncbi.nlm.nih.gov/29320748/ [Accessed: 4 February 2025].

Jeyakumar, L.H. et al. 2001. FKBP binding characteristics of cardiac microsomes from diverse vertebrates. *Biochemical and biophysical research communications* 281(4), pp. 979–986. Available at: https://pubmed.ncbi.nlm.nih.gov/11237759/ [Accessed: 31 January 2025].

Jiang, D. et al. 2004. RyR2 mutations linked to ventricular tachycardia and sudden death reduce the threshold for store-overload-induced Ca2+ release (SOICR). *Proceedings of the National Academy of Sciences of the United States of America* 101(35), pp. 13062–13067. Available at: https://pubmed.ncbi.nlm.nih.gov/15322274/ [Accessed: 26 February 2025].

Jiang, D. et al. 2005. Enhanced store overload-induced Ca2+ release and channel sensitivity to luminal Ca2+ activation are common defects of RyR2 mutations linked to ventricular tachycardia and sudden death. *Circulation research* 97(11), pp. 1173–1181. Available at:

https://pubmed.ncbi.nlm.nih.gov/16239587/ [Accessed: 26 February 2025].

Jiang, D., Chen, W., Wang, R., Zhang, L. and Chen, S.R.W. 2007. Loss of luminal Ca2+ activation in the cardiac ryanodine receptor is associated with ventricular fibrillation and sudden death. *Proceedings of the National Academy of Sciences of the United States of America* 104(46), pp. 18309–18314. Available at: https://pubmed.ncbi.nlm.nih.gov/17984046/ [Accessed: 26 February 2025].

Jiang, M.T., Lokuta, A.J., Farrell, E.F., Wolff, M.R., Haworth, R.A. and Valdivia, H.H. 2002. Abnormal Ca2+ release, but normal ryanodine receptors, in canine and human heart failure. *Circulation research* 91(11), pp. 1015–1022. Available at: https://pubmed.ncbi.nlm.nih.gov/12456487/ [Accessed: 19 February 2025].

Johnson, C.K. 2006. Calmodulin, Conformational States, and Calcium Signaling. A Single-Molecule Perspective. *Biochemistry* 45(48), p. 14233. Available at: https://pmc.ncbi.nlm.nih.gov/articles/PMC2533622/ [Accessed: 5 February 2025].

Johnson, D.A., Akamine, P., Radzio-Andzelm, E., Madhusudan and Taylor, S.S. 2001. Dynamics of cAMP-dependent protein kinase. *Chemical reviews* 101(8), pp. 2243–2270. Available at: https://pubmed.ncbi.nlm.nih.gov/11749372/ [Accessed: 12 February 2025].

Kaestner, L., Tian, Q. and Lipp, P. 2012. Action Potentials in Heart Cells. In: Jung, G. ed. *Fluorescent Proteins II*. Springer Series on Fluorescence. Berlin, Heidelberg: Springer Berlin Heidelberg, pp. 163–182. Available at: https://link.springer.com/10.1007/978-3-642-23377-7 [Accessed: 13 February 2025].

Kannankeril, P., Roden, D.M. and Darbar, D. 2010. Drug-Induced Long QT Syndrome. *Pharmacological Reviews* 62(4), p. 760. Available at: https://pmc.ncbi.nlm.nih.gov/articles/PMC2993258/ [Accessed: 15 December 2025].

Kashimura, T., Briston, S.J., Trafford, A.W., Napolitano, C., Priori, S.G., Eisner, D.A. and Venetucci, L.A. 2010. In the RyR2R4496C mouse model of CPVT, β-adrenergic stimulation induces ca waves by increasing SR Ca content and not by decreasing the threshold for Ca Waves. *Circulation Research* 107(12), pp. 1483–1489. Available at: /doi/pdf/10.1161/CIRCRESAHA.110.227744?download=true [Accessed: 16 November 2025].

Kato, T. et al. 2017. Correction of impaired calmodulin binding to RyR2 as a novel therapy for lethal arrhythmia in the pressure-overloaded heart failure. *Heart Rhythm* 14(1), pp. 120–127. Available at: https://pubmed.ncbi.nlm.nih.gov/27771553/ [Accessed: 8 October 2025].

Kentish, J.C., McCloskey, D.T., Layland, J., Palmer, S., Leiden, J.M., Martin, A.F. and Solaro, R.J. 2001. Phosphorylation of troponin I by protein kinase A accelerates relaxation and crossbridge cycle kinetics in mouse ventricular muscle. *Circulation Research* 88(10), pp. 1059–1065. Available at: https://www.ahajournals.org/doi/10.1161/hh1001.091640 [Accessed: 15 January 2025].

Kermode, H., Williams, A.J. and Sitsapesan, R. 1998. The interactions of ATP, ADP, and inorganic phosphate with the sheep cardiac ryanodine receptor. *Biophysical journal* 74(3), pp. 1296–1304. Available at: https://pubmed.ncbi.nlm.nih.gov/9512027/ [Accessed: 25 January 2025].

Kiarash, A., Kelly, C.E., Phinney, B.S., Valdivia, H.H., Abrams, J. and Cala, S.E. 2004. Defective glycosylation of calsequestrin in heart failure. *Cardiovascular Research* 63(2), pp. 264–272. Available at: https://dx.doi.org/10.1016/j.cardiores.2004.04.001 [Accessed: 6 August 2025].

Kim, E.J., Youn, B., Kemper, L., Campbell, C., Milting, H., Varsanyi, M. and Kang, C.H. 2007. Characterization of human cardiac calsequestrin and its deleterious mutants. *Journal of molecular biology* 373(4), pp. 1047–1057. Available at: https://pubmed.ncbi.nlm.nih.gov/17881003/ [Accessed: 31 January 2025].

Knighton, D.R., Xuong, N.H., Taylor, S.S. and Sowadski, J.M. 1991a. Crystallization studies of cAMP-dependent protein kinase. Cocrystals of the catalytic subunit with a 20 amino acid residue peptide inhibitor and MgATP diffract to 3.0 A resolution. *Journal of molecular biology* 220(2), pp. 217–220. Available at: https://pubmed.ncbi.nlm.nih.gov/1856856/ [Accessed: 12 February 2025].

Knighton, D.R., Zheng, J., Ten Eyck, L.F., Ashford, V.A., Xuong, N.H., Taylor, S.S. and Sowadski, J.M. 1991b. Crystal structure of the catalytic subunit of cyclic adenosine monophosphate-dependent protein kinase. *Science (New York, N.Y.)* 253(5018), pp. 407–414. Available at: https://pubmed.ncbi.nlm.nih.gov/1862342/ [Accessed: 12 February 2025].

Kohlhaas, M. et al. 2006. Increased sarcoplasmic reticulum calcium leak but unaltered contractility by acute CaMKII overexpression in isolated rabbit cardiac myocytes. *Circulation research* 98(2), pp. 235–244. Available at: https://pubmed.ncbi.nlm.nih.gov/16373600/ [Accessed: 19 February 2025].

De Koninck, P. and Schulman, H. 1998. Sensitivity of CaM kinase II to the frequency of Ca2+ oscillations. *Science (New York, N.Y.)* 279(5348), pp. 227–230. Available at: https://pubmed.ncbi.nlm.nih.gov/9422695/ [Accessed: 11 February 2025].

Kooij, V. et al. 2013. PKCα-Specific Phosphorylation of the Troponin Complex in Human Myocardium: A Functional and Proteomics Analysis. *PLOS ONE* 8(10), p. e74847. Available at: https://journals.plos.org/plosone/article?id=10.1371/journal.pone.0074847 [Accessed: 13 February 2025].

Korn, E.D. 1969. Cell membranes: structure and synthesis. *Annual review of biochemistry* 38(Volume 38, 1969), pp. 263–288. Available at: https://www.annualreviews.org/content/journals/10.1146/annurev.bi.38.070169.001403 [Accessed: 16 November 2025].

Kushnir, A., Shan, J., Betzenhauser, M.J., Reiken, S. and Marks, A.R. 2010. Role of CaMKIIdelta phosphorylation of the cardiac ryanodine receptor in the force frequency relationship and heart failure. *Proceedings of the National Academy of Sciences of the United States of America* 107(22), pp. 10274–10279. Available at: https://pubmed.ncbi.nlm.nih.gov/20479242/ [Accessed: 12 February 2025].

Kuźnicki, J., Kuźnicki, L. and Drabikowski, W. 1979. Ca2+-binding modulator protein in protozoa and myxomycete. *Cell Biology International Reports* 3(1), pp. 17–23. doi: 10.1016/0309-1651(79)90064-X.

Lai, Y., Nairn, A.C., Gorelick, F. and Greengard, P. 1987. Ca2+/calmodulin-dependent protein kinase II: identification of autophosphorylation sites responsible for generation of Ca2+/calmodulin-independence. *Proceedings of the National Academy of Sciences of the United States of America* 84(16), pp. 5710–5714. Available at: https://pubmed.ncbi.nlm.nih.gov/3475699/ [Accessed: 11 February 2025].

Landstrom, A.P., Dobrev, D. and Wehrens, X.H.T. 2017. Calcium Signaling and Cardiac Arrhythmias. *Circulation Research* 120(12), pp. 1969–1993. Available at: https://www.ahajournals.org/doi/abs/10.1161/circresaha.117.310083 [Accessed: 11 March 2022].

Lanner, J.T., Georgiou, D.K., Joshi, A.D. and Hamilton, S.L. 2010. Ryanodine receptors: structure, expression, molecular details, and function in calcium release. *Cold Spring Harbor perspectives in biology* 2(11). Available at: https://pubmed.ncbi.nlm.nih.gov/20961976/ [Accessed: 20 January 2025].

Laver, D.R. 2001. THE POWER OF SINGLE CHANNEL RECORDING AND ANALYSIS: Its application to ryanodine receptors in lipid bilayers. *Proceedings of the Australian Physiological and Pharmacological Society* (1), p. 32.

Laver, D.R. 2007. Ca2+ Stores Regulate Ryanodine Receptor Ca2+ Release Channels via Luminal and Cytosolic Ca2+ Sites. *Biophysical Journal* 92(10), p. 3541. Available at: https://pmc.ncbi.nlm.nih.gov/articles/PMC1853142/ [Accessed: 22 January 2025].

Laver, D.R. 2010. Regulation of RyR Channel Gating by Ca2+, Mg2+ and ATP. *Current Topics in Membranes* 66(C), pp. 69–89. doi: 10.1016/S1063-5823(10)66004-8.

Ledbetters, M.W., Preinero, J.K., Louis+, C.E. and Mickelsonon, J.R. 1994. Tissue Distribution of Ryanodine Receptor Isoforms and Alleles Determined by Reverse Transcription Polymerase Chain Reaction*. *THE JOURNAL OF BIOLOGICAL CHEMISTRY* 269(50), p. 3154431551. doi: 10.1016/S0021-9258(18)31728-9.

Leenhardt, A., Lucet, V., Denjoy, I., Grau, F., Ngoc, D. Do and Coumel, P. 1995. Catecholaminergic polymorphic ventricular tachycardia in children. A 7-year follow-up of 21 patients. *Circulation* 91(5), pp. 1512–1519. Available at: https://pubmed.ncbi.nlm.nih.gov/7867192/ [Accessed: 26 February 2025].

Lezoualc'H, F., Fazal, L., Laudette, M. and Conte, C. 2016. Cyclic AMP sensor EPAC proteins and their role in cardiovascular function and disease. *Circulation Research* 118(5), pp. 881–897. Available at: https://www.ahajournals.org/doi/10.1161/CIRCRESAHA.115.306529 [Accessed: 13 February 2025].

Li, J., Imtiaz, M.S., Beard, N.A., Dulhunty, A.F., Thorne, R., vanHelden, D.F. and Laver, D.R. 2013. ß-Adrenergic Stimulation Increases RyR2 Activity via Intracellular Ca2+ and Mg2+ Regulation. *PLoS ONE* 8(3). Available at: https://pubmed.ncbi.nlm.nih.gov/23533585/ [Accessed: 3 July 2025].

Li, N. et al. 2012. Inhibition of CAMKII phosphorylation of RyR2 prevents induction of atrial fibrillation in FKBP12.6 knockout mice. *Circulation Research* 110(3), pp. 465–470. Available at: https://www.ahajournals.org/doi/pdf/10.1161/CIRCRESAHA.111.253229?download=true [Accessed: 5 July 2025].

Limpitikul, W.B., Dick, I.E., Joshi-Mukherjee, R., Overgaard, M.T., George, A.L. and Yue, D.T. 2014. Calmodulin Mutations Associated with Long QT Syndrome Prevent Inactivation of Cardiac L-type Ca2+ Currents and Promote Proarrhythmic Behavior in Ventricular Myocytes. *Journal of molecular and cellular cardiology* 74, p. 115. Available at: https://pmc.ncbi.nlm.nih.gov/articles/PMC4262253/ [Accessed: 13 December 2025].

Lin, X., Jo, H., Sakakibara, Y., Tambara, K., Kim, B., Komeda, M. and Matsuoka, S. 2006. Beta-adrenergic stimulation does not activate Na+/Ca2+ exchange current in guinea pig, mouse, and rat ventricular myocytes. *American journal of physiology. Cell physiology* 290(2). Available at: https://pubmed.ncbi.nlm.nih.gov/16207789/ [Accessed: 15 January 2025].

Linck, B., Qiu, Z., He, Z., Tong, Q., Hilgemann, D.W. and Philipson, K.D. 1998. Functional comparison of the three isoforms of the Na+/Ca2+ exchanger (NCX1, NCX2, NCX3). *The American journal of physiology* 274(2). Available at: https://pubmed.ncbi.nlm.nih.gov/9486131/ [Accessed: 15 January 2025].

Lipp, P. and Niggli, E. 1996. Submicroscopic calcium signals as fundamental events of excitation-contraction coupling in guinea-pig cardiac myocytes. *Journal of Physiology* 492(1), pp. 31–38. doi: 10.1113/JPHYSIOL.1996.SP021286.

Little, S.C. et al. 2015. Protein phosphatase 2A regulatory subunit B56α limits phosphatase activity in the heart. *Science signaling* 8(386). Available at: https://pubmed.ncbi.nlm.nih.gov/26198358/ [Accessed: 25 February 2025].

Litwin, S.E., Zhang, D. and Bridge, J.H.B. 2000. Dyssynchronous Ca(2+) sparks in myocytes from

infarcted hearts. *Circulation research* 87(11), pp. 1040–1047. Available at: https://pubmed.ncbi.nlm.nih.gov/11090550/ [Accessed: 21 May 2024].

Liu, B. et al. 2018. Gene Transfer of Engineered Calmodulin Alleviates Ventricular Arrhythmias in a Calsequestrin-Associated Mouse Model of Catecholaminergic Polymorphic Ventricular Tachycardia. *Journal of the American Heart Association: Cardiovascular and Cerebrovascular Disease* 7(10), p. e008155. Available at: https://pmc.ncbi.nlm.nih.gov/articles/PMC6015318/ [Accessed: 8 October 2025].

Liu, N. et al. 2011. Calmodulin kinase II inhibition prevents arrhythmias in RyR2R4496C+/- mice with catecholaminergic polymorphic ventricular tachycardia. *Journal of Molecular and Cellular Cardiology* 50(1), pp. 214–222. Available at: https://pubmed.ncbi.nlm.nih.gov/20937285/ [Accessed: 28 August 2025].

Liu, Y. et al. 2017. CPVT-associated cardiac ryanodine receptor mutation G357S with reduced penetrance impairs Ca2+ release termination and diminishes protein expression. *PLoS ONE* 12(9). Available at: /pmc/articles/PMC5621672/ [Accessed: 25 May 2023].

Loaiza, R. et al. 2013. Heterogeneity of ryanodine receptor dysfunction in a mouse model of catecholaminergic polymorphic ventricular tachycardia. *Circulation Research* 112(2), pp. 298–308. Available at: https://pubmed.ncbi.nlm.nih.gov/23152493/ [Accessed: 21 August 2025].

Lock, J.T., Parker, I. and Smith, I.F. 2015. A comparison of fluorescent Ca2+ indicators for imaging local Ca2+ signals in cultured cells. *Cell calcium* 58(6), p. 638. Available at: https://pmc.ncbi.nlm.nih.gov/articles/PMC4658286/ [Accessed: 14 September 2025].

Lokuta, A.J., Meyers, M.B., Sander, P.R., Fishman, G.I. and Valdivia, H.H. 1997. Modulation of cardiac ryanodine receptors by sorcin. *The Journal of biological chemistry* 272(40), pp. 25333–25338. Available at: https://pubmed.ncbi.nlm.nih.gov/9312152/ [Accessed: 2 February 2025].

Lokuta, A.J., Rogers, T.B., Lederer, W.J. and Valdivia, H.H. 1995. Modulation of cardiac ryanodine receptors of swine and rabbit by a phosphorylation-dephosphorylation mechanism. *The Journal of Physiology* 487(Pt 3), p. 609. Available at: https://pmc.ncbi.nlm.nih.gov/articles/PMC1156649/ [Accessed: 1 July 2025].

Luo, T., Yan, N., Xu, M., Dong, F., Liang, Q., Xing, Y. and Fan, H. 2022. Junctophilin-2 allosterically interacts with ryanodine receptor type 2 to regulate calcium release units in mouse cardiomyocytes. *Gen. Physiol. Biophys* 41, pp. 133–140. doi: 10.4149/gpb_2022007.

Lytton, J. 2013. Membrane Transporters: Na+/Ca2+ Exchangers. *Encyclopedia of Biological Chemistry: Second Edition*, pp. 44–48. doi: 10.1016/B978-0-12-378630-2.00132-8.

MacDonnell, S.M., García-Rivas, G., Scherman, J.A., Kubo, H., Chen, X., Valdivia, H. and Houser, S.R. 2008. Adrenergic regulation of cardiac contractility does not involve phosphorylation of the cardiac ryanodine receptor at serine 2808. *Circulation research* 102(8). Available at: https://pubmed.ncbi.nlm.nih.gov/18388322/ [Accessed: 19 February 2025].

MacDougall, L.K., JONES, L.R. and COHEN, P. 1991. Identification of the major protein phosphatases in mammalian cardiac muscle which dephosphorylate phospholamban. *European journal of biochemistry* 196(3), pp. 725–734. Available at: https://pubmed.ncbi.nlm.nih.gov/1849481/ [Accessed: 25 February 2025].

Makita, N. et al. 2014. Novel calmodulin mutations associated with congenital arrhythmia susceptibility. *Circulation: Cardiovascular Genetics* 7(4), pp. 466–474. Available at: http://circgenetics.ahajournals.org/lookup/suppl/doi:10.1161/CIRCGENETICS.113.000459/-/DC1. [Accessed: 30 April 2022].

Marengo, J.J., Hidalgo, C. and Bull, R. 1998. Sulfhydryl oxidation modifies the calcium dependence of ryanodine- sensitive calcium channels of excitable cells. *Biophysical Journal* 74(3), pp. 1263–1277. Available at: https://pubmed.ncbi.nlm.nih.gov/9512024/ [Accessed: 18 February 2026].

Marks, A.R., Marx, S.O. and Reiken, S. 2002. Regulation of Ryanodine Receptors via Macromolecular Complexes: A Novel Role for Leucine/Isoleucine Zippers. *Trends in Cardiovascular Medicine* 12(4), pp. 166–170. doi: 10.1016/S1050-1738(02)00156-1.

Marx, S.O., Gaburjakova, J., Gaburjakova, M., Henrikson, C., Ondrias, K. and Marks, A.R. 2001. Coupled gating between cardiac calcium release channels (ryanodine receptors). *Circulation research* 88(11), pp. 1151–1158. Available at: https://pubmed.ncbi.nlm.nih.gov/11397781/ [Accessed: 4 February 2025].

Marx, S.O., Reiken, S., Hisamatsu, Y., Jayaraman, T., Burkhoff, D., Rosemblit, N. and Marks, A.R. 2000. PKA phosphorylation dissociates FKBP12.6 from the calcium release channel (ryanodine receptor): defective regulation in failing hearts. *Cell* 101(4), pp. 365–376. Available at: https://pubmed.ncbi.nlm.nih.gov/10830164/ [Accessed: 25 April 2022].

Maylie, J., Bond, C.T., Herson, P.S., Lee, W.S. and Adelman, J.P. 2003. Small conductance Ca2+-activated K+ channels and calmodulin. *The Journal of Physiology* 554(Pt 2), p. 255. Available at: https://pmc.ncbi.nlm.nih.gov/articles/PMC1664776/ [Accessed: 13 November 2025].

Meyer, T., Hanson, P.I., Stryer, L. and Schulman, H. 1992. Calmodulin trapping by calcium-calmodulin-dependent protein kinase. *Science (New York, N.Y.)* 256(5060), pp. 1199–1202. Available at: https://pubmed.ncbi.nlm.nih.gov/1317063/ [Accessed: 11 February 2025].

Meyers, M.B., Puri, T.S., Chien, A.J., Gao, T., Hsu, P.H., Hosey, M.M. and Fishman, G.I. 1998. Sorcin associates with the pore-forming subunit of voltage-dependent L-type Ca2+ channels. *The Journal of biological chemistry* 273(30), pp. 18930–18935. Available at: https://pubmed.ncbi.nlm.nih.gov/9668070/ [Accessed: 2 February 2025].

Milescu, L.S., Nicolai, C. and Bannen, J. 2000. QuB Software.

Mukherjee, S. 2014. *The human cardiac ryanodine receptor gating behaviour: a study of mechanisms*. Cardiff University. Available at: https://orca.cardiff.ac.uk/id/eprint/70227 [Accessed: 4 October 2025].

Mukherjee, S., Thomas, N.L. and Williams, A.J. 2012. A mechanistic description of gating of the human cardiac ryanodine receptor in a regulated minimal environment. *The Journal of general physiology* 140(2), pp. 139–158. Available at: https://pubmed.ncbi.nlm.nih.gov/22802361/ [Accessed: 22 January 2025].

Muthukumar, G., Nickerson, A.W. and Nickerson, K.W. 1987. Calmodulin levels in yeasts and filamentous fungi. *FEMS Microbiology Letters* 41(3), pp. 253–255. Available at: https://dx.doi.org/10.1111/j.1574-6968.1987.tb02206.x [Accessed: 7 February 2025].

Myers, J.B., Zaegel, V., Coultrap, S.J., Miller, A.P., Bayer, K.U. and Reichow, S.L. 2017. The CaMKII holoenzyme structure in activation-competent conformations. *Nature*

communications 8. Available at: https://pubmed.ncbi.nlm.nih.gov/28589927/ [Accessed: 11 February 2025].

Nakai, J., Imagawa, T., Hakamata, Y., Shigekawa, M., Takeshima, H. and Numa, S. 1990. Primary structure and functional expression from cDNA of the cardiac ryanodine receptor/calcium release channel. *FEBS letters* 271(1–2), pp. 169–177. Available at: https://pubmed.ncbi.nlm.nih.gov/2226801/ [Accessed: 13 April 2022].

Napolitano, C., Mazzanti, A., Bloise, R. and Priori, S.G. 2022. Catecholaminergic Polymorphic Ventricular Tachycardia. *Encyclopedia of Cardiovascular Research and Medicine* 1–4, pp. 542–552. Available at: https://www.ncbi.nlm.nih.gov/books/NBK1289/ [Accessed: 26 February 2025].

Niggli, E. and Shirokova, N. 2007. A guide to sparkology: the taxonomy of elementary cellular Ca2+ signaling events. *Cell calcium* 42(4–5), pp. 379–387. Available at: https://pubmed.ncbi.nlm.nih.gov/17428535/ [Accessed: 9 January 2025].

Nikolaienko, R., Bovo, E. and Zima, A. V. 2024. Expression level of cardiac ryanodine receptors dictates properties of Ca2+-induced Ca2+ release. *Biophysical Reports* 4(4), p. 100183. Available at: https://www.sciencedirect.com/science/article/pii/S2667074724000429 [Accessed: 6 August 2025].

Nojima, H. and Sokabe, H. 1986. Structure of rat calmodulin processed genes with implications for a mRNA-mediated process of insertion. *Journal of Molecular Biology* 190(3), pp. 391–400. doi: 10.1016/0022-2836(86)90010-0.

Nyegaard, M. et al. 2012. Mutations in calmodulin cause ventricular tachycardia and sudden cardiac death. *American journal of human genetics* 91(4), pp. 703–712. Available at: https://pubmed.ncbi.nlm.nih.gov/23040497/ [Accessed: 27 February 2025].

Okabe, Y. et al. 2024. An inherited life-threatening arrhythmia model established by screening randomly mutagenized mice. *Proceedings of the National Academy of Sciences* 121(17), p. e2218204121. Available at: /doi/pdf/10.1073/pnas.2218204121?download=true [Accessed: 16 November 2025].

Van Oort, R.J. et al. 2010. Ryanodine receptor phosphorylation by calcium/calmodulin-dependent protein kinase II promotes life-threatening ventricular arrhythmias in mice with heart failure. *Circulation* 122(25), pp. 2669–2679. Available at: https://pubmed.ncbi.nlm.nih.gov/21098440/ [Accessed: 24 February 2025].

Otsu, K., Fujii, J., Periasamy, M., Difilippantonio, M., Uppender, M., Ward, D.C. and MacLennan, D.H. 1993. Chromosome mapping of five human cardiac and skeletal muscle sarcoplasmic reticulum protein genes. *Genomics* 17(2), pp. 507–509. Available at: https://pubmed.ncbi.nlm.nih.gov/8406504/ [Accessed: 20 January 2025].

Otsus, K., Willard&, H.F., Khannas, V.K., Zorzatojyl, F., Green11, N.M. and Maclennans, D.H. 1990. Molecular Cloning of cDNA Encoding the Ca2+ Release Channel (Ryanodine Receptor) of Rabbit Cardiac Muscle Sarcoplasmic Reticulum. 265(23), pp. 13472–13483. doi: 10.1016/S0021-9258(18)77371-7.

Paludan-Müller, C. et al. 2017. Integration of 60,000 exomes and ACMG guidelines question the role of Catecholaminergic Polymorphic Ventricular Tachycardia-associated variants. *Clinical genetics* 91(1), pp. 63–72. Available at: https://pubmed.ncbi.nlm.nih.gov/27538377/ [Accessed: 26 February 2025].

Pedrozo, Z. et al. 2010. Calpains and proteasomes mediate degradation of ryanodine receptors in a model of cardiac ischemic reperfusion. *Biochimica et Biophysica Acta - Molecular Basis of Disease* 1802(3), pp. 356–362. Available at: https://pubmed.ncbi.nlm.nih.gov/20026269/ [Accessed: 18 February 2026].

Pegues, J.C. and Friedberg, F. 1990. Multiple mRNAs encoding human calmodulin. *Biochemical and Biophysical Research Communications* 172(3), pp. 1145–1149. doi: 10.1016/0006-291X(90)91567-C.

Peng, W. et al. 2016. Structural basis for the gating mechanism of the type 2 ryanodine receptor RyR2. *Science (New York, N.Y.)* 354(6310). Available at: https://pubmed.ncbi.nlm.nih.gov/27708056/ [Accessed: 19 April 2022].

Perchenet, L., Hinde, A.K., Patel, K.C.R., Hancox, J.C. and Levi, A.J. 2000. Stimulation of Na/Ca exchange by the beta-adrenergic/protein kinase A pathway in guinea-pig ventricular

myocytes at 37 degrees C. *Pflugers Archiv : European journal of physiology* 439(6), pp. 822–828. Available at: https://pubmed.ncbi.nlm.nih.gov/10784358/ [Accessed: 15 January 2025].

Pereira, L. et al. 2007. The cAMP binding protein Epac modulates Ca2+ sparks by a Ca2+/calmodulin kinase signalling pathway in rat cardiac myocytes. *The Journal of physiology* 583(Pt 2), pp. 685–694. Available at: https://pubmed.ncbi.nlm.nih.gov/17599964/ [Accessed: 13 February 2025].

Pereira, L. et al. 2013. Epac2 mediates cardiac β1-adrenergic-dependent sarcoplasmic reticulum Ca2+ leak and arrhythmia. *Circulation* 127(8), pp. 913–922. Available at: https://pubmed.ncbi.nlm.nih.gov/23363625/ [Accessed: 13 February 2025].

Pérez-Hernández, M. et al. 2018. Brugada syndrome trafficking-defective Nav1.5 channels can trap cardiac Kir2.1/2.2 channels. *JCI insight* 3(18). Available at: https://pubmed.ncbi.nlm.nih.gov/30232268/ [Accessed: 31 May 2023].

Pinnell, J., Turner, S. and Howell, S. 2007. Cardiac muscle physiology. *Continuing Education in Anaesthesia Critical Care & Pain* 7(3), pp. 85–88. doi: 10.1093/BJACEACCP/MKM013.

Postma, A. V. et al. 2005. Catecholaminergic polymorphic ventricular tachycardia: RYR2 mutations, bradycardia, and follow up of the patients. *Journal of medical genetics* 42(11), pp. 863–870. Available at: https://pubmed.ncbi.nlm.nih.gov/16272262/ [Accessed: 26 February 2025].

Potenza, D.M., Janicek, R., Fernandez-Tenorio, M., Camors, E., Ramos-Mondragón, R., Valdivia, H.H. and Niggli, E. 2019. Phosphorylation of the ryanodine receptor 2 at serine 2030 is required for a complete β-adrenergic response. *The Journal of general physiology* 151(2), pp. 131–145. Available at: https://pubmed.ncbi.nlm.nih.gov/30541771/ [Accessed: 20 February 2025].

Potenza, D.M., Janicek, R., Fernandez-Tenorio, M. and Niggli, E. 2020. Activation of endogenous protein phosphatase 1 enhances the calcium sensitivity of the ryanodine receptor type 2 in murine ventricular cardiomyocytes. *Journal of Physiology* 598(6), pp. 1131–1150. Available at: https://pubmed.ncbi.nlm.nih.gov/31943206/ [Accessed: 1 July 2025].

Prakash, O. et al. 2022. CPVT-associated calmodulin variants N53I and A102V dysregulate Ca2+ signalling via different mechanisms. *Journal of cell science* 135(2). Available at: https://pubmed.ncbi.nlm.nih.gov/34888671/ [Accessed: 29 April 2022].

Prakash, O. et al. 2023. Calmodulin variant E140G associated with long QT syndrome impairs CaMKIIδ autophosphorylation and L-type calcium channel inactivation. *Journal of Biological Chemistry* 299(1). Available at: https://pubmed.ncbi.nlm.nih.gov/36496072/ [Accessed: 28 August 2025].

Prestle, J. et al. 2001. Overexpression of FK506-binding protein FKBP12.6 in cardiomyocytes reduces ryanodine receptor-mediated Ca2+ leak from the sarcoplasmic reticulum and increases contractility. *Circulation Research* 88(2), pp. 188–194. Available at: https://www.ahajournals.org/doi/10.1161/01.RES.88.2.188 [Accessed: 31 January 2025].

Priori, S.G. et al. 2001. Mutations in the cardiac ryanodine receptor gene (hRyR2) underlie catecholaminergic polymorphic ventricular tachycardia. *Circulation* 103(2), pp. 196–200. Available at: https://pubmed.ncbi.nlm.nih.gov/11208676/ [Accessed: 26 February 2025].

Priori, S.G. et al. 2002. Clinical and molecular characterization of patients with catecholaminergic polymorphic ventricular tachycardia. *Circulation* 106(1), pp. 69–74. Available at: https://pubmed.ncbi.nlm.nih.gov/12093772/ [Accessed: 26 February 2025].

Priori, S.G. et al. 2015. 2015 ESC Guidelines for the management of patients with ventricular arrhythmias and the prevention of sudden cardiac death: The Task Force for the Management of Patients with Ventricular Arrhythmias and the Prevention of Sudden Cardiac Death of the European Society of Cardiology (ESC). *European heart journal* 36(41), pp. 2793–2867l. Available at: https://pubmed.ncbi.nlm.nih.gov/26320108/ [Accessed: 26 February 2025].

Prosser, B.L. et al. 2008. S100A1 binds to the calmodulin-binding site of ryanodine receptor and modulates skeletal muscle excitation-contraction coupling. *The Journal of biological chemistry* 283(8), pp. 5046–5057. Available at: https://pubmed.ncbi.nlm.nih.gov/18089560/ [Accessed: 2 February 2025].

Prosser, B.L., Hernández-Ochoa, E.O. and Schneider, M.F. 2011. S100A1 and calmodulin regulation of ryanodine receptor in striated muscle. *Cell calcium* 50(4), pp. 323–331. Available

at: https://pubmed.ncbi.nlm.nih.gov/21784520/ [Accessed: 2 February 2025].

Qian, Y. et al. 2023. Arrhythmogenic mechanism of a novel ryanodine receptor mutation underlying sudden cardiac death. *EP Europace* 25(7), pp. 1–15. Available at: https://dx.doi.org/10.1093/europace/euad220 [Accessed: 16 November 2025].

Qin, J. et al. 2008. Luminal Ca2+ regulation of single cardiac ryanodine receptors: insights provided by calsequestrin and its mutants. *The Journal of general physiology* 131(4), pp. 325–334. Available at: https://pubmed.ncbi.nlm.nih.gov/18347081/ [Accessed: 23 January 2025].

Rebbeck, R.T., Nitu, F.R., Rohde, D., Most, P., Bers, D.M., Thomas, D.D. and Cornea, R.L. 2016. S100A1 Protein Does Not Compete with Calmodulin for Ryanodine Receptor Binding but Structurally Alters the Ryanodine Receptor·Calmodulin Complex. *The Journal of biological chemistry* 291(30), pp. 15896–15907. Available at: https://pubmed.ncbi.nlm.nih.gov/27226555/ [Accessed: 2 February 2025].

Reed, G.J., Boczek, N.J., Etheridge, S.P. and Ackerman, M.J. 2015. CALM3 mutation associated with long QT syndrome. *Heart Rhythm* 12(2), pp. 419–422. Available at: https://pubmed.ncbi.nlm.nih.gov/25460178/ [Accessed: 13 December 2025].

Reiken, S. et al. 2003. Protein kinase A phosphorylation of the cardiac calcium release channel (ryanodine receptor) in normal and failing hearts. Role of phosphatases and response to isoproterenol. *The Journal of biological chemistry* 278(1), pp. 444–453. Available at: https://pubmed.ncbi.nlm.nih.gov/12401811/ [Accessed: 25 February 2025].

Rellos, P., Pike, A.C.W., Niesen, F.H., Salah, E., Lee, W.H., von Delft, F. and Knapp, S. 2010. Structure of the CaMKIIδ/Calmodulin Complex Reveals the Molecular Mechanism of CaMKII Kinase Activation. *PLOS Biology* 8(7), p. e1000426. Available at: https://journals.plos.org/plosbiology/article?id=10.1371/journal.pbio.1000426 [Accessed: 11 February 2025].

Respress, J.L. et al. 2012. Role of RyR2 Phosphorylation at S2814 during Heart Failure Progression. *Circulation Research* 110(11), p. 1474. Available at: https://pmc.ncbi.nlm.nih.gov/articles/PMC3371642/ [Accessed: 12 February 2025].

Roden, D.M., Lazzara, R., Rosen, M., Schwartz, P.J., Towbin, J. and Michael Vincent, G. 1996. Multiple mechanisms in the long-QT syndrome. Current knowledge, gaps, and future directions. The SADS Foundation Task Force on LQTS. *Circulation* 94(8), pp. 1996–2012. Available at: https://pubmed.ncbi.nlm.nih.gov/8873679/ [Accessed: 12 December 2025].

Rodriguez, P., Bhogal, M.S. and Colyer, J. 2003. Stoichiometric phosphorylation of cardiac ryanodine receptor on serine 2809 by calmodulin-dependent kinase II and protein kinase A. *The Journal of biological chemistry* 278(40), pp. 38593–38600. Available at: https://pubmed.ncbi.nlm.nih.gov/14514795/ [Accessed: 19 February 2025].

Rosenberg, O.S., Deindl, S., Sung, R.J., Nairn, A.C. and Kuriyan, J. 2005. Structure of the autoinhibited kinase domain of CaMKII and SAXS analysis of the holoenzyme. *Cell* 123(5), pp. 849–860. Available at: https://pubmed.ncbi.nlm.nih.gov/16325579/ [Accessed: 11 February 2025].

Roston, T.M., Sanatani, S. and Chen, S.R.W. 2017. Suppression-of-function mutations in the cardiac ryanodine receptor: Emerging evidence for a novel arrhythmia syndrome? *Heart Rhythm* 14(1), pp. 108–109. Available at: https://www.heartrhythmjournal.com/action/showFullText?pii=S1547527116310050 [Accessed: 26 February 2025].

Rousseau, E. and Meissner, G. 1989. Single cardiac sarcoplasmic reticulum Ca2+-release channel: activation by caffeine. *The American journal of physiology* 256(2 Pt 2). Available at: https://pubmed.ncbi.nlm.nih.gov/2537030/ [Accessed: 25 January 2025].

Rousseau, E., Smith, J.S. and Meissner, G. 1987. Ryanodine modifies conductance and gating behavior of single Ca2+ release channel. *The American journal of physiology* 253(3 Pt 1). Available at: https://pubmed.ncbi.nlm.nih.gov/2443015/ [Accessed: 25 January 2025].

Ruan, Y., Liu, N., Napolitano, C. and Priori, S.G. 2008. Therapeutic strategies for long-QT syndrome: does the molecular substrate matter? *Circulation. Arrhythmia and electrophysiology* 1(4), pp. 290–297. Available at: https://www.ahajournals.org/doi/abs/10.1161/CIRCEP.108.795617 [Accessed: 31 May 2023].

Ruiz-Hurtado, G., Morel, E., Domínguez-Rodríguez, A., Llach, A., Lezoualc'h, F., Benitah, J.P. and Gomez, A.M. 2013. Epac in cardiac calcium signaling. *Journal of molecular and cellular cardiology* 58(1), pp. 162–171. Available at: https://pubmed.ncbi.nlm.nih.gov/23220153/ [Accessed: 13 February 2025].

Ruknudin, A., He, S., Lederer, W.J. and Schulze, D.H. 2000. Functional differences between cardiac and renal isoforms of the rat Na+-Ca2+ exchanger NCX1 expressed in Xenopus oocytes. *The Journal of physiology* 529 Pt 3(Pt 3), pp. 599–610. Available at: https://pubmed.ncbi.nlm.nih.gov/11118492/ [Accessed: 15 January 2025].

Saljic, A., Muthukumarasamy, K.M., la Cour, J.M., Boddum, K., Grunnet, M., Berchtold, M.W. and Jespersen, T. 2019. Impact of arrhythmogenic calmodulin variants on small conductance Ca2+-activated K+ (SK3) channels. *Physiological Reports* 7(19), p. e14210. Available at: /doi/pdf/10.14814/phy2.14210 [Accessed: 13 November 2025].

Santonastasi, M. and Wehrens, X.H.T. 2007. Ryanodine receptors as pharmacological targets for heart disease 1. *Acta Pharmacol Sin* 28(7), pp. 937–944. doi: 10.1111/j.1745-7254.2007.00582.x.

Savio-Galimberti, E. and Knollmann, B.C. 2015. Channel Activity of Cardiac Ryanodine Receptors (RyR2) Determines Potency and Efficacy of Flecainide and R-Propafenone against Arrhythmogenic Calcium Waves in Ventricular Cardiomyocytes. *PLOS ONE* 10(6), p. e0131179. Available at: https://journals.plos.org/plosone/article?id=10.1371/journal.pone.0131179 [Accessed: 16 November 2025].

Scheinman, M.M. and Lam, J. 2006. Exercise-induced ventricular arrhythmias in patients with no structural cardiac disease. *Annual review of medicine* 57, pp. 473–484. Available at: https://pubmed.ncbi.nlm.nih.gov/16409161/ [Accessed: 26 February 2025].

Schwartz, P.J. et al. 2009. Prevalence of the congenital long-qt syndrome. *Circulation* 120(18), pp. 1761–1767. Available at: /doi/pdf/10.1161/CIRCULATIONAHA.109.863209?download=true [Accessed: 12 December 2025].

Shan, J. et al. 2010. Phosphorylation of the ryanodine receptor mediates the cardiac fight or

flight response in mice. *The Journal of clinical investigation* 120(12), pp. 4388–4398. Available at: https://pubmed.ncbi.nlm.nih.gov/21099118/ [Accessed: 19 February 2025].

Shen, X. et al. 2019. 3D dSTORM imaging reveals novel detail of ryanodine receptor localization in rat cardiac myocytes. *The Journal of physiology* 597(2), pp. 399–418. Available at: https://pubmed.ncbi.nlm.nih.gov/30412283/ [Accessed: 4 February 2025].

Shimada, T., Kawazato, H., Yasuda, A., Ono, N. and Sueda, K. 2004. Cytoarchitecture and intercalated disks of the working myocardium and the conduction system in the mammalian heart. *The anatomical record. Part A, Discoveries in molecular, cellular, and evolutionary biology* 280(2), pp. 940–951. Available at: https://pubmed.ncbi.nlm.nih.gov/15368339/ [Accessed: 10 January 2025].

Shimamoto, K. et al. 2022. Impact of cascade screening for catecholaminergic polymorphic ventricular tachycardia type 1. *Heart (British Cardiac Society)* 108(11), pp. 840–847. Available at: https://pubmed.ncbi.nlm.nih.gov/35135837/ [Accessed: 26 February 2025].

Shirokova, N., González, A., Kirsch, W.G., Ríos, E., Pizarro, G., Stern, M.D. and Cheng, H. 1999. *Perspective Calcium Sparks: Release Packets of Uncertain Origin and Fundamental Role*. Available at: http://www.jgp.org.

Sigalas, C., Bent, S., Kitmitto, A., O'Neill, S. and Sitsapesan, R. 2009. Ca(2+)-calmodulin can activate and inactivate cardiac ryanodine receptors. *British journal of pharmacology* 156(5), pp. 794–806. Available at: https://pubmed.ncbi.nlm.nih.gov/19220289/ [Accessed: 29 May 2024].

di Silvio, A., Rolland, J.F. and Stucchi, M. 2016. Identification of state-dependent blockers for voltage-gated calcium channels using a FLIPR-based assay. *Methods in Molecular Biology* 1439, pp. 197–206. Available at: https://link.springer.com/protocol/10.1007/978-1-4939-3673-1_13 [Accessed: 24 November 2025].

Sitsapesan, R. and Williams, A.J. 1994. Gating of the native and purified cardiac SR Ca(2+)-release channel with monovalent cations as permeant species. *Biophysical Journal* 67(4), pp. 1484–1494. Available at: https://pubmed.ncbi.nlm.nih.gov/7819484/ [Accessed: 4 October 2025].

Sleiman, Y., Lacampagne, A. and Meli, A.C. 2021. “Ryanopathies” and RyR2 dysfunctions: can we further decipher them using in vitro human disease models? *Cell Death & Disease 2021 12:11* 12(11), pp. 1–19. Available at: https://www.nature.com/articles/s41419-021-04337-9 [Accessed: 27 April 2022].

Smyth, J.W. and Shaw, R.M. 2010. Forward Trafficking of Ion Channels: What the Clinician Needs to Know. *Heart rhythm : the official journal of the Heart Rhythm Society* 7(8), p. 1135. Available at: /pmc/articles/PMC2917321/ [Accessed: 31 May 2023].

Søndergaard, M.T. et al. 2019. Diminished inhibition and facilitated activation of RyR2-mediated Ca2+ release is a common defect of arrhythmogenic calmodulin mutations. *FEBS Journal* 286(22), pp. 4554–4578. doi: 10.1111/FEBS.14969.

Song, L.S., Guatimosim, S., Gómez-Viquez, L., Sobie, E.A., Ziman, A., Hartmann, H. and Lederer, W.J. 2005. Calcium Biology of the Transverse Tubules in Heart. *Annals of the New York Academy of Sciences* 1047, p. 99. Available at: https://pmc.ncbi.nlm.nih.gov/articles/PMC1484521/ [Accessed: 10 January 2025].

Song, Z., Karma, A., Weiss, J.N. and Qu, Z. 2016. Long-Lasting Sparks: Multi-Metastability and Release Competition in the Calcium Release Unit Network. *PLoS Computational Biology* 12(1), p. e1004671. Available at: https://pmc.ncbi.nlm.nih.gov/articles/PMC4701461/ [Accessed: 6 October 2025].

Sorensen, A.B., Søndergaard, M.T. and Overgaard, M.T. 2013a. Calmodulin in a Heartbeat. *FEBS Journal* 280(21), pp. 5511–5532. doi: 10.1111/FEBS.12337.

Sorensen, A.B., Søndergaard, M.T. and Overgaard, M.T. 2013b. Calmodulin in a Heartbeat. *The FEBS Journal* 280(21), pp. 5511–5532. Available at: https://onlinelibrary.wiley.com/doi/full/10.1111/febs.12337 [Accessed: 8 June 2023].

Stange, M., Xu, L., Balshaw, D., Yamaguchi, N. and Meissner, G. 2003. Characterization of recombinant skeletal muscle (Ser-2843) and cardiac muscle (Ser-2809) ryanodine receptor phosphorylation mutants. *The Journal of biological chemistry* 278(51), pp. 51693–51702. Available at: https://pubmed.ncbi.nlm.nih.gov/14532276/ [Accessed: 19 February 2025].

Stevens, F.C. 1983. Calmodulin: an introduction. *Canadian journal of biochemistry and cell biology = Revue canadienne de biochimie et biologie cellulaire* 61(8), pp. 906–910. Available at: https://pubmed.ncbi.nlm.nih.gov/6313166/ [Accessed: 7 February 2025].

Sumandea, M.P., Pyle, W.G., Kobayashi, T., De Tombe, P.P. and Solaro, R.J. 2003. Identification of a Functionally Critical Protein Kinase C Phosphorylation Residue of Cardiac Troponin T. *Journal of Biological Chemistry* 278(37), pp. 35135–35144. doi: 10.1074/JBC.M306325200.

Sumitomo, N. et al. 2003. Catecholaminergic polymorphic ventricular tachycardia: electrocardiographic characteristics and optimal therapeutic strategies to prevent sudden death. *Heart (British Cardiac Society)* 89(1), pp. 66–70. Available at: https://pubmed.ncbi.nlm.nih.gov/12482795/ [Accessed: 26 February 2025].

Sun, J., Yamaguchi, N., Xu, L., Eu, J.P., Stamler, J.S. and Meissner, G. 2008. Regulation of the Cardiac Muscle Ryanodine Receptor by O2 Tension and S-Nitrosoglutathione†. *Biochemistry* 47(52), pp. 13985–13990. Available at: https://pubs.acs.org/doi/abs/10.1021/bi8012627 [Accessed: 18 February 2026].

Sutko, J.L. and Kenyon, J.L. 1983. Ryanodine modification of cardiac muscle responses to potassium-free solutions. Evidence for inhibition of sarcoplasmic reticulum calcium release. *The Journal of general physiology* 82(3), pp. 385–404. Available at: https://pubmed.ncbi.nlm.nih.gov/6631403/ [Accessed: 20 January 2025].

Swan, H. et al. 1999. Arrhythmic disorder mapped to chromosome 1q42-q43 causes malignant polymorphic ventricular tachycardia in structurally normal hearts. *Journal of the American College of Cardiology* 34(7), pp. 2035–2042. Available at: https://pubmed.ncbi.nlm.nih.gov/10588221/ [Accessed: 26 February 2025].

Swindells, M.B. and Ikura, M. 1996. Pre-formation of the semi-open conformation by the apo-calmodulin C-terminal domain and implications binding IQ-motifs. *Nature structural biology* 3(6), pp. 501–504. Available at: https://pubmed.ncbi.nlm.nih.gov/8646534/ [Accessed: 7 February 2025].

Takasago, T., Imagawa, T., Furukawa, K. ichi, Ogurusu, T. and Shigekawa, M. 1991. Regulation

of the cardiac ryanodine receptor by protein kinase-dependent phosphorylation. *Journal of biochemistry* 109(1), pp. 163–170. Available at: https://pubmed.ncbi.nlm.nih.gov/1849885/ [Accessed: 12 February 2025].

Takasago, T., Imagawa, T. and Shigekawa, M. 1989. Phosphorylation of the Cardiac Ryanodine Receptor by cAMP-Dependent Protein Kinase. *The Journal of Biochemistry* 106(5), pp. 872–877. Available at: https://dx.doi.org/10.1093/oxfordjournals.jbchem.a122945 [Accessed: 12 February 2025].

Takeshima, H. et al. 1989. Primary structure and expression from complementary DNA of skeletal muscle ryanodine receptor. *Nature 1989 339:6224* 339(6224), pp. 439–445. Available at: https://www.nature.com/articles/339439a0 [Accessed: 13 April 2022].

Takeshima, H. et al. 1994. Excitation-contraction uncoupling and muscular degeneration in mice lacking functional skeletal muscle ryanodine-receptor gene. *Nature* 369(6481), pp. 556–559. Available at: https://pubmed.ncbi.nlm.nih.gov/7515481/ [Accessed: 20 January 2025].

Takeshima, H. et al. 1996. Generation and characterization of mutant mice lacking ryanodine receptor type 3. *The Journal of biological chemistry* 271(33), pp. 19649–19652. Available at: https://pubmed.ncbi.nlm.nih.gov/8702664/ [Accessed: 20 January 2025].

Takeshima, H., Komazaki, S., Hirose, K., Nishi, M., Noda, T. and Iino, M. 1998. Embryonic lethality and abnormal cardiac myocytes in mice lacking ryanodine receptor type 2. *The EMBO journal* 17(12), pp. 3309–3316. Available at: https://pubmed.ncbi.nlm.nih.gov/9628868/ [Accessed: 20 January 2025].

Tarifa, C. et al. 2023. Spatial Distribution of Calcium Sparks Determines Their Ability to Induce Afterdepolarizations in Human Atrial Myocytes. *JACC: Basic to Translational Science* 8(1), pp. 1–15. doi: 10.1016/j.jacbts.2022.07.013.

Terentyev, D. et al. 2008. Modulation of SR Ca Release by Luminal Ca and Calsequestrin in Cardiac Myocytes: Effects of CASQ2 Mutations Linked to Sudden Cardiac Death. *Biophysical Journal* 95(4), pp. 2037–2048. doi: 10.1529/BIOPHYSJ.107.128249.

Terentyev, D. et al. 2009. miR-1 overexpression enhances Ca(2+) release and promotes

cardiac arrhythmogenesis by targeting PP2A regulatory subunit B56alpha and causing CaMKII-dependent hyperphosphorylation of RyR2. *Circulation research* 104(4), pp. 514–521. Available at: https://pubmed.ncbi.nlm.nih.gov/19131648/ [Accessed: 25 February 2025].

Terentyev, D. and Hamilton, S. 2016. Regulation of sarcoplasmic reticulum Ca2+ release by serine-threonine phosphatases in the heart. *Journal of molecular and cellular cardiology* 101, pp. 156–164. Available at: https://pubmed.ncbi.nlm.nih.gov/27585747/ [Accessed: 19 February 2025].

Terentyev, D., Viatchenko-Karpinski, S., Gyorke, I., Terentyeva, R. and Gyorke, S. 2003. Protein Phosphatases Decrease Sarcoplasmic Reticulum Calcium Content by Stimulating Calcium Release in Cardiac Myocytes. *The Journal of Physiology* 552(Pt 1), p. 109. Available at: https://pmc.ncbi.nlm.nih.gov/articles/PMC2343319/ [Accessed: 1 July 2025].

Tester, D.J. et al. 2020. Molecular characterization of the calcium release channel deficiency syndrome. *JCI Insight* 5(15). Available at: https://pubmed.ncbi.nlm.nih.gov/32663189/ [Accessed: 6 August 2025].

Thanassoulas, A. et al. 2023. Life-threatening arrhythmogenic CaM mutations disrupt CaM binding to a distinct RyR2 CaM-binding pocket. *Biochimica et Biophysica Acta (BBA) - General Subjects* 1867(4), p. 130313. doi: 10.1016/J.BBAGEN.2023.130313.

Thomas, N.L., George, C.H. and Lai, F.A. 2006. Role of ryanodine receptor mutations in cardiac pathology: more questions than answers? *Biochemical Society Transactions* 34(5), pp. 913–918. Available at: /biochemsoctrans/article/34/5/913/65988/Role-of-ryanodine-receptor-mutations-in-cardiac [Accessed: 26 February 2025].

Timerman, A.P., Onoue, H., Xin, H.B., Barg, S., Copello, J., Wiederrecht, G. and Fleischer, S. 1996. Selective binding of FKBP12.6 by the cardiac ryanodine receptor. *The Journal of biological chemistry* 271(34), pp. 20385–20391. Available at: https://pubmed.ncbi.nlm.nih.gov/8702774/ [Accessed: 31 January 2025].

Tombes, R.M., Faison, M.O. and Turbeville, J.M. 2003. Organization and evolution of multifunctional Ca2+/CaM- dependent protein kinase genes. *Gene* 322(1–2), pp. 17–31. Available at: https://pubmed.ncbi.nlm.nih.gov/14644494/ [Accessed: 11 February 2025].

Tomek, J., Nieves-Cintron, M., Navedo, M.F., Ko, C.Y. and Bers, D.M. 2023. SparkMaster 2: A New Software for Automatic Analysis of Calcium Spark Data. *Circulation Research* 133(6), pp. 450–462. Available at: /doi/pdf/10.1161/CIRCRESAHA.123.322847?download=true [Accessed: 3 September 2025].

Toutenhoofd, S.L., Foletti, D., Wicki, R., Rhyner, J.A., Garcia, F., Tolon, R. and Strehler, E.E. 1998. Characterization of the human CALM2 calmodulin gene and comparison of the transcriptional activity of CALM1, CALM2 and CALM3. *Cell calcium* 23(5), pp. 323–338. Available at: https://pubmed.ncbi.nlm.nih.gov/9681195/ [Accessed: 7 February 2025].

Tripathy, A., Xu, L., Mann, G. and Meissner, G. 1995. Calmodulin activation and inhibition of skeletal muscle Ca2+ release channel (ryanodine receptor). *Biophysical journal* 69(1), pp. 106–119. Available at: https://pubmed.ncbi.nlm.nih.gov/7669888/ [Accessed: 6 February 2025].

Tunwell, R.E.A., Wickenden, C., Bertrand, B.M.A., Shevchenko, V.I., Walsh, M.B., Allen, P.D. and Lai, F.A. 1996. The human cardiac muscle ryanodine receptor-calcium release channel: identification, primary structure and topological analysis. *The Biochemical journal* 318 (Pt 2)(Pt 2), pp. 477–487. Available at: https://pubmed.ncbi.nlm.nih.gov/8809036/ [Accessed: 20 January 2025].

Uchinoumi, H. et al. 2010a. Catecholaminergic polymorphic ventricular tachycardia is caused by mutation-linked defective conformational regulation of the ryanodine receptor. *Circulation research* 106(8), pp. 1413–1424. Available at: https://pubmed.ncbi.nlm.nih.gov/20224043/ [Accessed: 26 February 2025].

Uchinoumi, H. et al. 2016. CaMKII-dependent phosphorylation of RyR2 promotes targetable pathological RyR2 conformational shift. *Journal of Molecular and Cellular Cardiology* 98, pp. 62–72. doi: 10.1016/J.YJMCC.2016.06.007.

Valdivia, H.H. 1998. Modulation of intracellular Ca2+ levels in the heart by sorcin and FKBP12, two accessory proteins of ryanodine receptors. *Trends in pharmacological sciences* 19(12), pp. 479–483. Available at: https://pubmed.ncbi.nlm.nih.gov/9871407/ [Accessed: 2 February 2025].

Van Veen, T.A.B., Van Rijen, H.V.M. and Opthof, T. 2001. Cardiac gap junction channels:

modulation of expression and channel properties. *Cardiovascular Research* 51(2), pp. 217–229. Available at: https://dx.doi.org/10.1016/S0008-6363(01)00324-8 [Accessed: 14 January 2025].

Viero, C., Thomas, N.L., Euden, J., Mason, S.A., George, C.H. and Williams, A.J. 2012. Techniques and methodologies to study the ryanodine receptor at the molecular, subcellular and cellular level. *Advances in Experimental Medicine and Biology* 740, pp. 183–215. Available at: https://link.springer.com/chapter/10.1007/978-94-007-2888-2_8 [Accessed: 17 November 2025].

Villarroel, A. et al. 2014. The Ever Changing Moods of Calmodulin: How Structural Plasticity Entails Transductional Adaptability. *Journal of Molecular Biology* 426(15), pp. 2717–2735. doi: 10.1016/J.JMB.2014.05.016.

Waddell, H.M.M., Mereacre, V., Alvarado, F.J. and Munro, M.L. 2023. Clustering properties of the cardiac ryanodine receptor in health and heart failure HHS Public Access. *J Mol Cell Cardiol* 185, pp. 38–49. Available at: http://creativecommons.org/licenses/by/4.0/ [Accessed: 4 February 2025].

Walker, C.A. and Spinale, F.G. 1999. The structure and function of the cardiac myocyte: a review of fundamental concepts. *The Journal of thoracic and cardiovascular surgery* 118(2), pp. 375–382. Available at: https://pubmed.ncbi.nlm.nih.gov/10425017/ [Accessed: 10 January 2025].

Wallace, E., Howard, L., Liu, M., O'Brien, T., Ward, D., Shen, S. and Prendiville, T. 2019. Long QT Syndrome: Genetics and Future Perspective. *Pediatric cardiology* 40(7), pp. 1419–1430. Available at: https://pubmed.ncbi.nlm.nih.gov/31440766/ [Accessed: 12 December 2025].

Walweel, K. et al. 2014. Differences in the regulation of RyR2 from human, sheep, and rat by Ca^{2+} and Mg^{2+} in the cytoplasm and in the lumen of the sarcoplasmic reticulum. *The Journal of general physiology* 144(3), pp. 263–271. Available at: https://pubmed.ncbi.nlm.nih.gov/25156119/ [Accessed: 22 January 2025].

Walweel, K. et al. 2017. Calmodulin Mutants Linked to Catecholaminergic Polymorphic Ventricular Tachycardia Fail to Inhibit Human RyR2 Channels. *Journal of the American College*

of Cardiology 70(1), pp. 115–117. Available at: /doi/pdf/10.1016/j.jacc.2017.04.055?download=true [Accessed: 5 October 2025].

Walweel, K., Oo, Y.W. and Laver, D.R. 2017b. The emerging role of calmodulin regulation of RyR2 in controlling heart rhythm, the progression of heart failure and the antiarrhythmic action of dantrolene. *Clinical and experimental pharmacology & physiology* 44(1), pp. 135–142. Available at: https://pubmed.ncbi.nlm.nih.gov/27626620/ [Accessed: 24 April 2022].

Wang, H.G., George, M.S., Kim, J., Wang, C. and Pitt, G.S. 2007. Ca2+/Calmodulin Regulates Trafficking of CaV1.2 Ca2+ Channels in Cultured Hippocampal Neurons. *Journal of Neuroscience* 27(34), pp. 9086–9093. Available at: https://www.jneurosci.org/content/27/34/9086 [Accessed: 13 November 2025].

Wang, Y.Y. et al. 2017. RyR2R420Q catecholaminergic polymorphic ventricular tachycardia mutation induces bradycardia by disturbing the coupled clock pacemaker mechanism. *JCI Insight* 2(8). Available at: https://doi.org/10.1172/jci.insight.91872 [Accessed: 19 June 2024].

Wehrens, X.H.T. et al. 2003. FKBP12.6 deficiency and defective calcium release channel (ryanodine receptor) function linked to exercise-induced sudden cardiac death. *Cell* 113(7), pp. 829–840. Available at: https://pubmed.ncbi.nlm.nih.gov/12837242/ [Accessed: 31 January 2025].

Wehrens, X.H.T. 2011. CaMKII Regulation of the Cardiac Ryanodine Receptor and SR Calcium Release. *Heart Rhythm* 8(2), pp. 323–325. doi: 10.1016/j.hrthm.2010.09.079.

Wehrens, X.H.T., Lehnart, S.E., Reiken, S., Vest, J.A., Wronska, A. and Marks, A.R. 2006. Ryanodine receptor/calcium release channel PKA phosphorylation: a critical mediator of heart failure progression. *Proceedings of the National Academy of Sciences of the United States of America* 103(3), pp. 511–518. Available at: https://pubmed.ncbi.nlm.nih.gov/16407108/ [Accessed: 19 February 2025].

Wehrens, X.H.T., Lehnart, S.E., Reiken, S.R. and Marks, A.R. 2004. Ca2+/calmodulin-dependent protein kinase II phosphorylation regulates the cardiac ryanodine receptor. *Circulation research* 94(6). Available at: https://pubmed.ncbi.nlm.nih.gov/15016728/ [Accessed: 25 April 2022].

White, S.H. 1986. The Physical Nature of Planar Bilayer Membranes. *Ion Channel Reconstitution*, pp. 3–35. Available at: https://link.springer.com/chapter/10.1007/978-1-4757-1361-9_1 [Accessed: 3 October 2025].

Williams, A. and Thomas, N.L. 2019. Reconstitution of Ion Channels from Intracellular Membranes and Bacteria Not Amenable to Conventional Electrophysiological Techniques. *Encyclopedia of Biophysics*, pp. 1–11. Available at: https://link.springer.com/rwe/10.1007/978-3-642-35943-9_372-1 [Accessed: 17 November 2025].

Witcher, rick R., KovacsS, R.J., Schulmans, H., Cefali, D.C. and Jones, L.R. 1991. Unique Phosphorylation Site on the Cardiac Ryanodine Receptor Regulates Calcium Channel Activity. *THE JOURNAL OF BIOLOGICAL CHEMISTRY* 266(17), pp. 11144–11152. doi: 10.1016/S0021-9258(18)99140-4.

Wleklinski, M.J., Kannankeril, P.J. and Knollmann, B.C. 2020. Molecular and tissue mechanisms of catecholaminergic polymorphic ventricular tachycardia. *The Journal of physiology* 598(14), pp. 2817–2834. Available at: https://pubmed.ncbi.nlm.nih.gov/32115705/ [Accessed: 26 February 2025].

Wong, M.H. et al. 2019. The KN-93 Molecule Inhibits Calcium/Calmodulin-Dependent Protein Kinase II (CaMKII) Activity by Binding to Ca2+/CaM. *Journal of Molecular Biology* 431(7), pp. 1440–1459. Available at: https://pubmed.ncbi.nlm.nih.gov/30753871/ [Accessed: 21 July 2025].

Wright, N.T., Prosser, B.L., Varney, K.M., Zimmer, D.B., Schneider, M.F. and Weber, D.J. 2008. S100A1 and Calmodulin Compete for the Same Binding Site on Ryanodine Receptor. *The Journal of Biological Chemistry* 283(39), p. 26676. Available at: https://pmc.ncbi.nlm.nih.gov/articles/PMC2546546/ [Accessed: 2 February 2025].

Wu, X. and Bers, D.M. 2007. Free and Bound Intracellular Calmodulin Measurements in Cardiac Myocytes. *Cell calcium* 41(4), p. 353. Available at: /pmc/articles/PMC1868497/ [Accessed: 19 June 2024].

Wu, Y. et al. 2009. Calmodulin kinase II is required for fight or flight sinoatrial node physiology.

Proceedings of the National Academy of Sciences of the United States of America 106(14), pp. 5972–5977. Available at: https://pubmed.ncbi.nlm.nih.gov/19276108/ [Accessed: 12 February 2025].

Xia, M., Imredy, J.P., Koblan, K.S., Bennett, P. and Connolly, T.M. 2004. State-dependent inhibition of L-type calcium channels: cell-based assay in high-throughput format. *Analytical Biochemistry* 327(1), pp. 74–81. Available at: https://www.sciencedirect.com/science/article/pii/S0003269704000752?via%3Dihub [Accessed: 24 November 2025].

Xiao, B. et al. 2005. Characterization of a novel PKA phosphorylation site, serine-2030, reveals no PKA hyperphosphorylation of the cardiac ryanodine receptor in canine heart failure. *Circulation Research* 96(8), pp. 847–855. Available at: https://www.ahajournals.org/doi/10.1161/01.RES.0000163276.26083.e8 [Accessed: 20 February 2025].

Xiao, B. et al. 2007. Functional Consequence of Protein Kinase A-dependent Phosphorylation of the Cardiac Ryanodine Receptor: SENSITIZATION OF STORE OVERLOAD-INDUCED Ca2+ RELEASE. *Journal of Biological Chemistry* 282(41), pp. 30256–30264. doi: 10.1074/JBC.M703510200.

Xiao, B., Sutherland, C., Walsh, M.P. and Chen, S.R.W. 2004. Protein kinase A phosphorylation at serine-2808 of the cardiac Ca2+-release channel (ryanodine receptor) does not dissociate 12.6-kDa FK506-binding protein (FKBP12.6). *Circulation research* 94(4), pp. 487–495. Available at: https://pubmed.ncbi.nlm.nih.gov/14715536/ [Accessed: 19 February 2025].

Xiao, J. et al. 2007. Removal of FKBP12.6 Does Not Alter the Conductance and Activation of the Cardiac Ryanodine Receptor or the Susceptibility to Stress-induced Ventricular Arrhythmias. *Journal of Biological Chemistry* 282(48), pp. 34828–34838. doi: 10.1074/JBC.M707423200.

Xu, L., Eu, J.P., Meissner, G. and Stamler, J.S. 1998. Activation of the cardiac calcium release channel (ryanodine receptor) by poly-S-nitrosylation. *Science (New York, N.Y.)* 279(5348), pp. 234–237. Available at: https://pubmed.ncbi.nlm.nih.gov/9422697/ [Accessed: 18 February

2026].

Xu, L., Mann, G. and Meissner, G. 1996. Regulation of cardiac Ca2+ release channel (ryanodine receptor) by Ca2+, H+, Mg2+, and adenine nucleotides under normal and simulated ischemic conditions. *Circulation research* 79(6), pp. 1100–1109. Available at: https://pubmed.ncbi.nlm.nih.gov/8943948/ [Accessed: 25 January 2025].

Xu, L. and Meissner, G. 1998. Regulation of cardiac muscle Ca2+ release channel by sarcoplasmic reticulum lumenal Ca2+. *Biophysical Journal* 75(5), p. 2302. Available at: https://pmc.ncbi.nlm.nih.gov/articles/PMC1299904/ [Accessed: 23 January 2025].

Yang, L., Liu, G., Zakharov, S.I., Morrow, J.P., Rybin, V.O., Steinberg, S.F. and Marx, S.O. 2005. Ser1928 is a common site for Cav1.2 phosphorylation by protein kinase C isoforms. *The Journal of biological chemistry* 280(1), pp. 207–214. Available at: https://pubmed.ncbi.nlm.nih.gov/15509562/ [Accessed: 13 February 2025].

Yang, Y. et al. 2013. Cardiac Myocyte Z-line Calmodulin is Mainly RyR2-Bound and Reduction is Arrhythmogenic and Occurs in Heart Failure. *Circulation research* 114(2), p. 295. Available at: https://pmc.ncbi.nlm.nih.gov/articles/PMC4004530/ [Accessed: 15 September 2025].

Yang, Z., Ikemoto, N., Lamb, G.D. and Steele, D.S. 2006. The RyR2 central domain peptide DPc10 lowers the threshold for spontaneous Ca2+ release in permeabilized cardiomyocytes. *Cardiovascular Research* 70(3), pp. 475–485. Available at: https://dx.doi.org/10.1016/j.cardiores.2006.03.001 [Accessed: 28 February 2025].

Yang, Z. and Steele, D.S. 2002. Effects of phosphocreatine on SR Ca(2+) regulation in isolated saponin-permeabilized rat cardiac myocytes. *The Journal of physiology* 539(Pt 3), pp. 767–777. Available at: https://pubmed.ncbi.nlm.nih.gov/11897848/ [Accessed: 16 November 2025].

Yano, M., Yamamoto, T., Ikemoto, N. and Matsuzaki, M. 2005. Abnormal ryanodine receptor function in heart failure. *Pharmacology & Therapeutics* 107(3), pp. 377–391. doi: 10.1016/J.PHARMTHERA.2005.04.003.

Yap, K.L., Kim, J., Truong, K., Sherman, M., Yuan, T. and Ikura, M. 2000. Calmodulin target

database. *Journal of structural and functional genomics* 1(1), pp. 8–14. Available at: https://pubmed.ncbi.nlm.nih.gov/12836676/ [Accessed: 7 February 2025].

Yasuda, R., Hayashi, Y. and Hell, J.W. 2022. CaMKII: a central molecular organizer of synaptic plasticity, learning and memory. *Nature Reviews Neuroscience 2022 23:11* 23(11), pp. 666–682. Available at: https://www.nature.com/articles/s41583-022-00624-2 [Accessed: 11 February 2025].

Yin, C.C. and Lai, F.A. 2000. Intrinsic lattice formation by the ryanodine receptor calcium-release channel. *Nature cell biology* 2(9), pp. 669–671. Available at: https://pubmed.ncbi.nlm.nih.gov/10980710/ [Accessed: 6 October 2025].

Yin, L. et al. 2021. Impaired Binding to Junctophilin-2 and Nanostructural Alteration in CPVT Mutation. *Circulation Research* 129(3), pp. E35–E52. Available at: https://www.ahajournals.org/doi/suppl/10.1161/CIRCRESAHA.121.319094. [Accessed: 28 May 2024].

Yuchi, Z., Lau, K. and Van Petegem, F. 2012. Disease mutations in the ryanodine receptor central region: crystal structures of a phosphorylation hot spot domain. *Structure (London, England : 1993)* 20(7), pp. 1201–1211. Available at: https://pubmed.ncbi.nlm.nih.gov/22705209/ [Accessed: 14 February 2025].

Zalk, R., Lehnart, S.E. and Marks, A.R. 2007. Modulation of the ryanodine receptor and intracellular calcium. *Annual review of biochemistry* 76, pp. 367–385. Available at: https://pubmed.ncbi.nlm.nih.gov/17506640/ [Accessed: 28 April 2022].

Zhai, D. et al. 2022. LINC01194 recruits NUMA1 to promote ubiquitination of RYR2 to enhance malignant progression in triple-negative breast cancer. *Cancer letters* 544. Available at: https://pubmed.ncbi.nlm.nih.gov/35750275/ [Accessed: 18 February 2026].

Zhang, H. et al. 2012a. Hyperphosphorylation of the cardiac ryanodine receptor at serine 2808 is not involved in cardiac dysfunction after myocardial infarction. *Circulation research* 110(6), pp. 831–840. Available at: https://pubmed.ncbi.nlm.nih.gov/22302785/ [Accessed: 20 February 2025].

Zhang, J.Z., Waddell, H.M.M., Wu, E., Dholakia, J., Okolo, C.A., McLay, J.C. and Jones, P.P. 2016. FKBPs facilitate the termination of spontaneous Ca2+ release in wild-type RyR2 but not CPVT mutant RyR2. *The Biochemical journal* 473(14), pp. 2049–2060. Available at: https://pubmed.ncbi.nlm.nih.gov/27154203/ [Accessed: 26 February 2025].

Zhang, L., Kelley, J., Schmeisser, G., Kobayashi, Y.M. and Jones, L.R. 1997. Complex formation between junctin, triadin, calsequestrin, and the ryanodine receptor. Proteins of the cardiac junctional sarcoplasmic reticulum membrane. *The Journal of biological chemistry* 272(37), pp. 23389–23397. Available at: https://pubmed.ncbi.nlm.nih.gov/9287354/ [Accessed: 31 January 2025].

Zhang, M. et al. 2012b. Structural basis for calmodulin as a dynamic calcium sensor. *Structure (London, England : 1993)* 20(5), pp. 911–923. Available at: https://pubmed.ncbi.nlm.nih.gov/22579256/ [Accessed: 6 February 2025].

Zhang, T., Maier, L.S., Dalton, N.D., Miyamoto, S., Ross, J., Bers, D.M. and Brown, J.H. 2003. The deltaC isoform of CaMKII is activated in cardiac hypertrophy and induces dilated cardiomyopathy and heart failure. *Circulation research* 92(8), pp. 912–919. Available at: https://www.ahajournals.org/doi/pdf/10.1161/01.RES.0000069686.31472.C5?download=true [Accessed: 17 November 2025].

Zhang, Y.H., Hinde, A.K. and Hancox, J.C. 2001. Anti-adrenergic effect of adenosine on Na(+)-Ca(2+) exchange current recorded from guinea-pig ventricular myocytes. *Cell calcium* 29(5), pp. 347–358. Available at: https://pubmed.ncbi.nlm.nih.gov/11292391/ [Accessed: 15 January 2025].

Zhu, W., Bian, X. and Lv, J. 2024. From genes to clinical management: A comprehensive review of long QT syndrome pathogenesis and treatment. *Heart Rhythm O2* 5(8), pp. 573–586. Available at: https://www.sciencedirect.com/science/article/pii/S2666501824002253 [Accessed: 12 December 2025].

Zhu, X., Dunand, C., Snedden, W. and Galaud, J.P. 2015. CaM and CML emergence in the green lineage. *Trends in Plant Science* 20(8), pp. 483–489. doi: 10.1016/J.TPLANTS.2015.05.010.

Zima, A. V., Picht, E., Bers, D.M. and Blatter, L.A. 2008. Termination of Cardiac Ca2+ Sparks:

Role of Intra-SR [Ca2+], Release Flux, and Intra-SR Ca2+ Diffusion. *Circulation research* 103(8), p. e105. Available at: https://pmc.ncbi.nlm.nih.gov/articles/PMC2678058/ [Accessed: 24 January 2025].

Zissimopoulos, S. et al. 2025. Compromised repolarization reserve in a murine model of catecholaminergic polymorphic ventricular tachycardia caused by RyR2-R420Q mutation. *Journal of Molecular and Cellular Cardiology* 206, pp. 127–140. Available at: https://www.sciencedirect.com/science/article/pii/S0022282825001373#ec0005 [Accessed: 6 September 2025].

Zissimopoulos, S. and Lai, F.A. 2005. Interaction of FKBP12.6 with the cardiac ryanodine receptor C-terminal domain. *The Journal of biological chemistry* 280(7), pp. 5475–5485. Available at: https://pubmed.ncbi.nlm.nih.gov/15591045/ [Accessed: 31 January 2025].

Zorzato, F. et al. 1990. Molecular Cloning of cDNA Encoding Human and Rabbit Forms of the Ca2' Release Channel (Ryanodine Receptor) of Skeletal Muscle Sarcoplasmic Reticulum. 265(4), p. 199. doi: 10.1016/S0021-9258(19)39968-5.

Zuidscherwoude, M., Grigore, T., van de Langenberg, B., Witte, G., van der Wijst, J. and Hoenderop, J.G. 2024. Calmodulin regulates TRPV5 intracellular trafficking and plasma membrane abundance. *Journal of Physiology* 602(24), pp. 6871–6888. Available at: /doi/pdf/10.1113/JP286182 [Accessed: 13 November 2025].